In re: Oil Spill by the Oil Rig "Deepwater Horizon" in
The Gulf of Mexico, on April 20, 2010

UNITED STATES DISTRICT COURT
EASTERN DISTRICT OF LOUISIANA
MDL NO. 2179, SECTION J
JUDGE BARBIER; MAGISTRATE JUDGE SHUSHAN
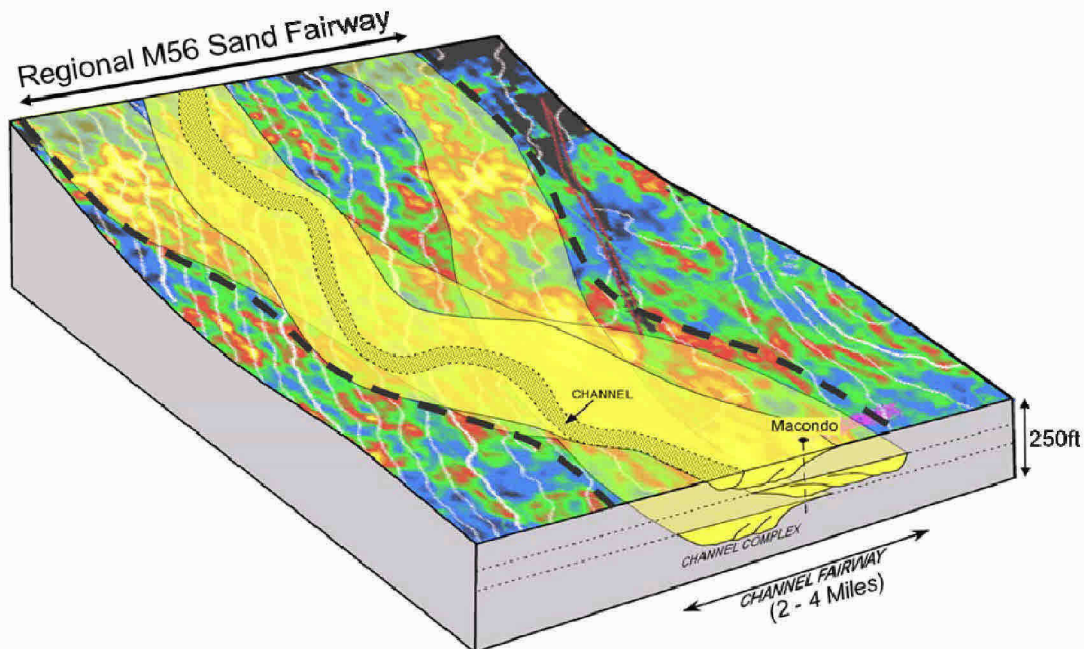
Modelling Macondo

A calculation of the volume of oil released during the *Deepwater Horizon* incident

Prepared on Behalf of BP Exploration & Production Inc. and Anadarko

Prepared by:

Martin J. Blunt

Department of Earth Science and Engineering
Imperial College, London SW7 2AZ, UK
May 1st, 2013

Table of Contents

1. Professional background

I am a professor of petroleum engineering at Imperial College London.

My speciality is the study of oil flow through rocks underground, a field known as reservoir engineering. I have taught the fluid flow principles presented in this report for over 20 years. My students have gone on to teach and practise petroleum engineering in universities and oil companies around the world. For instance, Dr. Hughes, at Louisiana State University, one of the leading reservoir engineers who consulted for the US Government's Macondo Flow Rate Technical Group, is one of my former PhD students from Stanford University. I have also taught classes for industry in the UK, US, China, Brazil, Iran and Saudi Arabia.

I have published over 200 papers which have been cited over 7,000 times.

I am a distinguished member of the Society of Petroleum Engineers (SPE). I served as an SPE Distinguished Lecturer in 2001. I received the SPE Cedric Ferguson medal for the best paper written under the age of 33, discussing a new method for using computers to simulate hydrocarbon fluid flow through reservoirs. I also received the 2011 SPE Lester Uren award for contributions to petroleum engineering technology made before the age of 45. I was given the 2012 Darcy Award for lifetime achievement by the Society of Core Analysts.

I am the editor of the scientific journal *Transport in Porous Media*.

I served as Head of the Department of Earth Science and Engineering at Imperial College from 2006-2011.

I have helped found, and am Chief Scientist of, two companies providing services to the oil industry.

I received a PhD in physics from Cambridge University in 1988. When I graduated, I worked for four years for BP. I developed new methods to improve the accuracy of reservoir simulators. These simulators predict oil recovery as an aid to reservoir management. For this work BP awarded me its Tallow Chandlers prize. I then joined the faculty of Stanford University. At Stanford my research on improving oil recovery was funded by the US Government and a consortium of major oil companies. I left Stanford to become a professor at Imperial College in 1999.

I have never testified as an expert witness before and my compensation is not dependent on the outcome.

1.1 Scope of Work

I have calculated the amount of oil spilt during the *Deepwater Horizon* incident using the methods of my field, reservoir engineering. I have drawn on the work of other BP experts, including the pressure transient analysis of Professor Alain Gringarten; the rock-compressibility results of Professor Robert Zimmerman; the pressure data generated by Professor Martin Trusler; the fluids analysis of Professor Curtis Whitson; and ████████████████████████████████████

My analysis uses a well-established method from my field called material balance. My Imperial College London colleague Professor Gringarten is submitting a report estimating cumulative flow using different techniques from his field of expertise, pressure-transient analysis. I make use of some of the results of his study, while he uses the results of some of my analysis. Even though there are a few steps in our respective calculations that use the same principles and interim methodologies, our determinations of cumulative flow are independent and involve distinct approaches. For example, Professor Gringarten does not directly use the main principle in my approach, material balance. And I do not use the method that Professor Gringarten pioneered, called deconvolution.

2. Executive summary of analysis and contrast with Government estimates

I calculate that the volume of oil released from the Macondo reservoir was 3.26 million stock tank barrels (MMstb). I have used conservative assumptions to avoid under-statement of the volume. I find a range of oil released between 2.9 and 3.7 MMstb.

This is the total volume of all the oil that left the reservoir, including any oil burnt or collected, converted to a volume at surface (stock tank) conditions of 60°F and 1 atmosphere pressure.

My calculation uses the same reservoir engineering principle employed by the Government's reservoir engineering experts Drs. Kelkar & Raghavan, namely material balance.

In material balance, three quantities – the oil volume connected to the well, compressibility and pressure depletion – are multiplied together to calculate cumulative oil flow.

Compressibility determines how much oil is released from the rock as the pressure drops. The main difference between my estimate and those of Dr. Kelkar & Raghavan and another US Government expert Dr. Hsieh, is that they double the compressibility from the value measured on Macondo rock samples at an independent service laboratory. This is a switch from the approach that Dr. Kelkar used when he first evaluated Macondo oil flow for the US Flow Rate Technical Group in 2010, where he took a measured value for rock compressibility, as I do in this report. Dr. Kelkar & Raghavan's expert report acknowledges that if they use the same rock compressibility as I do, they obtain roughly my value for cumulative flow.[1] Similarly, when Dr. Hsieh input into his model the measured compressibility, he obtained an estimate of cumulative flow in my range.[2] Neither Dr. Kelkar nor Dr. Hsieh have provided a scientific justification for their decision to double the rock compressibility from the measured values.

We will see that this has been a repeated problem in the work of the Government experts. In order to obtain their estimates of 5 MMstb oil released, they had to make assumptions that disagree significantly with direct measurements of the Macondo rock and fluid properties. The Government investigators each disregarded vital pieces of experimental evidence without justification; not all of their errors were identical, yet they arrived at the same final answer. There is a choice: either accept their calculation of 5 MMstb, despite the lack of any scientific explanation of why the measurements are wrong; or perform a calculation consistent with the data and arrive at a lower value. I have chosen the latter approach.

Nevertheless, there is an implicit consensus on many of the inputs into a calculation of oil released, which highlights the remaining disagreements. The table below isolates the most important biases in the Government calculations, juxtaposes my approach, and shows the net effect of each difference:

---

[1] *See* Kelkar & Raghavan expert report [KR], page 45. (*Bracketed information refers to the table of sources in Appendix N, which contains a full description of the referenced documents.*)

[2] *See* Dr. Hsieh's deposition [42], page 267, line 5 ("*Q. And if you input a rock compressibility of 6 microsips, your model yielded a cumulative flow estimate of 3.4 million barrels? A. That's correct*"); page 269, line 3 ("*A. I believe that it will give a number similar, close to 2.9 million barrels*"); Exhibit 8635, pages 73 and 74.

highlighted in red are assumptions that have a significant impact (>0.5 MMstb) on the calculated cumulative release of oil. Each key input is discussed in more detail in the Section indicated in the table.

SUMMARY OF DIFFERENCES BETWEEN THIS REPORT AND GOVERNMENT EXPERTS[3]

Expert and method used	Inputs into the material balance equation			Other key assumptions and comments	Impact on oil released
	Connected oil volume (See Section 4.1)	Compressibility (See Section 4.2)	Pressure drop (See Section 4.3)		
My analysis: material balance	112 MMstb	21.4 microsips (total) 6 microsips (rock)	1,367 psi	*Based on measured data or pre-incident analyses & independent experts.*	**3.26 MMstb**
Drs. Kelkar & Raghavan: *material balance*	124 MMstb (110-137 MMstb) • *Unsupported assumption of full reservoir connectivity.* • *Over-stated conversion from reservoir to surface volumes.*	27.7 microsips (total) 12 microsips (rock) • *No evaluation of laboratory data to justify doubling of measured values for rock compressibility.*	1,460 psi • *Used curve-fitting method to extrapolate pressure.* • *Wrong conversion from capping stack to reservoir pressures.*	*Calculated alternative estimate of 3.4 MMstb oil released using 6 microsips rock compressibility and an oil volume of 110 MMstb (See Appendix F.3).*	**+ 1.74 MMstb**
	+0.48 MMstb	**+1.04 MMstb**	**+0.22 MMstb**		
Dr. Hsieh: *reservoir simulation*	110 MMstb • *Assumed full connectivity.* • *Overall value close to mine.*	28.3 microsips (total) 12 microsips (rock) • *No evaluation of laboratory data and unjustified doubling of measured values for rock compressibility.*	1,583 psi • *Poor late-time match between pressure data and model simulation.* • *Wrong conversion from capping stack to reservoir pressures.*	*Assumed constant outflow path, with no analysis of erosion (See Section 3.5).* *Admitted in deposition that model showed release of 2.9 MMstb using lab measurement of 6 microsips for rock compressibility (See footnote 2).*	**+ 1.66 MMstb**
	-0.08 MMstb	**+1.22 MMstb**	**+0.52 MMstb**		
Dr. Pooladi-Darvish: *reservoir simulation*	137 MMstb • *Unsupported assumption of full reservoir connectivity.* • *Over-stated conversion from reservoir to surface volumes.*	22.2 microsips (total) 6 microsips (rock) • *Used same number for rock compressibility as my analysis, contrary to Drs. Kelkar & Raghavan and Dr. Hsieh.*	1,654 psi • *Wrong pressure conversion from capping stack to reservoir pressures, with under-estimated weight of well-bore oil.*	*Assumed constant outflow path, failing to disprove historical changes from erosion (See Appendix F.4).*	**+ 1.77 MMstb**
	+0.93 MMstb	**+0.15 MMstb**	**+0.68 MMstb**		

---

[3] Sources: Kelkar & Raghavan report [KR], mid-range value, with a connected oil volume of 123.5 MMstb; Pooladi-Darvish report base case; for my values, I have averaged my calculation for the three sets of fluid data using the mid-range rock compressibility: see Section 4; I use an effective compressibility, not the total compressibility – see Appendix A – so that oil released is found by multiplying the values of the three variables together. Further details are provided in Appendix F.5. Note there is some rounding in the calculations for purposes of summary presentation.

There are three other overarching problems in the Government expert reports.

1. **Government experts assumed an unchanging outflow path, predetermining a total flow estimate of 5 MMstb**. The experts who did not use the material balance method – Dr. Hsieh, Dr. Griffiths and Dr. Pooladi-Darvish – took an estimate of the final flow rate before shut-in, approximately 50,000 stb per day, and assumed that the flow rate during the preceding 86 days was even higher. Of course, simple mathematics dictates that the outcome of a cumulative-flow calculation based on this assumption will exceed 4.5 MMstb. They justified this approach by assuming that there were no impediments to oil flow in the well-bore, blow-out preventer or tubing that might have caused flow to be lower in those preceding days. They did not prove this assumption; indeed, they hardly discussed it. By contrast, the material balance method used here is not tied to an assumption about historical flow rates (*see* Section 3.5).

2. **Government experts assumed the reservoir oil was completely connected to the Macondo well, omitting to analyze geological features that the Government's non-litigation expert consultant said would limit connectivity**. None of the Government experts analyzed the evidence from the Macondo geology and seismic analysis that indicates that the oil reservoir was not completely connected to the well. This is a change from prior expert analysis commissioned by the Government. Dr. Hsieh was told by the Government's consultant Prof. Fleming from the University of Texas that the *"geological evidence"* pointed to *"a significant probability of poor connectivity"* in the Macondo reservoir.[4] The Government estimates therefore have an implicit upward bias from ignoring evidence that some of the oil was likely compartmentalized and hence cut off from flowing to the well (*see* Section 4.1).

3. **Government experts over-estimated flow by over-stating the pressure depletion in the reservoir. They used an improper conversion from the pressure measurements at the capping stack to the pressure inferred in the reservoir**. **They did not account for pressure increases as the oil trapped in the well-bore cooled.** The estimates of oil flow by Drs. Kelkar & Raghavan, Hsieh and Pooladi-Darvish over-stated the reservoir pressure depletion that drove the flow. All of these experts used the pressure measurements taken from the capping stack mounted above the blow-out preventer, as do I. These were used to deduce the bottom-hole or reservoir pressure. But between the capping stack and the reservoir was a column of trapped oil thousands of feet tall. So the reservoir pressure was higher than at the capping stack – it had a column of oil sitting above it. This "head" is a function of the density of the trapped oil. The density rose following the shut in. The oil was hot as it flowed from the reservoir to the ocean. When flow stopped, the oil cooled down, gradually becoming heavier. The Government experts based their calculation on measurements of capping stack pressure increasing slowly over time, but the reservoir pressure was rising faster than they suggest: there was an extra factor – the weight of oil – that was also increasing. As we will see below, none of the Government experts presented an analysis accounting for this changing oil density. By assuming the oil was hotter and lighter than it actually was, indeed unfeasibly hot, they end up over-estimating pressure depletion, and hence the oil flow (*see* Section 4.3).

---

[4] *See* Exhibit 8624 (presentation to the USGS) [64], slide 7.

3. The material balance method to calculate oil released

This Section explains the methodology used in my analysis, known as material balance, which also was used by the Government experts Drs. Kelkar & Raghavan.

Flow from the Macondo well involved two distinct physical systems. One consisted of the well-bore and equipment through which hydrocarbons flowed upward and into the ocean. Before entering the well-bore, the hydrocarbons had to flow through the rock in which they had been stored. This second system is called the reservoir.

I will first provide a brief overview of reservoir engineering as it pertains to this case, then introduce the particular methodology used in my analysis.

3.1 Introduction to reservoir engineering best practice

One hundred years ago at Imperial College London, where I teach, Vincent Illing began pioneering methods for appraising petroleum reservoirs. Reservoir engineering has evolved ever-more-modern tools to predict the behaviour of hydrocarbon fields, harnessing the power of high-speed computing. I have helped develop some of these tools, and have founded two start-up companies to pursue innovative approaches to predict fluid flow. But the results from any model, no matter how sophisticated, are only valid if the inputted data are sound. Therefore, best practice requires the reservoir engineer to check the model against measurements and analysis from other disciplines, such as geology.

The Government experts have (1) repeatedly inputted data contradicted by laboratory measurements and then (2) omitted the important process of geological verification. Thus they have: overlooked the likelihood that the reservoir was not fully connected to the well (*see* Section 4.1); ignored laboratory measurements of rock compressibility (Dr. Hsieh and Drs. Kelkar & Raghavan, *see* Section 4.2); and neglected the changing temperature of the oil in the well-bore column, thereby over-stating the pressure depletion (all Government experts, *see* Section 4.3).

3.2 The material balance method used by Government experts and me

The most basic principle in reservoir engineering, and the cornerstone of this report, is material balance.[5] As the Government expert report by Drs. Kelkar & Raghavan states, *"material balance [is] a standard petroleum engineering calculation based on the principle of conservation of mass."*[6] Because conservation of mass is a universal law of physics, material balance calculations can be used to analyze the work of the other Government experts as well, since their software packages (if they are valid) are written to conserve mass. This is why, for example, Government expert Dr. Hsieh calculated the same

---

[5] *See*, for instance, the standard textbook by Dake (1978).
[6] Kelkar & Raghavan report [KR], page 23.

cumulative production that I do when he input a rock compressibility consistent with laboratory measurements.[7]

Here is how material balance works. When the well is drilled through the reservoir, it encounters the fluids in the reservoir rock: oil and water. These fluids are stored at very high pressures in tiny pore spaces. Figure 3.1 shows a core sample of the Macondo rock, accompanied by a microscopic image of a sandstone with similar properties. The rock is under enormous pressure from the weight of rock above it. The well allows a release of oil out of the reservoir to the surface. As oil starts to flow through the rock's connected pores, the pressure of the oil in the reservoir decreases. When the pressure decreases, the remaining oil expands, pushing the oil out of the reservoir. As the pressure of the fluids within the rock pores drops, the rock is compressed down, squeezing the pore spaces, pushing out more oil. The material balance principle says that the volume of oil that comes out of the reservoir must be equal to the combined volume expansion of oil (and to a lesser extent water) and the compression of the rock pore space. To calculate the oil produced from this fluid expansion and rock compression, we need know only the compressibility of the fluids and rock, the size of the reservoir connected to the well, and the change in pressure. These are the three variables that will be discussed throughout the remainder of this report.
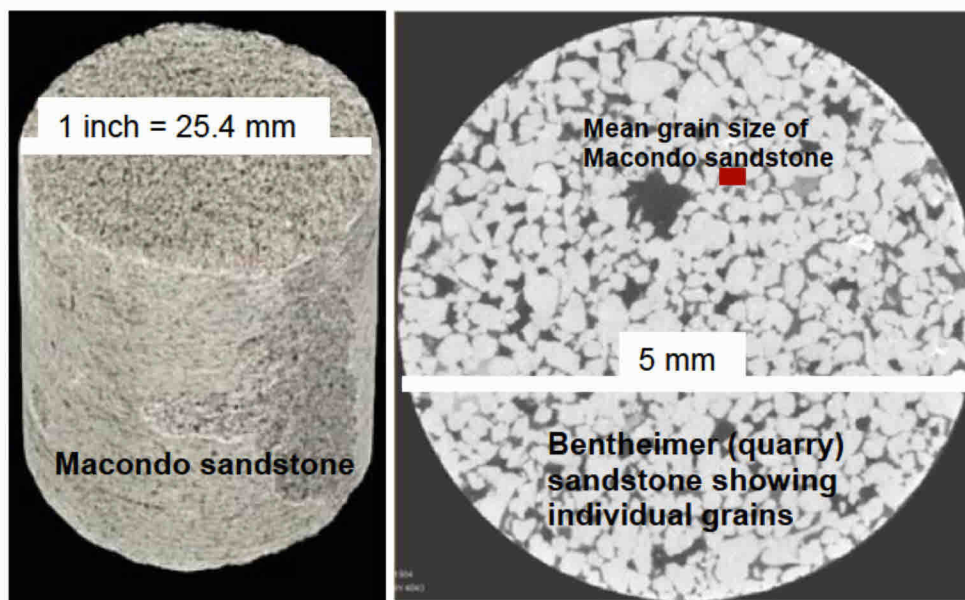
Figure 3.1. Macondo sandstone core (left) and a microscopic cross-section of a quarry sandstone called Bentheimer.[8] The mean grain size of the Macondo sandstone is indicated by the red bar.[9] The Macondo sandstone has a similar average porosity, but a smaller grain size than Bentheimer. Bentheimer sandstone is used in buildings, including the pedestal of the Statue of Liberty.

---

[7] *See* Dr. Hsieh's deposition [42], page 267, line 5; page 269, line 3; Exhibit 8635, pages 73 and 74.
[8] Taken from Blunt *et. al* (2013).
[9] BP-HZN-2179MDL02394186 (Weatherford's grain size analysis) [25]. The picture is taken from WFT-MDL-00039841 (Weatherford's core photographs) [51].

In even simpler terms: the pressure-driven change in the volume of oil, water and rock pore space in the reservoir is equal to what comes out of the well. This is the central concept in reservoir engineering: we relate what was produced to changes in the reservoir. We keep track of the volume of oil produced by calculating the volume of oil displaced from fluid expansion and pore contraction.

The measurement that gauges how much oil is produced is the reservoir pressure. This concept is illustrated in Figure 3.2 by analogy with a barbecue propane tank. The gauge on the tank measures the gas pressure. Likewise, in the material balance method, one input is the change in reservoir pressure.

In the barbecue propane tank, the volume of the tank determines how much gas is produced for each incremental drop in pressure. Likewise, the larger the original volume of oil in the reservoir, the more oil is produced for a given pressure drop. Thus, the original (connected) volume of oil in place is another input in the material balance equation.

The driving factor of compression is also analogous between the barbecue tank and the reservoir. While barbecuing, the propane gas expands in the tank, propelling the flow, just as in the Macondo reservoir, the expansion of oil and the compression of rock pore space drove the flow of oil. This combined compressibility of oil, water and rock (the first two expanding, the third contracting) is the final material balance variable.

I calculate that the Macondo pressure gauge indicates that 2.9% of the oil in the reservoir was produced during the spill: this equates to around 3.3 MMstb (*see* Sections 4.2 and 4.3).

Figure 3.2. A schematic of material balance using a barbecue propane tank as an analogy. The gauge records the fraction of gas remaining in the tank. At the end of the incident, I calculate that the Macondo oil gauge read 97.1% (shown by the red arrow): 2.9% of the oil connected to the well had been released. This represents a pressure drop of almost 1,400 psi.

The advantage of the material balance approach is that it does not require knowledge of changing flow rates over time, instead computing directly the total amount of oil produced. It avoids the error of the Government's experts in assuming an unchanging flow path of the oil from the reservoir to the surface. This Government error led to the extrapolation of a final flow rate of 50,000 stb per day (or higher) to the whole period of the spill, pre-ordaining the outcome of the cumulative flow calculation (*see* Section 3.5).

3.3   Material balance equation

The material balance equation for the oil released, N_p, can be written as follows:

Oil released ⟶

Oil volume connected to the well – from seismic surveys, geology and pressure anlaysis ⟶

$$N_p = N \times c \times \Delta p$$

⟵ Pressure drop – from capping stack pressure analysis

Compressibility of rock and fluids – from fluid and core measurements

(3.1)

3.3.1 Oil connected to the well. The oil volume contained by the Macondo reservoir, N, can be calculated from an analysis of the seismic survey – performed before the well was drilled – that finds the overall extent of the field. Each of the Government experts used this method, as do I. In petroleum engineering it is common to refer to the stock tank oil initially in place, or STOIIP. This is the total amount of oil in the whole field. In a proper material balance analysis, however, it is not STOIIP that we need, but the volume of oil that was connected to the well. As we discuss later in Sections 4.1 and 5, it is unlikely that this one well was connected to all the sandstone channels in Macondo: the N we use in the equation can be less than the STOIIP determined from the seismic survey. The value of N is informed by the seismic survey, the geology of the field and the analysis of the pressure data.

3.3.2 Compressibility. This is the combined compressibility of the rock, water and oil in the pore space.[10] It measures the fractional change in volume per unit decrease in pressure. Technically, this is called "compressibility," even though in our case the fluids are expanding. An analogy would be the air in a bicycle tyre. If you release the pressure, the air expands and flows out of the valve. More compressible fluids expand more as the pressure is dropped, pushing out more oil.   In the reservoir, the fluid pressure drops and the fluids (oil and water) expand, pushing oil out through the rock pores and into the well. The rock also gets compressed – like squeezing a sponge to release water – and this adds to the production. Unlike sponges or air, the compressibility of the rock and fluids we consider is much lower, so the change in volume is relatively smaller.

3.3.3 Pressure drop. The third and final quantity in the material balance equation is Δp, the pressure drop in the reservoir. This is the difference between the initial reservoir pressure and the final pressure: $\Delta p = p_i - p_f$. The final pressure is the average pressure in the reservoir at the end of the spill after the well has been closed: it is the pressure in the well at reservoir depth only after a very long time, once the pressure everywhere in the reservoir equalizes, which takes time, since it involves communication through tiny rock pores, rather than the open space of a bicycle tyre. Thus, we cannot simply derive this number by using the pressure in the well when the capping stack was shut and the spill ended, nor even when the well was cemented in almost three weeks later: the pressures at these earlier times vary across the reservoir and will be lowest at the well. It takes a long time for the pressures throughout the reservoir to even out, so the final equilibrium pressure is always greater than that measured at the well soon after the flow ceases.

---

[10] *See* Appendix A.4 for the precise derivation the compressibility, c, defined so as to obey material balance exactly. The equations more normally employed – Eqs. (A.6) and (A.7) – are exactly equivalent to Eq. (3.1).

12

Thus, to deduce the final average pressure, we need to extrapolate the final pressure readings to very late times. As do my Government expert counterparts, I obtain the final average reservoir pressure by constructing a mathematical model. This model predicts the pressure increases that would have occurred after the well was cemented and measurements were thereby cut off. This is discussed in Section 4.3.

3.4 Each input into my material balance equation was adopted, at some point, by a Government expert

For every key input that I use in the material balance equation, there is a Government investigator who agreed with my value: the problem is simply that none of the Government expert reports consistently used data that corresponded to measured values throughout their calculations. Table 3.1 provides a pictorial illustration of the three key variables employed in the material balance equation by the Government investigators: it is a simplification of the Section 2 summary table. Green indicates that they considered values in line with my calculations, while red indicates the use of values that contradict direct measurements. They all made different mistakes to arrive at the same answer of 5 MMstb.

Investigator	Oil volume	Compressibility	Pressure drop
Drs. Kelkar & Raghavan[11]	🟥🟩🟥🟩🟥🟩	🟥	🟩
Dr. Hsieh	🟩	🟥	🟥
Dr. Pooladi-Darvish[12]	🟥	🟩	🟥

Table 3.1. Table showing where the values for the three key properties in the material balance equation employed by Government investigators broadly correspond to my determinations (green), or are significantly different (red).

Before proceeding with a more in-depth discussion of these differences, I will briefly contrast the material balance method and the methodologies of Government experts Drs. Hsieh and Pooladi-Darvish that take a final flow rate and extrapolate back in time to find the total oil released.

3.5 Contrast with the non-material balance methods used by Government experts

3.5.1 Calculating the final flow rate and then extrapolating it backward for the entire spill period makes the unproven assumption of no outflow configuration changes over time. The expert reports of Drs. Hsieh and Dr. Pooladi-Darvish take a calculated flow rate of around 50,000 stb/day near the end of the spill, and then assume or posit that the rate was higher throughout the preceding period of the incident.[13] The end result will necessarily be a cumulative flow calculation of 4.5 MMstb or more. It is based on the assertion that the resistance of the flow path of oil from reservoir to the ocean remained unchanged; the only influence on rate would be the depletion of reservoir pressure, causing the rate to fall gradually over time.

---

[11] *See* Kelkar & Raghavan report [KR], page 28: lower bound case assumes STOIIP of 110 MMstb, consistent with my analysis; upper case assumes a value of 137 MMstb, which is not.

[12] Dr. Pooladi-Darvish's overall compressibility lies within the range of the measurements, although the oil compressibility is over-stated; *see* Section 4.2.

[13] *See* Pooladi-Darvish report [PD] between 51,600 and 54,200 stb/day; Dr. Hsieh has 52,603 stb/day (Exhibit 8617 (Hsieh pressure analysis)) [44].

This constraint explains how Dr. Pooladi-Darvish, who considered 25 quite different scenarios, can apparently match the pressure data with only a narrow range of cumulative-release numbers at or near 5 MMstb; when he relaxed the assumption of a constant outflow, he was able to find lower values.[14] His superficially impressive array of seemingly diverse simulations essentially answers the question: "If I *assume* a cumulative flow of around 5 MMstb, what are the consistent reservoir properties?" As I show in Section 4 and in Appendix F.4, the reservoir properties that he input to make his model match the pressure data lie outside the measured values, precluding the ability to validate his assumption of constant outflow. This is a key flaw in this approach: since it is not possible to know the outflow with any certainty during the earlier part of the spill, these assumptions are, at best, somewhat speculative, and in any event, do not truly amount to an independent assessment of cumulative flow.

3.5.2 Evidence for an increasing flow rate caused by erosion of obstacles in the flow path. There is persuasive evidence that the outflow configuration did, in fact, change over time. For example, Phase 1 expert Dr. Emilsen concludes that at the time of the blow-out, the oil flowed into the well-bore over a restricted interval of the reservoir, perhaps because of residual cement blocking the flow. This would lead to an additional pressure drop between the reservoir and the well-bore, causing a slower flow rate at the outset of the incident, rather than the higher rate assumed by the Government experts. At the end of the incident, just before the well was cemented, the injectivity test showed negligible resistance: the measured pressure increase on injection was an order of magnitude less than if these impediments were still present.[15]

Outflow impediments in oil wells are common: petroleum engineers are accustomed to planning for huge losses in pressure (the driving force of flow rate) from such restrictions. However, petroleum engineers generally consider them to be fixed over time, unless particular efforts are made to increase the flow from the well (by injecting acid, fracturing or making new perforations through the casing). This perhaps explains why Dr. Hsieh neglected this effect completely, while Dr. Pooladi-Darvish considered only a constant additional flow resistance.

Unlike a normal well, the Macondo oil flow was unplanned and uncontrolled: the flow resistance between the reservoir and the well-bore most likely decreased over time, as the oil forced its way through more of the formation, perhaps through erosion of the cement, and as abrasive materials in the oil (such as sand or cement fragments) eroded barriers to flow, either in the blow-out preventer or in the equipment clogging the bottom of the hole. It is likely that initially there was a very large pressure loss down-hole, giving a low initial flow rate, which then rose over time as the restrictions eroded, even if we ignore changes in the surface equipment. It is very difficult to make a reliable estimate the magnitude or duration of this effect, making any calculation of cumulative flow that depends on assumptions about historical flow rates – particularly in the early period of the spill – highly unreliable. Government estimates that assume away this problem (Drs. Hsieh, Pooladi-Darvish, and Griffiths) are therefore unreliable. This confirms why it is so important to have an independent analysis that assesses the cumulative flow directly, such as the material balance method used here. Indeed, this is accepted

---

[14] *See* Pooladi-Darvish report [PD], page 26.
[15] *See* Final Emilsen report [27] and Appendix E.3 for further discussion and quantitative analysis.

by Drs. Kelkar & Raghavan who, while they estimated a final flow rate, used material balance to compute the cumulative release.

3.5.3 Analogy that illustrates the advantage of the material balance method over the Government method of assuming a constant outflow configuration and extrapolating backward from a final flow rate. Imagine that one evening a police officer arrests a thief who is emerging from a hole through the side of a building that connects to a bank vault. The thief is arrested and found to be carrying around $53,000. The police look at closed circuit television pictures and notice that this hole has been present for 86 days. Then they guess that the daily take was higher at the outset, perhaps because the thief initially selected stacks of higher denominations, so they assume an average daily loss of, say, $58,000. The newspaper headlines say "$5 million taken in bank heist." Through a well-meaning series of unverified assumptions, this would exaggerate, if not the amount stolen, then the degree of underlying uncertainty. As we have discussed, this is akin to the erroneous assumptions and extrapolations made by some Government investigators.

Now, imagine further that the bank is insured for this loss, so they contact their insurers with these estimates and ask for $5 million in compensation. Would the insurers pay? No, they would ask the bank to check their records and say how much was in the bank vault before the hole was made, and then return to the vault, count the money and report the difference. This may be more or less than $5 million, but avoids the somewhat difficult and problematic analysis of exactly how much was stolen on each of the 86 days.

Material balance is the petroleum engineering equivalent to counting the money in the vault. It accounts for the oil volume in the reservoir before and after the spill, to provide a direct calculation of the total volume of oil released. It does not rely on an assessment of flow rate at any given time.

3.6   Sequence of the material balance method to be discussed here

Figure 3.3 is a flowchart that summarizes the approach I will follow. I will determine the value for the three parameters in the material balance equation – volume of oil, compressibility and pressure drop – based on measured data or pre-incident analysis supplemented by independent expert assessment.

I find an effective compressibility of around 21 microsips, including the 6 microsips for rock compressibility, based on independent laboratory measurements. I find the pressure drop to be 1,367 psi. If we multiply the compressibility by the pressure drop, we obtain the fraction of the oil in the reservoir released: this is 0.029 or 2.9%. I deduce that the connected oil volume is likely to be around 112 MMstb. Then the volume of oil released is 112 MMstb multiplied by 0.029, giving 3.26 MMstb.[16]

I will also calculate a range of cumulative flow, from 2.9 to 3.7 MMstb, defined by the range in values assigned to the material balance equation variables. The range for those variables is derived from the variation of laboratory measurements of fluid and rock properties (*see* Appendix A). Thus, my cumulative flow calculation is based on experimental measurements, but my quoted range is also tied directly to the variability of measurements. In other words, my approach is data based.

---

[16] *See* Section 4 for actual numbers used; for this introduction I am using averages of my mid-range calculations.

My calculations are also conservative. Where the data are susceptible to interpretation, I take values that would lead to the highest estimate of oil released. For oil volume, I have assumed a connectivity consistent with the highest plausible assessment of permeability (the ability for fluids to flow) (*see* Section 4.1). For compressibility, I allow the highest measured value from one rock sample, even though it appears inconsistent with my review of the literature (*see* Section 4.2). For pressure drop, I ignore the effects of cooling from the ocean that would make the oil denser, leading to a larger pressure drop (*see* Appendix B).

In the Sections that follow, and in the Appendices, I will carefully assess every input, reviewing the direct measurements and placing them in the context of the scientific literature. I also take information from independent experts who have looked at different aspects of this problem: pressure analysis, fluid properties, pressure readings and rock mechanics. I also look for mutual consistency between different assessments of reservoir properties. This follows best practice: a conscientious reservoir engineer combines insights from experimental measurements, geophysical surveys (the seismic) and geology. Finally, I will contrast the approach to each variable used by the Government experts, highlighting where they have departed from measured data.

Material balance methodology

$$N_p = N.c.\Delta p$$

$$3.26 \text{ MMstb} = 112 \text{ MMstb} \times 21 \text{ microsips} \times 1,367 \text{ psi}$$

Size and connectivity of the reservoir from the seismic, geology and pressure response

Section 4.1

Connected oil volume, *N*

Seismic image of Macondo geology

Measurements of fluid and rock properties

Section 4.2

Fluid and rock compressibility, *c*

Fluid samples

Rock cores

Sample: 1-2R
Depth: 18163.10 feet

Match the measured capping stack pressure to a mathematical model

Section 4.3
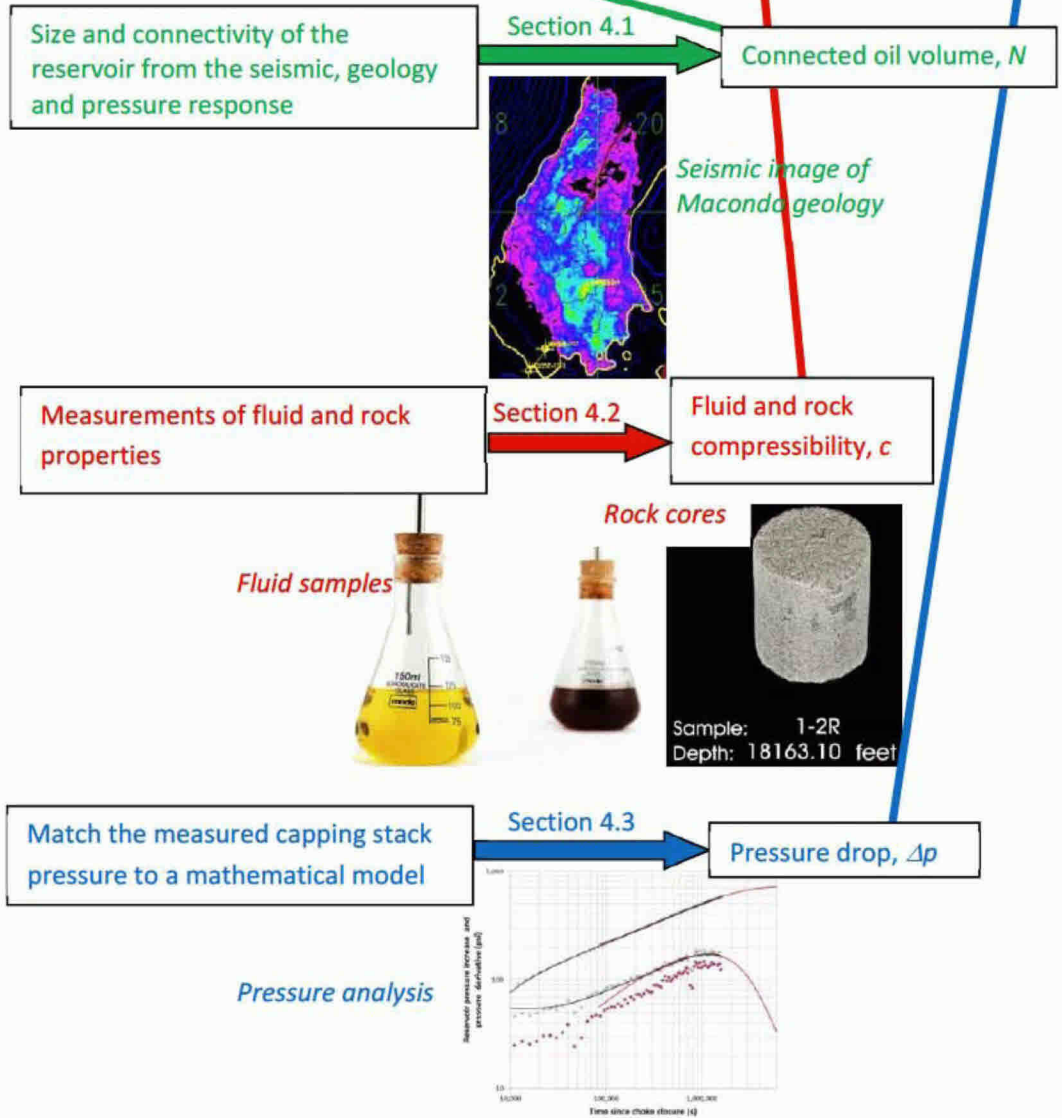
Pressure drop, *Δp*

Pressure analysis

Figure 3.3. Flowchart summarizing the approach followed in this report to calculate the volume of oil released from Macondo. The colours indicate which part of the material balance equation the analysis informs.

The seismic image in Figure 3.3 above is HIGHLY CONFIDENTIAL

TREX-011553-R.0017

4. Determination of the parameters used in the material balance equation

This Section has three parts, each discussing one of the three properties in the material balance equation, which when multiplied together give the total oil released: the oil volume; the compressibility of fluids and rock; and the pressure drop. The Government counterpart to this discussion in found in the report of Drs. Kelkar & Raghavan, who apply material balance in their Section III, at pages 23-28.

4.1 First variable: connected oil volume

Each of the Government experts who have studied the Macondo reservoir has used the same number as I do for connected oil volume – around 110 MMstb – as either their sole value, an alternative base case, or as one end of their range of input values. Dr. Hsieh employed this value exclusively; Dr. Pooladi-Darvish adopted it for what he termed his analytical case; while Drs. Kelkar & Raghavan used it as their low-end estimate.[17]

Drs. Kelkar & Raghavan and Dr. Pooladi-Darvish used a higher value of 137 MMstb for their high-end and simulation base cases, respectively. Their starting point though was the same as mine: they accepted BP's pre-drill seismic analysis of the volume of reservoir rock. We part ways in two subsequent steps in the calculation. Firstly, they assumed that all the oil contained in the reservoir was connected to the Macondo well, as I discuss immediately below. Secondly, they over-estimated the translation to surface oil volumes, using a conversion factor different from that measured directly on Macondo oil samples. I will discuss this issue in Section 4.1.8.

4.1.1 Geological complexity is ignored in the Government assumption of 100% oil connectivity. None of the Government reports considered the reservoir geology. They assumed – without discussion – that all the oil in the field is connected to the well. The US Geological Survey (USGS) did consider the geology of Macondo in an internal presentation co-authored by Prof. Flemings from the University of Texas, who concluded: *"It is geologically reasonable that there is limited channel connectivity,"*[18] yet Dr. Hsieh from the USGS did not mention connectivity in his published analysis.

Connectivity directly affects the calculation of the amount of oil released, which under the material balance equation is proportional to the volume of oil contacted by the well; if the reservoir has limited connectivity, then less oil flows. The connectivity is controlled by the structure of the sandstone channels comprising the reservoir, so some discussion of the geology is in order.

4.1.2 Geological history and resulting complexity of reservoir structure. For 50 million years the Mississippi River and its tributaries have been transporting sediment from the erosion of the North American mountain ranges – grain by grain – down to the Mississippi delta.

---

[17] Sources: IGS642-000215 (Dr. Hsieh's 10/13/2010 Pre-decisional draft report, Tables 1 and 2) [11]; Drs. Kelkar & Raghavan [KR], page 28, Tables 9 and 10; Dr. Pooladi-Darvish [PD], Appendix II, slide 31 mentions *"OOIP=109 MMSTB."*

[18] *See* Exhibit 8624 (Geological evidence for an elongate, heterogeneous reservoir) [64], slide 6.

Some of these sediments became the Macondo field, which lies 40 miles off the shore of Louisiana, approximately 130 miles SE of New Orleans, beneath the Gulf of Mexico – see Figure 4.1. The water depth is almost 5,000 ft and the oil reservoir itself lies a further 13,000 ft under the sea bed.

NORTHERN GULF OF MEXICO
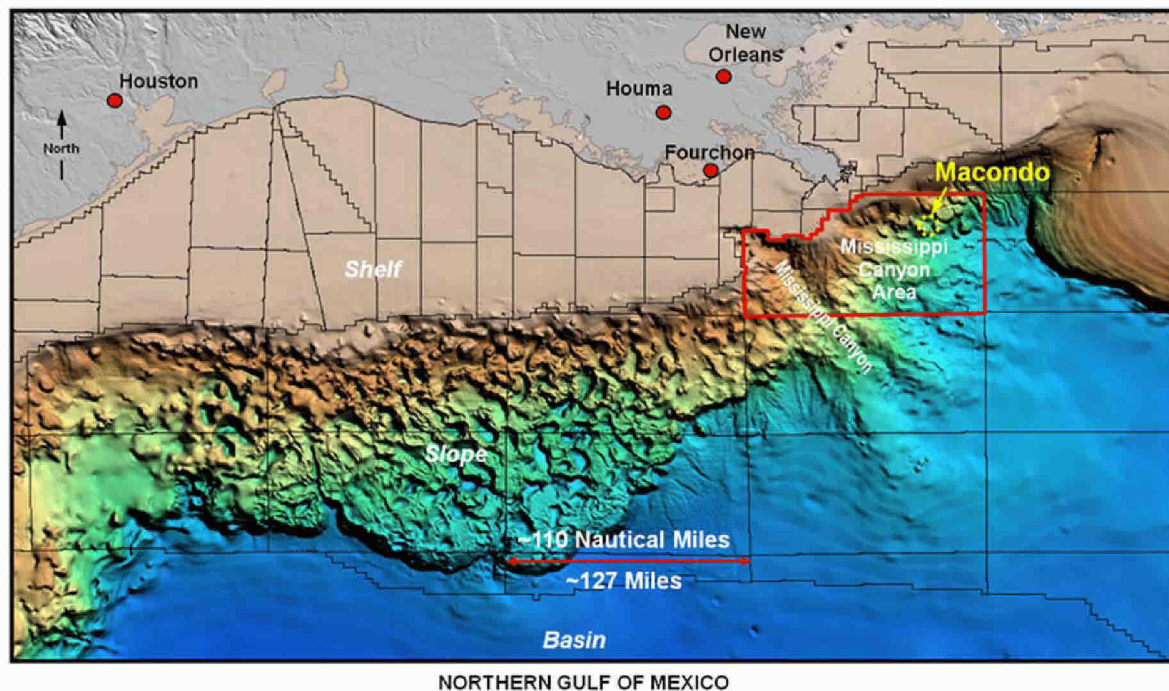
Figure 4.1. The location of the Macondo field under the Gulf of Mexico in the Mississippi Canyon area. The field is below deep water, just off the continental shelf. [19]

The Macondo reservoir is formed of sand deposited in the Middle-Miocene age – around 13 million years ago.[20] The sand was deposited in underwater flows called turbidites. These flows follow a variable path over the course of geologic time, forming long, sinuous channels that can accumulate in different geometric patterns like those shown in Figure 4.2. The reservoir was formed of several of these channels with impermeable mud in between. They were deposited within a NW-to-SE trending "fairway" several miles wide. Over time, huge volumes of further sediment have been laid down, crushing the sand at very high pressures and temperatures, fusing the grains together and forming sandstone. Sandstone is porous, and if the pores are sufficiently connected, oil can flow into and through them. The mud sediments that were deposited in between the sandstone channels became shale upon burial over geologic time. Shale is largely impermeable to the flow of oil.

---

[19] BP-HZN-2179MDL00059145 (BP Shallow Hazards presentation, [29].
[20] BP-HZN-2179MDL03290054 (BP Post-Well Subsurface Technical Memorandum) [6], page 3; BP-HZN-2179MDL05181294 (Macondo Review, slide 24) [36].
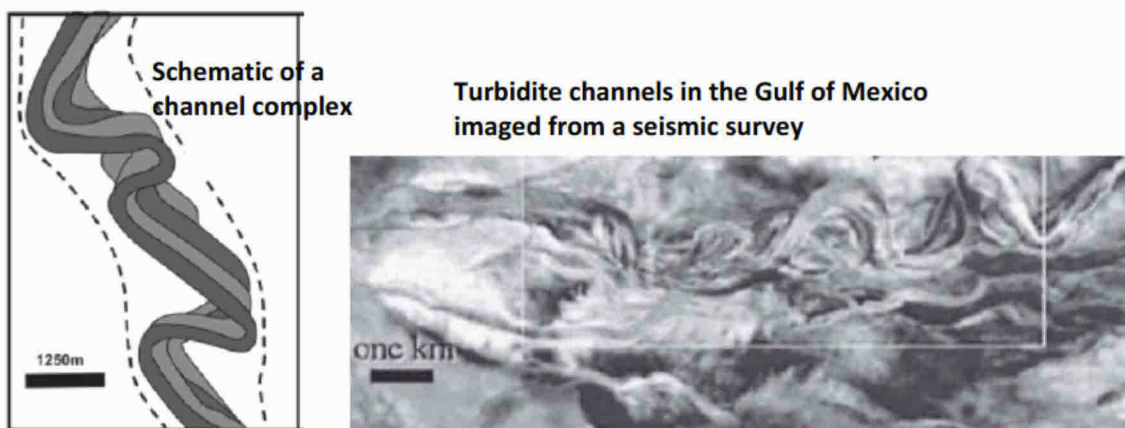
Figure 4.2. Left is a schematic of the structure of a turbidite channel complex, an arrangement of individual sinuous sandstone channels.[21] Right is a seismic (sound wave) image showing such channels from the Gulf of Mexico.[22] Macondo was so deep though that seismic surveys could not discern individual channels.

Figure 4.3 shows a cliff face of part of a turbidite channel complex, highlighting the shale lenses and layers that can cut off continuity of flow between adjacent sand channels.
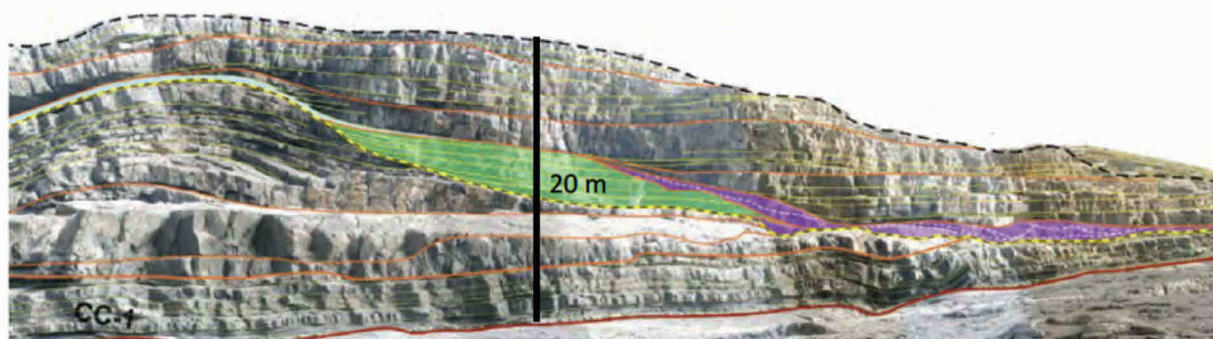
Figure 4.3. A cliff face at Fisherman's Point in Ireland illustrating the interbedding of shale and sandstone typical of a turbidite channel complex.[23] The green shows a channel margin (or edge, where the sand is interspersed with less permeable sediment) while the red lines delineate individual channels (the layers of rock). The pale blue (top left) and purple (right) indicate impermeable shale and mudstone, at the sides of the channels, which blocks the flow between channels.

4.1.3 Connectivity analysis of the Macondo geology. If we knew the exact geometric relationships of the various channels making up the Macondo reservoir – which ones were connected, and to what extent any were compartmentalized by shale layers or faults – then we could quantify what percentage of the total oil in the reservoir sandstones was drained by the Macondo well. However, the information needed to determine connectivity is incomplete and not conclusive. But as we will see, there is strong evidence of compartmentalization. Let us examine this evidence.

The figure on the cover page of this report shows how the oil-bearing sandstone channels connected to the Macondo well might be arranged. The reservoir is composed of several meandering channel

---

[21] McHargue *et al.* (2011).
[22] Posamentier and Kolla (2003).
[23] Alpak *et al.* (2013).

complexes.[24] Each channel complex is approximately 40-100 ft (15-30 m) thick, and up to a mile (1,600 m) wide. The reservoir is several miles long. This image is BP's interpretation of a seismic survey,[25] which sends sound waves through the rock; the waves that return produce an image of the subsurface.

Figure 4.4 is a schematic showing how the well cut through three sandstone channel complexes (layers). Also shown in red is a so-called seismic wavelet, to show that the wavelength of the sound waves sent through the rock to image the field is longer than the thickness of the sandstone channels, and so the waves cannot discretely resolve them. We do not know exactly how the channels are arranged in the subsurface; the seismic survey only indicates where the hydrocarbon-bearing sandstone is likely to be located, on average.
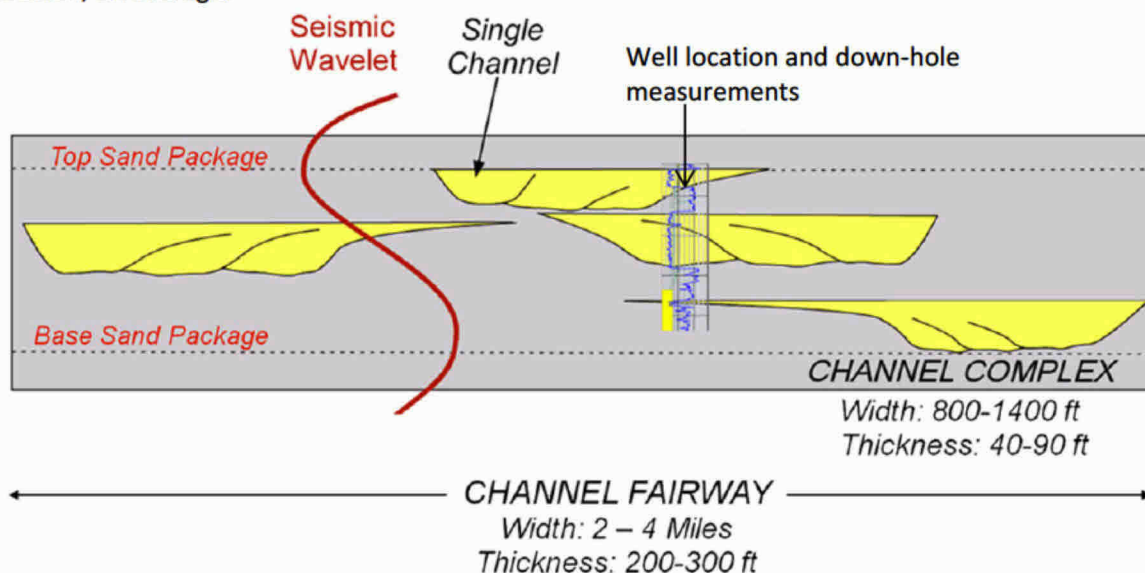
Figure 4.4. Schematic showing that the Macondo well cut through three sandstone channel complexes (layers).[26] Note the channel complex on the left that is not connected to the well.

I will now consider the possible structure of the Macondo reservoir in Figure 4.5, juxtaposed with the BP's pre-drill seismic interpretation. The BP seismic image by itself does not discern individual channels, let alone reveal their degree of connectivity. Instead what is shown is the presence and inferred thickness of oil-bearing sandstone: green represents a relatively thick layer, with blue then purple indicating – on average – less oil. Black represents water-filled rock, or impermeable shale or salt.

---

[24] *See* McHargue *et al.* (2011) and Alpak *et al.,* 2013) for more precise descriptions of the variable levels of complexity and corresponding refinements of terminology of turbidite complexes. I will use a simplified vocabulary: a channel complex comprises one layer encountered by the well and makes a connected path through the reservoir.

[25] BP-HZN-2179MDL04440238 (BP seismic survey presentation, slide 10) [17].

[26] BP-HZN-2179MDL04440238 (BP seismic survey presentation, slide 1) [17].
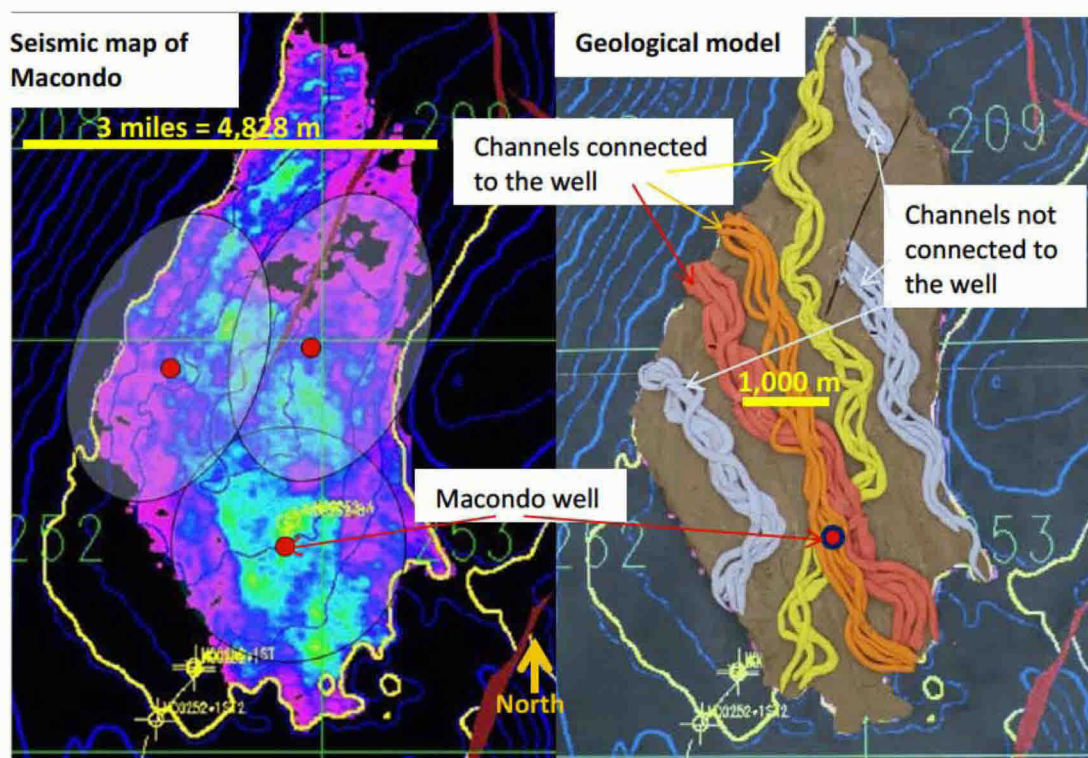
Figure 4.5. Left is BP's seismic map of the Macondo field.[27] Green suggests a likely thick layer of oil-bearing sandstone on average, while areas marked in blue, then purple are progressively thinner. The black indicates shale or water-saturated sandstone. The red circles indicate the location of the Macondo well (lowest circle) and two other planned wells. On the right is a photograph of a model of the field made by me using coloured modelling clay, placed over this map, showing the putative location of individual channels. The brown is shale – this lies below, between and above the channels. The yellow, orange and red indicate the three channel complexes (layers) encountered by the Macondo well. The lilac-coloured channels are not connected to the well.

BP, unsurprisingly, targeted the middle of the thickest likely portion of oil-bearing sandstone with the Macondo well, indicated by the lower red circle. Two other planned wells are also shown – these were not drilled.

My own interpretation of possible channel interrelationships is superimposed on the same horizontal area on the right of Figure 4.5. While I do not know the exact location of every channel, nor have I attempted to capture every nuance of their structure, the following qualitative features are important, relevant and supported by the evidence from the pressure analysis (Section 4.3), seismic survey and geology.

1. The reservoir is formed from a series of channel complexes, themselves composed of individual channels.
2. The channels are sinuous and run approximately North-West to South-East.
3. Oil can flow along the channels. But there may be little or no flow between channel complexes. This is the problem overlooked by the Government experts in assuming 100% connectivity of all the oil-bearing sands in the Macondo reservoir.

---

[27] BP-HZN-2179MDL02107723 (BP's Technical Assurance Memorandum, Section 3, row 60) [10].

The seismic image in Figure 4.5 above is HIGHLY CONFIDENTIAL

TREX-011553-R.0022

4. The Macondo well likely contacted three of these complexes: these are the three layers encountered when drilling the well – shown in Figure 4.5 as the red, orange and yellow strands of clay.

5. The oil volume contacted by the Macondo well represents the majority of the total volume of the field, but not all of it. The oil in some of the channels cannot flow to the well. These are the lilac-coloured channels in the picture. This is consistent with BP's interpretation – see Figure 4.4 – where the channel complex to the left is not connected to the well.

6. There could be other sources of compartmentalization, such as faults, and there is some indication in the seismic data that faults cut the Macondo channels.[28]

4.1.4 Evidence for limited connectivity in channelled reservoirs. The original development plan for Macondo proposed drilling three wells to produce the field.[29] Three wells – as opposed to one – would lead to higher production rates, but also has the advantage of ensuring that the vast majority of the reservoir volume would indeed be connected to at least one of these wells. To quote from BP's *pre-drill* assessment[30] "*Estimate 80% of prospect resource recoverable from wells on MC 252.*" What this means is that even with three wells and a production time of several years, BP considered that only 80% of the field would be drained. BP stated that a single well "*will confirm 63% of the predicted resource volume.*"[31] BP considered "*In the event of a compartmentalized reservoir, additional wells may be required to adequately drain the reservoir.*"[32] In the opinion of BP geophysicist Dr. Ritchie "*I think it is a very unlikely case that one well would drain the fully connected volume.*"[33] He also states "*.. the fully connected volume I believe is unrealistic.*"[34] BP's geological review states:[35] "*Flooding along the axis of the channel may result in good … communication. Flooding across the channel ….. with the risk that permeability barriers prevent pressure support at the producer.*"

Based on BP's analysis *before* the accident and the interpretation of their geologists, the Government experts' assumption that the well drained the entire field will over-state *N* in the material balance equation. It is very likely that not all the oil-bearing sandstone channels in Macondo intersect or otherwise conduct flow across the shale barriers that separate them.

Published petroleum reservoir literature also recognizes that the connectivity of turbidite channel reservoirs is a problem in field development:[36] "*operators have encountered severely impaired reservoirs ….. attributed in large part to reservoir compartmentalization.*"[37] Dr. Kelkar is a co-author on a paper[38] that states, in reference to deepwater fields, "*some of these reservoirs are highly*

---

[28] For instance the red line in the BP seismic (upper part of the figure).

[29] BP-HZN-2179MDL06566208 (BP Pre-Drill Review) [31], slide 24.

[30] *Id.,* slide 24 [31]; BP-HZN-2179MDL02107723 (BP Technical Assurance Memorandum, Section 3, row 11) [10].

[31] BP-HZN-2179MDL02107723 (BP's Technical Assurance Memorandum, [10]) Section 3, row 11.

[32] *Id.,.*

[33] *See* Bryan Ritchie Deposition [46], page 322, line 21.

[34] *Id.,* page 324, line 17 [46]; see also *Id.,* page 325, line 13 [46]

[35] BP-HZN-2179MDL06604338 (BP's presentation of reservoir geology, slide 2) [39].

[36] *See,* for instance, Abreu *et al.* (2003), Ragagnin and Moraes (2008), and Alpak *et al.* (2010).

[37] Alpak *et al.* (2010).

[38] Liu *et al.* (2008).

compartmentalized." Limited connectivity has hampered production in channelled turbidites in the Schiehallion field West of Shetlands, the Bittern Field in the North Sea, and the Ram Powell field in the Gulf of Mexico.[39]

4.1.5 Government experts deduce smaller reservoir areas without reducing connected volume. Later in this report we will discuss how both the Government experts and I use measurements of the pressure build-up after well shut-in to deduce the size and shape of the Macondo reservoir (*see* Section 4.3). Every expert found that the connected reservoir has a smaller area (and width) than determined from BP's seismic analysis in Figure 4.5.[40] BP likewise used pressure analysis after choke closure and also presented a model with a smaller area.[41] This suggests that the well-known geological phenomenon of compartmentalization of turbidite systems has indeed limited the connectivity of the greater Macondo reservoir shown by BP's seismic analysis. Yet the Government experts omit the next step of proportionately reducing their connected volume of initial oil. *"The primary job of a reservoir engineer,"* Drs. Kelkar & Raghavan tell us, *"is to obtain a production forecast . . . after addressing three primary questions: . . . (3) how much of the available quantity of fluid may be produced."*[42] Yet they did not assess what percentage of the Macondo field could be produced by the single Macondo well.

Finding a smaller area from a pressure analysis does not alone prove poor connectivity: the geology has to be considered carefully to determine if it is plausible that the whole field can drain to the well in the times indicated by the pressure analysis: I suggest that this is not possible for the BP seismic interpretation (*see* Section 5). It is unreasonable to suggest that oil located far beyond the boundaries detected by the pressure analysis can reside within these confines.

4.1.6 My method for assessing connectivity and connected oil volume. I use the area I compute from the pressure analysis. I take the largest plausible permeability value, which gives the largest area. I assume that the oil outside this area is not connected to the well, but that the reservoir thickness is only 10 ft in these regions: the purple areas shown in Figure 4.5. 10 ft is the limit of the seismic interpretation,[43] so this is a lower bound on the disconnected volume, or an upper bound on connectivity. This is the most optimistic assessment of connectivity that is consistent with the pressure analysis, the seismic interpretation and calculations of permeability. The details are given in Section 5: dependent on the fluid and rock properties assumed, the connectivity is 87-90%. From Figure 4.5, this is evidently a very generous interpretation, placing the vast majority of the oil in the yellow, red and orange channels while making the lilac channels very thin in comparison. This approach will give a plausible upper bound on oil released.

---

[39] Govan *et al.* (2006), Alpak *et al.* (2010), Alpak *et al.* (2013).

[40] IGS642-00215 (Hsieh's draft report, page 12, Table 2 (1,958 acres: 22,270 ft length times 3,830 ft width) [11]; Pooladi-Darvish report [PD], Appendix V, slides 4 and 5 (between 1,686 and 2,228 acres, using the quoted widths and lengths); BP's mid-range area is 4,482 acres. BP-HZN-2179MDL05173765 (BP gross rock volume assessment) [30].

[41] *See* Dr. Levitan's deposition [56], page 141, lines 14 and 15 (2,185 acres).

[42] *See* Kelkar & Raghavan report, [KR], page 31.

[43] *See* BP-HZN-2179MDL05173765 (BP's gross rock volume assessment) [30], slide 1, most likely case: *"10 ft cutoff footprint (noise background)."*

I contrast my approach with that of the other Government investigators in Table 4.1 below. I allow a larger connected area than all the other experts, but this is still smaller than inferred by BP in their seismic interpretation (4,482 acres). In brief, the Government investigators squeezed too much oil into their models of the reservoir.

4.1.7 Oil volume underground. Table 4.1 also shows the total oil volume in the reservoir. Having calculated the extent of the rock containing oil, we need to determine how much oil is in this rock. This is done using logs of down-hole measurements of porosity (the fraction of the rock that is void space) and saturation (the fraction of the void space that contains oil – the rest contains water). I follow the same approach here as Dr. Kelkar & Raghavan and find virtually identical numbers; Dr. Pooladi-Darvish and Dr. Hsieh also used values that correspond to mine. Since there is no disagreement on this part of the analysis – either in terms of the method or the conclusions – and since it is standard in any oil industry assessment, I leave the details to Appendix A.2. Bear in mind, however, that while we agree on translating reservoir rock volume to reservoir oil volume, the similar numbers mask the issue discussed in the preceding sections: the Government numbers do not account for the geological evidence of incomplete connectivity.

Expert	Reservoir area from pressure analysis (acres)	Connectivity	Reservoir volume (MM reservoir barrels)	Surface volume (MMstb)
My analysis[44]	1,931-2,590	87-90%	258	109-114 (112 mid range)
Drs. Kelkar & Raghavan[45]	Not stated	Assumed to be 100%	293	110-137 (124 mid range)
Dr. Hsieh[46]	1,958	Assumed to be 100%	259	110
Dr. Pooladi-Darvish[47]	2,167	Assumed to be 100%	296	137

Table 4.1. Areas and oil volumes connected to the well proposed by me and the Government experts.

4.1.8 Conversion of oil volume to surface conditions. Our focus now switches from the rock to the fluids contained within them. Macondo oil samples were collected using down-hole tools before the accident. Three laboratories – Schlumberger, Intertek (Westport Labs) and Core Labs (Pencor)[48] –

---

[44] I show the full range of connected areas and connectivity, the mid-range determination of reservoir volume and the range of surface volumes using the mid-range rock compressibility. *See* Section 5 and Appendix D.1.6 for further details.

[45] From Kelkar & Raghavan report [KR], page 27. Also considers 110 MMstb, ([KR], page 28) so the mid-range oil volume is 124 MMstb quoted in the summary table in Section 2 and Table 4.1.

[46] Values computed from values in Dr. Hsieh's draft report [11], Tables 1 and 2.

[47] Dr. Pooladi-Darvish base case [PD], values from Appendix IV, slide 10. Surface volumes found using B_{oi} = 2.15306 in his simulation input files.

[48] I have taken data directly from their reports: BP-HZN-2179MDL04440732 (Intertek fluid property report) [18], BP-HZN-2179MDL00063016 (Core Labs fluid property report) [19]; BP-HZN-2179MDL00063084 (Core Labs fluid property report with cover page) [20]; BP-HZN-2179MDL01608973 (Schlumberger Fluid Analysis on Macondo samples) [34]; BP-HZN-2179MDL01872218 (Core Labs fluid properties report) [35]; see Appendix A.1 for further details.

independently measured the properties of these samples. The measurements include a quantity called the formation volume factor (B_o): the ratio of the reservoir volume of oil to the surface volume.

The inconsistency in the estimates of original oil in place between the Government experts Drs. Kelkar & Raghavan and Dr. Pooladi-Darvish (137 MMstb) and me (around 110 MMstb, see Table 4.1) arises from both the consideration of connectivity (addressed above) and from a different conversion of a reservoir volume of oil to a volume measured at the surface (which we will discuss below). Background on *why* oil changes volume between the reservoir and surface will help resolve the correct method for *how* that translation should be calculated.

4.1.9 Shrinkage of the reservoir oil volume from exsolution of dissolved gas with changing pressure.
Oil is a mixture of hundreds of different hydrocarbon components. Some of these – methane, ethane, propane and butane – are gases at the surface, which we refer to as stock tank conditions. When the pressure in the oil drops (for instance, as oil flows to the surface up the well-bore), these gaseous components come out of solution – see Figure 4.6.
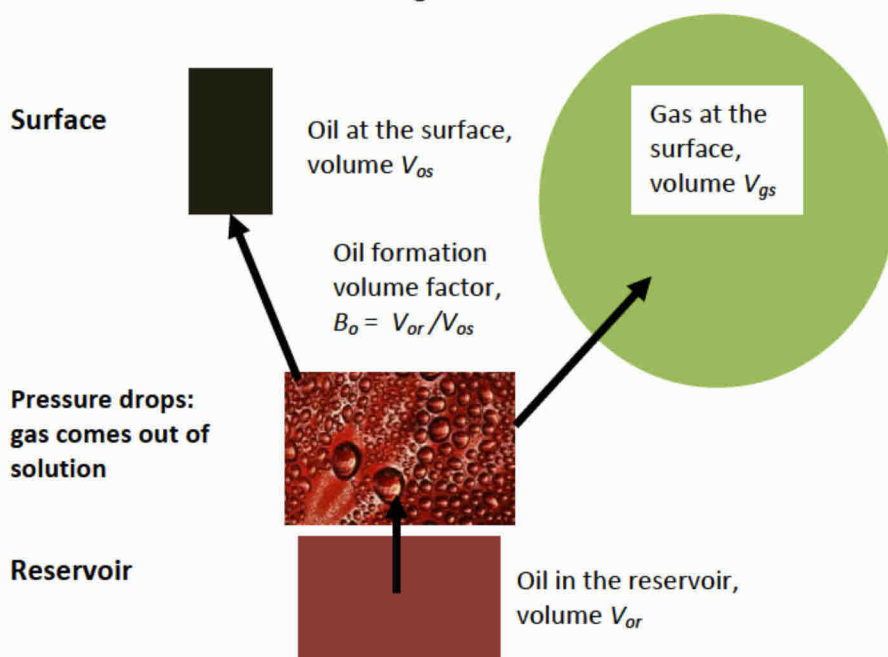
Figure 4.6. When oil flows up to the surface, its pressure drops. Bubbles of gas exsolve from the oil. At the surface, both oil and gas are produced. The volume of oil at the surface is lower than that in the reservoir, because gas has come out of solution. The oil formation volume factor is the ratio of the reservoir volume of oil to the volume at standard or stock tank conditions (60°F and atmospheric pressure). In this analysis I calculate oil volumes at stock tank conditions.[49]

The pressure when the first gas appears is called the bubble point. The same phenomenon occurs when you open a can of soda: prior to opening, carbon dioxide is dissolved in the liquid at high pressure. When you release the pressure by opening the can, carbon dioxide comes out of solution and produces bubbles.

---

[49] Image from dehaanservices.ca

Macondo was an exceptionally light oil which shrank significantly when taken to the surface. As a result the shrinkage coefficient B_o plays a major role in the calculation of oil released.

4.1.10 Two different methods to convert to surface volumes. Two approaches are used in the oil industry to convert from oil volume in the reservoir to oil volume at surface conditions. A higher amount of produced oil is calculated using the conversion factor produced by the Government's fluid expert Dr. Zick. He used a method known as multistage separation. This is what is used by oil companies to maximize volume during normal, planned production. When oil companies normally produce oil, they separate the oil and exsolved gas through a deliberately-engineered series of separators at a succession of decreasing temperatures and pressures. This multistage separation is designed to produce as much (valuable) oil, and as little (less valuable) gas as possible. The value of B_o depends on the exact sequence of separations. It will be the lowest possible B_o, in order to produce the highest possible surface volume. Dr. Zick tries to construct the high-volume separation process that he asserts BP was planning to use if it produced oil from Macondo for sale. But of course, the Macondo oil was not produced in such a fashion. It flowed through various openings at different depths, temperatures and pressures over 86 days. BP's fluids expert Dr. Whitson tries to reconstruct what the actual multistage separation would have been during the incident, and derives a higher number for B_o, which yields a translation to fewer barrels at surface conditions. He also concludes, as do I, that the complexity of this analysis can be avoided by using the other industry method for conversion to stock tank conditions, known as a single-stage separation. This occurs when the oil and gas remain in contact as they are brought to surface conditions. Dr. Whitson finds that the number for B_o using this definition is close the value derived from the appropriate multistage process. Thus, I will use the values of B_o from the single-stage separation in my calculations.[50]

The measured value of B_o for the single-stage separation used in my calculations ranges from 2.3 to 2.4 depending on the reservoir pressure.[51] Government expert Dr. Hsieh used a value similar to mine: 2.35.[52] Dr. Pooladi-Darvish and Drs. Kelkar & Raghavan used a significantly lower number of approximately 2.1.[53] Dr. Pooladi-Darvish, however, said that he used a single-stage method for the conversion,[54] so his number should be closer to mine.[55]

4.1.11 Connected oil volume: 109-114 MMstb. Table 4.2 shows my determinations of initial oil in place: there are three values, derived from the values of B_o measured by the three different laboratories. Thus, as will be the case for each input variable, I base the range on the measured data.

I arrive at a number – around 110 MMstb – which has been agreed as plausible by all the Government investigators.[56] However, we arrive there by different methods. The Government experts omitted the

---

[50] *See* Appendix F.2 and Appendix A.2.

[51] *See* Table A.4.

[52] Dr. Hsieh's draft report [11], Table 1.

[53] Dr. Pooladi-Darvish value of 2.15306 for initial formation volume factor for his base case simulation model taken from his computer input files; Drs. Kelkar & Raghavan used 2.14 ([KR] page 27).

[54] See Pooladi-Darvish report [PD], Appendix II, slide 45.

[55] *See* Appendix F.2, Table F.1 and Table A.4.

[56] All but one of Dr. Pooladi-Darvish's "good match" simulation models over-state the oil volume – Appendix F.4.

step of evaluating the geology and selecting and justifying an estimate of connectivity to the well of the various sandstone channels comprising the Macondo field. Thus, their value for oil volume implicitly assumed a connectivity of 100%. Furthermore, the conversion from reservoir to surface conditions used values that were not justified by direct measurements. Thus, their analysis was incomplete and their calculations were biased to over-state the oil released.

	High case Intertek	Middle case Schlumberger	Low case Core Labs	Average value
Connected oil volume	114 MMstb	112 MMstb	109 MMstb	**112 MMstb**

Table 4.2. Connected oil volume using the three sets of fluid properties.[57]

---

[57] This assumes the mid-range rock compressibility; *see* Section 5 for further discussion.

4.2   Second variable: compressibility

4.2.1 Introduction to compressibility. Compressibility is the second variable in the material balance equation. In this Section we evaluate the data for fluid and rock compressibility. As mentioned in Section 2 (and the summary table) Dr. Hsieh and Drs. Kelkar & Raghavan used a value for rock compressibility outside the range of the measurements, leading to a significant over-estimate of oil released.

Figure 4.7 shows a schematic of what is meant by the compressibility of fluids and rock, and how it contributes to oil production. As the pressure drops, the oil and water expand. The rock grains – held apart by the high fluid pressure – begin to crush together, resulting in a decrease in porosity.
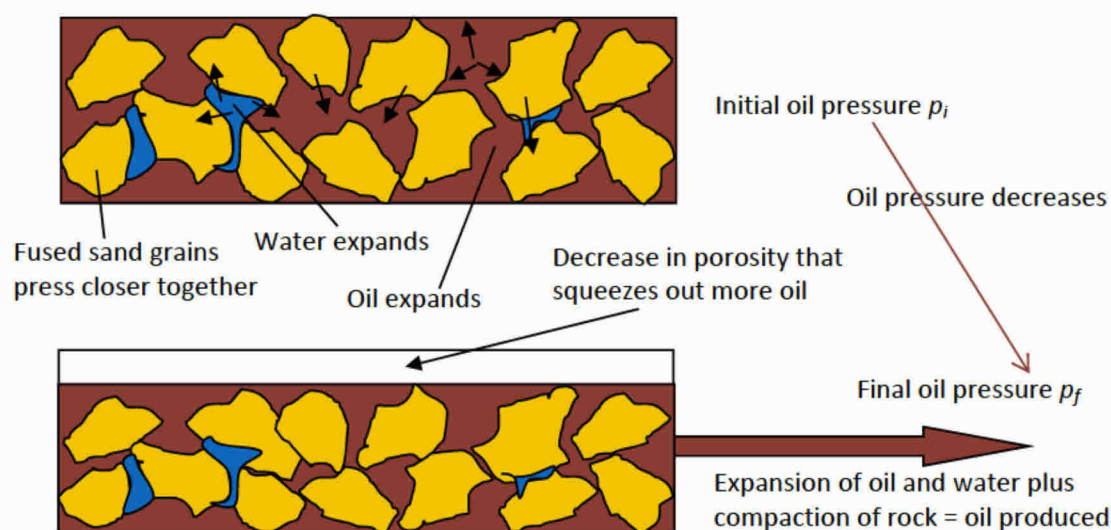
Figure 4.7. Schematic explanation of compressibility. As the oil pressure drops, oil and water expand, while the rock compresses. The arrows indicate the expansion of the oil and water and the collapse of the sand grains into the pore space (this effect – a change of less than 1% in the pore space – has been exaggerated for clarity). All three phenomena contribute to oil production. The change in volume is the oil produced.

Compressibility is measured in units of inverse pressure, called sips. A microsip is a millionth of a sip: if the compressibility is 10 microsips, a pressure drop of 1,000 psi (around 70 times atmospheric pressure) will result in a 1% change in volume.

4.2.2 Oil compressibility: 13.7 – 14.8 microsips.   This range covers the compressibilities (or "expandibilities") from the three sets of fluid measurements introduced in Section 4.1. I compute oil compressibility so that it provides exactly the measured change in volume from initial to final reservoir pressures: the details are provided in Appendix A.2. While there are variations in the values between the three laboratories, I would consider them broadly consistent.   I will use all three values in the calculations that follow.

Dr. Pooladi-Darvish's analytical model used an oil compressibility of 28 microsips, twice the measured value.[58] This is the main contributor to his overstatement of oil produced. Furthermore, his simulation models took another value which is also outside the measured range.[59] While he presented reasonable values in his report, the numbers used in quantitative calculations depart significantly from the measurements, a problem that we will see again in his treatment of pressure.[60]

4.2.3 Water compressibility: 3 microsips. Water is much less compressible that the reservoir oil. There are no direct measurements of the compressibility of the reservoir brines at Macondo conditions. Since the water saturation is low, different plausible values of water compressibility make a negligible (less than 0.3%) difference in calculated oil released. I take an upper bound value based on my reading of the literature: **3 microsips.**[61] The Government experts used a similar value as well.

4.2.4 Pore volume compressibility: 4.3 − 8.6 microsips. This is the main source of the departure between my estimate of cumulative production and those of Government experts Dr. Hsieh and Drs. Kelkar & Raghavan (see the summary table in Section 2).

Rock properties were measured on core samples by Weatherford laboratories. These cores were extracted from the well during drilling. These measurements provide the only direct assessment of the compressibility and permeability.[62] Neither Dr. Hsieh nor Drs. Kelkar & Raghavan used these measurements or provided a scientific explanation for disregarding them.

Before drilling, BP predicted that Macondo rock compressibility would be 5 - 6 microsips, based on property correlations from other fields in the Gulf of Mexico.[63] A comprehensive review of production in the Gulf of Mexico, co-authored by Dr. Kelkar, considered a range of 1-10 microsips, with a mid-range value of 3 microsips for fields of similar geological age to Macondo.[64] Once experimental data were available, a value of 6 microsips was taken for BP's reservoir modelling.[65] This value was also used by Dr. Pooladi-Darvish.[66] Dr. Kelkar, when working for the Macondo Flow Rate Technical Group in 2010, used a base-case value of 5.61 microsips.[67]

So, the mid-range value I will use, based on the measurements, is also around 6 microsips.

---

[58] A value of 28.5 microsips; Pooladi-Darvish report [PD], Appendix II, slides 30 and 31.

[59] 15.3 microsips, see Appendix F.4.6.

[60] *See* Section 4.3 and Appendix B.4. Values in Pooladi-Darvish report [PD], Appendix III, slides 8 and 9.

[61] Osif (1988).

[62] The raw data from the measurements of pore volume compressibility are given in spreadsheet form; BP-HZN-2179MDL02394185 (Weatherford pore volume compressibility) [24]. A summary of the measurements is also provided; BP-HZN-2179MDL02393883 (Weatherford summary of pore volume compressibility) [26]. The results of permeability measurements are reported in BP-HZN-2179MDL02394182 (Weatherford permeability measurements) [23].

[63] *See* Figure A.1 taken from BP-HZN-2179MDL06566208 (BP Pre-Drill Review, slide 17) [31].

[64] *See* Liu *et al.* (2008), Table 2.

[65] See, for instance, Pinky Vinson's deposition [47], page 300, line 15. Also Dr. Merrill deposition [54], page 214: 21-23.

[66] Pooladi-Darvish report [PD], Appendix III, slide 8.

[67] *See* Don Maclay's deposition [62], page 393, line 9 to page 394, line 1.

However, Dr. Hsieh[68] and Drs. Kelkar & Raghavan,[69] in their expert reports, used a value of 12 microsips. The origin of this value appears to be BP's work in support of the well integrity test. This was as part of evaluating a worst-case scenario.[70] In any event, I consider BP's opinions largely irrelevant here – after all I don't accept their connectivity (*see* Section 5), pressure drop (*see* Section 4.2) or B_o (Section 4.1) estimates either: I base my analysis on the experimental evidence.

Rather than discuss this further – there is no scientific evidence or analysis for this value to discuss – I will instead carefully outline why I have chosen my values.

Weatherford measured the pore volume compressibility on three core samples from the Macondo well. In Appendix A, I show how pore volume compressibility is found from the Weatherford data. The calculation exactly reproduces the change in volume – and hence oil production – associated with rock compression as the fluid pressure drops.
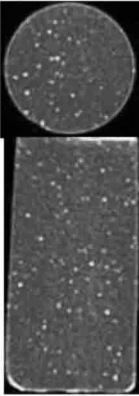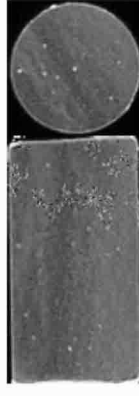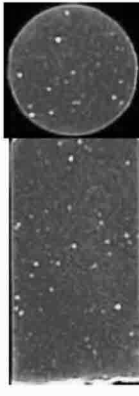
Sample name	3-6R	3-16R	3-22R	
Location and CT scans of the cores in axial and longitudinal directions	Top layer	Middle layer	Middle layer	
Porosity, ϕ	0.217	0.206	0.214	**Average compressibility**
c_f (microsips; $\times 10^{-6}$ psi^{-1})	8.57	4.34	6.14	**6.35**

Table 4.3. Measured pore volume compressibilities. Also shown are X-ray CT scans of the cores in axial and longitudinal directions: they are approximately 1 inch in diameter and 1.7 inches long. The images show the uniform internal structure of the rock.[71]

The values I quote in Table 4.3 are taken from the expert report of Dr. Zimmerman. He has employed the same approach as I have, but pruned out the initial period of the experimental test when the rock deformed slowly in response to the change in fluid pressure. He also accounts for the compressibility of the solid grains themselves. This leads to slightly higher values of compressibility than simply taking all

---

[68] IGS642-000215 (Draft Hsieh report) [11] Table 1.

[69] Kelkar-Raghavan report [KR], page 28.

[70] Pinky Vinson's deposition; [47], page 300, line 15. Also Dr. Merrill's deposition; [54], page 192, line 5; page 214, line 23; and page 216, line 15 onwards.

[71] From Weatherford's X-ray CT scans; [52].

the raw data. I will defer to his superior expertise, noting that using his values leads to higher estimates of oil released.[72] I will consider values that cover the full range of the measurements.

Published literature regarding Gulf of Mexico fields also supports the reliability of the Weatherford measurements.[73] For instance, a comprehensive review of compressibility measurements in the literature is provided by Newman (1973). His measurements for consolidated sandstones of similar porosity to that encountered in Macondo indicate values of around 3.5 microsips or lower. However, he states: *"The salient conclusion is that to evaluate rock compressibility for a given reservoir it is necessary to measure compressibility in the laboratory."*

Following Newman's advice, I will use the measured compressibilities in my calculations, even though they appear at the upper end of likely values based on the other evidence I have presented.

4.2.5 Effective compressibility for input into the material balance equation: 18.7 − 24.5 microsips.

Table 4.4 reports the values of effective compressibility that I will use in the material balance equation.[74] I have combined the values of oil, water and rock compressibility together in a way that exactly reproduces the volume change as the reservoir pressure declines. There are nine values: three sets of fluid measurements times three rock compressibilities: the high, middle and low cases. This covers the *full range* of the measurements.

Effective compressibility, c (microsips)	Fluid properties		
	High case Core Labs	Middle case Schlumberger	Low case Intertek	**Average value (mid case)**
High case rock compressibility	24.48	23.64	23.45	
Mid case rock compressibility	22.01	21.16	20.97	**21.38**
Low case rock compressibility	19.76	18.91	18.72	

Table 4.4. Values of effective compressibility that will be used to compute oil released in the material balance equation.

---

[72] *See* Appendix A.2 for further discussion.
[73] For more detail *see* Appendix A.3.
[74] *See* Appendix A.4 for a discussion of compressibility definitions.

4.3   Third variable: pressure drop

The third parameter in the material balance equation is the pressure drop in the reservoir caused by the outflow of oil. My analysis here departs from that of the Government experts in two significant respects: the conversion from capping stack to down-hole pressure; and the extrapolation to find the final reservoir pressure.

4.3.1 Conversion from capping stack to down-hole pressure. We need to know the pressure in the reservoir. However, there was no pressure gauge there during and after the incident. The pressure data was measured on a gauge in the capping stack. This was separated from the reservoir by a column of trapped oil thousands of feet tall.

During the build-up period (when the well was closed) there was no flow, and the down-hole pressure was the capping stack pressure plus the weight of fluid from the capping stack to the reservoir: this is called the head. I have performed this conversion for the three sets of measured fluid data.[75] The Government experts have all performed this translation incorrectly. It is the biggest source of error in their derivation of the pressure-change input into the material balance equation.

Here is the part of that analysis that the Government experts got wrong. During the spill, hot oil rose through the well, heating the casing, cement and surrounding rock from the reservoir to the sea bed. When flow ceased, the rock, and the oil in the well-bore, cooled down again. Colder fluids are denser, and so the pressure difference between the capping stack and the reservoir increased over time. To account for this changing head properly requires an analysis of heat transport – conservation of energy – in the well-bore and the surrounding rock. This is presented in Appendix B.

The capping stack pressure increased slowly, very slowly indeed by the beginning of August. This misled the Government experts: from the gradual rise of the capping stack pressure they mistakenly concluded that the reservoir was highly permeable. More permeable reservoirs allow oil to flow more easily, and hence build up less pressure. However, even when the capping stack pressure was flat, the reservoir pressure continued to rise: this cooling oil was pressing down more and more. The rising reservoir pressure was masked by the apparent flattening of pressure readings at the capping stack. If the Government experts had accounted for the extra pressure rise due to cooling, they would have deduced a lower permeability and flow rate, as we discuss below.

4.3.2 The poor conversion of the capping stack pressures is the principal problem with the pressure analysis of the Government investigators. In Appendix B.4 I quantify the effect of using a poor conversion from capping stack to reservoir on the pressure drop and oil released in the Government reports.[76] Here I will provide an overview to highlight its importance to their over-estimates of oil produced.

---

[75] The details are presented in Appendix B.
[76] Further details of my critique are also provided in Appendices F and G.

33

To find the final reservoir pressure (and hence the pressure depletion) there are two steps: converting the capping stack pressure to down-hole values, and then predicting the additional increase in pressure after the well was cemented in. I focus on this first step here, before moving to the second.

The Government experts assumed that there was a fixed pressure difference between the capping stack and the reservoir of between 3,100 and 3,200 psi.[77] My values change with pressure and temperature. They are typically 150 psi higher: this discrepancy alone has a 10% (0.5 MMstb) impact on the Government's estimated oil released. However, Dr. Hsieh considered a conversion close to mine, but never used it,[78] while Dr. Pooladi-Darvish calculated a wide range of values yet inexplicably chose a value below them all for his base case simulation model.[79]

The critical part of the calculation is to assess the cooling rate of the oil trapped between the capping stack gauge and the reservoir at the bottom of the hole. I show that the oil became cooler than the Government experts presumed, hence the reservoir pressure was higher than they realized, and the depletion lower. My calculations err on the side of higher temperature, hence lower reservoir pressure and more oil produced: I calculate that the temperature of the oil near the sea bed cools from close to reservoir temperatures to around 95°F at the time of cementing the well: this is still much warmer than the surrounding ocean and sediment, which is at 40°F.[80] What temperature did the Government investigators assume? I have extracted the temperature that would give the pressure conversion they used (using data for oil density).[81] The temperature values I calculate are implausible: close to or above the maximum recorded flowing temperature of 221°F,[82] and, for Drs. Pooladi-Darvish and Griffiths, in excess of the reservoir temperature itself (243°F).

The Government investigators made the oil unfeasibly hot; they implied that oil sitting in the capping stack, surrounded by cold steel and deep ocean for 19 days, would remain as hot as, or hotter than, the deep reservoir. This is impossible. Technically, the Government calculations disobeyed the second law of thermodynamics: hot things cool down.

This pressure conversion error caused large errors in the simulation work of Dr. Hsieh and Dr. Pooladi-Darvish: not only did it lead to an over-statement of pressure drop that drives the flow, but also of the permeability, the connectedness of the rock pores that also directly governs the flow rate, discussed later in this Section. The correct pressure head conversion would have led these investigators to halve their estimates of oil released.

I will now discuss the second step in the pressure analysis: extrapolating to late times to find the final reservoir pressure, and hence the pressure drop to input into the material balance equation.

---

[77] The sources and precise values are: Drs. Kelkar & Raghavan [KR], page 19 (3,220 psi); Dr. Hsieh, (pressure analysis) (3,199 psi) [44]; Dr. Pooladi-Darvish [PD], Appendix III, slide 23, base case model assuming a well-head temperature of 220°F (3,137 psi); Dr. Griffiths, [SKG], Appendix F, page 39 ("*calculated static head of 3190 psi*").

[78] Exhibit 8617; in digital format as IGS770-000026 (Dr. Hsieh's spreadsheet), first tab, cell H2 (3,350 psi).

[79] *See* Pooladi-Darvish report [PD], Appendix III, slide 23 (range 3,318-3,148 psi).

[80] Appendix B.3.

[81] Appendix B.1.

[82] Reddy *et al.* (2012).

4.3.3 Pressure analysis to determine reservoir size and pressure decline. In standard oilfield operations, a so-called pressure transient or well test is often performed. The pressure in the well is measured as a function of time while the well is flowing, declining in what is called the draw-down. After the well is shut in, the pressure increases in what is called the build-up.

During a draw-down or build-up, pressure changes radiate outward from the well-bore, like a wave moving through the reservoir. This so-called pressure transient can be thought of as ripples in a pond moving out in circles until they encounter some barrier to flow (such as the river bank). Just as the reaction of ripples to the river bank can be seen with the eye, the encounter of the pressure waves with reservoir boundaries can be detected in changes in the slope of the pressure response. This is shown in Figures 4.8 and 4.9 below; we will review how I deduce the Macondo reservoir boundaries from the pressure transient in the following sections.

We will also use the pressure measurements to determine the final variable in the material balance equation, reservoir pressure depletion. The Macondo the well produced for almost 86 days. Then the well was closed. The pressure at the capping stack was measured before the well was closed, and for 19 days afterwards. That pressure was still increasing when the well was cemented in, so we need to use proper methods of extrapolation to determine the final average reservoir pressure and hence the depletion from the initial pressure to obtain our third material balance variable. This will be analyzed in Sections 4.3.6 - 11.

4.3.4 Radial flow period to determine permeability. Government experts Drs. Hsieh and Pooladi-Darvish arrive at enormously over-stated flow estimates because their models double the correct value for permeability. Permeability is a rock property that measures how easily the oil can move through the tiny, tortuous pathways connecting the pores between the grains of sand, shown previously in Figure 3.1. Higher values for permeability give higher flow rates. Permeability is controlled by the size of the pores (larger pores allow more flow) and by how well they are connected together.

The Government experts all assumed a permeability of over 500 mD.[83] That is more than twice the most likely value, and proportionately inflates the Government estimates of flow. To understand how the Government experts made this mistake, and to determine an appropriate value for permeability ourselves, we need to introduce the methods for interpreting the pressure changes that occur when a reservoir stops producing and builds up pressure.

To represent the pressure response, we treat the reservoir as a box, shown schematically in Figure 4.8, as has every other investigator who has studied Macondo. This box contains all the oil-bearing sandstone *connected* to the well.

If we return to the analogy of the ripples in the pond, the pressure signal moves out in circles (radially) before it encounters a boundary (the edges of the reservoir channel or channel complex). This is depicted in Figure 4.9. Permeability is deduced from identifying the initial radial flow period. We will plot the Macondo radial flow pressure transient to calculate the permeability in Section 4.3.8.

---

[83] *See* Section 4.3.8. Appendix C discusses permeability in more mathematical detail.
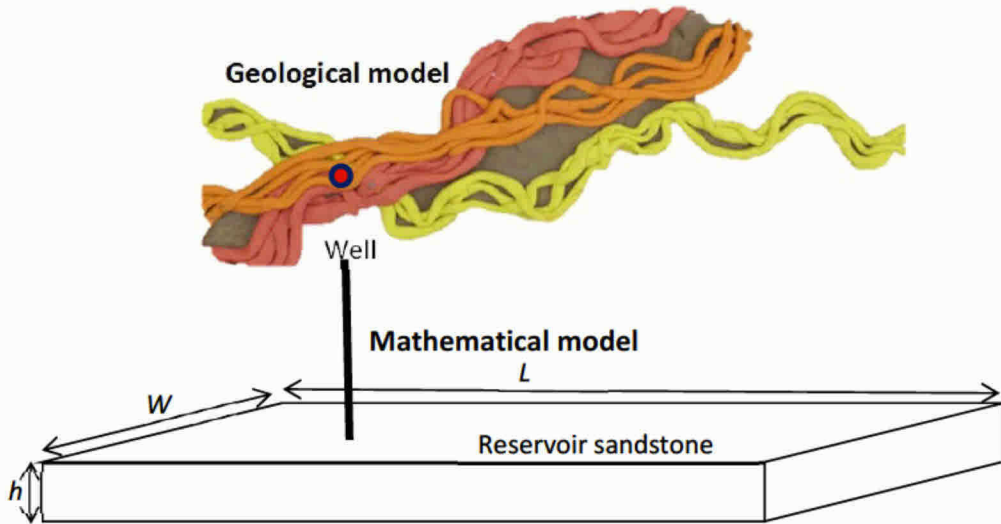
Figure 4.8. Schematic of the reservoir geometry used in our analysis of the pressure response. At the top are the three sandstone channels connected to the Macondo well extracted from the geological model shown in Figure 4.5. We represent this in our mathematical model by a box of length L, width W and height h: this box contains all the oil-bearing sandstone connected to the well. We assume that the well is drilled through the centre-line of the box middle at some point along the length.
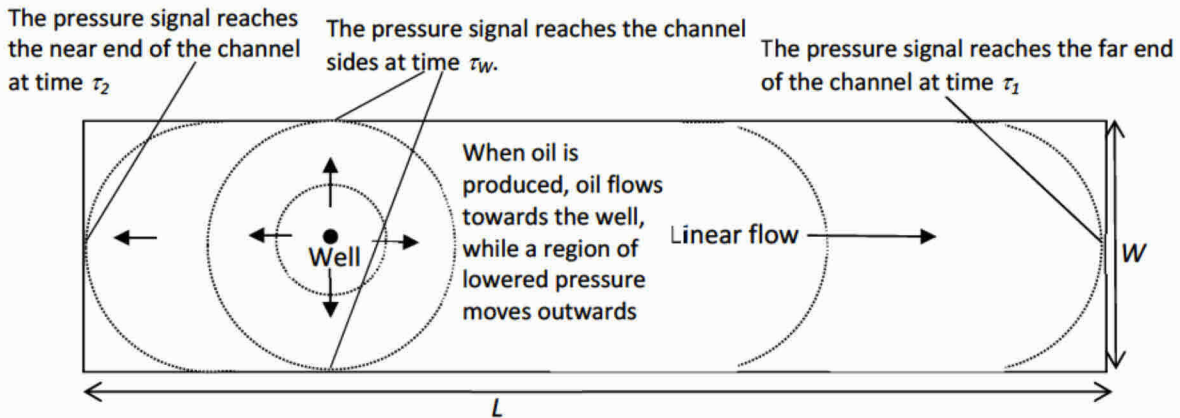
Figure 4.9. A horizontal cross-section of the reservoir, indicating radial and linear flow regimes. At early times the pressure decreases in an approximately circular manner from the well. This radial flow period ends when the pressure reaches the boundary of the channel at time τ_w – around 17 hours or 60,000 s for Macondo. There then follows a longer period of linear or channel flow. It is possible to find the times to reach the two ends of the channel using the analysis techniques described in this report.

4.3.5 Linear or channel flow. When the radial flow pressure transient hits the nearest boundary of the reservoir – the sides of the channel – the flow begins moving in a linear direction along the channel. As depicted in Figure 4.9, the time for the transition from radial to channel flow – τ_w – can be used to calculate the reservoir width. To obtain distances from travel time, we need to know the speed.[84] The speed of the pressure transient is proportional to permeability. So having derived the permeability from

---

[84] Technically this is a diffusivity, defined in Appendix C.

the radial flow analysis as described in the previous section, we will be able to deduce the size of the connected reservoir from the times at which the pressure transient hits the boundaries.

From the geological interpretation of the field it is reasonable to consider that the reservoir is composed of one or more channel complexes, which – for simplicity – I will refer to as channels from now on. Once the period of radial flow ends, our analysis shifts to the movement of pressure along the channel – this is one-dimensional or linear flow. We can detect the times when the pressure wave hits the two ends of the channel, and calculate the length of the channels. From the width and the length we can determine the area of the reservoir connected to the well: the area of the box in Figure 4.8.

I employ a rectangular flow model to study radial flow and the transition to flow in a channel, and a linear flow model for the late-time behaviour to determine the times to reach the ends of the reservoir and the pressure drop.

We now have the principles for analyzing the pressure data as a function of time. We will show how it provides us with four important pieces of information: (1) the final reservoir pressure, used to calculate pressure depletion, a direct input into the material balance equation; (2) permeability, the critical determinant of flow rate, from the rate of pressure build-up in the radial flow period; (3) the time for the pressure response to hit the sides of the channel, which will be used to measure reservoir width and check connectivity; and (4) the times for the pressure response to reach the two ends of the channel, which will be used to help assess original oil volume and exclude the possibility of aquifer support to the production of oil.

4.3.6 Pressure prediction. We start with a plot of the build-up of pressure as a function of the time after the capping stack was shut in. I have plotted this pressure response in Figure 4.10 together with the predictions of my analytical rectangular and linear flow models.[85] I obtain a close match to the measured pressure, demonstrating that my model is an accurate depiction of the behaviour by reservoir engineering standards:[86] this is shown by the red and black lines in Figure 4.10.

But there is a more powerful methodology for plotting and analyzing the pressure build-up. It focuses on the trend, or slope of the data. Analyzing the changes in slope provides insight into the characteristics of the reservoir. Matching the slope changes with a model is an extra litmus test of model validity.

4.3.7 Pressure derivative methodology and its importance. A revolution in the ability to interpret pressure tests and thereby determine reservoir properties occurred in the 1980s,[87] when reservoir engineers began to focus on the plot of the change in pressure as a function of time. Using this plot, characteristic shapes appear in the slope, from which an engineer can determine the structure of the reservoir and the permeability. Like a physician with a chest X-Ray, a reservoir engineer can diagnose

---

[85] *See* Appendices C and D.
[86] I have derived all the equations I use by hand, and have not relied on commercial pressure transient analysis software. Such software requires an assumed flow rate (see, for instance, M. Levitan deposition [56]; page 216, lines 19,20).
[87] Bourdet *et al.* (1983; 1989).

the properties of the reservoir from the so-called derivative plot. This has been the standard approach in the oil industry for the last 25 years. I am not going to go through the technical details;[88] instead I will illustrate the concept with some examples.
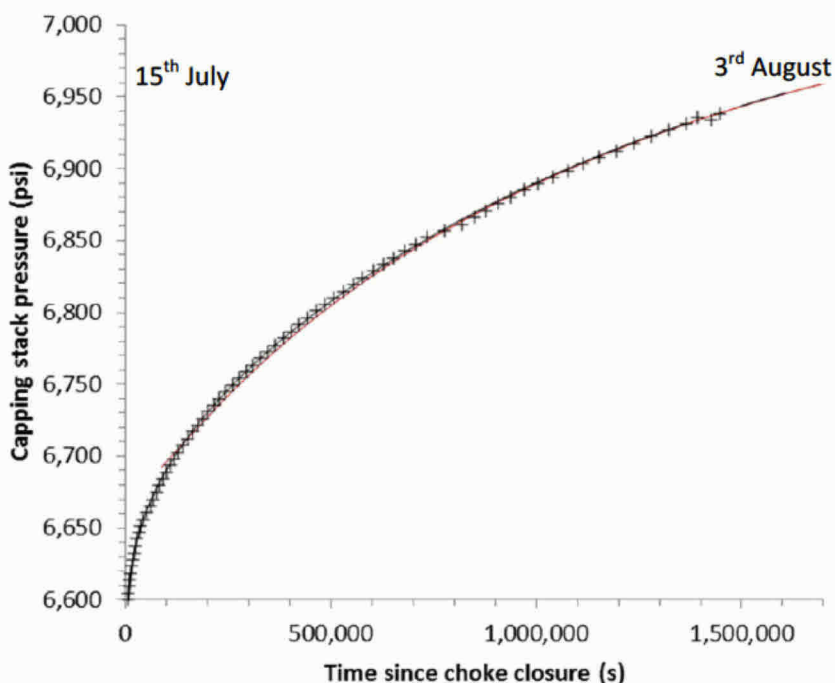
Figure 4.10. The measured capping stack pressure. Time is measured in seconds from well closure until the injectivity test prior to cementing the well. For reference 1,000,000 (one million) s is around 11 days and 14 hours. The red line is my prediction using a linear flow model, after one day (86,400 s), while the black line uses a rectangular flow model.

Figure 4.11 is a textbook graph of the pressure and the pressure derivative (the slope of the pressure as a function of time). After around 10 hours (36,000 s) the derivative reaches a constant value: this is radial flow from which permeability is calculated. A higher derivative means a lower permeability.

I also show a field example from a deepwater channelled turbidite (like Macondo).[89] Here we detect radial flow (at 3 hours or about 10,000 s) followed by channel flow (after 10 hours or 36,000 s), when the derivative starts to increase. In these figures the points are the data, while the lines are matches using a rectangular model, which I will employ to study Macondo. Note that both pressure and derivative are accurately predicted by the models.

A good engineer would look at the field example below and determine that there was an initial period of radial flow. The increase in derivative that occurs later – the slope is ½ – tells you that flow then became confined to a channel. Then the engineer would match the data to a mathematical model to quantify

---

[88] The mathematical details are presented in Appendix D.

[89] Govan *et al.* (2006). The field is Schiehallion on the Atlantic margin of the United Kingdom Continental Shelf. In the paper, the BP engineers describe a variety of methods to predict production and reservoir connectivity. The analysis includes material balance and the use of pressure derivatives.

38

the permeability, the pressure drop, and the size of the reservoir connected to the well. So, let's do the same for Macondo.
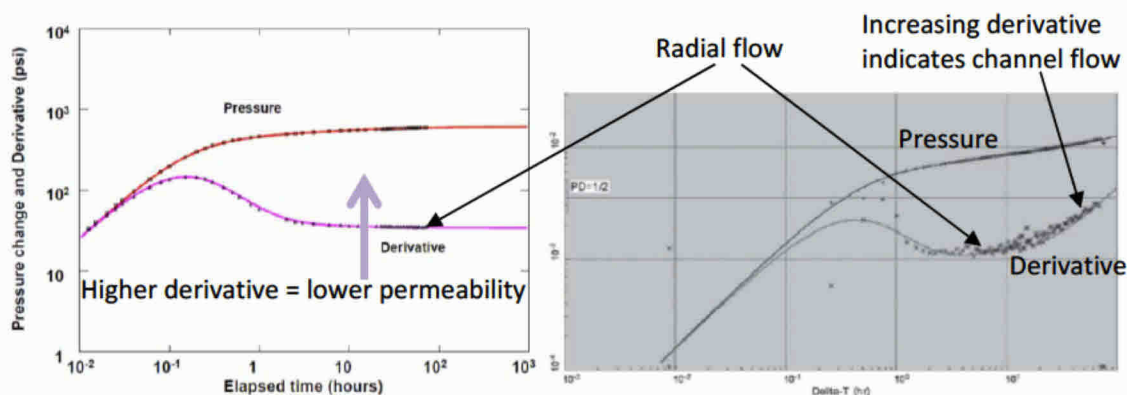
Figure 4.11. Left: exemplar pressure build-up and derivative.[90] The pressure build-up appears to show little information but the derivative – the slope of the plot – reveals the behaviour of the reservoir in great detail. The constant value of the derivative seen after around 10 hours indicates radial flow, from which permeability can be calculated: the higher the value the lower the permeability. **Right: a field example of the pressure and derivative in a channelled deepwater turbidite oilfield (Govan *et al.*, 2006; © Society of Petroleum Engineers)** showing similar features. The points are data and the lines the model match: note how the model is expected to reproduce the data and its derivative almost exactly.

4.3.8 Pressure derivative for Macondo. Figure 4.12 is the centre-piece of the pressure analysis. It shows the measured and predicted reservoir pressure derivative, as well as the pressure rise itself. This is the traditional presentation of pressure analysis in petroleum engineering. It is similar to the field example above: radial flow apparent at around 10,000 s and an increase in slope – showing channel flow – coming later (in this case around 60,000 s or 17 hours).

The graph contains a lot of valuable information. There are two main points to note.

1. The pressure and derivative are accurately matched by the analytical models. The pressure is matched with an error of 2 psi or less – this is superior to all the matches presented in the expert reports of Dr. Pooladi-Darvish and Dr. Hsieh.[91] I have matched the data using both a linear flow model, applicable after 1 day (86,400 s), and a rectangular flow model that better represents the transition from radial to linear flow.[92] The sensitivity of the pressure gauge is only 5 psi, so we can consider this – by engineering standards – a more-or-less exact match.

2. The permeability can be estimated from the value of the derivative in the radial flow period. I find a value of approximately 300 mD.[93] This value is consistent with Macondo core and log measurements.[94] Using a fixed reservoir-to-capping stack conversion means that – to match the

---

[90] Taken from the lecture notes of Dr. Gringarten (2012).

[91] *See* Tables D.2 and D.3; Pooladi-Darvish report [PD], Table 1, page 3; for Dr. Hsieh *see* Appendix G.

[92] The linear model equations are given in Appendix C; the rectangular model is standard in well test analysis and was first derived by Earlougher *et al.* (1968).

[93] The equations are presented in Table D.1, the best match in Table D.3 for the rectangular model (Core Labs properties – see Table A.1 for viscosity). I assume a final flow rate of 45,000 stb/day.

[94] *See* Appendix A.5 for a detailed discussion of the permeability data.

pressure – the Government investigators assumed that the rise in reservoir pressure was the same as in the capping stack, with a lower derivative. This corresponds to a higher permeability of around 560 mD.[95] This almost exactly matches the 550 mD used by Dr. Pooladi-Darvish[96] and 593 mD employed by Dr. Hsieh:[97] they did indeed match the pressure, but the wrong pressure to find the wrong permeability, which lay outside the averages from log and core measurements. The flow rate is proportional to the permeability, so their simulation models significantly over-estimated the flow rate (and hence cumulative oil released).
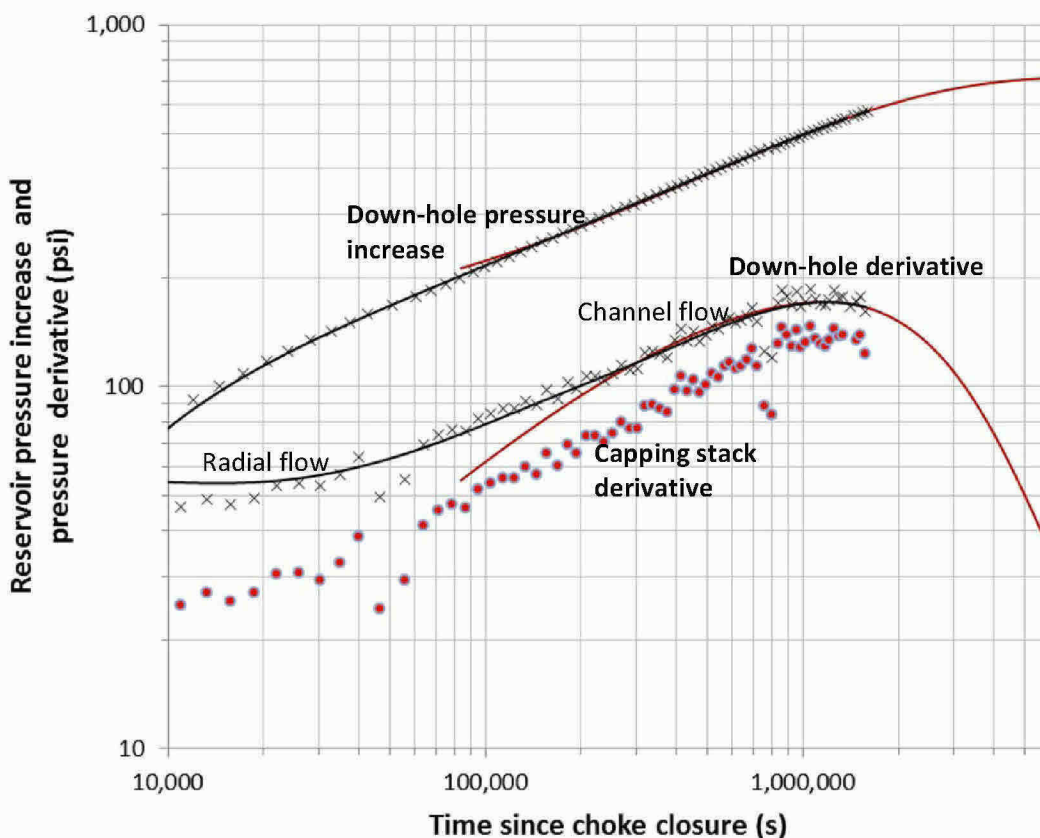
Figure 4.12. The pressure derivative and the pressure rise plotted as a function of time since choke closure. The red points are the derivative measured at the capping stack, while the crosses show the down-hole (reservoir) pressure derivative, which is higher, indicating lower permeability. I show best match predictions to the reservoir behaviour using both rectangular (black lines) and linear flow models (red lines). The linear flow model shows a deviation at early times, since it cannot represent the transition to radial flow.

4.3.9 Reservoir pressure predictions. The analysis of the pressure in the first day (86,400 s) has some uncertainties: cooling from the ocean, the thermal properties of the annulus around the well, and the complex sequence of flow rates during choke closure all impact the early pressure transient. I consider the permeability calculated in the expert report of Dr. Gringarten, 238 mD, which avoids these problems through using down-hole pressure measurements, more robust than my determination presented

---

[95] Assuming a radial flow stabilization in the capping stack derivative of 32 psi in Figure 4.12.
[96] Dr. Pooladi-Darvish's base case model [PD], Appendix III, slide 8.
[97] Exhibit 8615 (10/22/2010 Hsieh Draft Report, Table 2) [67].

above, although my value lies in his statistical range.[98] The emphasis of my calculations will be on late times, beyond a day, when there is linear flow. A close match to the pressure in this regime is important to determine the final reservoir pressure and the location of the far reservoir boundary.

My base case assumes a constant (albeit unspecified) flow rate. The flow rate history does impact the pressure response, as stated above. However, for times beyond a day or so, the pressure response is governed by the average rate alone.[99]

Figure 4.13 shows the down-hole pressure plotted against time compared to the pressure predicted by my model: the inset shows the pressure prediction for later times, indicating that the pressure stabilizes to its final value of 10,433 psi around three months after choke closure. The final reservoir pressure that I use in my material balance calculation ranges from 10,433 to 10,531 psi, depending on which sets of the fluid properties are used.[100]

The Government reports all estimate a final reservoir pressure that lies below my values.[101] None of these reports compare their predictions to the data using the X-ray examination of the pressure derivative.[102] Dr. Hsieh omitted this analysis, even though the BP engineers with whom he was working did use derivative plots.[103] However, my value is lower than the value presented in a press release by BP: *"industry-standard techniques predict the final reservoir pressure to be approximately 10,600 psi."*[104] I find a lower final pressure than that derived by BP, resulting in a higher calculated cumulative flow.

Dr. Hsieh and Dr. Pooladi-Darvish significantly over-estimated the pressure drop and consequently over-stated the oil released; this effect is quantified in the summary table in Section 2. Drs. Kelkar & Raghavan made two errors that partially cancelled: they under-estimated the head, but slightly over-estimated the pressure rise, leading to a more reasonable final assessment of pressure drop (see Appendix B.4).

---

[98] Dr. Gringarten [ACG] quotes a range of 170-329 mD.

[99] See Appendix E.

[100] The fluid properties determine the conversion from capping stack to reservoir properties (Appendix B) and so the predictions are different for the three sets of measurements. In this Section I show model comparisons using the Core Labs properties; my analysis is, however, performed for all three sets of data.

[101] Dr. Hsieh, 10,267 psi (*see* Exhibit 8617 (Hsieh pressure analysis)) [44]; Dr. Griffiths, 10,310 psi [SKG] Appendix F, page 39; Dr. Pooladi-Darvish [PD] , Appendix V, slides 4 and 5: 10,053 to 10, 382psi from his simulations; Drs. Kelkar and Raghavan [KR] , page 23: 10,235-10,396 psi.

[102] Dr. Pooladi-Darvish [PD] presented a pressure and derivative match for his analytical model, Appendix II, slides 30 and 31; however, for all his simulation runs, he only showed matches of pressure alone.

[103] *See* Dr. Merrill's deposition [55], page 344, line 18 where Dr. Merrill mentions *"Bourdet derivative plots"*.

[104] BP press release, page 6, second paragraph [50].
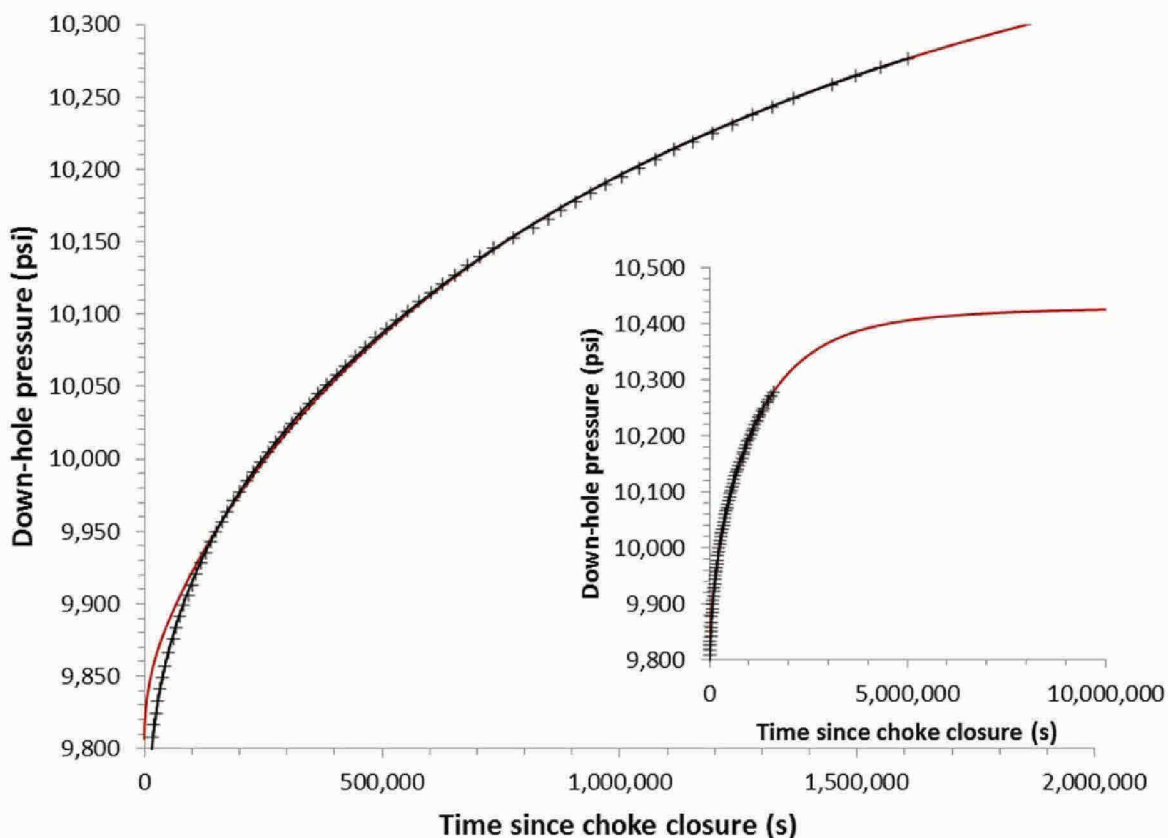
Figure 4.13. Down-hole (reservoir) pressure data (crosses) compared to the predicted pressure for linear (red line) and rectangular (black line) models. The inset shows the extrapolation to late time showing that the final reservoir pressure (10,433 psi) is reached around 3 months after choke closure.

4.3.10 Pressure drop: 1,325 − 1,423 psi.[105] For completeness, we end this section with Table 4.5, which presents the final reservoir pressure and pressure drop Δp (the initial pressure, 11,856 psi, minus the final pressure) using the three sets of fluid data. The pressure drop is the third and final component in the material balance equation: its value lies between 1,325 psi and 1,423 psi.

Property	High case Core Labs	Middle case Intertek	Low case Schlumberger	Average values
Final reservoir pressure, p_f (psi)	10,433	10,502	10,531	**10,489**
Pressure drop, Δp (psi)	**1,423**	**1,354**	**1,325**	**1,367**

Table 4.5. Final reservoir pressure and pressure drops determined from the pressure match for the three sets of fluid properties.

---

[105] These values are found using the linear flow model. See Appendix D, Tables D.2 and D.3.

42

5. Confirming the consistency of the calculations with other evidence

Before we multiply our three numbers together to calculate the oil released, we need to pause to check if the different inputs to our calculation are mutually consistent. It is standard in reservoir engineering to check if the predictions of the pressure analysis agree with the geology of the reservoir. We have assembled the pieces of the Macondo jigsaw in this analysis; now we will analyze whether they fit together to construct a coherent picture of the reservoir. This vital assessment was not performed by any of the *Government* investigators: such a check would have shown (as we will show here) that their *analysis was incompatible with the measurements*.

In Section 4.1 we showed how the Government investigators assumed without geologic analysis that the total reservoir volume was connected to the well. In Section 5.1, I will combine the seismic and pressure analysis to show that the reservoir is not 100% connected. In Section 5.2 I will explain how my approach of using the range of values from the data for each parameter ends up defining a range of calculated flow volumes that is more certain and reliable than other approaches to uncertainty.

5.1 Cross-checking seismic and pressure-transient indications of reservoir size, dimensions and connectivity

5.1.1 Reservoir length. It could be possible for the connected reservoir to be shorter than the length of the field. For example, in the seismic interpretation introduced in Section 4.1, faults were mapped cutting across the axis of the channel orientation. I would arrive at a much smaller connected reservoir and lower connected oil volume (and hence cumulative flow) if I adopt such an assessment.

Figure 5.1 shows a BP interpretation of the seismic survey where individual channels are identified. The analysis suggested that the channels were not necessarily continuous in a North-South direction. From this, BP made an assessment of the area connected to the Macondo well – before the capping stack pressure data was available – that gave values between 50 and 225 acres.[106] By comparison, the entire area in BP's seismic analysis is much larger – 4,482 acres. If I were to use the smaller connected area suggested in this BP study, the calculated volume of oil released would be at most between 80,000 and 440,000 stb.

While BP's analysis is not unreasonable from a geological standpoint, I will show in this Section that the pressure response clearly indicates that the connected area is considerably larger than this.

Thus, I will not consider the possibility that the reservoir is compartmentalized by a fault or other barrier cutting across the channels. Instead, I believe the pressure-transient evidence (outlined below) suggests that the limitation on connectivity is associated principally with the reservoir width, that is, how far it extends East-West or NE-SW.

---

[106] BP-HZN-2179MDL04440238 (BP seismic survey presentation, slide 3 and 4, respectively) [17]. Other estimates of the connected oil volume made during the spill by BP include 650 acres – see Dr. Levitan's deposition [56]; page 95, lines 7,8 – which is still much lower than indicated by the pressure response once the well was closed.
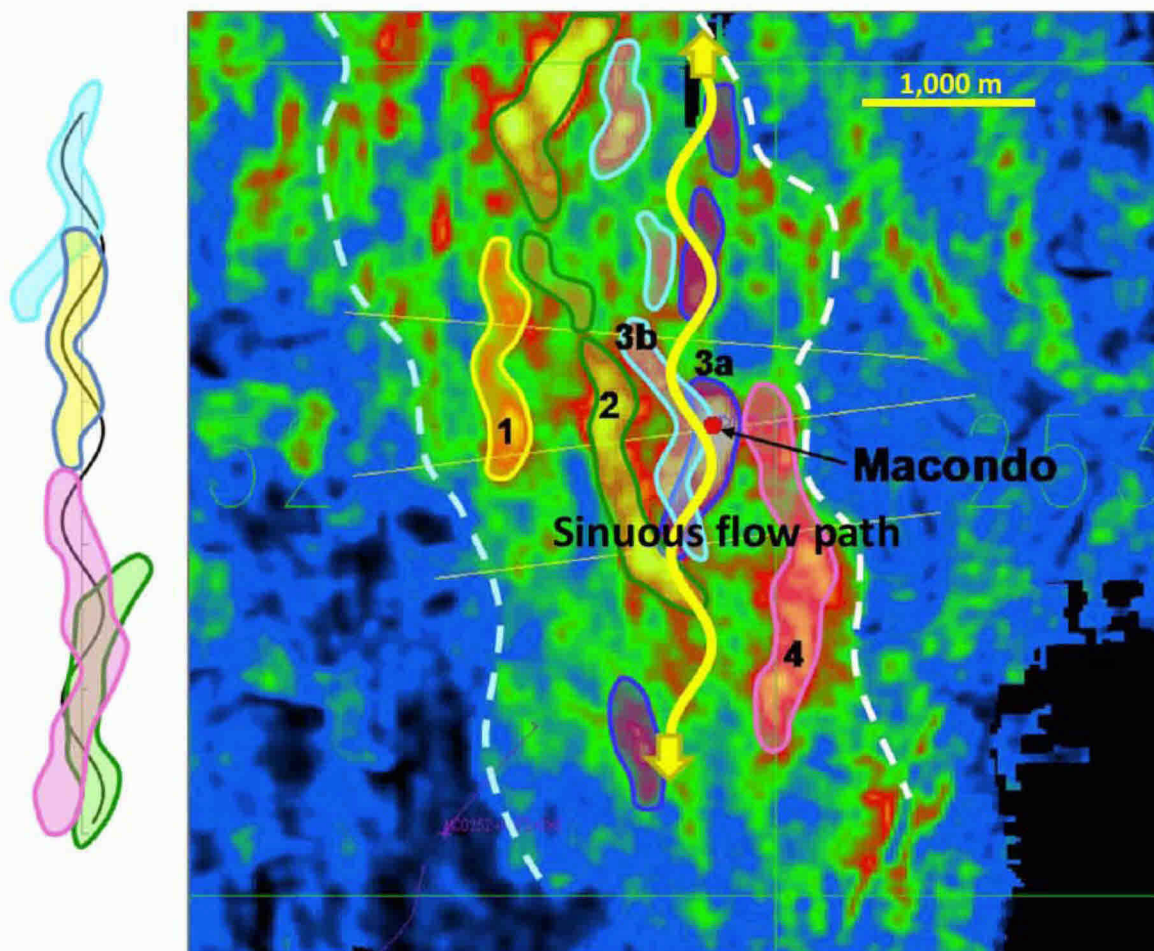
Figure 5.1. Map of the Macondo field.[107] This is a detailed view of Figure 4.5 where the location of sandstone channels is postulated – it is not possible to determine their locations, connectivity and shape exactly, but what is shown is a reasonable inference from the likely geology and seismic survey. Flow – and pressure – follows a sinuous path along the channels. On the left, I have taken the channels marked 1-4 on the figure, rotated and flipped them and placed them to lie – approximately – on a sine wave. I assume that the flow follows the sinusoidal path shown – this is approximately 14% longer than a straight line. Note that some channels, 1 for instance, are not connected to the well.

5.1.2 Interpretation of the pressure response and connected reservoir areas. In Sections 4.3.4 and 4.3.5 we introduced the general method of using the pressure transient after well shut-in to find the reservoir boundaries. Figure 4.9 showed that we would use the times to hit the boundaries, denominated by the Greek letter τ and multiply that by the pressure wave speed, which is a function of permeability, to find distances. I have used this method to find the times τ_1 and τ_2 for the pressure to detect boundaries to the North-West and South-East (or South) of the well respectively, while τ_w is the time taken to detect the width of the channels in a roughly East-West (or SW-NE) direction. (The precise times are derived in Appendix D and shown in Tables D.2 and D.3.) These are no-flow boundaries, meaning that no oil or water moves beyond the extent of this connected reservoir volume.

---

[107] BP-HZN-2179MDL04440238 (BP seismic survey presentation, slide 2 [17].

TREX-011553-R.0044

Once we know the times to see the boundaries of the (connected) reservoir, we need to derive the rate at which the pressure signal propagates. If we know this speed and the times, then we can find the physical locations of these boundaries. In Sections 4.3.4 and 4.3.5 we discussed that this rate is a function of permeability. Higher permeability allows faster flow and a more rapid propagation of the pressure signal. Hence higher permeability gives a larger area and greater connectivity.

The speed of the pressure transient is also a function of the rock compressibility. A more compressible rock retards the speed of pressure transmission. Hence reservoir engineers use a term for pressure-transient speed called diffusivity, which proportional to permeability but inversely proportional to compressibility.[108]

With our pressure-transient deductions of times to hit boundaries, combined with possible ranges of values for diffusivity, I can calculate a likely upper bound on the reservoir's connectivity. I will take the largest permeability value from the expert report of Prof. Gringarten: 329 mD.[109] This is above the value I deduced from pressure analysis (300 mD – see Section 4.3) and from down-hole measurements (219 mD – see Appendix A.5).

Using this upper bound on permeability, the connected area I calculate varies from 1,931 to 2,590 acres (see Table 4.1).[110]

5.1.3 Meandering flow path. Figure 5.1 shows that the pressure response (and the oil) does not move in a straight line – it follows the winding path of the sandstone channels. Hence the pressure signal (and the flowing oil) travels a longer-than-straight-line distance. To calculate the path length I have taken some of the channels indicated in Figure 5.1 and modelled their shape as sine waves. This is a standard geometric approach in geology.[111] I calculate that the true distance travelled is around 14% longer than a straight line.[112] In reality, the flow path could be more tortuous still, taking detours along locally the thickest sands in three dimensions. I used this sinuosity in constructing my model in Figure 4.5.

5.1.4 Combining pressure and seismic analysis to deduce connected area. In Figure 5.2, the left side overlays the reservoir size estimated from pressure analysis onto the size predicted by the seismic analysis. The horizontal lines indicate the width of the field as interpreted from the pressure analysis. The pressure-inferred size is smaller, which suggests that the field is poorly connected, requiring a reduction of the initial-volume input for material balance from the value used by the Government. A possible reason is shown on the right side of Fig. 5.2, my geological (clay) model, showing how individual oil-filled channels may be disconnected laterally from the well.

---

[108] Using Eq. (C.4).

[109] The Gringarten report [G] has a range 170-329 mD with a most likely case of 238 mD. Technically, this means that there is a 10% probability of the permeability exceeding 329 mD.

[110] *See* Appendix D.1 for the mathematical details of how distances and areas are calculated.

[111] See, for instance, Posamentier (2003), Dystra and Kneller (2008).

[112] *See* Appendix D.1 for the mathematical details.
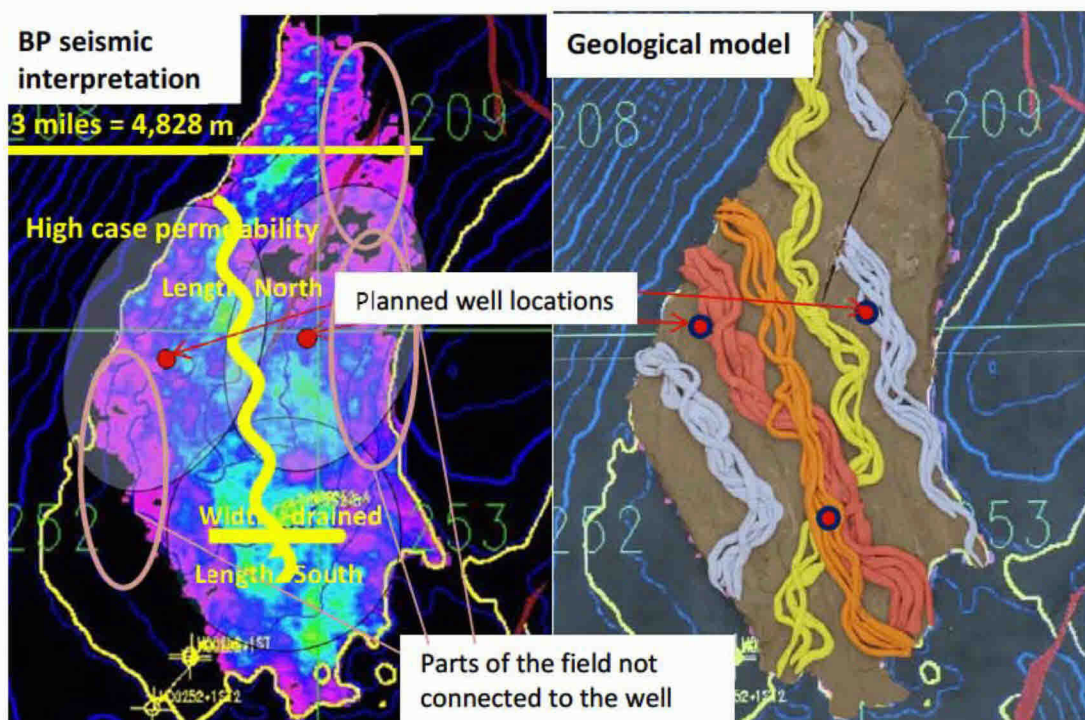
Figure 5.2. Left is the BP interpretation of the seismic, right is my reservoir model (see Figure 4.5). The horizontal yellow lines indicate the width of the connected oil volume predicted from the pressure analysis. The wavy lines indicate the predicted extent of the reservoir. I have considered a high case permeability. The lilac ovals indicate regions of the field that are unlikely to be connected.

The wavy lines show the extent of the field to the North-West and South.[113]

We appear to have hit a sweet spot: the extent of the field to the North-West predicted from the pressure transient is consistent with the seismic interpretation. This provides confidence in our pressure analysis and our assessment of the rock and fluid properties that go into the compressibility component of diffusivity, the speed of the pressure wave.

Figure 5.2, combined with our pressure analysis (Section 4.3), indicate the following:

1. **The channels are well connected longitudinally.** Along the sandstone channels the Macondo well drains all or most of the field.
2. **The width of the region drained by the well is roughly one half the total width of the field near the well.** This suggests that the connectivity of the field in a transverse direction, between – rather than along – channels is poorer. The well does not necessarily connect to the entire volume of oil-bearing sandstone. This is consistent with the geology – flow is well-connected along a channel, but restricted between channels that may not intersect and are separated by

---

[113] The lengths from the pressure analysis are the path lengths along the sinuous channels indicated: the straight-line path is some 14% shorter.

46

low permeability shale.[114] In Figure 5.2, I have indicated by the lilac ovals regions of the field that I consider are unlikely to be connected to the well.

3. The clear signature of channel flow, the restricted width of the channel, and evidence of no-flow boundaries along all sides of the region connected to the well, strongly indicate that **there is no aquifer support**. There is no evidence that we are seeing a drainage region that extends beyond the oilfield.

We will now address possible objections to this interpretation.

1. **Permeability.** The higher numbers for permeability assumed by the Government experts would suggest higher connectivity. However, Prof. Gringarten's report uses a superior method for deducing permeability that is based on pre-spill measurements and dynamic flowing data, considered the gold standard for permeability assessment. He derives a permeability of 238 mD. I am using a higher value of 329 mD – the upper end of his range. It is not possible to reconcile significantly higher permeabilities – of 500 mD and above – as used by the Government investigators[115] with measurements on rock samples from Macondo (average 364 mD), log (down-hole) analysis (average 219 mD),[116] and my pressure analysis (300 mD, Section 4.3).

   There is another source of evidence that the Governments high permeabilities are highly improbable. If the permeability had been 500 mD or higher, then the effect of well cooling may well have exceeded the slow reservoir pressure rise after choke closure on July 15th 2010. The capping stack pressure might have stabilized and then fallen slightly in the first day. This is likely to have been misinterpreted as a sign of poor well integrity, the choke would have been re-opened, and oil would have continued to spill, unnecessarily, into the Gulf until the relief well was drilled.[117]

2. **Compressibility.** As discussed earlier, some Government experts asserted a higher compressibility, leading to a higher calculation of cumulative flow. However, this would lead to a slower-moving pressure signal, since the diffusivity is inversely proportional to compressibility. Hence, their assumption of higher compressibility must result in an interpretation of the pressure transient yielding a smaller calculated drainage region. A low compressibility, in contrast, allows the pressure signal to travel faster and encounter more of the field. Notice two competing effects of compressibility: while – for a fixed oil volume and pressure drop – a high compressibility leads to more oil released, a high compressibility indicates a smaller oil volume. So, allowing a much larger compressibility is inconsistent with the seismic extent of the field, unless the field is poorly connected.

---

[114] Posamentier (2003).

[115] *See* Appendices F and G.

[116] *See* Appendix A.5.

[117] *See* Appendix B.3 for a fuller discussion.

3. **Aquifer.** During the incident, investigators from both the Government and BP considered that an aquifer drive could provide pressure support and additional recovery in Macondo;[118] this was a reasonable hypothesis to consider, but the impact of the aquifer would require production periods of some years, while the pressure response indicates flow boundaries were encountered during the time-scale of the incident. For an aquifer – located to the sides and end of the main oil-bearing channels – to contribute to oil production, the pressure response has to pass through poorly-connected, low permeability regions between channels, or pass beyond the longitudinal extent of the reservoir. This flow response takes several months or years to contribute noticeably to production. This conclusion is consistent with the modelling work of all the Government investigators and the analysis performed shortly after capping stack closure by BP. BP's reservoir engineer Dr. Merrill says that he *"excluded an aquifer"*[119] as the easiest and simplest way to match the measured pressures.

4. **Analysis of the implicit Government premise that the well drained the entire width** of the field. I have calculated that – approximately – half the width of the field near the well is contacted.[120] To double this, so that the whole width is encountered, would require an increase of my value of τ_w by a factor of four – from around 17 hours to more than three days.[121] Despite the ambiguities associated with the interpretation of the pressure response at early times, a clear indication of channel flow is encountered within a day. Furthermore, I have assumed that the average permeability across or between channel complexes (including low permeability shale that separates individual channels) is the same as the permeability along a channel. This again is unlikely,[122] and so – if anything – my calculated width is likely an over-estimate.

5.1.5 Deducing connectivity from the overlay of pressure and seismic analysis. I will take a generous approach, which – while it likely over-states the connected oil volume – provides a robust upper bound. As outlined in Section 4.1, I place the oil connected to the well in the area predicted from the pressure analysis. I assume that outside this area, the oil does not flow to the well. The thickness of the oil in these regions is assumed to be 10 ft on average – this is the limit of the seismic interpretation.[123] The overall average thickness of the whole field 44 ft, while the thickness at the well is 93 ft, so I am placing very little oil outside the main, connected channels.[124] I find a connectivity of between 87 and 90% dependent on the fluid properties.[125] I find it implausible that the connectivity is better than this: the seismic interpretation places oil further to the East and West of the well than can be possibly connected to it. I cannot, however, exclude a lower case with more restricted connectivity, based on the most likely value of permeability in the Gringarten report.

---

[118] BP-HZN-2179MDL06566208 (BP Pre-Drill Review, slide 18) [31].

[119] Dr. Merrill deposition [55], page 442, line 27.

[120] τ_w indicates the transition from radial flow to channel flow and so, technically, is used to find the connected reservoir width near the well.

[121] Since this is a diffusive process, to travel twice the distance takes four times longer.

[122] *See* BP's geological review; [39], slide 2.

[123] *See* BP's gross rock volume assessment; [30], slide 1, most likely case: *"10 ft cutoff footprint (noise background)."*

[124] *See* Table A.3 and [31], slide 15.

[125] *See* Appendix D.1.6 for the mathematical details and Table D.4 for the values.

My assumptions are consistent with the *upper bound* of permeability. I can only allow a larger connected area by reducing the compressibility. This may allow more oil to be connected, but less oil is released for a given pressure drop. The two effects cancel out. Or, I allow a larger permeability, outside the values assigned by robust pressure analysis and down-hole measurements. It is not possible to use plausible rock and fluid properties and allow a cumulative oil release that lies above my range.

5.2 Consistency with flow rate history

5.2.1 Pressure analysis and flow rate history. I will now mention one last, further, consistency check related to the pressure analysis. The pressure was matched by a mathematical model that assumed a fixed (albeit unspecified) flow rate. To yield my calculation of total oil released, if the flow rate was constant, it was in the range of 34,000 – 43,000 stb/day. This is inconsistent with the Government assumption of flow rates that were either constant or decreasing over time with final value of around 50,000 stb/day. If this final flow rate is correct, then my analysis asserts that the flow rate must, overall, have increased on average during the spill period.

In Appendix E.2 I match the pressure response using different possible flow rate histories. This approach is standard in pressure transient analysis, where – for many reasons – the flow at any given well may vary. I can obtain good matches for various flow rate histories, including those with a final flow rate consistent with Government estimates, while arriving at my mid-range calculation of total oil released.

Furthermore, analysis of the accident suggests that oil flow into the well-bore was initially highly restricted, but the restriction(s) had disappeared by the end of the spill, as indicated by the injectivity test just before cementing the well, which showed negligible resistance to flow.[126] This also supports the conclusion that flow became less impeded during the spill, allowing the flow rate to increase.

The available evidence indicates that even if we accept the Government estimates of flow rate for the latter period of the spill, it is likely that the flow rate *increased* on average over time, giving a cumulative oil released significantly below the totals assumed by the Government investigators.

5.2.2 Statistical analysis and a likely range of oil released. When petroleum engineers are evaluating a new oilfield, they often use statistical methods to estimate ranges of each input into their calculations – permeability, compressibility, oil formation volume factor, porosity, saturation and gross rock volume. Then, the statistics of a combined quantity – such as oil originally in place (STOIIP) – are computed. This is valuable to quantify uncertainty leading up to investment decisions.[127] For example, a range of outcomes with associated probabilities for each can be used for cost-benefit decisions. I have not followed this approach for two reasons. Firstly, such quantification of uncertainty involves a series of somewhat subjective inputs. Secondly, this statistical approach is most valuable *before* production, when data on many properties that determine reservoir behaviour are completely absent.

In Macondo, a well was drilled that produced oil. This provides information that helps narrow the uncertainty in our calculations. For instance, the most likely case seismic analysis suggested that the

---

[126] *See* Appendix E.3 and the Emilsen report [27] for further discussion.
[127] For instance, BP presents a statistical analysis of STOIIP in its Macondo pre-drill report [9]; Section 6.19.

49

well would encounter 96 ft of oil-bearing sandstone: it encountered 93 ft.[128] In the seismic interpretation, BP was uncertain as to the lateral (East-West) extent of the field with a predicted maximum height of up to 140 ft at the well:[129] the pressure response demonstrates that the flow into the well was confined to a channel that may not have encompassed the entire width of the field. Data from the well and the pressure analysis considerably reduce the uncertainty in connected oil volume. The mutual consistency between the results of the pressure analysis, measured rock and fluid properties, and the geology of the field significantly shrinks the uncertainty in reservoir properties.

I have taken an unbiased approach, defining my ranges of likely outcomes based on the ranges in the data, allowing for the full range of measured fluid and rock properties. The resulting range of oil released is ±12%. The approach taken here in the determination of cumulative flow is more robust and avoids the unsupported extrapolations, poor analysis and scant regard for measured data in the Government's analyses. For the reasons given above, I consider it highly unlikely that the oil released from Macondo lies significantly above the values I present in the next Section.

---

[128] *See* Table A.3 and [31], slide 15. Also BP's gross rock volume assessment; [30], slide 1, most likely case: *"96 ft at proposed location."*
[129] See BP's gross rock volume assessment; [30], slide 3: *"Scale Up from 96 to 140 at proposed location."*

6. Range of cumulative oil released

We will now recap our values of each of the three fundamental inputs to the material balance equation, and then calculate the volume of oil released. Recall that the simplified presentation of the material balance equation was:

$$N_p = N.c.\Delta p$$

(6.1)

6.1.1 Connected oil volume, _N_, is 107 to 116 MMstb. The discussion in Section 5 demonstrates that the connected oil volume I use is a possible upper bound. There are nine values, dependent on which set of laboratory data is used to convert from reservoir to surface volumes, and the compressibilities used.[130]

Connected oil volume, _N_ (MMstb)	Fluid properties			
	High (Intertek)	**Middle** (Schlumberger)	**Low** (Core Labs)	_Average (mid case)_
High case rock compressibility	113	111	107	
Mid case rock compressibility	114	112	109	**112**
Low case rock compressibility	116	114	110	

Table 6.1. The calculated volume of oil connected to the Macondo well. These are values of _N_ input directly into the material balance equation.

6.1.2 Effective compressibility, _c_, is 19 to 24 microsips. The compressibility values I use cover the full range of the measured rock and fluid data, Table 4.4 (Section 4.2).

Effective compressibility, _c_ (microsips)	Fluid properties			
	High (Core Labs)	**Middle** (Schlumberger)	**Low** (Intertek)	_Average (mid case)_
High case rock compressibility	24.48	23.64	23.45	
Mid case rock compressibility	22.01	21.16	20.97	**21.38**
Low case rock compressibility	19.76	18.91	18.72	

Table 6.2. The effective compressibility, _c_, that will be used to compute oil released in the material balance equation.

6.1.3 Pressure drop, _ΔP_, is 1,325 to 1,423 psi. Here we have three values for the different fluid properties used (Section 4.3).

	High	Middle	Low	_Average_
Pressure drop, _Δp_ (psi)	1,423	1,354	1,325	**1,367**

Table 6.3. Pressure drops, _Δp_, determined from the pressure match.

6.1.4. Calculated oil released is 2.9 to 3.7 MMstb. I multiply the values for the connected oil volume, compressibility and pressure drop together, Table 6.4. I take values corresponding to the same set of fluid data for consistency. I allow for the full range of measured fluid and rock property data. This is the

---

[130] Tables 4.1 and 4.2 only showed the volumes for the mid-range rock compressibility.

amount of oil released from the reservoir, not what entered the ocean. Oil burnt or collected before reaching the ocean is not subtracted from this total.

I consider that the mid-range compressibility to be most consistent with the data: averaging the numbers for the three sets of fluid properties gives a base-case calculated volume of **3.26 MMstb**.
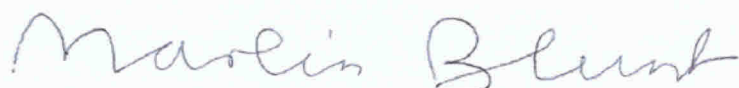
Oil Released (MMstb)		Fluid Properties			
		High	Middle	Low	Averaged
Rock Properties	High	3.74	3.57	3.47	
	Middle	3.41	3.24	3.15	3.26
	Low	3.10	2.94	2.86	

Table 6.4. The predicted oil released in million stb (MMstb) using the material balance equation (6.1).

6.1.5. Conclusion. This report contains all my analysis, my conclusions and the reasons for them. The opinions that I have expressed are based on my review of the documents referred to in this report,[131] in the light of my education and experience.[132] I may do further analysis to supplement my findings after receiving any subsequent Government expert reports or other relevant information.

I am receiving £280 per hour for my work on this case, though I understand that the contracting agency of my university, by whom I am paid, receives £350 per hour.

May 1, 2013

Martin Blunt

_____

---

[131] A complete bibliographic list of the documents referred to in forming my opinion is provided in Appendix N.
[132] My academic CV is provided in Appendix L and my full publications list in Appendix M.

Appendix A.   Data analysis details

A.1.   Introduction and data sources

Table A.1 shows the data that I have used with a brief justification of the choice.

Quantity	Symbol	Data source	Value	Unit	Comments
Connected Oil Volume, _N_: 107-116 MMstb					
Gross rock volume	V	BP seismic interpretation [9]	1,530	rb	Assess 87-90% connectivity
Porosity	ϕ	Log analysis [6]	0.217		Thickness-weighted average over 93 ft
Oil saturation	S_o	Log analysis [6]	0.878		Thickness-weighted average
Initial oil formation volume factor	B_{oi}	Service laboratory reports [18,20,32,34]	2.2708-2.3595	rb/stb	Use values from three laboratories
Compressibility, _c_: 18.7-24.5 microsips					
Oil compressibility	c_o	Service company reports [18,20,32,34]	13.70; 13.90; 14.82	microsips	Track exact change in volume for calculated pressure drop for three sets of service company data
Pore volume compressibility	c_f	Weatherford measurements [24,26] and Dr. Zimmerman [Z]	4.34; 6.35; 8.57	microsips	Range based on measured data to match change in pore volume
Water compressibility	c_w	Literature value, Osif (1988)	3	microsips	Has negligible impact on the calculation
Pressure Drop, _Δp_: 1,325; 1,354; 1,423 psi					
Densities for conversion from capping stack to reservoir	ρ	Whitson tables [W] and Core Labs measurements [20]	Varies	kgm^{-3}	The Whitson tables provide a consistent extrapolation for temperatures lower than studied experimentally. Retain direct data for Core Labs to provide an experimentally-based lower bound.
Temperatures for density values	T	Solution of heat transport equations, Appendix B	40-243	°F	Take literature values of thermal properties. At late time, behaviour insensitive to values used.
Pressure difference between capping stack and reservoir	$p_w\text{-}p_{cs}$	Calculation of head, Appendix B	3,210-3,435	psi	Computed for three sets of fluid properties. Conversion tabulated as a function of capping stack pressure and time since choke closure.
Pressure readings	$P_{cs}(t)$	Trusler report [T]	Varies	psi	Capping stack pressures after choke closure
Final reservoir pressure	p_f	Section 4.3, Appendices C and D	10,433-10,531	psi	From fit to analytical linear flow model
Times to reach reservoir boundaries	τ	Section 4.3, Appendices C and D	Varies	s	Using analytical linear and rectangular flow models
Subsidiary variables used in the consistency check, Section 5					
Permeability	K	Gringarten report [ACG], core measurements [1,23] and pressure analysis, Section 4.3, Appendix E	170-329	mD	From Gringarten expert report including upper range
Viscosity	μ	Whitson table [W] for Core Labs sample 19 at 9,800 psi and 10,500 psi	0.205, 0.2197	mPa.s	Measured data inconsistent between labs. Use well-bore pressure in radial flow period, final pressure for reservoir boundaries.

Table A.1. Summary of the data used in my calculations.

I have relied on data in the reports provided by the independent service laboratories mentioned below. For Core Labs I have taken the data from the less dense sample,[133] giving the higher estimate of oil released: additional data is summarized in BP's Post-Well Technical Memorandum.[134] I have also employed values for fluid and rock properties determined from expert reports, although I have performed my own appraisal of the data.

A.1.1 Core Labs (Pencor) data. Core Labs received the down-hole Macondo fluid samples shortly after collection. Later they provided samples to Intertek and Schlumberger for analysis. The Core Labs data I use is taken from a spreadsheet.[135] The formation volume factor for a single-stage flash at the saturation pressure (the bubble point pressure, when gas first exsolves from the oil) and a temperature of 242°F is given in tab "Res. Fluid Summary C50" cell C48 (the value is 2.618). I use the tables of fluid density from tabs "CCE at 100 °F", "CCE at 170 °F" and "CCE at 242 °F". The densities are found at a given temperature and pressure by linear extrapolation, as outlined below, from the tabulated values. The formation volume factor is the value at saturation pressure multiplied by the ratio of the density to the density at the saturation pressure. Viscosity as a function of temperature and pressure is taken from the tables in the "Viscosity" tab.

A.1.2 Schlumberger data. Here the data is taken from the pdf document [34]. The formation volume factor at the saturation pressure, 2.539, is taken from the table at the bottom of page 4 (called the "zero flash"). Tables 24 and 25 are used for fluid densities. I use the Anton Parr values (the other set of values are similar to less than 0.2%). Viscosities were not measured.

A.1.3 Intertek data. Here the spreadsheet [32] is used to find the formation volume factor at the saturation pressure, 2.5104 ("Summary" tab, cell C27). Then another spreadsheet [18] contains tabulated data for fluid density at the reservoir temperature, 243°F (Table 3, located, confusingly, under tab "Table 4"). I have used the values with a mixer – a magnetic stirrer – since this more rapidly establishes thermodynamic equilibrium in the system. While measurements were taken at a lower temperature of 100°F, there are no absolute measurements of fluid density (no single-phase flash was performed at this temperature to obtain these values). I use the viscosity data in Table 8 of [18].

A.2 Fluid properties and petrophysical analysis

A.2.1 How compressibility is calculated. The definition of the isothermal compressibility for oil is:

$$c_o = -\frac{1}{V_o}\frac{\partial V_o}{\partial p}$$

(A.1)

---

[133] *See* the Pencor deposition [66], exhibit 8584, page 5, that shows a reservoir condition density of 0.583 g/cm^3. This is from sample 19 and is the data I use. Compare with sample 53: exhibit 8583, where the same measurement gives a higher value of 0.587 g/cm^3.

[134] BP-HZN-2179MDL03290054 (BP Post-Well Subsurface Technical Memorandum, [6] , pages 40 and 41).

[135] BP-HZN-2179MDL00063084 (for sample 19) (Core Labs fluid property report) [20]. Core labs did analyse another sample, 53, and obtained similar results; I have not used this data directly though. I have used the sample with the lower density as mentioned in the main text.

where V_o is the oil volume. However, the compressibility of the oil (and rock) is not constant, but varies with pressure. In the material balance equation (and the analytic analysis – Appendix C) a single compressibility value is used: this is not the derivative of volume change with pressure, as in Eq. (A.1) but a difference, so that $c\Delta p$ is strictly the fractional change in volume for a pressure drop Δp in Eq. (3.1).

In reservoir engineering, we normally define oil expansion in terms of the oil formation volume factor: the derivation that follows is a little clumsy but straightforward. Originally the oil volume in the reservoir is $V_{oi} = Ah\phi S_o$; at the surface its volume is $N=V_{oi}/B_{oi}$. The reservoir pressure drops and finally reaches a value p_f with oil formation volume factor B_{of}. The surface volume is the same, but the reservoir volume at this final, lower, pressure is larger $V_{of}=NB_{of} = V_{oi} B_{of}/B_{oi}$. The difference is the volume produced. This has a reservoir volume $V_{oi}(B_{of}/B_{oi} -1) = Ah\phi S_o(B_{of}-B_{oi})/B_{oi}$. Using Eqs. (A.1) and (3.1) this defines c_o as:

$$c_o = \frac{B_{of} - B_{oi}}{B_{oi}\Delta p}$$

(A.2)

In the material balance analysis I can find the appropriate value of c once I know the pressure drop Δp. I take the Δp determined from the pressure analysis (see Appendix D, Section 4.3 and Table A.5). There is a negligible change in properties if other possible values of Δp are used.

A.2.2 I use linear extrapolation to find properties. In all calculations, to find properties at a given temperature and pressure, I use linear extrapolation between the closest sets of data (that is measured data at the nearest pressure and temperature conditions). This is a standard approach and employed, for instance, in reservoir simulators. The equations are readily used in a spreadsheet.

I wish to find the value of a property A at a known temperature T and pressure P. Imagine that I have the tables below. The two values of temperature and pressure chosen will be those closest to T and P – usually values above and below the required values.

Then I calculate:

$$A(T,p) = (T - T_1)\left[\frac{(p - p_{2a})A_{2b} + (p_{2b} - P)A_{2a}}{(T_2 - T_1)(p - p_{2a})}\right] + (T_2 - T)\left[\frac{(p - p_{1a})A_{1b} + (p_{1b} - p)A_{1a}}{(T_2 - T_1)(p - p)}\right]$$

(A.3)

A.2.3 Log analysis. When the Macondo well was drilled it encountered three layers of sandstone that contained oil with impermeable shale in between, shown in Figure 4.4.[136] The oil-bearing rock was

---

[136] In this report I will accept BP's interpretation of hydrocarbon-bearing sandstone encountered in BP-HZN-2179MDL04440267 (Macondo OOIP) [8]; BP-HZN-BLY00120160 (BP summary of permeability, porosity and saturation) [16] and will consider the layers M56 D, E and F to comprise the Macondo reservoir. I will include M56F despite the suggestion by Pinky Vinson from BP that this may not be hydrocarbon bearing (*see* Pinky Vinson's deposition [48], page 341, lines 14-24). Excluding M56F from the analysis would reduce my calculations of oil released by 100,000 - 140,000 stb (3-4% of the total).

detected through logs – these are down-hole measurements of density and electrical conductivity that can be used to infer the presence of oil. These measurements were used to find water saturation (the fraction of the void space of the rock filled with water – the rest is filled with oil) and porosity. Fluid samples were collected down-hole and analyzed. Rock core samples about an inch in diameter and almost two inches long were drilled out of the side of the well-bore, and their properties were measured.[137] The fluid samples were used to determine – among other things – the ratio of the volume of oil in the reservoir to its volume at surface conditions. Porosity was measured on the rock samples to calibrate the calculations from the logs.

$T=T_1$

Pressure	Value of A
p_{1a}	A_{1a}
p_{1b}	A_{1b}

$T=T_2$

Pressure	Value of A
p_{2a}	A_{2a}
p_{2b}	A_{2b}

Table A.2. Example data at different temperatures and pressures to illustrate linear extrapolation of values.

The results of this analysis, taken from BP's reports, are tabulated in Table A.3. I have then determined average values of porosity and oil saturation.[138] The average porosity[139] calculated from the logs – 21.7% – is close to the average of the core measurements – 22.2%.[140] For reference, BP's calculated permeability values are also shown.[141]

Anadarko also performed a preliminary petrophysical analysis. Their conclusions would lead to a smaller oil volume – and hence oil released. However, their results were not calibrated against core data, since this was not available at the time. This is discussed further in Appendix A.7.

---

[137] These were rotary sidewall cores: cylindrical samples of rock drilled out from the side of the well. They are typically around 1.7 inches (4 cm) long with a diameter of 1 inch (2.5 cm).

[138] I use a thickness weighting of the values in each layer as shown in Table A.3. *See* BP-HZN-2179MDL04440267 (Macondo OOIP) [8]; BP-HZN-BLY00120160 (BP summary of permeability, porosity and saturation) [16].

[139] This is the average porosity for the 16 core samples taken from layers M56D and M56E for which permeability – see Appendix A.5 – was also measured; BP-HZN-2179MDL02394182 (Weatherford permeability measurements) [23].

[140] The 16 core measurements have an average porosity of 0.222. Using this value (as opposed to 0.217 in Table A.3) would increase the volume of oil released by approximately 2% (60,000 stb) because of a larger calculated oil volume. However, the log-derived values – from the whole 93 ft of oil-bearing sandstone encountered by the well – are more representative of the reservoir than the average of 16 core measurements on samples around 2 inches long.

[141] These values are discussed further in Appendix A.5: they are the geometric averages in each layer, corrected for oil flow and the presence of water.

Layer	Layer thickness (ft)	Porosity	Permeability (mD)	Oil saturation
Top (M56D)	22	0.2067	86.53	0.8283
Middle (M56E)	64.5	0.2208	275.22	0.903
Bottom (M56F)	6.5	0.2108	110.39	0.7815
Average (total)	93 (total)	0.217	219	0.878

Table A.3. The properties of the three oil-bearing sandstone layers penetrated by the Macondo well.[142] I have computed the average porosity, permeability and oil saturation using a pore-volume weighted average. The permeability is shown for reference: it is the geometric average of the permeability calculated within each layer, corrected for oil flow and the presence of water.

A.2.4 Steps to find the initial oil in place. BP analyzed the seismic data to calculate the initial oil in place *before* the Macondo well was drilled. There are four steps in the calculation: determining the volume of rock that contains oil; correcting for the fact that most of the rock is solid; correcting for the percentage of pore space containing water; and converting the reservoir volume of oil to surface volume. I will describe each step in turn: this is the standard approach used universally in the industry. I also arrive at essentially the same number found in the Kelkar & Raghavan report.[143]

BP determined the total horizontal area, A (4,482 acres) over which it expected to encounter oil and the average height of permeable oil-bearing sandstone over this area, h (44 ft).[144] The volume of oil-bearing rock is therefore Ah. This is called the gross rock volume.

The reservoir rock is composed of solid grains fused together, with pore space in between containing oil and water. We are only interested in the oil volume. To find that oil volume, Ah is multiplied by the porosity ϕ, the fraction of the rock volume that is pore space. The result is the volume of void space in the reservoir rock – the space that can be filled with fluid. This is called the pore volume.

We then multiply the void space of the reservoir by the oil saturation, S_o – the fraction of the void space that contains oil. This is less than 1, as there is always some water present in reservoir rock: the rock was originally saturated with water, and oil migrated into the reservoir, forcing out most – but not all – the water. This gives us $Ah\phi S_o$, which is the oil volume in the reservoir.

Then the oil volume at the surface, called the stock tank oil initially in place, STOIIP, is given by:

$$STOIIP = Ah\phi S_o / B_{oi}$$

(A.4)

A.2.5 Summary of fluid properties. The three sets of measured data are broadly consistent. I will use all three in my calculations. Table A.4 below compares values of oil formation volume factor with those

---

[142] BP-HZN-BLY00120160 (BP summary of permeability, porosity and saturation) [16]; *see also* BP-HZN-2179MDL04440691 (BP summary of log analysis) [15], slide 25.

[143] While the reservoir oil volume is similar in the Kelkar & Raghavan report, they not use a measured value to convert this to a surface volume (*see* Section 4.1), and assumed full connectivity.

[144] BP-HZN-2179MDL05173765 (BP gross rock volume assessment, slide 1) [30], for the most likely case. *See also* BP-HZN-2179MDL06566208 (BP Pre-Drill Review) [31], slide 15; and BP-HZN-2179MDL04440267 (Macondo OOIP, row 12) [8] for height h (44ft), and row 26 for area A (4,482 acres).

from the BP fluid property tables (see the discussion below).[145] As a basis of comparison, I show here the calculated properties at the initial reservoir pressure (p_i=11,856 psi)[146] and at the final pressure (determined from the pressure analysis, Section 4.3). For the calculation of initial oil in place, I need to know only the initial B_{oi}, but the final-pressure B_{of} will be used later for the calculation of compressibility. Table A.5 shows the oil compressibilities (Section 4.2).

The three sets of measured data give consistent values of B_o and c_o: the discrepancy in values is around 5%. These are difficult measurements made on a complex fluid at high temperatures and pressures.

Property	Core Labs	Schlumberger	Intertek	BP tables
B_{oi}	2.3595	2.3031	2.2708	2.1431
B_{of}	2.4093	2.3455	2.3129	2.1841
p_f (psi)	10,433	10,531	10,502	10,502

Table A.4. Comparison of fluid data used in the analysis. The subscript i refers to initial conditions (pressure of 11,856 psi) and f to final reservoir conditions. B_o is the oil formation volume factor. p_f is the predicted final pressure from an analysis of the capping stack pressure build-up presented in Section 4.3: I find different values dependent on which set of fluid data is used. The final pressure is not calculated for the BP tables: the Intertek value is used to determine properties for comparison only.

Property	Core Labs	Schlumberger	Intertek
c_o (microsips; ×10^{-6} psi^{-1})	14.819	13.899	13.703

Table A.5. Comparison of measured oil compressibility. This is one component of the total or effective compressibility used in the material balance calculation.

A.2.6 BP fluid property tables, and the value of B_o used by the Government, have a bias. BP created tables of oil properties for Macondo.[147] These use thermodynamic correlations[148] tuned to match the data to construct a convenient tabulation of properties for use in further analysis, including simulation tools. As seen in Table A.4, there is a significant discrepancy between the oil formation volume factor in the BP table used by the Government and the appropriate value of formation volume factor for this problem.[149] Any conversion from reservoir to surface volumes is inversely proportional to the value of B_o used. Use of these BP tables leads to approximately a 6-10% increase in calculated oil volume released, dependent on what measurement it is compared to. Since these BP tables are not reports of direct measurements, and because we do not know the purpose or origin of these tables, I conclude that they should not be used for this analysis.

[145] Viscosity was also measured by Core Labs and Intertek (see Appendix A.1 and BP-HZN-2179MDL00063016 (Core Labs fluid property report) [19];BP-HZN-2179MDL04440732 (Intertek fluid property report) [18]; For reference, the Core Labs data gives values of 0.2026 and 0.1876 mPa.s for initial and final reservoir conditions respectively, while the Intertek measurements give 0.2610 and 0.2462 mPa.s for initial and final conditions respectively. I do note that the difference in these measurements may be the result of different experimental techniques. I will use the viscosities computed using an equation of state in the Whitson report in this analysis.
[146] See Appendix A for a justification of this value.
[147] BP-HZN-2179MDL04578104 (BP fluid property tables) [5]. In the oil industry these are called "black oil" tables. While crude oil is indeed black in colour, this is a technical term referring to the characterization of the oil as being liquid (stock tank oil) containing gas that is dissolved in the oil at reservoir conditions.
[148] Technically these correlations are called equations of state.
[149] It is not clear if the BP Tables record single-stage or multistage separation values, which could explain the discrepancy. In any event, my approach is to stick to the measured data.

However, the value of B_o in one BP table was also used in both the Kelkar & Raghavan and Pooladi-Darvish reports. This is the principal reason for their over-statement of oil volume. This value was also used in the Griffiths report, again introducing a bias.[150]

A.2.7 Data summary. For reference Table A.6 shows the information I will use to find oil in place. It helps illustrate the sequence of multiplications to find the reservoir volume of oil. Then I divide by the values of B_{oi} in Table A.4 to find the initial oil in place.

Area, A (acres)	Average height, h (ft)	Gross rock volume, Ah (MMrb)	Porosity, ϕ	Oil saturation, S_o	Reservoir oil volume, $Ah\phi S_o$ (MMstb)	Connectivity %	Connected oil volume Mid case (MMrb)
4,482	44	1,530	0.217	0.878	291	87-90	258

Table A.6. Compilation of data used to find the reservoir volume of oil in the Macondo reservoir. I assume that 87-90% of the oil is connected to the well. I then divide by B_{oi} to find the connected oil volume measured at surface conditions: Table A.4.

A.2.8 Gas/oil ratios. In addition to the comparison of properties presented in Table A.4, I have also compared the measured gas/oil ratios: this is the ratio of gas volume to oil volume measured at stock tank conditions for a single-stage flash. Table A.7 shows numbers that are broadly consistent across the three laboratories. Here the BP tables are almost exactly the same as the Intertek data.

The gas/oil ratio has been used to convert a total flow of oil and gas in the ocean determined from *in situ* observations, to an effective oil flow rate at the surface.

Property	Core Labs	Schlumberger	Intertek	Average of the measurements	BP tables
R_s (scf/stb)	2,906	2,945	2,831	2,894	2,833

Table A.7. Comparison of measured gas/oil ratios R_s. scf is a standard cubic foot and stb is a stock tank barrel.[151]

A.2.9 Definition of oil formation volume factor. Oil is more valuable than gas, and so fields are operated to collect as much oil as possible. The heavier gas components – propane and butane – can, with judicious chemical engineering, be dissolved in the oil phase, leaving a lower volume of a so-called lean gas composed almost entirely of methane and ethane. You can increase the amount of oil recovered by preferentially separating out the gas at higher pressures (and temperatures) and then letting the depleted oil reach equilibrium with the remaining dissolved gas. This can happen naturally in the reservoir below the bubble point (the saturation pressure), if gas is preferentially produced: this is called differential liberation (of gas). The amount of oil collected can also be maximized through multistage separators at the surface that are designed to collect as much liquid (oil) as possible. I note that much of the fluid property data concerns measurements of differential liberation and multistage separator

---

[150] *See* Section 4.1 and Appendix F for more details.

[151] BP-HZN-2179MDL00063084 (Core Labs fluid property report, "Res. Fluid Summary" tab, cell B48 for single-phase flash) [20]; BP-HZN-2179MDL01608973 (Schlumberger Fluid Analysis on Macondo Samples, , zero flash value) [34] , page 4; and BP-HZN-2179MDL04440977 (Intertek multi-state separator tests and compositions) value from "Summary" tab, cell C28 (for single-stage separator test) [32]. The Whitson [W] table values are the average of the values provided based on the samples analyzed by the different laboratories.

tests.[152] These can give lower values of B_o (meaning more oil at the surface). I will not use these values, as they do not correspond to the circumstances of the Macondo spill. The oil remained above the bubble point in the reservoir, and oil and gas remained in equilibrium in the well-bore before being released to the ocean, or collected. I quote from Muskat's classic work *The Physical Principles of Oil Production* (p76):

Implicit ... has been the assumption that the solubility and shrinkage properties of crude-oil and natural-gas systems are independent of the thermodynamic paths followed between terminal points, i.e., reservoir and atmospheric conditions. This, of course, will be true if the total hydrocarbon content be kept fixed and the gas and liquid phases are maintained in continuous contact... Such a process (for fixed total composition) is termed "flash liberation" or "flash vaporization." An example of its occurrence in practice is the variation in pressure and temperature of the stream of oil and gas as it flows up the well bore to the surface under steady-state conditions.

During the Macondo spill, the oil and gas maintained continuous contact from the reservoir to the exit point. Hence, the single-stage flash (called flash liberation in the quotation above) B_o – and not the B_o obtained from a separator analysis has been used in my calculations. This is discussed further in Appendix F.2.

A.3   Rock properties

As with oil, the compressibility – the fractional change in volume per unit change in pressure – changes with pressure. To track exactly the volume change for the calculated change in pressure in the reservoir, I define the pore volume compressibility as follows, to be consistent with material balance Eq. (3.1):

$$c_f = \frac{\epsilon(p_f)}{\phi(p_i - p_f)}$$

(A.5)

where ε is the volumetric strain (the fractional change in rock volume) as a function of pressure. As before, I take p_f to be 10,500 psi – the final answer is insensitive to the exact choice within around 100 psi. ϕ is the initial porosity and p_i is the initial pressure (when the strain is 0) which – in these experiments – is 11,800 psi.

Using this approach I obtain values of 7.41, 3.74 and 5.32 microsips for the three samples.

Dr. Zimmerman in his expert report [RWZ] examined the Weatherford pore volume compressibility. I will use his (higher) values – in Table 4.3 – for my calculations.

There is little definitive public domain data that might help constrain the value of pore volume compressibility further than discussed in the main text. A paper published by authors from Chevron, ENI and Baker Atlas (Wolfe *et al.*, 2005) by the Society of Petroleum Engineers reports laboratory measurements of c_f that lie between 1 and 2 microsips for deep Gulf of Mexico sandstones. They

---

[152] See, for instance, BP-HZN-2179MDL04440977 (Intertek multi-state separator tests and compositions) [32]; BP-HZN-2179MDL04440978 (Intertek multi-state separator test results) [33].

propose a method to calculate pore volume compressibility from logs that shows reasonable agreement with direct measurements on both whole cores and rotary sidewall cores. Liu *et al.* (2008) quote a range of compressibility between 1 and 10 microsips for Gulf of Mexico reservoir of similar geological age to Macondo, with a base case of 3 microsips.

Ostermeier from Shell (2001) presents an overview of the compressibility of Gulf of Mexico sandstones. He distinguishes two classes of sandstone: the first are poorly consolidated and highly compressible with a compressibility that increases as the fluid pressure declines. He reports compressibilities as high as 100 microsips. In Macondo, however, the sandstone is of the second class (again this is clear from a study of data from other fields in the Gulf of Mexico provided by BP[153]), with a lower porosity and a compressibility that declines with declining pore pressure. He reports one set of measurements with values less than 10 microsips.

There are correlations in the literature to predict pore volume compressibility from porosity for sandstones. For instance, the Hall (1953) correlation can be used to calculate compressibility from porosity. For Macondo, this gives a value of 3.5 microsips.

The mineralogy of the sandstone also suggests a relatively incompressible rock compared to other samples from the Gulf of Mexico. Weatherford determined that the Macondo sandstone is 93% quartz (ranging from 91-94% on the core samples studied) with on average 3% clay.[154] Ostermeier, from Shell, in a Distinguished Author article in the *Journal of Petroleum Technology* (Ostermeier, 2001), provides a review of Gulf of Mexico rock compressibility. He comments that rocks with high quartz content – as in Macondo – have low compressibilities: the quartz is very hard compared to more ductile, or easily deformed, components of the rock, such as clay. Quartz-rich sandstones can have a high compressibility only if the grains contact at sharp points: the grains can then easily rotate and compress into the pore space. However, for a system of this relatively low porosity, and buried at high temperature, there is likely a relatively high degree of cementation (the grains are stuck or fused together).

It is not possible to make a more definitive statement on likely pore volume compressibility: I will be guided by the direct measurements that do appear to be in a plausible range, albeit at the upper end, based on my reading of the literature.

I conclude, for reference, with Figure A.1 which shows the correlations used by BP to estimate compressibility before drilling. While consistent with a value of 6 microsips, the considerable scatter emphasizes the importance of checking the value with directly measured data.

---

[153] BP-HZN-2179MDL06566208 (BP Pre-Drill Review, slide 17) [31].
[154] BP-HZN-2179MDL02394187 (Weatherford rock composition analysis) [37].
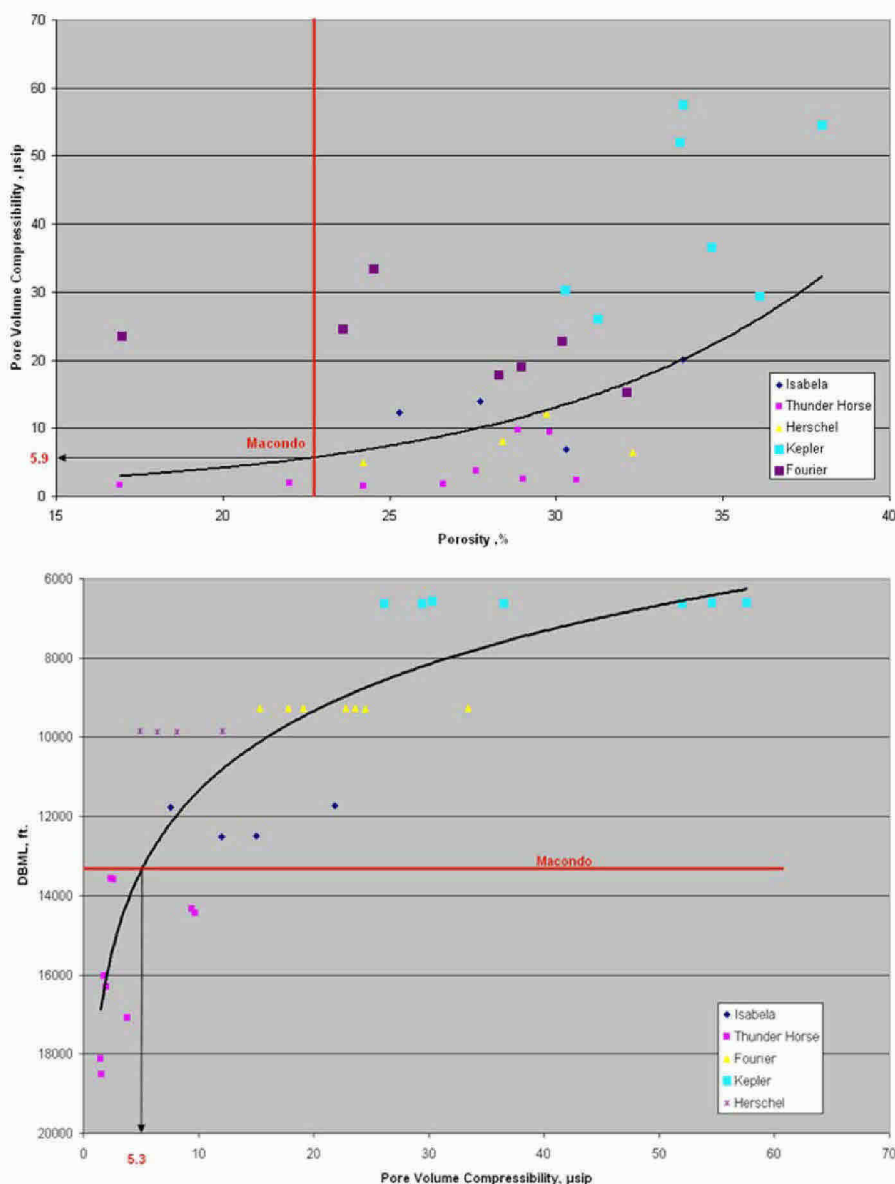
Figure A.1. The correlation between pore volume compressibility and porosity (top figure) and depth (bottom figure) for Gulf of Mexico fields taken from a BP report prepared before drilling.[155] 1 μsip is a microsip or 10^{-6} psi^{-1}. The graphs – with some scatter – indicate a compressibility of between 5 and 6 microsips, close to the average of the measurements – Table 4.3.

A.4   Total compressibility

I simplified the material balance equation (3.1) to emphasize the key data that contribute to the calculation of oil released: equation (3.1) is correct but requires a non-standard definition of compressibility presented in Section 4.2. The more standard expression in the oil industry (Dake, 1978) for material balance is as follows:

---

[155] BP-HZN-2179MDL06566208 (BP Pre-Drill Review, slide 17) [31].

$$N_p = LWh\phi \cdot c_t \cdot \Delta p / B_{of}$$

(A.6)

$LWh\phi$ is the connected pore volume of the reservoir, Δp is the pressure drop and B_{of} is the oil formation volume factor at the final reservoir pressure.

c_t is the total compressibility:

$$c_t = c_r + S_o c_o + S_w c_w$$

(A.7)

where the subscripts r, o and w stand for the rock, oil and water respectively. c_t is the combined compressibility of the rock, oil and water. The void space is full of fluid, hence S_o + S_w =1.

The effective compressibility used in the main text is $c = \left(\frac{B_{oi}}{B_{of}}\right)\left(\frac{c_t}{S_o}\right)$ where the total compressibility is given by Eq. (A.7).

Table A.8 provides the values of total compressibility multiplied by porosity that I calculate. This is – traditionally – the direct input into the material balance equation (A.6).[156] I take a fixed value of pore volume compressibility, but average the fluid compressibilities for each layer using the height-weighted average to find the effective value for a given set of fluid and rock properties.

Total compressibility times porosity (microsips)	Core Labs	Schlumberger	Intertek
High case	4.76	4.58	4.54
Mid case	4.28	4.10	4.06
Low case	3.84	3.67	3.63

Table A.8. The total compressibility multiplied by porosity, using the full range of measured pore volume compressibility and oil compressibility from the three sets of fluid data.

A.5   Permeability

While permeability does not enter into the material balance equation directly, it is a key component of a consistent model of the reservoir. This is because permeability ties together the variables in the material balance analysis, allowing us to confirm (or question) the reliability of our values for each variable.

The permeability will allow us to assess the size of the connected reservoir – determined from the pressure response – and to compare this with the seismic interpretation.

Permeability is also a crucial parameter in the Hsieh and Pooladi-Darvish reports that use reservoir simulation: the flow rate is directly proportional to permeability. Hence, through over-stating the permeability, they over-estimated the volume of oil released.

Hence it is important to review the permeability measurements.

---

[156] The approach in the main text and here are mathematically equivalent and give exactly the same values of oil released.

Permeability is typically the most uncertain parameter in a reservoir engineering analysis. Hence, it is unwise to hinge a prediction of flow rate – and hence oil released – directly on one inference of its value without checking for consistency with other parameters. Furthermore, in this report we carefully compare and critique permeability determined by different methods: direct measurements on core samples, correlations to down-hole measurements, measurements on neighbouring fields and deduction from pressure analysis.

Like pore volume compressibility, permeability is measured on inch-long rock samples taken from the reservoir. In the laboratory, permeability is found from the relationship between flow rate and pressure gradient – embodied in Darcy's law which we describe mathematically in Appendix C. It is relatively easy to perform this measurement using a dry core (with no liquid inside) by measuring air flow. However, air and oil flow are not identical and a correction needs to be made to reduce the air-measured permeability. Furthermore, in the reservoir, the rock also contains water. This water does not flow, but it restricts the volume occupied by oil and further reduces the permeability to oil.

There are four main sources of evidence for permeability that I review below: Weatherford's direct core measurements, BP's down-hole (log) analysis, data from other fields in the Gulf of Mexico, and literature values. In addition, in the main text (Section 4.3), I calculate permeability directly from the pressure analysis. Finally, and most importantly, Dr. Gringarten has provided the most robust determination of permeability from pressure measurements made down-hole just after drilling the well. I will use these values in my calculations for the reasons outlined in this Section.

A.5.1. Core measurements: permeability is 364 mD. Weatherford reported a series of measurements of permeability on the core samples taken from the reservoir sandstones contacted by the Macondo well.[157] Permeability was measured using two synthetic oils flowing through 19 cores: the values obtained ranged from 7 to 181 mD. The arithmetic mean (average) of all the oil measurements is 75 mD. The oil flow measurements were made on the cores as they were received in the laboratory and before they were cleaned and dried.[158] As a consequence, the pore spaces of the rock could be clogged with drilling fluid ("mud") and associated sand dislodged during drilling and extraction of the core samples. Hence, while oil flow reproduces the conditions pertaining in the reservoir under production, these values may be unrepresentative. However, this observation indicates that the rock in the near-well-bore region had a reduced permeability. This could have restricted flow, particularly in the early period of the spill.[159]

Weatherford also reported air permeability measurements on 16 cleaned cores that were drilled from the two main sandstone layers: M56D (6 samples) and M56E (10 samples): photographs of these cores are shown in Figure A.2. The average air permeability is 474 mD with a range from 64 to 756 mD. The

---

[157] These are contained in a series of spreadsheets: BP-HZN-2179MDL05223139 (Weatherford permeability measurements to oil) [1]; BP-HZN-2179MDL00470598 (Weatherford summary of cores collected) [21]; BP-HZN-2179MDL00470599 (Weatherford rotary core summary) [22] provide summaries of the cores collected and tested; while BP-HZN-2179MDL02394182 (Weatherford permeability measurements) [23] reports the measurements on cleaned samples.

[158] See Pinky Vinson's deposition [47], page 110, lines 9-11.

[159] This is discussed further in Appendix E.3.

air permeability was corrected to represent liquid (oil) flow.[160] I have calculated an average (mean) of 442 mD.[161]

M56D – upper sandstone layer

M56E – middle sandstone layer
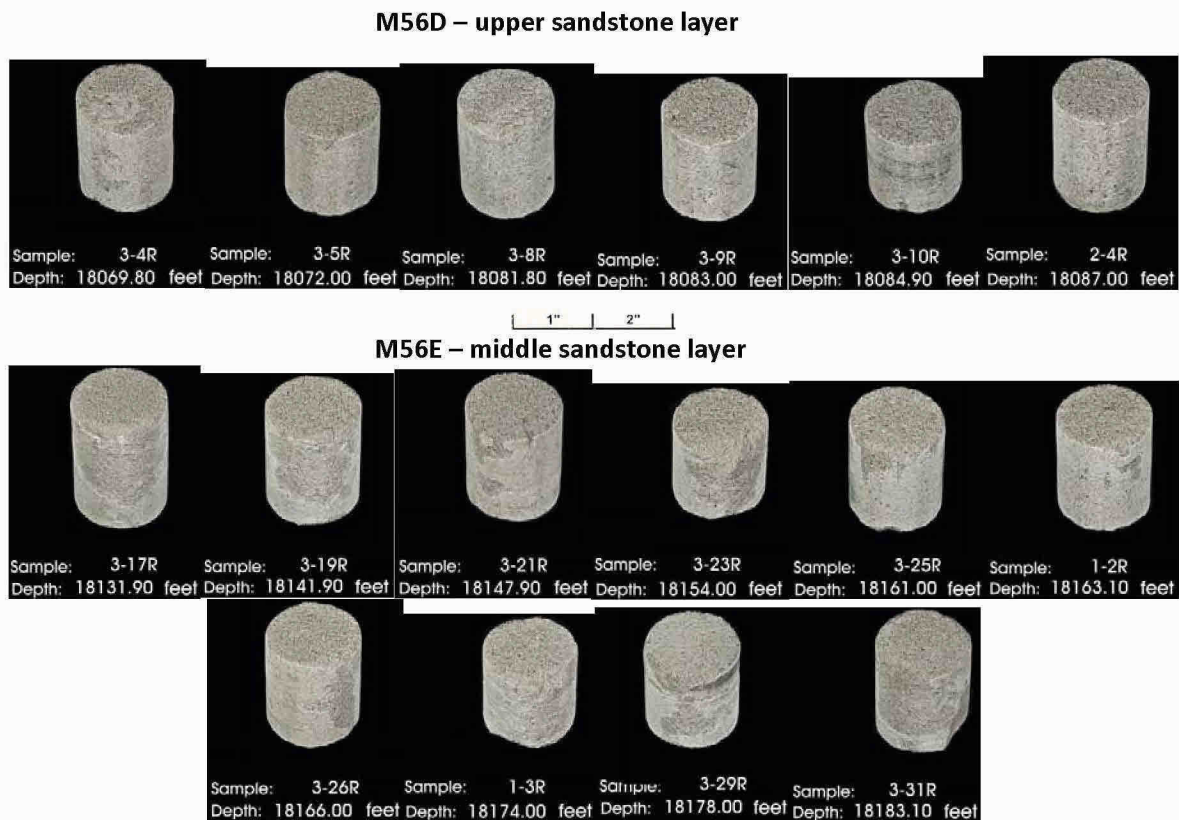
Figure A.2. Photographs of the 16 cores from the two main sandstone layers M56D and M56E, for which permeability was measured.[162] The flow-based average permeability to oil is 364 mD.

It is not best practice simply to use the mean of the permeability measurements to represent the average for field-scale production. For three-dimensional flow, the geometric average within each layer[163] is more representative, since this better captures the flow conditions in the reservoir. I also

---

[160] Air permeability is modified using the "Klinkenberg correction" to account for "gas slippage". Physically, the gas has a finite flow near the solid grain boundaries at the microscopic scale, whereas in a liquid (such as oil) the flow is strictly zero at the solid. This means that the air-measured permeability is higher than the oil-measured values.

[161] My averages are higher than those quoted by Weatherford; I have excluded lower permeability samples that are not from the main sandstone layers as defined in BP-HZN-BLY00120160 (BP summary of permeability, porosity and saturation) [16].

[162] Taken from WFT-MDL-00039841 (Weatherford's core photographs) [51].

[163] Mathematically, this is found from computing the mean value of the logarithm of permeability and then finding the exponential.

correct for the presence of water in the pore space.[164] This makes the oil flow-based average of the Weatherford measurements **364 mD.**[165]

A.5.2. Down-hole measurements: permeability is 219 mD. BP related down-hole (log) readings to core measurements of air permeability.[166] These down-hole measurements use sophisticated tools lowered in the well which record the density and electrical conductivity of the rock – and the fluids within them – close to the well-bore. They provide reliable values of porosity and water saturation. They do not directly study fluid flow; instead a correlation is determined between down-hole readings and permeability measurements taken from rock samples at the same depth. The data from these samples are used with the logs to interpolate the permeability along the entire oil-bearing interval of 93 ft. This is a standard approach and the log-based values are often considered more representative than the average of the core measurements. BP presents the geometrically averaged permeability:[167] as mentioned above, this best reflects the overall behaviour in the layers of sandstone through which the oil flows. This permeability is corrected to account for the presence of water in the pore space. BP calculated average permeabilities[168] of 87, 275 and 110 mD for the top (M56D), middle (M56E) and lower (M56F) sandstones respectively, with an overall average of **219 mD** (Table A.3).[169]

A.5.3. Correlations from other fields in the Gulf of Mexico:[170] **permeability is 400 mD.** BP also presented an overview of permeability measurements on other fields in the Gulf of Mexico and correlated permeability with porosity, shown in Figure A.3 – this is a universally applied method in the oil industry. The expected permeability, using a porosity of 0.225, is around 500 mD. With the measured porosity of 0.217 (Table A.3) the likely permeability based on this correlation is around 400 mD. This is at the upper end of the numbers quoted above.

A.5.4 Literature values. Ostermeier (1996) presents an overview of permeability in Gulf of Mexico sandstones. He considers sandstones with porosities in the range 0.344-0.256, which is significantly higher than the values we see in Macondo (around 0.21-0.22). It is difficult to make a definitive assessment of likely permeability based on the data presented, but extrapolating his measurements to a lower porosity range and accounting for grain size, using his data I would calculate that likely permeabilities are around 200 mD or lower in Macondo.

---

[164] I multiply by 0.85 – see the discussion of BP's log analysis in Appendix A.5.2.

[165] Mathematically, I take the geometric mean of the 6 measurements in layer M56D and the geometric mean of the 10 measurements in layer M56E. I then use the height-weighted average of these two values.

[166] This analysis is presented in BP-HZN-2179MDL03290054 (BP Post-Well Subsurface Technical Memorandum) [6]; permeability values uncorrected for oil flow and water are shown in Figure 35.

[167] These are provided for each layer in the BP spreadsheet; [16].

[168] These are the Klinkenberg-corrected geometrically-averaged air permeabilities multiplied by 0.85 to account for the presence of water. In the absence of direct experimental data, the factor of 0.85 was taken from the Santa Cruz field in the Gulf of Mexico (see Pinky Vinson's deposition [48], page 254, line 25, and page 355, lines 1 and 2).

[169] This is the layer thickness-weighted average of the values.

[170] BP studied other fields in the Gulf Mexico whose data were used by BP to develop correlations between rock properties (for instance, between porosity and permeability) that were then employed to calculate rock properties for Macondo. It does not imply that the value of a property measured at another field is the same at Macondo.

A.5.5 Gringarten pressure analysis: permeability is 238 mD. Dr. Gringarten has analyzed the pressure measurements down-hole performed by Schlumberger before cementing the well in his expert report [ACG]. These provide a valuable flow-based estimate of permeability. This analysis avoids the complexities associated with estimating permeability from the capping stack response because the down-hole measurements include both accurate assessments of rate history and pressure.

The Gringarten analysis provides a reliable estimate of permeability that represents reservoir flow in a region that extends several 100s of ft around the well and so is a flow-based average, rather than a measurement on a small core sample.

As a consequence, I consider his analysis – close to the average of the log measurements – to provide most valid determination of permeability. He quotes a statistical range of possible values between approximately 170 and 329 mD, with 238 mD representing the mid-range (P50) case.

A.5.6 Data-informed permeability range: 200-400 mD. If we exclude the relatively low permeabilities to oil measured by Weatherford, all the other data indicate an average permeability in the range **200-400 mD**. However, the value of permeability does not directly affect the material balance analysis if other properties – oil volume, compressibility and pressure drop – are known.

The Gringarten analysis suggests that the flow-based average permeability in the field is at the lower end of this range.
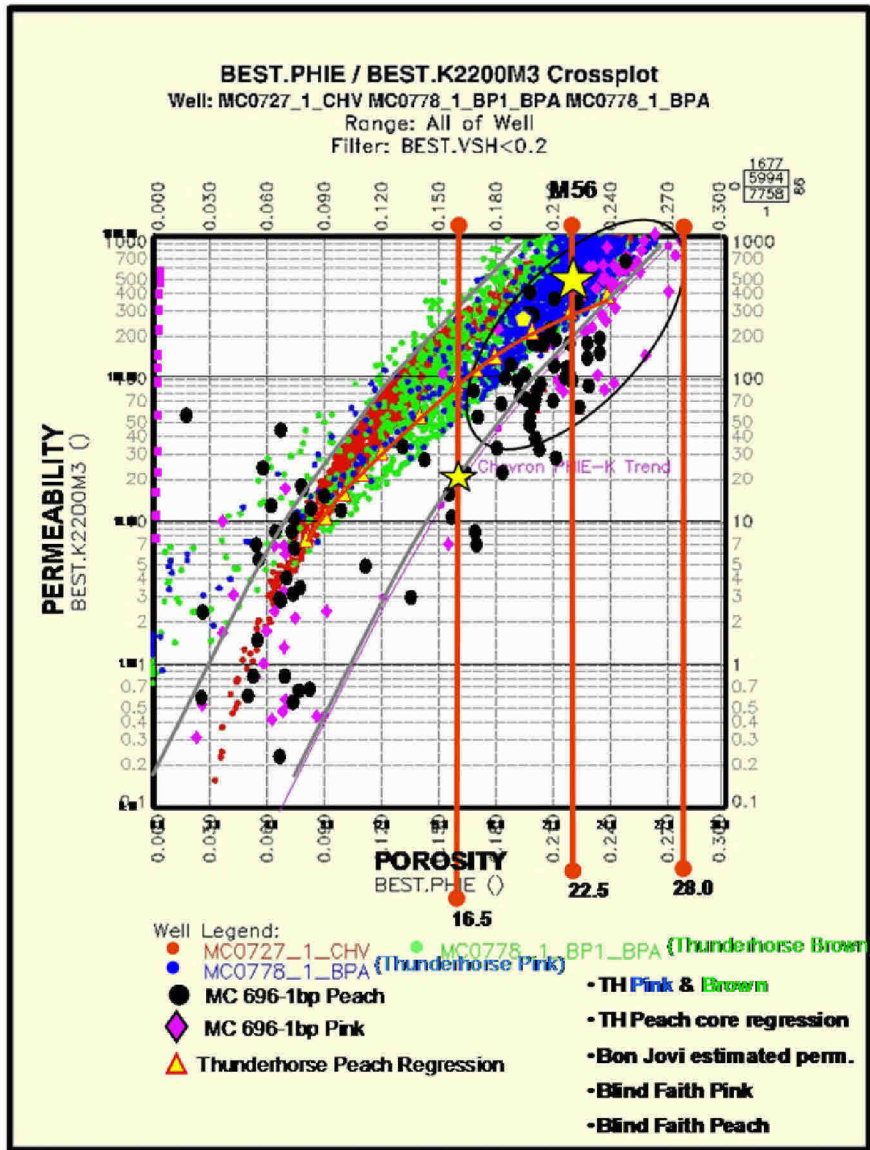
Figure A.3. The correlation between permeability and porosity for Gulf of Mexico fields.[171] BP estimated a mean porosity – before drilling – of 0.225 giving an expected permeability of approximately 500 mD for Macondo. With the measured porosity of 0.217 (see Table A.3), the average permeability is approximately 400 mD.

---

[171] BP-HZN-2179MDL06566208 (BP Pre-Drill review, slide 14) [31].

TREX-011553-R.0068

A.6   Datum depths, pressures and temperatures

Using the BP technical notes [14] and emails [4] the pressure transducers in the capping stack were located at a depth of 4,912 ft below the sea surface. This is 12 ft below the top of the HC connector [14].

The sea floor is at a water depth of 4,992 ft [4].

I need to relate the capping stack pressure to the reservoir pressure. Using the BP summary spreadsheet [16] I choose a datum depth approximately mid-way through the middle – thickest – layer. The top layer is at 18,034.1 TVDSS (true vertical depth sub-sea) and the bottom is at 18,105.0 ft. The middle is therefore at 18,069.6 ft. The datum depth given is 18,065 ft which is close to the middle of the sandstone. However, there may be a transcribing error in the spreadsheet, since the original Schlumberger MDT report [63] implies a different depth, 18,056 ft, which I use.[172]

The initial reservoir pressure is hence 11,856 psi[173] at a depth of 18,056 TVDSS.[174] The initial reservoir temperature is 243°F.[175]

The vertical distance from the capping stack transducer to the datum reservoir depth is 18,056-4,912 = 13,144 ft (rounded to the nearest ft).

A schematic of the reservoir, well bore and capping stack is shown in Figure A.4 that explains the distances mentioned above.

A.7   Anadarko petrophysical analysis

Anadarko, a part-owner of Macondo at the time, performed an independent analysis of the log (down-hole) data prior to the accident. These results are preliminary, since it is usual – as for the BP analysis presented earlier in this Appendix – to calibrate the results against direct measurements on core samples taken from the well. This was not done, since, at the time, the results of the Weatherford core analysis were not available.

Table A.9 presents the key Anadarko results compared to those from BP, and the values used in this report. Note that use of the Anadarko data would lead to lower estimates of oil released. However, as noted above, the lack of calibration means that their results are less likely to be representative of the field. I will note, however, that the logs do indicate a lower porosity and permeability than the averages of the core samples.

---

[172] BP-HZN-2179MDL03742328 (MDT report, page 7) mentions a pressure of 11,856 psi at a depth of 18,131 ft. [63]. Then page 28 mentions that the true depth below the sea is 75 ft lower than this, giving a datum depth of 18,131-75=18,056 ft.

[173] Taken from BP-HZN-2179MDL03742328 (MDT report, page 24 from the Test Point Table [63]; also [63] page 7.

[174] BP-HZN-BLY00120160 (BP summary of permeability, porosity and saturation, cell D12) [16].

[175] [BP-HZN-BLY00120160 (BP summary of permeability, porosity and saturation, cell T12) [16]. The initial reservoir pressure and temperature accord to that considered by Dr. Yun Wang at BP (see Edmond Shtepani's deposition [53] page 28, line 22).

The oil saturation estimate was not subject to calibration, and hence, of all the properties shown, is possibly as representative as the BP value. Using the Anadarko saturation would result in a lower estimate of oil released.
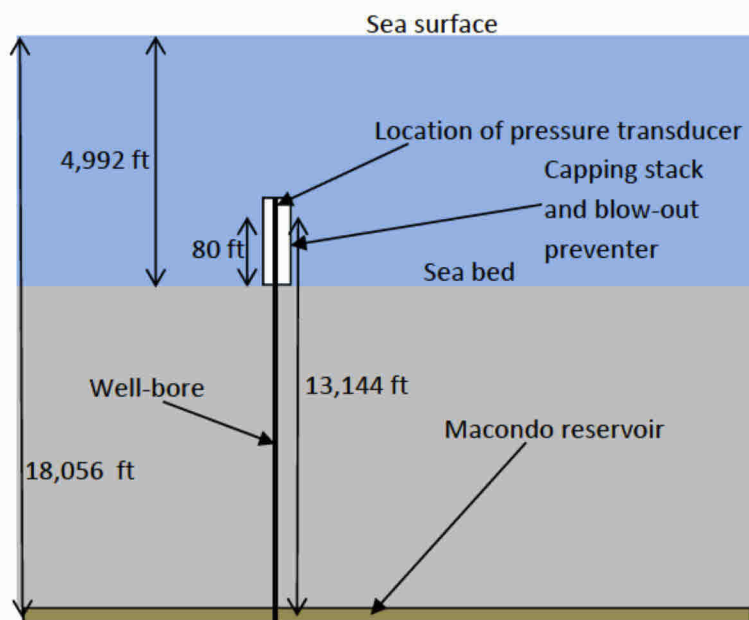
Figure A.4. A schematic of the well bore, capping stack and reservoir geometry taken from [4,14,16,63]. The figure is not to scale. We need to know the distance from the capping stack to the reservoir to calculate the weight of fluid in the well bore and hence to find the reservoir pressure from the measured capping stack pressure.

	Net pay (total layer thickness) (ft)	Porosity	Permeability (mD)	Oil saturation
BP log analysis	93	0.217	219	0.878
Anadarko log analysis	92	0.192	107	0.837
Values I use in my calculations	93	0.217	245	0.872
Effect on oil released of using Anadarko values (MMstb)	-0.04	-0.27	Implies reduced connectivity	-0.05

Table A.9. Comparison of the results of BP's and Anadarko's petrophysical analysis. Also shown is the impact of using each piece of Anadarko data on my estimates of oil released.[176]

---

[176] The BP data is taken from Table A.3. The Anadarko data is taken from Brian O'Neill's deposition [60], page 77, line 4 for net pay; page 79, line 1 for porosity; page 80, line 1 for saturation; and page 81, line 5 for average permeability.

Appendix B. Conversion from capping stack to down-hole pressures

B.1. Requirement to correct the data and the equation used

The measurements of fluid pressure in the capping stack provide valuable information about the reservoir. When the well was closed, the pressure increased over time and was continuing to rise – albeit slowly – when the well was cemented in. The final pressure (had the measurements continued for much longer) helps determine the total amount of oil that was released, Eq. (3.1).

We are interested in the pressure in the reservoir – strictly speaking the pressure down-hole, or the reservoir pressure at the well-bore and at the datum depth. We have measurements at the capping stack. Since – once the well is shut in – there is no net flow, the down-hole pressure is the capping stack pressure plus the weight of fluid from the capping stack to the reservoir. This is a familiar concept: atmospheric pressure is the weight of air above us, while pressure increases with depth in the sea (or a swimming pool) because of the weight of water above you. Indeed, the high fluid pressures encountered in deep oil reservoirs are a consequence of the weight of fluid (and rock) above them.

I will provide a careful analysis of this pressure conversion, since it does have a significant impact on the pressure analysis. Furthermore, this calculation has not been performed properly by any of the Government investigators: specifically they all took a fixed pressure difference, ignoring the increase in its value over time as a consequence of the increasing capping stack pressure and the cooling well-bore, both of which tend to make the oil denser.

The concept is simple, but the details – provided here – touch upon a number of fascinating, classical problems in fluid dynamics.

Mathematically, if the capping stack pressure transducer (where the pressure is measured) is at a depth z_{cs} and the reservoir is at a depth z_r (all depths are measured below the sea surface) then we can relate the down-hole (well) pressure p_w to the capping stack pressure p_{cs} by:

$$p_w = p_{cs} + \int_{z_{cs}}^{z_r} \rho(T,p)g \, dz$$

(B.1)

where ρ is the oil density and g is the acceleration due to gravity (9.81 ms^{-2} in SI units). We know the oil density as a function of temperature and pressure from the fluid property reports presented in Appendix A. The pressure at any depth is – as we have already said – the weight of fluid above it. We can compute density and hence pressure in a step-wise manner starting from the known (measured) capping stack pressure and integrating downwards.

71

B.2   Temperature changes in the well-bore

The deep ocean seawater has a temperature of approximately 40°F (4°C).[177] Below the sea bed, there is a natural geothermal gradient of around 30°C per km (20°F per 1,000 ft), meaning that the rock and fluids get hotter as we go deeper. We know that the Macondo oil is at a temperature of 243°F. It is a reasonable approximation to assume that before the spill the temperature decreased linearly with distance from 243°F in the reservoir to some lower temperature in the capping stack.

B.2.1 Heating the well and the surrounding rock. While Macondo was flowing, hot fluids moved rapidly up the well-bore, heating the well and the surrounding rock, as well as the blow-out preventer. Hence, the flowing temperature of the oil and gas was close to the reservoir temperature. This is a well-known scientific problem, analyzed comprehensively in 1961 by the founder of rigorous well-test analysis, Prof. Hank Ramey.[178] However, when the well was closed, the facilities on the sea bed, the well-bore and the surrounding rock cooled. The process can be modelled using heat transport equations that are similar in form to the ones we use to analyze pressure – this is considered in Section B.3.

B.2.2 Double-diffusive convection. Surrounded by cold sea water, the capping stack cooled rapidly. Cold fluids are denser than warm ones. Hence, the cold oil in the pipe in the capping stack was denser than the warmer fluid below it. This cold oil sunk and warm oil rose, as illustrated in Figure B.1. This is another fascinating problem in fluid mechanics that has received considerable attention, as the same physical phenomenon – the over-turning of fluids because of an unstable density variation – is seen in many circumstances, from the sea below Arctic ice, to the interior of large stars. I recommend the engaging review paper by Huppert and Turner (1981). Technically, our well-bore circulation could be described as double-diffusive convection.[179] The increase in pressure with depth makes the fluids denser, and so is stabilizing. The cooling of the oil at the top is, however, destabilizing. A mathematically similar problem for salt water in a well has been analyzed by Love *et al.* (2007). They define a critical Rayleigh number for the onset of this convection. As I show in Section B.3, this convection started a day or two after choke closure. While it does not directly impact the calculation of pressure difference, it does explain how – on average – we can maintain denser fluids above less dense ones: there was a continual circulation of fluid, which persisted until the well was cemented.

B.2.3 Data tabulation. I will start with the data, tabulating the pressure difference between the reservoir and the capping stack for different temperatures and pressures at the capping stack, Table B.1. I will assume that the temperature increases linearly with depth from some specified capping stack temperature to the reservoir temperature. I evaluate the integral Eq. (B.1) numerically over 10 ft depth increments using standard methods coded into a spreadsheet.

---

[177] See a detailed analysis of temperature in and below the Gulf of Mexico in Forrest *et al.* (2005).

[178] Prof. Ramey was Prof. Gringarten's PhD supervisor at Stanford University and trained the current elder generation of experts in well test analysis. He also co-authored the analytic derivation for flow in a rectangular reservoir used in Section 4.3. The paper referred to is Ramey (1961).

[179] Classically the instability comes from a combination of thermal and concentration gradients. Here it is a combination of thermal and pressure gradients, both of which are governed by diffusive processes.

I have used the fluid property tables provided by Dr. Whitson for the Intertek and Schlumberger fluid properties. These provide a smoother extrapolation than the measurements, while providing a physical basis for the prediction of density at temperatures lower than explored experimentally. I have used the experimental data for the lower-density Core Labs sample (Appendix A.1), which give the lowest pressure differences. The measured and predicted densities vary typically by no more than 0.1%, but the use of the experimental data directly leads to a slightly lower pressure difference, giving a larger estimate of oil released. In order to preserve a rigorous upper bound on my calculations of oil released constrained by the data, I therefore use the Core Labs measurements to provide a lower plausible bound on the pressure difference.

Then I will provide – in Section B.3 – an analysis of how the temperature is likely to have varied over time to provide this pressure conversion founded on basic principles of heat transport. In essence, I invoke conservation of energy.

After choke closure, the well-bore cooled and the capping stack pressure increased. Both effects led to a rise in the pressure difference over time. Using a fixed pressure difference – as do all the Government investigators – under-states the rate of pressure build-up in the reservoir, leading to an over-estimate of permeability (Section 4.3), an under-estimate of the final reservoir pressure and over-statement of the volume of oil released.
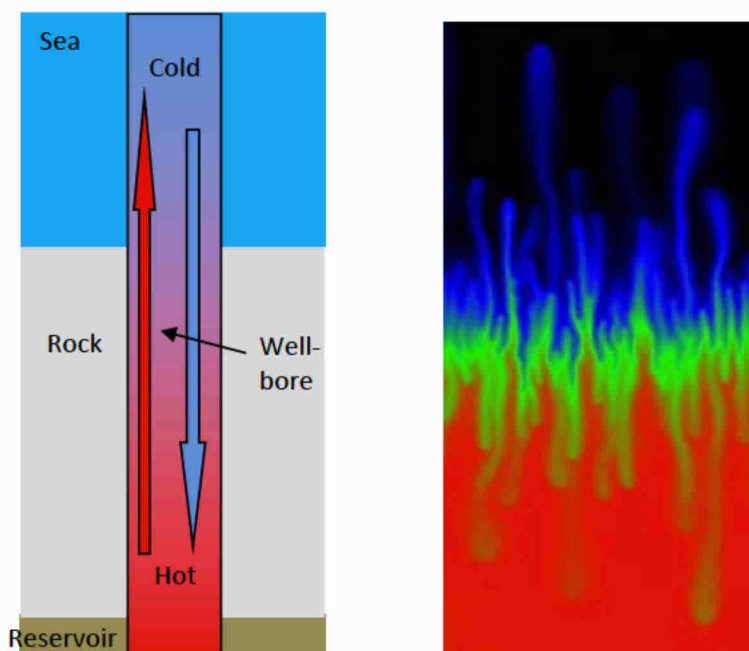
Figure B.1. Left, a schematic of the well-bore when the well was closed. While there is no net flow, cold, dense oil at the top of the well-bore can sink, while hot, buoyant oil rises. This circulation distributes heat along the well-bore and maintains a density that can decrease with depth. To the right is a visualization of an experiment showing a mathematically similar instability caused by concentration gradients of different chemicals dissolved in water.[180]

---

[180] See http://fluidflowvisualization.sandia.gov/double_diffusion.html; Pringle and Glass (2002) from Sandia.

Core Labs properties

Pressure difference between the reservoir and capping stack (psi)	Capping stack temperature (°F)								
Capping stack pressure (psi)	90	100	110	120	130	140	150	160	170
6,600	3,310	3,297	3,285	3,272	3,260	3,247	3,235	3,222	3,210
6,700	3,315	3,302	3,290	3,278	3,265	3,253	3,241	3,228	3,216
6,800	3,320	3,308	3,295	3,283	3,271	3,259	3,246	3,234	3,222
6,900	3,325	3,313	3,301	3,289	3,279	3,264	3,252	3,240	3,227
7,000	3,330	3,318	3,306	3,294	3,282	3,270	3,258	3,246	3,233
7,100	3,336	3,324	3,312	3,299	3,287	3,275	3,263	3,251	3,239
7,200	3,341	3,329	3,317	3,305	3,293	3,281	3,269	3,257	3,245

Schlumberger properties

Pressure difference between the reservoir and capping stack (psi)	Capping stack temperature (°F)								
Capping stack pressure (psi)	90	100	110	120	130	140	150	160	170
6,600	3,403	3,391	3,378	3,366	3,353	3,340	3,328	3,315	3,302
6,700	3,409	3,396	3,384	3,371	3,359	3,346	3,334	3,321	3,308
6,800	3,414	3,402	3,389	3,377	3,365	3,352	3,340	3,327	3,315
6,900	3,419	3,407	3,395	3,383	3,370	3,358	3,346	3,333	3,321
7,000	3,425	3,412	3,400	3,388	3,376	3,364	3,351	3,339	3,327
7,100	3,430	3,418	3,406	3,394	3,382	3,369	3,357	3,345	3,333
7,200	3,435	3,423	3,411	3,399	3,387	3,375	3,363	3,351	3,339

Intertek properties

Pressure difference between the reservoir and capping stack (psi)	Capping stack temperature (°F)								
Capping stack pressure (psi)	90	100	110	120	130	140	150	160	170
6,600	3,375	3,362	3,349	3,337	3,324	3,311	3,298	3,285	3,273
6,700	3,380	3,368	3,355	3,343	3,330	3,317	3,305	3,292	3,279
6,800	3,386	3,373	3,361	3,348	3,336	3,323	3,311	3,298	3,285
6,900	3,391	3,379	3,366	3,354	3,342	3,329	3,317	3,304	3,291
7,000	3,396	3,384	3,372	3,360	3,347	3,335	3,323	3,310	3,298
7,100	3,402	3,389	3,377	3,365	3,353	3,341	3,328	3,316	3,304
7,200	3,407	3,395	3,383	3,371	3,359	3,346	3,334	3,322	3,310

Table B.1. Calculated pressure difference between the capping stack and the reservoir for different capping stack pressures and temperatures.

We can, empirically, write the following equations to predict the pressure difference for specified capping stack temperatures and pressures using Table B.1. For the Core Labs properties we find:

$$p_w = p_{cs} + 3210 + \frac{7}{120}(p_{cs} - 6600) + \frac{5}{4}(170 - T_{cs})$$

(B.2)

with pressure, p, measured in psi and temperature, T, in °F. For the Schlumberger properties:

$$p_w = p_{cs} + 3302 + \frac{37}{600}(p_{cs} - 6600) + \frac{101}{80}(170 - T_{cs})$$

(B.3)

while for Intertek it is:

74

$$p_w = p_{cs} + 3273 + \frac{37}{600}(p_{cs} - 6600) + \frac{51}{40}(170 - T_{cs})$$

(B.4)

The final use of the tables and correlations is to note that convection is likely to start when the density is higher at the top of the well-bore than at the bottom. Using the Core Labs properties this occurs at a temperature of approximately 159°F, while for the Intertek and Schlumberger properties the temperature is 166°F.

B.3 Analysis of temperature changes in the well-bore

B.3.1 The Ramey number and heating the well. The reservoir temperature is 243°F and for 86 days hot oil from the reservoir flowed upwards. This hot fluid heated up the well-bore and the surrounding rock, the blow-out preventer and the capping stack. When flow ceased, the well-bore cooled.

Let us first consider the initial heating of the well and surrounding rock. As mentioned in Section B.2, this problem has been treated in the classic work of Ramey (1961). He found the well-bore temperature as a function of time and depth and used his expression to predict the temperature profiles measured in several wells. I will simplify his analysis. The temperature profile is a function of the following dimensionless number, which I will call the Ramey number R_n:[181]

$$R_n = \frac{\dot{m}C_o}{2\pi\kappa_s H}$$

(B.5)

where $\dot{m}$ is the mass flow rate, κ_s is the thermal conductivity of the rock (and brine within it), C_o is the heat capacity of the oil and H is the distance from the capping stack to the reservoir. The values I use are given in Table B.2. The mass flow rate is given a convenient round number in SI units, based on an average flow rate of around 40,000 stb/day.

B.3.2 I assume that during the spill the well-bore temperature is the reservoir temperature. I find a value of 6 for the Ramey number. For $R_n \gg 1$, the well-bore temperature is, to a good approximation, equal to the reservoir temperature. I will make this assumption: that the well-bore temperature is everywhere and for all times during the spill equal to the reservoir temperature. This is not a bad approximation, but it will tend to over-state the temperature in the well-bore after choke closure and hence under-estimate the fluid density and the final reservoir pressure, and over-estimate the amount of oil released. I will return to examine this approximation at the end of this Section.

B.3.3 Radial heat transport equation. I will now model the heating and cooling of the rock using a radial diffusion equation to represent heat transport. I assume that the temperature gradient with depth is small compared to radial temperature gradients (away from the well-bore). In this case, I can model the system in horizontal cross-section as shown in Figure B.2.

---

[181] This is *A/Zf(t)* using the nomenclature of Ramey (1961). *f(t)* is a time-dependent function that describes the heat transport, which we will quantify later. In this problem its value at the end of the spill is of order 1.

75

The governing partial differential equation is as follows:

$$\frac{1}{r}\frac{\partial}{\partial r}\left(\kappa_s r \frac{\partial T}{\partial r}\right) = \Gamma_T \frac{\partial T}{\partial t}$$

(B.6)

where r is the radial coordinate, T is temperature and t is time. κ_s is the thermal conductivity and Γ_T is the heat capacity (per unit volume) of the rock and fluids (or the annulus). In a homogeneous medium, Eq. (B.6) can be written:

$$\frac{1}{r}\frac{\partial}{\partial r}\left(r \frac{\partial T}{\partial r}\right) = \alpha_T \frac{\partial T}{\partial t}$$

(B.7)

where α_T is the inverse thermal diffusivity:

$$\frac{1}{\alpha_T} = \frac{\kappa_s}{\Gamma_T} = \frac{\kappa_s}{\phi \rho_w C_w + (1-\phi)\rho_s C_s}$$

(B.8)

C is the heat capacity (per unit mass), ρ is density and ϕ is the porosity. I take the values shown in Table B.2 in my calculations.

In Appendix C, I solve the same equation as (B.7) but for pressure. This is done analytically and I go through the derivation carefully, as it is important for the modelling of the pressure response. Here I employ similar techniques, but will provide a much briefer presentation.[182]

First, I need to solve for the initial heating for times $t_p \geq t > 0$, where t_p is the production time (length of the spill period). I assume $T(r > r_w, 0) = T_o$ and impose $T(r \leq r_w, t) = T_r$. The solution is known analytically if the thermal properties of the annulus and the formation – the rock – are the same.[183] Define $\Delta T = T - T_o$, then the Laplace transform is given by:[184]

$$\Delta \tilde{T} = (T_r - T_o)\frac{K_0(\sqrt{\alpha_T s}\, r)}{s K_0(\sqrt{\alpha_T s}\, r_w)}$$

(B.9)

where K_0 is a modified Bessel function of order 0. We then find the temperature profile at $t = t_p$, $T_i(r, t_p)$ and use this as the initial condition for the cooling period.

Formally, if we also consider heat transport in the well-bore itself, again assuming constant thermal properties, the solution for the well-bore temperature during cooling can be written as:

---

[182] More details can be found in the classic reference Carslaw and Jaeger (1946). To be consistent with the pressure analysis in Appendix C, my symbol α is the inverse diffusivity (not, as normal, the diffusivity).
[183] See Carslaw and Jaeger (1946).
[184] Carslaw and Jaeger (1946), page 335, Eq. (3).

$$T(r_w, \Delta t) = T_o + \frac{\alpha_T}{2\Delta t} \int_0^\infty \Delta T_i(r', t_p) e^{-\frac{\alpha_T(r' - r_w)^2}{4\Delta t}} dr'$$

(B.10)

where $\Delta t = t - t_p$ is the time since choke closure.

However, these expressions cannot accommodate different thermal properties for the rock, the oil, and the steel, cement and drilling mud in the annulus. Instead, to account these effects I will solve the equations numerically.

Quantity	Symbol	Value	Unit
Average mass flow rate of oil	$\dot{m}$	100	kgs^{-1}
Distance from capping stack to reservoir	H	4,004	m
Thermal conductivity of the rock and fluids	κ_s	0.7[185]-2.9[186] Base case 1.3	Wm^{-1}K^{-1}
Thermal conductivity of cement	κ_c	0.29[187]	Wm^{-1}K^{-1}
Thermal conductivity of oil	κ_o	0.137	Wm^{-1}K^{-1}
Porosity of sediment	ϕ	0.30	
Heat capacity of seawater	C_w	3,990[188]	Jkg^{-1}K^{-1}
Heat capacity of oil	C_o	2,000[189]	Jkg^{-1}K^{-1}
Heat capacity of sediment (sand or sandstone)	C_s	745	Jkg^{-1}K^{-1}
Heat capacity of cement	C_c	1,550[190]	Jkg^{-1}K^{-1}
Density of seawater	ρ_w	1,027	kgm^{-3}
Density of cement slurry	ρ_c	2,500	kgm^{-3}
Grain density (quartz)	ρ_s	2,660	kgm^{-3}
Reservoir temperature	T_r	243	$^\circ$F
Initial temperature	T_o	40	$^\circ$F
Well-bore radius	r_w	0.10795	m
Maximum well radius	r_m	0.46	m
Base case thermal diffusivity, Eq. (B.7)	$1/\alpha_T$	4.97×10^{-7}	m^{2}s^{-1}
Thermal diffusivity of (stainless) steel[191]	$1/\alpha_T$	4.1×10^{-6}	m^{2}s^{-1}
Thermal diffusivity of cement and oil[192]	$1/\alpha_T$	7.5×10^{-8}	m^{2}s^{-1}
Annular thermal diffusivity[193]	$1/\alpha_T$	16×10^{-8}	m^{2}s^{-1}

Table B.2. Parameters used for my calculation of well-bore cooling.

---

[185] Lower limit for Gulf of Mexico sediments taken from Newson and Brunning (2004).

[186] Sandstone (Berea) value from Incropera and DeWitt (1985), page 756, Table A.3. Also used for heat capacities.

[187] Cement and oil thermal properties from Skalle (2011), page 95, Table 7-1.

[188] Seawater properties taken from Sharqawy et al. (2010) for a salinity of around 35g/kg and a temperature of 5°C.

[189] Average value for fuel oil taken from http://www.engineeringtoolbox.com/specific-heat-fluids-d_151.html

[190] From http://www.engineeringtoolbox.com/specific-heat-solids-d_154.html

[191] Taken from Stankus et al. (2008); other types of steel have a higher thermal diffusivity.

[192] Calculated from the other properties in the table.

[193] A harmonic average of steel and annular values; the calculation is described in the text.

At all times, $T(r \rightarrow \infty) = T_o$

For $t \leq t_p$, $T(r=r_w)=T_r$

For $t>t_p$, constant total energy

$T_o = 40^{\circ}$F; $T_r = 243^{\circ}$F.
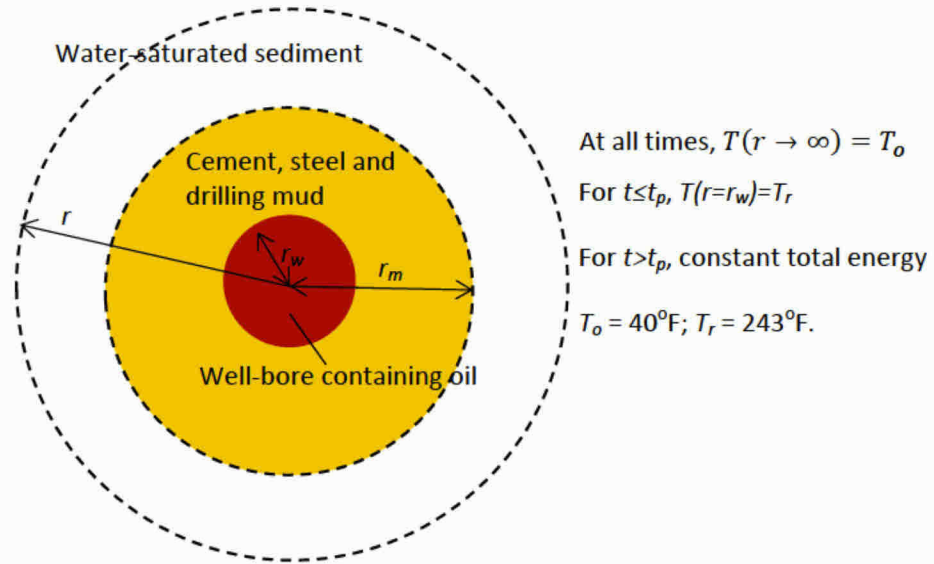
Figure B.2. A horizontal cross-section through the well-bore, the annulus (containing steel, cement and drilling mud) and the surrounding water-saturated sediment below the sea. I assume that during the spill, the oil in the well is at a reservoir temperature of 243°F, and heats the surrounding rock. After choke closure, the rock and oil in the well cool. I calculate the temperature in the well as a function of time using similar techniques employed in Appendix C to compute the pressure response, as, mathematically, the equations are the same. In the figure T is temperature.

I have solved Eq. (B.6) numerically using standard explicit finite differences, with linear increments in radius Δr (0.05-0.1 m) and small time steps δt (160 s in the cooling period) to ensure stability:

$$T_i^{n+1} = T_i^n + \frac{2\delta t}{\Gamma_{Ti}\Delta r^2(r_i + r_{i-1})}[\kappa_i r_i(T_{i+1}^n - T_i^n) - \kappa_{i-1} r_{i-1}(T_i^n - T_{i-1}^n)]$$

(B.11)

where the subscript i labels the radial grid block and the superscript n the time level. $r_{i=0} = r_w$ and I solve in the rock or annulus for $i \geq 1$.

The initial condition is: $T(r,t=0)=T_o$. During heating $T(r \leq r_w, t)=T_r$; during cooling I compute the temperature in the well using the oil heat capacity in Table B.2.

B.3.4 Predicted temperature profiles. Figure B.3 shows the temperature as a function of radius from the well at the end of the spill ($t=t_p=7.6\times10^6$ s or 85 days and 17 hours) and just before the well is cemented ($\Delta t = 1.6\times10^6$ s or almost 19 days later). We see that the hot oil heats the rock to a radius of around 3 m, consistent with a simple calculation that the affected region is given approximately by $2\sqrt{t_p/\alpha_T}$. In this calculation I have assumed that the annular region has the same thermal properties as the surrounding rock. I will return to challenge this assumption later.

The rate of heating – computed by summing up the excess heat energy introduced into the system – is approximately Π = 640 kW. This corresponds to an average temperature loss $\Delta T = \Pi/\dot{m}C_o$ in the flowing oil of around 3 K or 6°F. Hence, it is not a bad approximation to assume more-or-less constant

78

temperature conditions. However, closer to the sea bed, exposed to the cold ocean, there will be further cooling: the maximum temperature measured for oil collected from the well was 221°F,[194] indicating a 22°F temperature drop.
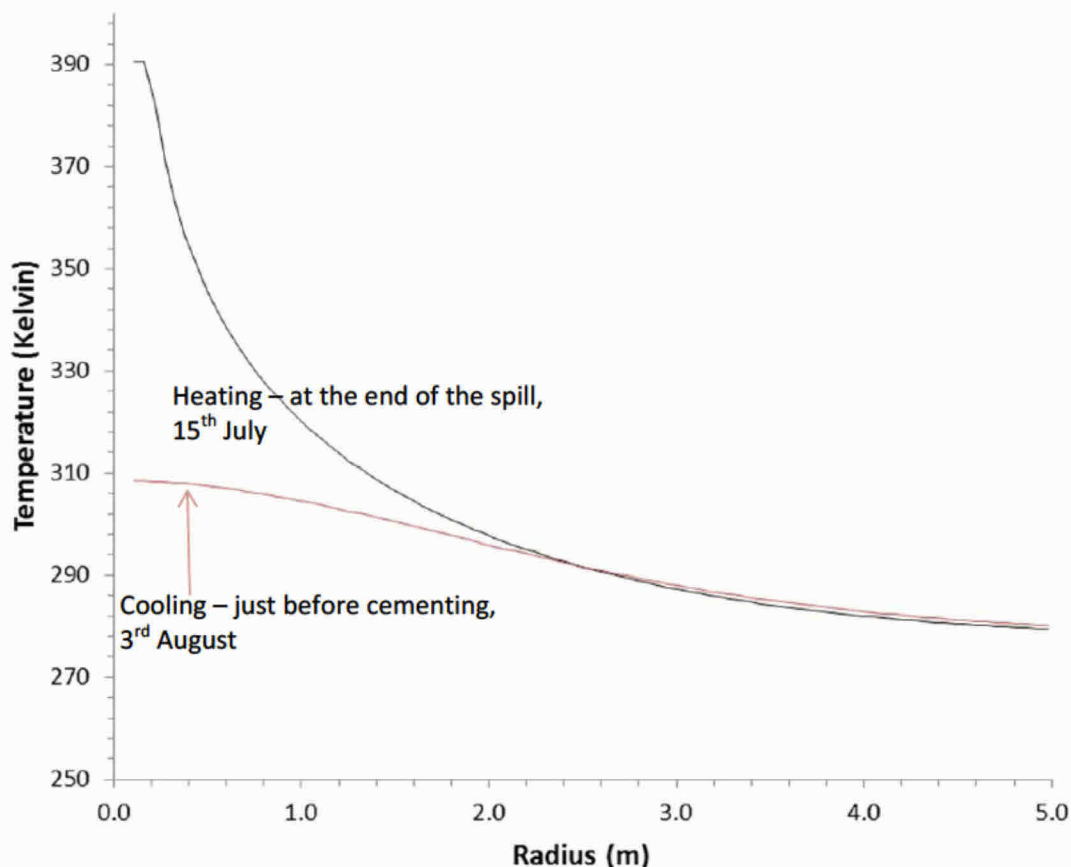
Figure B.3. Predicted temperature in the rock as a consequence of heating from the hot fluid in the well during the spill, followed by cooling after choke closure. The temperature profiles at the end of the spill, and just before the well is cemented are shown. The final well-bore temperature is around 310 K or 95°F.[195] This case shows the temperature close to the top of the well, just under the sea bed.

As discussed below, just as in the pressure analysis, at late time the build-up is dominated by the cumulative flow, here the cooling is controlled by how much heat energy entered the rock. Figure B.4 compares the heat flux into the rock as a function of time during heating (equivalent to the flow rate for a pressure analysis) compared to analytical solution for early time.[196] The agreement between the numerical solution and theory is excellent, indicating that my solutions are converged.

After choke closure, the temperature profile continues to spread, but with no net heat exchange. The temperature at the well drops to around 310 K or 95°F.

---

[194] 105°C measured by Reddy *et al.* (2012).

[195] I have performed these calculations in SI units.

[196] Taken from Carslaw and Jaeger (1946), page 336, Eq. (9).

79

Figure B.5 shows the temperature at the well as a function of depth. The profiles at the end of the spill and just before the well was cemented are shown. I have performed many simulations at different depths and – to a very good approximation – the temperature profile at any one time simply varies linearly from the value computed from Figure B.3 to 243°F at the reservoir depth.
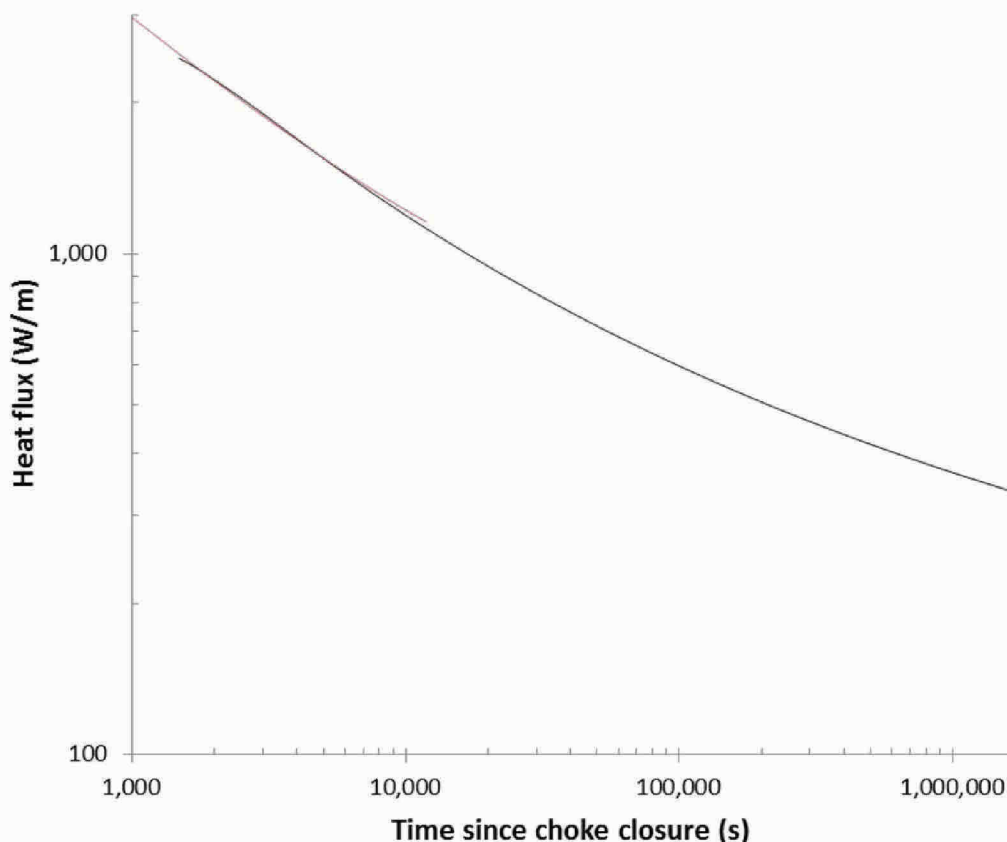
Figure B.4. Predicted heat flux as a function of time (black line) compared to analytical early-time solution of the heat transport equation (red curve). The predictions show an almost exact correspondence to the comparable Fig. 42, page 338, in Carslaw and Jaeger (1946).

Figure B.6 shows the temperature at the well-bore as a function of time after choke closure. Three cases are shown, assuming different thermal conductivities of the rock (the values shown in Table B.3). The fastest cooling occurs for the most conductive rock, representing consolidated sandstone, with slower cooling for less conductive, unconsolidated sediments. The base case is the upper end of the range measured for Gulf of Mexico sediments below the sea bed, but this conductivity is lower than deeper, more consolidated rock (see Table B.2). The final well-bore temperature, before cementing, is 95±5 °F at the sea bed.

Temperature (Fahrenheit)
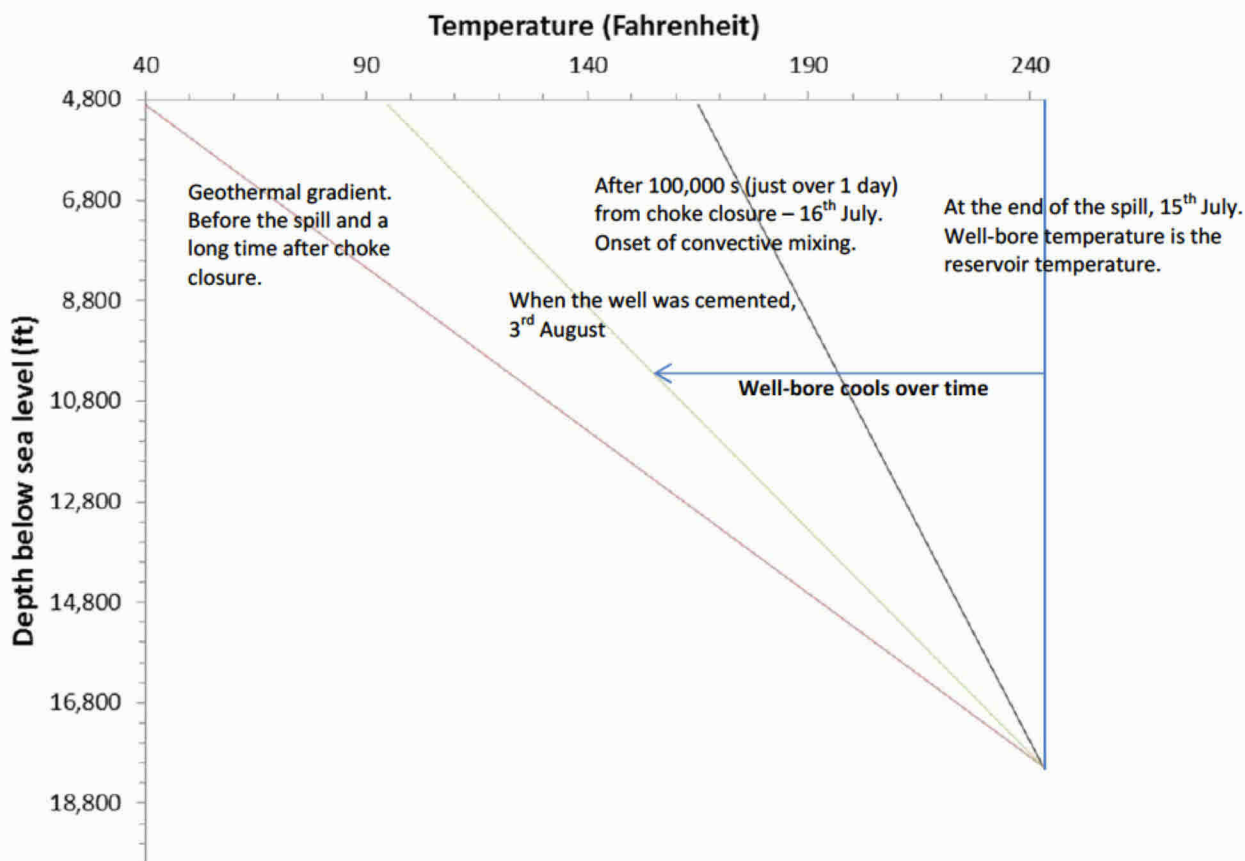
Figure B.5. Predicted temperatures at the well-bore as a function of depth, at different times. To a good approximation, at any given time the temperature varies linearly with depth from some (decreasing) value at the sea bed to 243°F at the reservoir. After around 1 day (100,000 s) we see the onset of convective mixing. This may locally distort the temperature profiles, giving regions of constant temperature with depth. However, conservation of energy prevents the average temperatures varying significantly from what is shown here.

It could be argued that the well-bore cools slower near the top because the sediments are less conductive, and faster at the bottom, where the rock is more consolidated. On the other hand, the extra cooling from the ocean (considered below) and the fact that – at the top of the well – the initial temperature is not exactly 243 °F at choke closure, means that the well-bore may in fact be cooler at the top than I have calculated. I consider it a reasonable approximation to take one base case, constant, value for the rock properties, and use this to compute the temperature profiles; these approximations are considered in more detail below.

The oil in the well-bore cools, on average, by 74°F. This represents a cooling rate of approximately 4 kW. This is less than 1% of the average rate of heating of the rock during the spill. I have also computed the temperature profiles assuming no heat exchange between the oil and the rock; this affects the temperature profile by less than 1 degree. Hence, the contribution to the energy balance of the oil in the well is small, but is included in the results I show here.

81
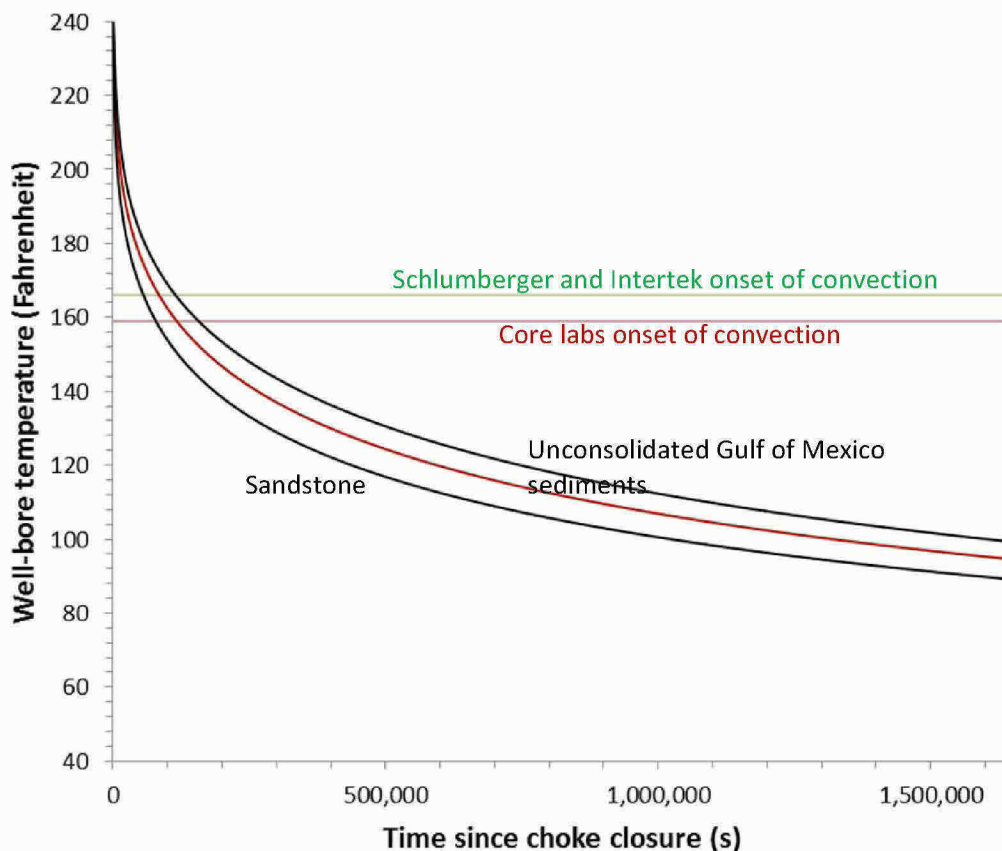
Figure B.6. The predicted well-bore temperature as a function of time near the sea bed. I then assume a linear increase in temperature with depth as shown in Figure B.5. The lowest curve assumes that the rock surrounding the well is sandstone, while the other curves show the range of properties for unconsolidated Gulf of Mexico sediments (see Table B.2). The red curve is the base case used in my calculations. Convection in the well-bore starts after about 1-2 days when the temperature marked by the horizontal lines is reached. When the well was cemented, the calculated well-bore temperature is 95±5 °F.

B.3.5 Cooling from the ocean. The other source of cooling is the ocean itself. The well and surface equipment sits some 92 ft above the sea bed and this will cool rapidly. It is possible to make a rough approximation of the degree of cooling using an empirical value of 300 $Wm^{-2}K^{-1}$ for heat transfer between fluids (seawater and oil) across steel.[197] The temperature drop driving the cooling is assumed to be the difference between the computed well-bore temperature and the sea temperature. Then taking an effective radius of the well-bore of around 0.4-0.5 m – the annular diameter near the top of the well – I estimate an average cooling rate of around 400 kW. This is comparable to the heating rate of the rock and so is potentially significant, leading to much lower temperatures in the well-bore. However, this very simple calculation over-states the cooling. The temperature in the oil above the sea bed will likely be close to 40 °F and the complex flow pathways in the capping stack and the blow-out preventer could possibly delay or prevent effective heat exchange with the well-bore below the ocean

---

[197] The value for the heat transfer is taken from http://www.engineeringtoolbox.com/overall-heat-transfer-coefficients-d_284.html

82

floor. I will ignore any additional cooling from the sea, but it does indicate that my assumptions are conservative: it is unlikely that the well-bore temperatures I have calculated are over-estimated.

B.3.6 Convective mixing in the wellbore. The final discussion — before getting to a quantitative relationship to convert capping stack to reservoir pressures — is to consider the impact of convection on this analysis. As shown in Figure B.6, after around 1 day the well-bore has cooled sufficiently that the oil at the top is denser than the oil at the bottom. This is unstable. This will lead to convective circulation — with hot oil rising and cold oil falling — if we are above a critical Rayleigh number R_a. Love *et al.* (2007) showed that for flow in a well, the onset of convection occurs for:

$$R_a = \frac{g\alpha_o\Delta\rho r_w^4}{\mu H} > 215.6$$

(B.12)

$\Delta\rho$ is the density difference between the top and the bottom of the well, while α_o is the inverse thermal conductivity of oil. I estimate that less than 1 degree of cooling below the temperature indicated in Figure B.6 is sufficient for the onset of convection, with Rayleigh numbers of 50,000 or more developing later. This convection is illustrated in Figure B.1.

There is no doubt that convection occurs, but what does this mean? Traditionally, for a system that is heated from below and cool at the top, the convection maintains an approximately constant temperature profile with depth apart from narrow boundary layers at the top and bottom. The temperature is close to the average of the top and bottom values. In Macondo this would lead to the deep oil being cooler than the rock and the oil further up being hotter. Since heat exchange with the rock is very efficient, on average the oil must maintain, more-or-less, the same temperature as the rock. I am not aware of any study of this interesting problem: it is possible that several convection cells develop with a stair-step change in temperature with depth, as seen in the ocean below the Arctic ice (Huppert and Turner, 1981). However, overall, simply from consideration of conservation of energy, in this essentially closed system, with the vast majority of the heat energy stored in the rock, I cannot conceive of any mechanism that will significantly change the average temperature in the well-bore from what I have calculated. Even if we were to allow the temperature to be constant with depth, at a value that is the average of my computed sea bed temperature and the reservoir temperature, this will reduce the pressure difference I present next by only approximately 10 psi out of a total of around 3,300 psi.

B.3.7 Radial heat transport. I will now convert the computed temperature as a function of time to a pressure difference between the capping stack and reservoir.

Figure B.7 shows the computed temperature profiles plotted as a function of the logarithm of time. Note that after around 1 day (100,000 s) the temperature decreases almost exactly in proportion to log(*Δt*). This is not coincidental. As I discuss in Appendix C, diffusion in a radial geometry — after the input of a constant heat flux (or a constant flow rate) followed by a no-flow period — leads to a temperature (or pressure) that decreases linearly with the logarithm of time at sufficiently late times. In this case the boundary conditions are different, but at late time the functional form of the heat

83

transport is largely independent of the boundary conditions: heat is added to the system and it diffuses radially.[198]

We will use the same concept later in our discussion of the pressure response: at late time, the behaviour is controlled solely by the total heat energy introduced (in this case) or the cumulative flow (for pressure): the analysis is insensitive to the details of the heat transfer or flow rates over time.
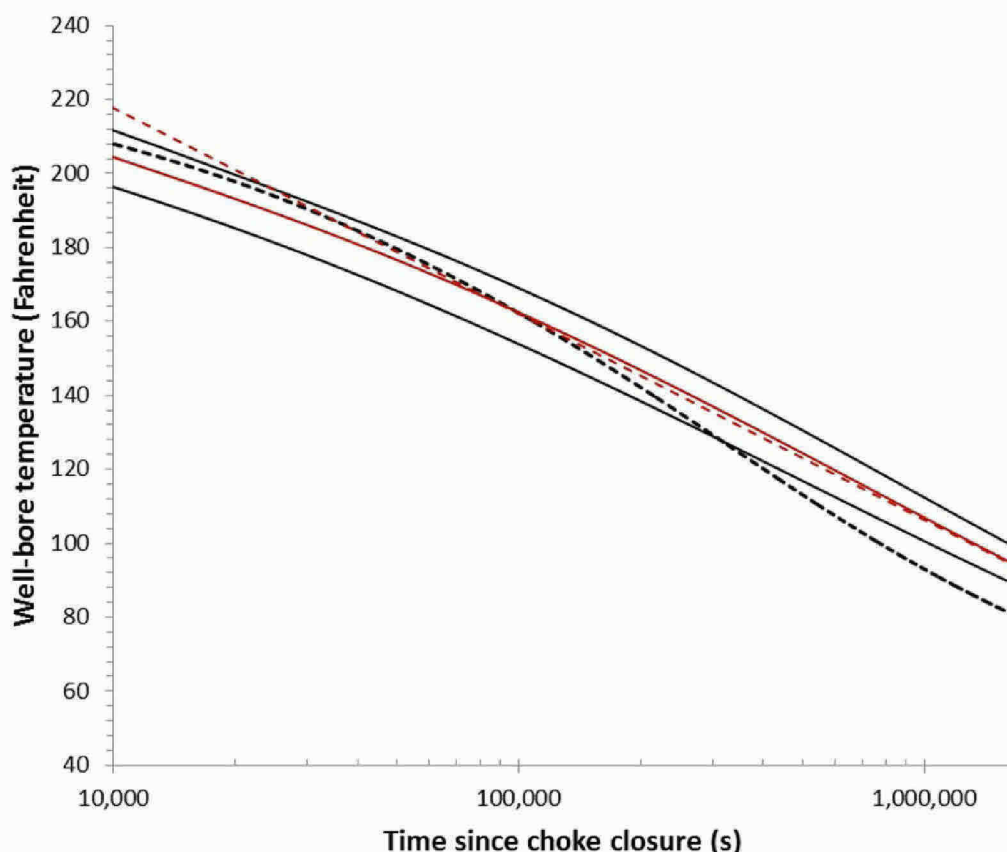
Figure B.7. The predicted well-bore temperature as a function of time near the sea bed. Here time is shown on logarithmic axes, indicating that the temperature decreases linearly with ln(Δt); this is the classical time dependence for radial transport, which we will encounter again in Appendix C for pressure. For times greater than around 100,000 s the temperature of the base case (middle curve in red) is given by: $T = 162 - 55.7 \log_{10}(\Delta t/100,000)$ for temperature in °F and time in s – this trend is shown by the dashed red line. The other solid lines are the cases shown in Figure B.6. The dashed black line shows the impact of assuming an annular region of lowered thermal conductivity near the sea bed.

The temperature decreases as ln(ΔT) with a slope η_T. Without a full derivation, which uses the results of Appendix C, this slope η_T is approximately:[199]

---

[198] This is discussed in Ramey (1961).

[199] Taken for the late-time expression of flux, Carslaw and Jaeger (1946), page 336 and using the final flux as an approximately constant heat transfer rate.

$$\eta_T \approx \frac{(T_r - T_o)}{\ln\left(\frac{4\alpha_T t_p}{r_w^2}\right) - 2\gamma}$$

(B.13)

where γ is Euler's constant (0.57722). This is relatively insensitive – as we see – to the fluid and rock properties used. Theoretically the value is 34°F; the slope of the line in Figure B.6 for late times (greater than 1 day or 100,000 s) is around 55.7°F, which gives η_T of 55.7/log(10) = 24°F, a somewhat lower value, since the slope is still, slowly, increasing, and we consider the cooling of oil in the well itself.

B.3.8 Consideration of heat transport in the annulus: a more-likely case. The Macondo well, as any deep oil well, consisted of a telescope-like arrangement of progressively smaller holes with depth. At the sea bed the hole had a radius of around 18 inches (0.46 m).[200] Surrounding the oil is a concentric arrangement of cement, steel casing and drilling mud. Steel conducts heat very efficiently, but the mud (mainly oil) and the cement will – generally – have a lower thermal conductance than the formation itself (see Table B.2).

I have adopted lower-bound estimates of the thermal properties of the Macondo well from the literature in Table B.2. In Figure B.7 I present a case where I have considered the impact of the annulus near the sea bed. I have made the following assumptions which I consider a more-likely case than the results presented previously:

- During the heating period I take a well-bore temperature of 237°F, corresponding to my predicted cooling of 6°F in the well; this is still less than the cooling (22°F) measured directly during the spill.[201] This accounts for the extra cooling during the spill from the ocean.
- I assume an annular radius of 0.46 m (36 inch diameter). At the sea bed, the inner 22 inches of the well contained 11.87 inches of metal casing.[202] I calculate an effective thermal diffusivity from a harmonic average of 11.87 inches of steel and 10.13 inches of cement and oil (the arithmetic average of α_T).[203] I then apply this value over the larger 36 inch diameter hole. Overall the presence of steel in the well approximately doubles the thermal diffusivity from its value with just oil and cement: the number I use is shown in Table B.2.

This case is very interesting: a slower initial cooling (in the first 10,000 s), and then a rapid cooling after around 100,000 s followed by – roughly – the same cooling rate, with a final temperature now of only 81°F.

Furthermore, I have ignored direct cooling from the ocean after choke closure. This is likely to be significant, leading to more cooling near the surface compared to my base case, not less, although the

---

[200] Hickman *et al.* (2012).

[201] Reddy *et al.* (2012).

[202] Taken from Appendix W of the BP Accident Report (2010), page 16, Tables 1.2-1.4.

[203] Strictly I find the harmonic average of the thermal conductivity and the volume-weighted average of the heat capacity (per unit volume). In this case though, within the approximations of the data in Table B.2, the heat capacities per unit volume of steel, oil and cement are similar: 3.7×10^6 Jm^{-3}K^{-1}.

effect is difficult to quantify. After all, it is almost certain that the oil actually in the capping stack is at, or very close to, the sea temperature to 40°F, so to presume that it is much hotter just below the sea bed is almost certain an over-statement.

There is one last uncertainty. The natural temperature change with depth below the Gulf of Mexico is not linear but often displays a dog-leg shape, meaning that the average temperature can be higher or lower than a straight-line extrapolation from the sea bed to reservoir depths.[204] The BP Accident Report shows a temperature profile with depth which is non-linear implying slightly higher temperatures on average.[205] I will ignore this, as it has little impact on the calculations.

In the pressure analysis, the key feature is the rate of cooling – the slope of the graph in Figure B.7. After 100,000 s any estimate of the thermal properties of the well and rock– supported by the literature – give almost the same behaviour. I am therefore confident that my analysis is valid in this time period because my pressure analysis is focussed on the late-time (>100,000 s) response, matched with a linear flow model that is insensitive to what may have happened in the first day after choke closure. I will take the mid-range case – the red line in Figure B.7 – for my quantitative analysis. To be conservative, I ignore the additional cooling likely as a consequence of the effects of the annulus and the ocean. In the end, the more likely case makes a difference of only 5 psi to the calculated pressure drop and a less than 0.5% decrease in oil released: I will note though that with this correction, the pressure match is better (to within 1.5-1.7 psi – compare with Table D.2).

B.3.9 Conversion from capping stack to reservoir pressures. I now insert the computed time dependence of temperature (Figure B.6) into Eqs. (B.2) – (B.4). I find, using the Core Labs measurements that

$$p_w = p_{cs} + 3210 + \frac{7}{120}(p_{cs} - 6600) + \frac{5}{4}\left[8 + 55.7\log_{10}\left(\frac{\Delta t}{100,000}\right)\right]$$

(B.14)

with pressure, p, measured in psi and time since choke closure, Δt, in s. For the Schlumberger properties the pressure conversion is:

$$p_w = p_{cs} + 3302 + \frac{37}{600}(p_{cs} - 6600) + \frac{101}{80}\left[8 + 55.7\log_{10}\left(\frac{\Delta t}{100,000}\right)\right]$$

(B.15)

while for Intertek it is:

$$p_w = p_{cs} + 3273 + \frac{37}{600}(p_{cs} - 6600) + \frac{51}{40}\left[8 + 55.7\log_{10}\left(\frac{\Delta t}{100,000}\right)\right]$$

(B.16)

---

[204] Forrest *et al.* (2005).
[205] Appendix W of the BP Accident Report (2010), page 15, Figure 1.5.

Note that this correction will add a constant amount to the predicted reservoir pressure derivative (Section 4.3): both temperature effects in the well-bore and the pressure response of the reservoir itself impact the predicted behaviour.

The correction Eqs. (B.14) – (B.16) is only applicable for late-times (Δt>100,000 s). For my quantitative analysis – to show the predicted reservoir pressures based on the capping stack measurements – I tabulate the temperature as a function of time using the middle case (red solid line) in Figure B.6, and insert this directly into Eqs. (B.2) – (B.4).

I consider this calculation to be robust for the late shut-in period – after around 1 day. It simply uses conservation of energy: during the spill the hot oil delivers heat to the formation and then the formation cools down. At late time, the temperature profile in the well-bore decays as ln(Δt), with a slope only weakly dependent on the rock properties. However, the early-time behaviour is sensitive to the near-well heat transport (just as in well test analysis, the early time build-up is affected by the rock properties close to the well). Hence, the conductivity of the casing, cement and fluid in the annulus could affect the behaviour until the heat transient moves beyond the well and into the rock. A numerical solution of both vertical and radial heat transport, as presented by Wooley (1980), could be used, if the thermal properties of the annulus were known. The focus of the analysis in my report, and any quantitative analysis, considers only the late-time linear or channel flow period.

B.3.10 Discussion of the impact of cooling. The preceding discussion has, inevitably, been rather mathematical. Now, I will try to discuss the behaviour a little more qualitatively, to draw attention to its significance, before quantifying how a neglect of this effect impacted the estimates of the Government investigators.

Why is the cooling insensitive to the thermal properties of the rock, and why does an insulating annulus increase the cooling rate? Imagine a hot cup of coffee. If it is in a thin plastic cup, it is too hot to hold and cools rapidly; put it in a thick, insulating Styrofoam and it cools slowly while the cup remains at worst lukewarm on the outside. So, by analogy, if the annulus is insulating, the surrounding rock stays cool. But this is not the whole situation for Macondo – it is more complex and subtle than that. Imagine now that we place the coffee (plus cup and lid) in a large bath of water. We have a little heater and keep the coffee hot for many hours. What happens now? Well, for the thin plastic cup, the heater is on more-or-less constantly and we end up with hot coffee in a hot bath. But for the Styrofoam cup, there is less heating and the bath water remains cold, even though the coffee stays hot. This is akin to the well flow – the oil is held at more-or-less reservoir temperatures for 86 days surrounded by rock and water and then it cools. When it cools, the hot coffee in the hot bath actually cools slowly – after all, you have to wait to cool down the entire bath first. The hot coffee in the Styrofoam initially stays hot, but eventually it is affected by the cold water around it: when this happens, the temperature falls, and it falls fast – just as in our Macondo oil simulation. So, an insulating annulus, with the properties I have estimated, leads to a more rapid cooling at around 1 day, and more cooling overall. Also, the properties of the formation have little impact: a more conductive rock heats up more and cools quickly, but is hotter when cooling starts, while a less conductive formation heats less but cools slower – the two effects almost cancel out.

I will now show the impact on the pressure response, anticipating the mathematical details in Appendices C and D. Figure B.8 shows the effect on the reservoir pressure derivative ($dp/d(ln(\Delta t))$) of the temperature correction alone, compared to the capping stack derivative, together with the reservoir derivative that I analyze in Section 4.3. Note that the temperature effects resemble a very long radial flow period. Indeed the temperature transient resembles the build-up for a reservoir with a permeability of around 550 mD (the constant derivative is around 30 psi, similar to that of the capping stack derivative at early time). The more likely case – with an insulating annulus – resembles the pressure transient with a skin effect (the hump in Figure 4.11 at early times), but a skin effect that is much, much more long-lasting than in normal pressure analysis.

The interesting point to note is that the derivative is around 30 psi or larger within a day of choke closure. Had I included the effects of cooling from the ocean this derivative (rate of cooling) would most likely be even larger. This explains why my estimated permeability using the base case – 300 mD – is higher than Dr. Gringarten's best estimate of around 240 mD: including these additional effects would lead to lower estimates of permeability in my analysis, closer to the determination by Dr. Gringarten from down-hole measurements. For instance, my more likely case gives a permeability of around 280 mD (from the constant pressure derivative value of around 60 psi in Figure B.8).

B.3.11. A reservoir permeability of 500 mD or more may have led to a reopening of the well.. Figure B.8 is a fascinating graph, made appealing (to the expert) through the mathematical correspondence between temperature and pressure transients. However, rather than dwell on this, I will illustrate one important, qualitative feature. If the reservoir pressure were 500 mD or larger, then the reservoir derivative would have a radial flow stabilization at around 30 psi.[206] My more-likely case has the same – and rising – derivative value at around 60,000 s (17 hours); if we include ocean cooling it is almost certainly even higher. Now, the capping stack derivative is the reservoir derivative minus the temperature correction.[207] So, the capping stack derivative could drop to zero and then go negative, before rising again when channel flow starts.

What does this mean? Within a day of choke closure on July 15th 2010, the capping stack pressure would have risen, then reached a maximum and then started to fall slightly. This was the well integrity test: a falling pressure would have likely been misinterpreted as evidence of leakage from the well-bore, the valves would have been re-opened, and oil would have continued, unnecessarily, to have been spilt until the relief well was drilled.

This somewhat dramatic comment does help to illustrate, clearly, the importance of the cooling on an interpretation of the pressure response.

---

[206] Using the equations in Table D.1 and the methodology of Section 4.3.
[207] Precisely there is an extra correction for pressure effects in Eqs, (B.2)-(B.4), so the capping stack derivative is even lower.
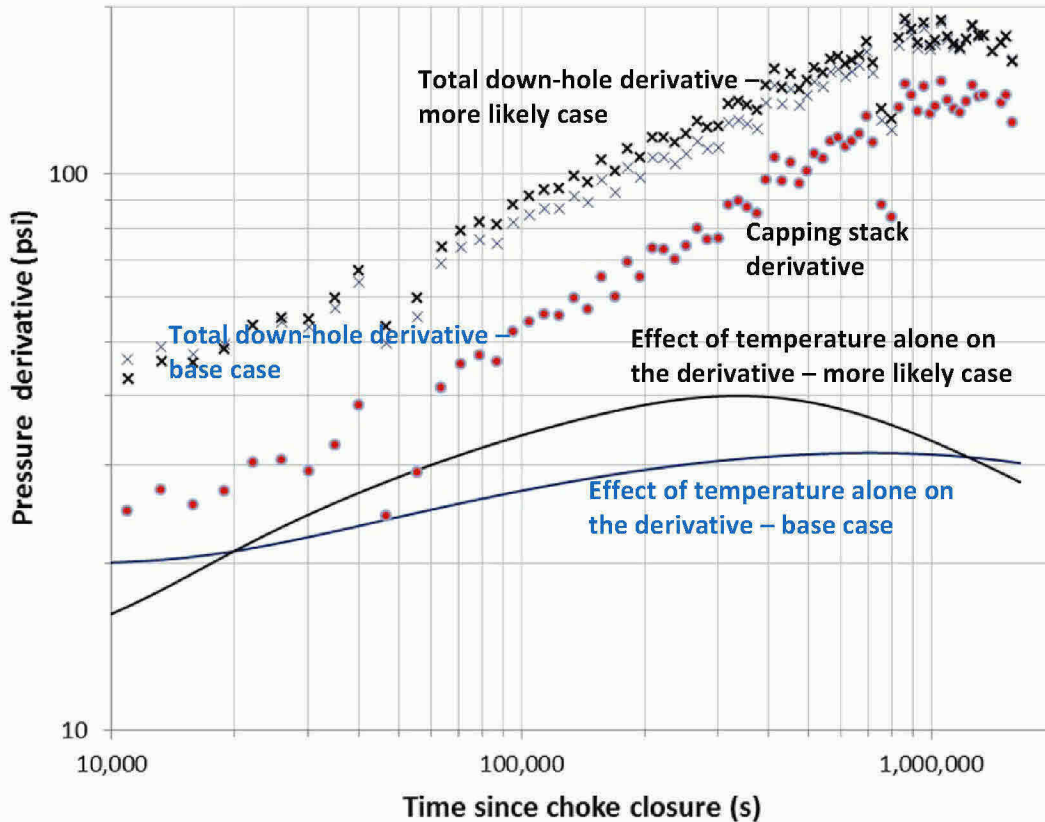
Figure B.8. The capping stack pressure derivative, the effect of the temperature correction alone and the total reservoir derivative used in this analysis (see Figure 4.12). I show the base case (used for quantitative calculation) and a more likely case, with more rapid cooling overall.

B.4 Effect of an incorrect pressure conversion on Government estimates of oil released

I now present the details of the analysis discussed in Section 4.3. In Table B.3 I present the conversion from capping stack to reservoir pressures given in the different Government reports. For comparison I show my own conversion – averaged over the three sets of fluid properties – for the last capping stack pressure measurement used in my analysis (6,952 psi when I predict the capping stack temperature to be 95°F). There is a large discrepancy between my value and the much lower numbers presented in the Government reports. I also show the pressure rise calculated from this final pressure measurement to the final pressure. In this case the discrepancies are less significant. I also show the likely impact on permeability of adding the temperature effects to the derivative (Section 4.3).

Finally, I present the impact on predicted oil released. I only consider the impact of the pressure conversion (not the analysis to find the final pressure) on the pressure drop in the material balance equation. For Dr. Hsieh and Dr. Pooladi-Darvish who have simulation models, I also incorporate the impact of the change in permeability, assuming that flow rate (and hence cumulative released) is proportional to permeability. For these two experts, the correction will more than halve their estimated oil released.

Investigator	Pressure head (psi)	My estimate of capping stack temperature (°F)[208]	Under-statement of head compared to my value (psi)	Pressure rise from last capping stack measurement (psi)[209]	Impact on permeability (mD)	Effect of using proper conversion on oil released (MMstb)[210]
My analysis	*3,378[211]*	*95*		*159*		
Drs. Kelkar & Raghavan[212]	3,220	220	158	185	Used material balance	-0.54
Dr. Hsieh[213]	3,199	235	179	78	570 to 300	-2.62
Dr. Pooladi-Darvish[214]	3,137	>243	241	71	550 to 300	-2.69
Dr. Griffiths[215]	3,190	>243	188	126	Not a reservoir analysis	

Table B.3. A table summarizing the impact of the pressure conversion from capping stack to reservoir on the calculations of the Government experts. I show the pressure head, together with the capping stack temperature consistent with this value at the time of cementing the well. I also quote the further pressure rise from the last measurement to the final reservoir pressure. I demonstrate that the poor pressure conversion leads to an over-statement of both the pressure depletion and the permeability, which governs flow rate. These two effects have a huge impact on the results of Dr. Hsieh and Dr. Pooladi-Darvish.

I end this Appendix by noting the values of capping stack temperature consistent with the heads assumed by the Government researchers. I have used the tabulations of oil density to find what temperature (at a capping stack pressure of 6,952 psi) will give the values listed in Table B.3. I find capping stack temperatures of 220°F or higher. This is completely implausible because it ignores the impact of the oil cooling and leads to a substantial under-statement of the pressure difference between the capping stack and the reservoir, contributing to a significant over-estimate of oil released. Just because it is difficult to quantify the rate of cooling, this is not an excuse to ignore it and end up with a biased estimate of the pressure conversion based on near-reservoir temperatures throughout the oil column. Things that are hot cool down: this is a simple statement of the second law of thermodynamics. This cannot be ignored.

---

[208] I find the temperature that gives the estimated head averaging the three sets of fluid data using the tables in Appendix B. For reference a capping stack temperature of 243°F gives head values of 3,141, 3,232 and 3,202 psi (average 3,192 psi) for the Core Labs, Schlumberger and Intertek fluid properties respectively.

[209] Dr. Hsieh's values are taken from his spreadsheet [44]; Drs. Kelkar & Raghavan from their supporting spreadsheet "Av pr to DOJ"; Dr. Griffiths from [SKG], Appendix F, page 39; and for Dr. Pooladi-Darvish I assume his last pressure measurement was 6,994 psi, as the other Government investigators.

[210] To find the new cumulative flow, I multiply the estimated value by the ratio of the pressure drop accounting for the head conversion only to the estimated pressure drop, and by the ratio of permeabilities.

[211] Calculated at the end of the build-up period with a measured capping stack pressure of 6,952 psi and a temperature of 95°F, averaged over the three sets of data using the correlations in Appendix B.

[212] From Kelkar-Raghavan report [KR], page 19: "*The pressure drop due to the column of oil is 3,220 psi.*"

[213] From Dr. Hsieh's pressure analysis spreadsheet [44].

[214] From Dr. Pooladi-Darvish's report [PD], Appendix III, slide 23, using the base case model, for which he assumed a well-head temperature of 220°F using his estimates of fluid properties.

[215] From Griffiths report [SKG], Appendix F, page 39.

TREX-011553-R.0090

Appendix C.   Mathematical derivation of the model of the pressure response

This Appendix contains the derivations of the equations used to analyze the pressure response. The methodology is standard in the petroleum industry, but is included for completeness. I present here principally the linear model for flow. The equations for the rectangular model are not presented as they have already been derived in Earlougher *et al.* (1968).

C.1   Darcy's law and fluid flow

I will now introduce the second fundamental equation, after material balance, used in reservoir engineering. This is Darcy's law, originally proposed by the French Civil Engineer Henry Darcy in 1856 in a study of sand filters in public fountains: running the water through the sand effectively removes bacteria from the water. Darcy's law describes how fluid (oil) moves underground in porous rock. It can be written:

$$Q = -\frac{AK}{\mu}\nabla p$$

Area of the rock across which there is flow; Permeability; Oil flow rate; Oil viscosity; Pressure gradient

(C.1)

The flow rate (Q, the volume flowing per unit time) is proportional to the area that flows (A; in this context it is the height of the reservoir sandstone multiplied by the width). Q is inversely proportional to the viscosity, μ. Viscosity is a measure of how easily fluid flows, and is found from fluid property measurements. The flow rate is also proportional to the pressure gradient, ∇p: this is the driving force that pushes the fluid through the microscopic pore spaces of the rock. The minus sign is because flow goes from high pressure to low pressure. The remaining term in the equation, K, is the permeability. This is a rock property and quantifies how easily oil flows through the pore space. Its magnitude is related to the area of a typical pore (pore spaces are typically around one tenth to one thousandth of a millimetre across: see Figure 3.1) and hence has a very low value when measured in SI units (square metres, m^2). However, it is standard in petroleum engineering to measure permeability in units of a darcy (D), or millidarcy (mD, thousandths of a darcy) in honour of the discoverer of the equation. I D is approximately 10^{-12} m^2 (see Appendix I). Average permeabilities of a reservoir vary typically from around 1 mD to 1 D. Permeability is found from flow measurements on core samples and from an analysis of pressure behaviour: both approaches will be used in this report (Section 4.3 and Appendix A.5).

C.2   Radial flow

C.2.1. Radial flow equations. The analysis of radial flow is standard can be found in any reservoir engineering or well-testing textbook. I recommend Bourdet (2002). We assume that we have fluids of a constant compressibility obeying Darcy's law, Eq. (C.1).

We use Darcy's law and invoke conservation of volume in a system of constant compressibility we arrive at the following partial differential equation for the evolution of pressure:

$$\nabla^2 p = \alpha \frac{\partial p}{\partial t}$$

(C.2)

For radial flow, Eq. (C.2) is:

$$\frac{1}{r}\frac{\partial}{\partial r}\left(r\frac{\partial p}{\partial r}\right) = \alpha \frac{\partial p}{\partial t}$$

(C.3)

where r is the radial coordinate, p is pressure and t is time. α is the inverse diffusivity for pressure:

$$\alpha = \frac{\phi \mu c_t}{K}$$

(C.4)

where K is the (average) permeability, μ the viscosity and ϕ the porosity. The total compressibility c_t is defined by Eq. (A.7). We have already met similar equations for temperature in Appendix B, Eq. (B.7).

The initial condition is $p(r,0)=p_i$ (initial pressure in the reservoir). We assume a specified flow rate $-Q_o$ at the well ($r=r_w$, where r_w is the radius of the well); later we show how to accommodate a varying flow rate. The negative sign indicates that the flow is in the direction of decreasing r (flow out of the reservoir). Rate here is measured at reservoir conditions: to covert to surface condition rates you need to divide by the oil volume formation factor B_o.

We return to Darcy's law, Eq. (C.1) to relate the flow rate to pressure gradient. For horizontal radial flow of oil, the effective flow area is $2\pi rh$, or the surface of a cylinder:

$$Q = -2\pi rh \frac{K}{\mu}\frac{\partial p}{\partial r}$$

(C.5)

The constant well flow rate boundary condition is:

$$Q_0 = 2\pi rh \frac{K}{\mu}\frac{\partial p}{\partial r}\bigg|_{r=r_w}$$

(C.6)

The easiest way to solve this problem is to define a new variable:

$$y = \frac{\alpha r^2}{4t}$$

(C.7)

92

Then Eq. (C.2) becomes:

$$\frac{dp}{dy} + y\frac{d^2p}{dy^2} = -y\frac{dp}{dy}$$

(C.8)

We find:

$$\frac{dp}{dy} = \eta\frac{e^{-y}}{y}$$

(C.9)

where η is a constant found from the constant flow boundary condition:

$$Q_0 = 2\pi rh\frac{K}{\mu}\frac{\partial p}{\partial r}\Big|_{r=r_w} = \eta\frac{4\pi Kh}{\mu}e^{-y}|_{r=r_w}$$

(C.10)

While we will provide careful determinations of parameters later, it is instructive to note that for all but the earliest times y is very small. The well radius is approximately 4 inches (0.1 m) and the base case value of the parameter α is around 0.5 m^{2}s^{-1}.[216] Then y evaluated at the well is approximately $0.0013/t$ where time, t, is measured in seconds. Our interest is in times of around 1,000 to 1,000,000 s, so y is always very small (<<1) at the well. Hence we can set $e^{-y} = 1$ and we find:

$$\eta = \frac{\mu Q_0}{4\pi Kh}$$

(C.11)

and, to obey the initial conditions, we can write:

$$p_w = p_i - \eta\int_{\frac{\alpha r_w^2}{4t}}^{\infty}\frac{e^{-y}}{y}dy = p_i + \eta Ei\left(-\frac{\alpha r_w^2}{4t}\right)$$

(C.12)

where Ei is the exponential integral (Abramovich and Stegun, 1970). As mentioned above, for all the times we are interested in $\frac{\alpha r_w^2}{4t} \ll 1$ and so we can use the following approximation (Abramovich and Stegun, 1970):

$$Ei(-y) = \ln y + \gamma$$

(C.13)

---

[216] This is much smaller than the inverse thermal diffusivity introduced in Appendix B. Heat transports through rock much slower than pressure. Over the spill period, a noticeable temperature change was observed out to, at most, 3 m, whereas the pressure encountered reservoir boundaries some 5,000 m or more from the well.

93

for y<0.01 where γ is Euler's constant =0.57721. Hence we find, from Eq. (C.12):

$$p_w = p_i - \eta \ln\left(\frac{4t}{\alpha\gamma r_w^2}\right)$$

(C.14)

The pressure decreases as ln t – logarithmically with time – in the radial flow regime. The radial flow regime ends when the pressure wave hits the sides of the channel – see Figure 4.9. This occurs when $r=W/2$ at a time:

$$t = \tau_W = \frac{\alpha W^2}{16}$$

(C.15)

C.2.2. Inclusion of skin. It is likely that the oil did not flow unimpeded across the whole reservoir section. While it is difficult to model this in detail, since the precise nature of the well-bore damage is unknown, it is possible to account for this empirically. This is achieved through the inclusion of a so-called skin. This method is standard in the oil industry and accounts for any changes in effective permeability near the well. Skin is included in reservoir models simply as an additional pressure drop at the well that is linearly related to flow rate. We obtain (by definition):

$$p_w = p_i - \eta\left(\ln\left(\frac{4t}{\alpha\gamma r_w^2}\right) + 2S\right)$$

(C.16)

S is the (dimensionless) skin factor (not to be confused with saturation).

In Macondo, skin can account for deviations from radial flow near the well: it is unlikely that the flow into the damaged well is exactly radial near the well-bore, as the oil has to access the damaged portions of the cement and casing [27]. This is called the partial penetration skin. Furthermore, as discussed in Appendix E.6, this skin is likely to have varied over time.

C.2.3. Variable rate and pressure build-up. It is possible to account for varying flow rate by considering the response of a series of constant rates imposed at different times. This is called Duhamel's principle.

First we define p_D as the pressure response for a unit flow rate and with no skin and with zero initial pressure. From Eq. (C.14):

$$p_D(t) = \frac{\mu}{4\pi K h}\ln\left(\frac{4t}{\alpha\gamma r_w^2}\right)$$

(C.17)

At any time – using Duhamel's principle – the well pressure can be written as:

94

$$p_w = p_i - \delta(t)Q(t) + \int_0^t \frac{\partial Q(\tau)}{\partial \tau} p_D(t-\tau)d\tau$$

(C.18)

where δ accounts for skin, and can be a function of time, if S varies:

$$\delta = \frac{S\mu}{2\pi Kh}$$

(C.19)

C.2.4. Simple model of draw-down and build-up. We assume that from $t=0$ we have a constant rate $-Q_o$ and then at $t=t_p$ the well is closed and $Q=0$. We will only consider here the pressure build-up, $t>t_p$.

Consider this as the addition of two rates ($-Q_o$ for $t>0$ and Q_o added for $t>t_p$) in Eq. (C.18):

$$p_w = p_i - \eta \left(\ln \frac{4t}{\alpha r_w^2} - \ln \frac{4(t-t_p)}{\alpha r_w^2} \right) = p_i - \eta \ln \left(\frac{t_p + \Delta t}{\Delta t} \right)$$

(C.20)

where $\Delta t = t - t_p$.

Eq. (C.20) is the basis of the standard Horner plot in well test analysis: the pressure is plotted against the logarithm of Horner time $(t_p + \Delta t)/\Delta t$. A straight line indicates radial flow with the slope giving an indication of flow rate and permeability. This is also the same behaviour we saw for the temperature profile in Appendix B.3.

C.3   Linear flow

For linear flow Eq. (C.2) is:

$$\frac{\partial^2 p}{\partial x^2} = \alpha \frac{\partial p}{\partial t}$$

(C.21)

As before the initial condition is $p(x,0)=p_i$ (initial pressure in the reservoir). There is no flow at $x=L$: the end of the reservoir, as shown in Figure C.1. The specified flow rate $-Q_o$ is given at the well ($x=0$).
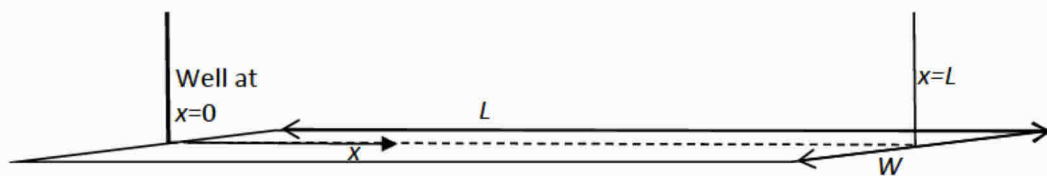
Figure C.1. Schematic of the model for linear flow: the reservoir is treated as a straight channel of length *L* and width *W*, with flow only in the *x* direction. The well is at one end (*x=0*).

As before, the relationship between flow rate and pressure gradient is given by Darcy's law, Eq. (C.1) where now the flow area is hW:

95

$$Q = -\frac{KhW}{\mu}\frac{\partial p}{\partial x}$$

(C.22)

Then the no-flow boundary condition at *x=L* is equivalent to:

$$\left.\frac{\partial p}{\partial x}\right|_{x=L} = 0$$

(C.23)

C.3.1. Laplace transform. A powerful and general way to solve pressure dissipation problems is to use the method of Laplace transforms (Carslaw and Jaeger, 1946). The Laplace transforms used are all taken from Abramovich and Stegun (1970). We take the Laplace transform of the governing partial differential equation, Eq. (C.21):

$$\frac{\partial^2 \tilde{p}}{\partial x^2} = \alpha s \tilde{p} - \alpha p_i$$

(C.24)

The tilde ~ represents the Laplace transform. The general solution is:

$$\tilde{p} = A(s)e^{-\sqrt{\alpha s}x} + B(s)e^{+\sqrt{\alpha s}x} + p_i/s$$

(C.25)

Then for the no-flow condition, Eq. (C.23):

$$B(s) = A(s)e^{-2\sqrt{\alpha s}L} = \varepsilon A(s)$$

(C.26)

where

$$\varepsilon = e^{-2\sqrt{\alpha s}L}$$

(C.27)

and is small for most times considered.

Then we consider the constant flow rate boundary condition at the well. Taking the Laplace transform of Eq. (C.22), we find

$$\tilde{Q} = -\frac{KhW}{\mu}\frac{\partial \tilde{p}}{\partial x} = \frac{KhW}{\mu}\sqrt{\alpha s}A(s)\left(e^{-\sqrt{\alpha s}x} - \varepsilon e^{+\sqrt{\alpha s}x}\right)$$

(C.28)

Then the boundary condition at *x=0* becomes:

96

$$Q_o/s = -\frac{KhW}{\mu}\sqrt{\alpha s}A(s)(1-\varepsilon)$$

(C.29)

From this we find *A(s)* and hence the Laplace transform of *p*.

$$A(s) = -\frac{\mu Q_o}{KhW\sqrt{\alpha}(1-\varepsilon)}s^{-3/2}$$

(C.30)

$$\tilde{p} = -\frac{\mu Q_o}{KhW\sqrt{\alpha}(1-\varepsilon)}s^{-3/2}\left(e^{-\sqrt{\alpha s}x} + \varepsilon e^{+\sqrt{\alpha s}x}\right) + p_i/s$$

(C.31)

At *x*=0 we define a well pressure p_0 (we account for skin later):

$$\widetilde{p_0} = -\frac{\mu Q_o}{KhW\sqrt{\alpha}}\frac{(1+\varepsilon)}{(1-\varepsilon)}s^{-3/2} + p_i/s$$

(C.32)

To invert the Laplace transform, we need to re-write the terms in ε that are functions of *s*.

$$\frac{(1+\varepsilon)}{(1-\varepsilon)} = 1 + 2\sum_{n=1}^{\infty}\varepsilon^n = 1 + 2\sum_{n=1}^{\infty}e^{-2n\sqrt{\alpha s}L}$$

(C.33)

We then use the following inverse Laplace transform (Abramovich and Stegun, 1970): for

$$\tilde{f}(s) = s^{-3/2}e^{-k\sqrt{s}}$$

(C.34)

the inverse transform is:

$$f(t) = 2\sqrt{\frac{t}{\pi}}e^{-k^2/4t} - k\,\text{erfc}\left(\frac{k}{2\sqrt{t}}\right)$$

(C.35)

Comparing Eqns. (C.34) and (C.35) with the terms in the sum in Eq. (C.33) we use:

$$k = 2n\sqrt{\alpha}L$$

(C.36)

Then from Eq. (C.33):

97

$$p_0 = p_i - \frac{2\mu Q_o}{KhW\sqrt{\pi\alpha}}\sqrt{t}\left[1 + 2\sum_{n=1}^{\infty}\left(e^{-\alpha n^2 L^2/t} - nL\sqrt{\frac{\pi\alpha}{t}}\ \text{erfc}\left(\frac{\sqrt{\alpha}nL}{\sqrt{t}}\right)\right)\right]$$

(C.37)

where erfc is the complementary error function (Abramovich and Stegun, 1970). Let's simplify Eq. (C.37) by defining:

$$\beta = \frac{2\mu Q_o}{KhW\sqrt{\pi\alpha}} = \frac{2Q_o}{hW}\sqrt{\frac{\mu}{\pi\phi c_t K}}$$

(C.38)

and:

$$\tau_L = \alpha L^2 = \frac{\phi\mu c_t}{K}L^2$$

(C.39)

Physically τ_L is the time taken for the pressure response to reach the no-flow boundary at $x=L$. Then:

$$p_0 = p_i - \beta\sqrt{t}\left[1 + 2\sum_{n=1}^{\infty}\left(e^{-n^2\tau_L/t} - n\sqrt{\pi}\sqrt{\frac{\tau_L}{t}}\ \text{erfc}\left(n\sqrt{\frac{\tau_L}{t}}\right)\right)\right]$$

(C.40)

C.3.2. Early time behaviour. In the linear flow regime, but before the pressure sees the boundary at $x=L$, $t \ll \tau_L$, from Eq. (C.40) all the terms in the bracket, bar the first, are small, and we see classic channel-flow behaviour with a square-root-of-time dependence:

$$p_0 = p_i - \beta\sqrt{t}$$

(C.41)

C.3.3. Late-time behaviour. Once the pressure wave has seen the boundaries, $t \gg \tau_L$, there is an approximately linear decrease in pressure with time. This is the so-called pseudo steady-state regime that is often employed in simple analyses of producing fields: it is seen after several months and continues through the decades-long life of the field.

This behaviour is more difficult to derive directly from Eq. (C.40) as, in the limit $t \gg \tau_L$, we have a sum of nearly equal terms. The way to derive this is to return to the Laplace transform solution, Eq. (C.32) in the limit of small s (this corresponds to large t). In this case, instead of Eq. (C.33) we write:

$$\frac{(1+\varepsilon)}{(1-\varepsilon)} = \frac{1 + e^{-2\sqrt{\alpha s}L}}{1 - e^{-2\sqrt{\alpha s}L}} \approx \frac{1 + 1 - 2\sqrt{\alpha s}L}{2\sqrt{\alpha s}L} \approx \frac{1}{\sqrt{\alpha s}L} = \frac{1}{\sqrt{\tau_L}}s^{-1/2}$$

(C.42)

to leading order in s.

98

TREX-011553-R.0098

Then from Eq. (C.32):

$$\widetilde{p_0} = -\frac{\sqrt{\pi}}{2}\frac{\beta}{\sqrt{\tau_L}}s^{-2} + p_i/s$$

(C.43)

and hence

$$p_0 = p_i - \frac{\sqrt{\pi}}{2}\frac{\beta}{\sqrt{\tau_L}}t$$

(C.44)

As mentioned above, the pressure declines linearly with time in response to a constant flow rate production.

A full solution, based around this late-time expression, can be found in Carslaw and Jaeger (1946), p112 (we do not derive it here as it is not used in the analysis):

$$p_0 = p_i - \frac{\sqrt{\pi}}{2}\frac{\beta}{\sqrt{\tau_L}}\left(t - \frac{2\tau_L}{\pi^2}\sum_{n=1}^{\infty}\frac{e^{-n^2\pi^2 t/\tau_L}}{n^2}\right)$$

(C.45)

C.3.4. Inclusion of skin. Here we define p_w as the measured well-bore pressure and obtain using Eqs. (C.16) and (C.19):

$$p_w = p_0 - \delta Q_0 = p_i - \delta(t)Q_0 - \beta\sqrt{t}\left[1 + 2\sum_{n=1}^{\infty}\left(e^{-n^2\tau_L/t} - n\sqrt{\pi}\sqrt{\frac{\tau_L}{t}}\,\mathrm{erfc}\left(n\sqrt{\frac{\tau_L}{t}}\right)\right)\right]$$

(C.46)

C.3.5. Variable rate and pressure build-up. As before, we use Duhamel's principle to find the response of the system as the sum of a series of constant rates imposed at different times.

First we define p_D as the pressure response for a unit flow rate and with no skin and with zero initial pressure. From Eq. (C.46):

$$p_D(t) = -\beta\sqrt{t}/Q_0\left[1 + 2\sum_{n=1}^{\infty}\left(e^{-n^2\tau_L/t} - n\sqrt{\pi}\sqrt{\frac{\tau_L}{t}}\,\mathrm{erfc}\left(n\sqrt{\frac{\tau_L}{t}}\right)\right)\right]$$

(C.47)

For reference the early time behaviour, Eq. (C.41):

$$p_D = -\beta\sqrt{t}/Q_0$$

(C.48)

and the late-time behaviour, Eq. (C.44):

99

$$p_D = -\frac{\sqrt{\pi}}{2Q_0}\frac{\beta}{\sqrt{\tau_L}}t$$

(C.49)

At any time – using Duhamel's principle – the well pressure can be written as:

$$p_w = p_i - \delta(t)Q(t) + \int_0^t \frac{\partial Q(\tau)}{\partial \tau}p_D(t-\tau)d\tau$$

(C.50)

C.3.6. Draw-down and build-up with constant rates. As before, at *t=0* we start producing at a constant rate -Q_o and then at *t=t$_p$* the well is closed and *Q=0*. We will only consider the pressure build-up, *t>t$_p$*.

As for the radial case, we either consider this as the addition of two rates (-Q_o for *t>0* and Q_o added for *t>t$_p$*) to find:

$$p_w = p_i - Q_o\left(p_D(t) - p_D(t-t_p)\right)$$

(C.51)

The early-time response is from Eq. (C.48):

$$p_w = p_i - \beta\left(\sqrt{t} - \sqrt{t-t_p}\right)$$

(C.52)

Usually in pressure transient analysis we define *Δt=t-t$_p$* and hence we have:

$$p_w = p_i - \beta\left(\sqrt{\Delta t + t_p} - \sqrt{\Delta t}\right)$$

(C.53)

This is the classic expression for channel flow that we will show is consistent with the Macondo pressure build-up.

C.3.7. Late-time and consistency with material balance. The late-time response, which we call p_f (this is the final reservoir pressure, when the pressure is constant throughout the domain) is, from Eq. (C.49):

$$p_f = p_i - \frac{\sqrt{\pi}}{2}\frac{\beta}{\sqrt{\tau_L}}\left(t - (t-t_p)\right) = p_i - \frac{\sqrt{\pi}}{2}\frac{\beta}{\sqrt{\tau_L}}t_p$$

(C.54)

There is a fixed final pressure drop. This expression has to be consistent with material balance which states that the amount of oil produced N_{pr} (at reservoir conditions) is given by:

$$N_{pr} = Q_o t_p = Vc_t(p_i - p_f) = Vc_t\Delta p$$

(C.55)

100

TREX-011553-R.0100

where V is the pore volume of the reservoir: $V = \phi hWL$. From Eq. (C.54) and using Eqs. (C.38) and (C.39), we find that the final term in Eq. (C.55) is:

$$Vc_t\Delta p = \frac{\sqrt{\pi}}{2}\frac{\beta}{\sqrt{\tau_L}}\phi hWLc_t t_p = \frac{\phi\mu c_t}{K\alpha}Q_o t_p = Q_o t_p$$

(C.56)

using Eq. (C.4) for α.

So – as it has to be – the late-time final pressure is consistent with material balance.

C.4   Well not at the end of the channel

C.4.1. Well geometry. Our model reservoir has the well exactly at one end. The Macondo well was, however, designed to be in the centre of the thickest layers of oil-bearing sandstone, near, but not at, the Southern end of the field. An improved representation is to place the well a distance L_1 from one boundary and L_2 from the other as shown schematically in Figure C.2.
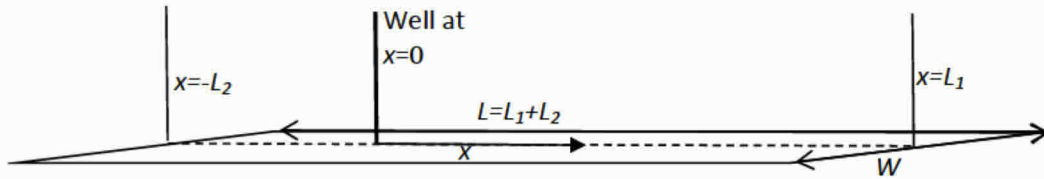
Figure C.2. Schematic of the reservoir with a well placed at an arbitrary location in the reservoir channel. This is the model that accurately predicts the measured pressure.

This case can be treated as two separate problems in each limb of the reservoir with the constraint that they give the same well pressure and that the two rates add to the specified rate at the well.

C.4.2. Analytic analysis. If we define Q as the total rate at the well, then $Q=Q_1+Q_2$ the sum of the rates on each branch. The rates on each branch may change with time even if Q is a constant.

We require the well pressures to be equal (we treat skin separately as an additional pressure drop proportional to Q):

$$p_{w1} = p_{w2} \text{ hence } \int_0^t \frac{\partial Q_1(\tau)}{\partial\tau}p_{D1}(t-\tau)d\tau = \int_0^t \frac{\partial Q_2(\tau)}{\partial\tau}p_{D2}(t-\tau)d\tau$$

(C.57)

From Eq. (C.50), where for either limb ($i=1$ or 2):

$$p_{Di}(t) = -\beta\sqrt{t}/Q_o\left[1 + 2\sum_{n=1}^{\infty}\left(e^{-n^2\tau_i/t} - n\sqrt{\pi}\sqrt{\frac{\tau_i}{t}}\,\text{erfc}\left(n\sqrt{\frac{\tau_i}{t}}\right)\right)\right]$$

(C.58)

101

and from Eq. (C.39):

$$\tau_i = \alpha L_i^2$$

(C.59)

For Eq. (C.57) to be valid for all times we equate the integrand and write $Q_2 = Q - Q_1$:

$$p_{D1}(t - \tau)\frac{\partial Q_1(\tau)}{\partial \tau} = \left(\frac{\partial Q(\tau)}{\partial \tau} - \frac{\partial Q_1(\tau)}{\partial \tau}\right) p_{D2}(t - \tau)$$

(C.60)

And hence we find an expression for Q_1:

$$\frac{\partial Q_1(\tau)}{\partial \tau} = \frac{p_{D2}(t - \tau)}{p_{D1}(t - \tau) + p_{D2}(t - \tau)}\frac{\partial Q(\tau)}{\partial \tau}$$

(C.61)

From Eq. (C.57) the general expression for pressure at the well is:

$$p_w = p_i - \delta(t)Q(t) + \int_0^t \frac{\partial Q_1(\tau)}{\partial \tau} p_{D1}(t - \tau)d\tau$$

(C.62)

which from Eq. (C.61) becomes:

$$p_w = p_i - \delta(t)Q(t) + \int_0^t \frac{\partial Q(\tau)}{\partial \tau}\frac{p_{D1}(t - \tau)p_{D2}(t - \tau)}{p_{D1}(t - \tau) + p_{D2}(t - \tau)}d\tau$$

(C.63)

One way of writing this is to use an expression similar Eq. (C.50) and define a new unit flow pressure response:

$$p_w = p_i - \delta(t)Q(t) + \int_0^t \frac{\partial Q(\tau)}{\partial \tau} p_{Db}(t - \tau)\, d\tau$$

(C.64)

where

$$p_{Db} = \frac{p_{D1} p_{D2}}{p_{D1} + p_{D2}}$$

(C.65)

with p_{Di} for $i=1,2$ given by Eq. (C.58).

If we consider our simple model of constant rate draw-down and build-up, then we use Eq. (C.51) as before but with p_{Db} in (C.65) substituted for p_D.

We will use the final pressure directly in our analysis. From (C.54) and (C.65) we find:

$$p_i - p_f = \Delta p = \frac{\sqrt{\pi}}{2} \frac{\beta}{(\sqrt{\tau_1} + \sqrt{\tau_2})} t_p$$

(C.66)

C.4.3. Coupling to a semi-analytic outflow model. The final stage of the analysis is to couple this reservoir model to the outflow performance. If we assume fully turbulent flow then the pressure drop from the well to surface can be expressed as (this is the assumption used in the Government reports [2,3]):

$$p_w - p_s = \xi(t) + \kappa(t)Q^2(t)$$

(C.67)

where ξ accounts for the weight of oil and gas and κ is the turbulent resistance factor. Both of these parameters may be functions of time. Then we can construct the following expression for pressure as a function of flow rate:

$$p_i - p_s = \xi(t) + \delta(t)Q(t) + \kappa(t)Q^2(t) - \int_0^t \frac{\partial Q(\tau)}{\partial \tau} p_{Db}(t - \tau)\,d\tau$$

(C.68)

If we know the parameters as a function of time, then $Q(t)$ can be obtained from Eq. (C.68) semi-analytically. While a little more sophisticated, Eq. (C.68) is quite easy to use. It could also be used in combination with independent calculations of outflow performance: a simple tank model of the reservoir could be replaced by the expressions in this report. However, this requires the somewhat uncertain determination of outflow performance κ and the effect of skin δ as a function of time.

Appendix D.   Additional pressure analysis

This Appendix provides additional results and the equations used in the analysis of the measured pressure data discussed in Section 4.3.

D.1.   Parameter matches, sensitivities and model comparisons

D.1.1 Definitions and best-match values. Table D.1 summarizes the properties that we can derive from the pressure analysis. They are all introduced in Appendix C. Table D.2 provides my values of these properties using the methods presented in Appendices C and E and Section 4.3.

Parameter	Defining equation	Meaning	Found from
η	$$\eta = \frac{\mu Q_0}{4\pi K h}$$ (C.11)	Draw-down in radial flow. Uses height h at the well (93 ft), and final flow rate.	Value of pressure derivative
τ_W	$$\tau_W = \frac{\alpha W^2}{16}$$ (C.15)	Time for pressure to see channel width	End of radial flow regime
τ_1	$$\tau_1 = \alpha L_1^2$$ (C.59)	Time for pressure to reach channel end	Match to channel flow pressure build-up
τ_2	$$\tau_2 = \alpha L_2^2$$ (C.59)	Time for pressure to reach the other channel end	Match to channel flow pressure build-up
β	$$\beta = \frac{2\mu Q_o}{K h W \sqrt{\pi \alpha}}$$ $$= \frac{\mu Q_o}{2\sqrt{\pi \tau_W} K h}$$ (C.38)	Draw-down in linear flow	Slope of channel flow pressure regime
Δp	$$\frac{\Delta p}{= \frac{\sqrt{\pi}}{2} \frac{\beta}{(\sqrt{\tau_1} + \sqrt{\tau_2})} t_p}$$ (C.66)	Pressure decline	Final stabilized pressure

Table D.1. Table of parameters that will be determined from fitting the analytical model in Appendix C to the measured pressure response.

Parameter	τ_1	τ_2	β	Δp	p_f	p_{csf}	Pressure error	Derivative error
Core Labs data	11,300,000	115,000	0.8011	1,423	10,433	7,040	2.03	12.00
Schlumberger data	12,000,000	87,900	0.7589	1,325	10,531	7,066	1.84	11.78
Intertek data	11,800,000	93,700	0.7713	1,354	10,502	7,041	1.89	11.85
Unit	s	s	psi.s$^{-1/2}$	psi	psi	psi	psi	psi

Table D.2. Parameters determined from the pressure match to the linear flow model. Table D.1 provides definitions and descriptions of each of these terms. The errors are the root-mean-square errors – Eqs. (D.2), (D.3). p_{csf} is the final capping stack pressure, computed using the methods in Appendix B once the temperature in the well-bore is the geothermal gradient – see Figure D.6.

Parameter	η	τ_W	τ_1	τ_2	β	Δp	p_f	Pressure error	Derivative error
Core Labs data	55.6	60,873	10,226,054	190,423	0.79939	1,444	10,412	1.37	11.14
Schlumberger data	53.4	61,791	11,020,620	165,194	0.76131	1,341	10,515	1.13	11.09
Intertek data	54.4	62,177	10,809,080	172,072	0.77329	1,371	10,485	1.37	11.14
Unit	psi	s	s	s	$psi.s^{-1/2}$	psi	psi	psi	psi

Table D.3. Parameters determined from the pressure match to a rectangular flow model. Table D.1 provides definitions and descriptions of each of these terms. The errors are the root-mean-square errors – Eqs. (D.2), (D.3).

The pressure data is presented in Figure 4.10 as 79 distinct values.[217] It is the *pressure measured* at the capping stack from shutting in the well to just before the well was cemented.[218] The pressure in the reservoir – deep underground – is estimated using the conversion presented in Appendix B: I will treat this as the measured reservoir pressure in my analysis. I have three conversions giving three sets of pressure matches for the three sets of fluid properties introduced in Appendix A.

The values shown in Table D.2 are best matches to the pressure data and the pressure derivative[219] using the linear flow model presented in Appendix C. This model is used for all the quantitative analysis to find the length of the reservoir and the pressure decline.

Table D.3 shows the pressure matches to an analytical rectangular flow model, which better captures the transition from radial to channel flow.[220] This model is useful to determine η, used to compute permeability in Section 4.3 and τ_W, used to find the connected width of the reservoir in Section 5. It also provides a check that the linear model arrives at similar values of τ_1 and the final pressure (within 21 psi, or a pressure drop difference of 1.5%), which is controlled by the late-time behaviour.

Note that we match the pressure to around 2 psi or better, which is well within the precision of the pressure gauge itself (around 5 psi).[221]

D.1.2 Objective function for matching. The match is found from minimizing the objective function, *O*,[222]

---

[217] I have taken pressure readings with the same value and averaged the times at which they were recorded. I have ignored the final five readings, which are perturbed by the injectivity test prior to cementing the well.

[218] I used the revised Ratzel report [3] to assume that there is no flow from the completion of the choke closure at 14:22 on 15th July. I take the end of the build-up period when the injectivity test started at 13:00 on 3rd August. Δt is the time since choke closure, while t_p is the production time. From the BP Accident Investigation Report (BP, 2010), I assume that the well started flowing at approximately 21:00 on 20th April 2010 (this is also consistent with the Emilsen Report [27]). This gives t_p (until choke closure) of 85 days, 17 hours and 22 minutes or 7,406,520 s.

[219] The derivative is computed as a difference between the previous and the subsequent pressure readings divided by the difference in the logarithm of time. There is a period late on 31st July when the pressure falls slightly [T] – this negative derivative is ignored in the analysis.

[220] The equations are not given here but can be found in Earlougher *et al.* (1968).

[221] It is possible to fit the data with an average accuracy better than the pressure gauge sensitivity, since we match to a discrete pressure at the average time that this pressure is recorded: at that time, the real pressure is almost certainly very close to what is recorded – much closer than the sensitivity of the gauge.

[222] The minimization has been performed using the Simplex algorithm. I have also checked the results by hand to confirm that a good match has been obtained.

$$O = \sum_{i=1}^{n} w_i \left(p_i - p_t(t_i)\right)^2 + \sum_{i=2}^{n-1} w_i \left(\frac{p_{i+1} - p_{i-1}}{\ln(t_{i+1}) - \ln(t_{i+1})} - \frac{dp_t}{dln(t)}\bigg|_{t_i}\right)^2$$

(D.1)

where we have n pressure points in the match (n=60 for the linear model, beyond Δt = 1 day; for the rectangular model we have 79 values after Δt = 3,600 s – one hour), p_i at times t_i, and the theoretical pressure p_t and its derivative $dp_t/dln(t)$ are computed from Eq. (C.64). The function O is minimized by varying the parameters β, τ_1 and τ_2 in the calculation of p_t for the linear model. The weighting factor w is the normalized length of time for which a given pressure value was recorded – this tends to weight the late-time behaviour more heavily. Using no weighting (w=1) has a negligible effect (less than 0.5%) difference to my predictions of pressure drop.
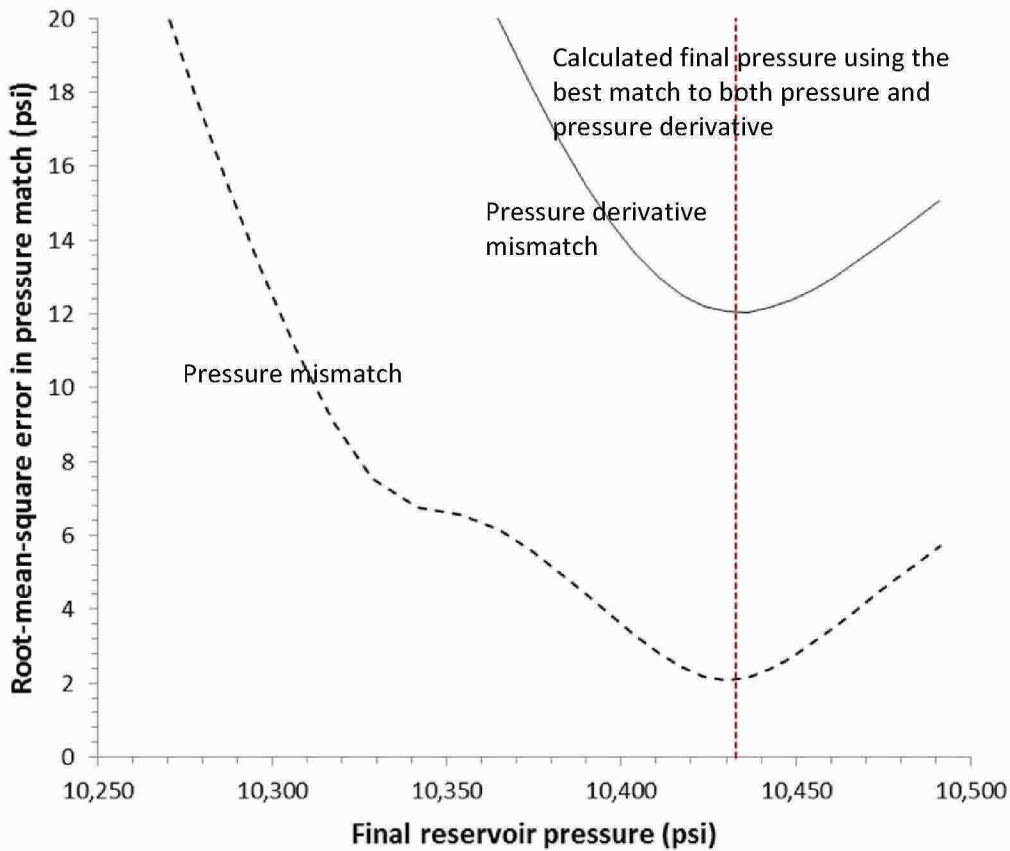
Figure D.1. The root-mean-square mismatch in pressure and pressure derivative for different assumed values of the final reservoir pressure. Note that our theoretical model can predict the measured pressure to, on average, around 2 psi. The vertical line is the best match – presented in Table D.2 – that uses the best fit to both pressure and its derivative. Here we use Core Labs fluid properties.

Tables D.2 and D.3 show the root-mean-square errors in the match, computed as follows:

106

$$\text{Root mean square error in pressure} = \sqrt{\frac{1}{n}\sum_{i=1}^{n} w_i(p_i - p_t(t_i))^2}$$

(D.2)

$$\text{Root mean square error in derivative} = \sqrt{\frac{1}{n-2}\sum_{i=2}^{n-1} w_i\left(\frac{p_{i+1} - p_{i-1}}{\ln(t_{i+1}) - \ln(t_{i-1})} - \frac{dp_t}{dln(t)}\bigg|_{t_i}\right)^2}$$

(D.3)
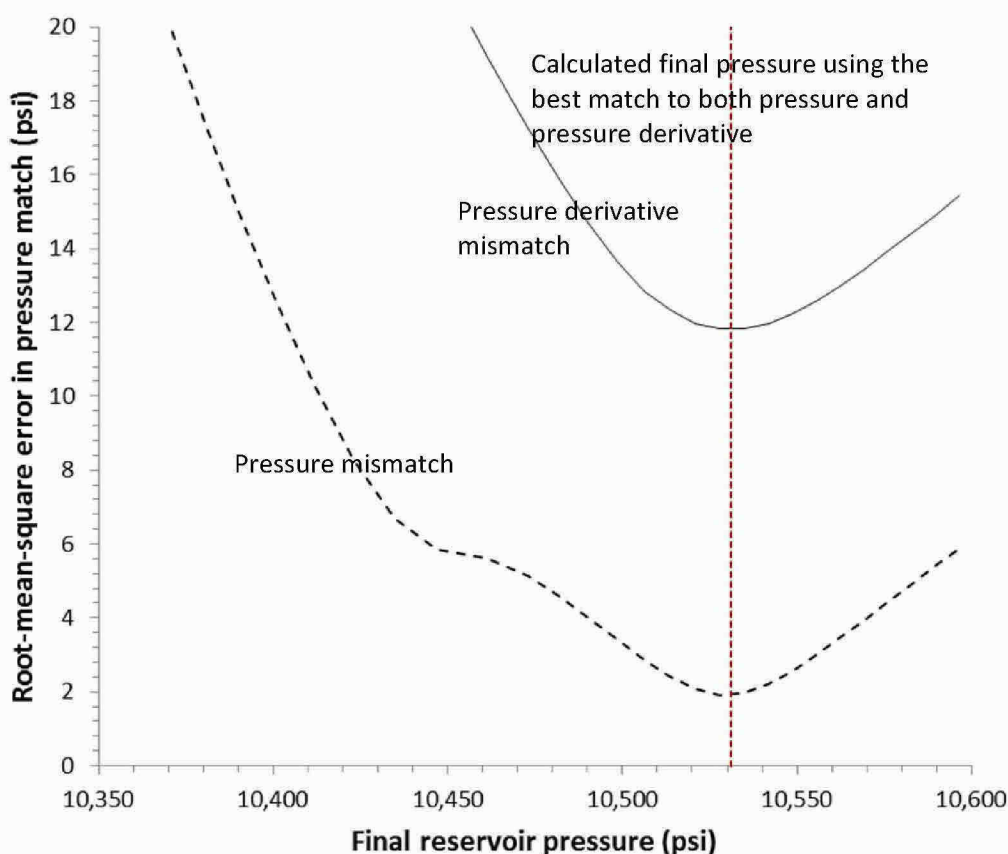
Figure D.2. The average absolute mismatch in pressure and pressure derivative for different assumed values of the final reservoir pressure. The vertical line is the best match – presented in Table D.2 – that uses the best fit to both pressure and its derivative. Here we use Schlumberger fluid properties.

D.1.3 Sensitivity to the final reservoir pressure. Figures D.1 to D.3 show the mismatch to the pressure data if we *assume* a final reservoir pressure and then find the best fit to the other parameters. So, Δp is fixed, while the times τ_1 and τ_2 to hit the boundaries are adjusted to obtain the best match to the data.

However, if we assume a pressure drop that is not optimal, the data match will always be poor, regardless of where we place the reservoir boundaries. We use the linear model.

My best match for the final reservoir pressure is the one that has the best combined fit to both the pressure and pressure derivative. We can shift the final pressure by only around 10 psi before a noticeably non-ideal fit is seen.
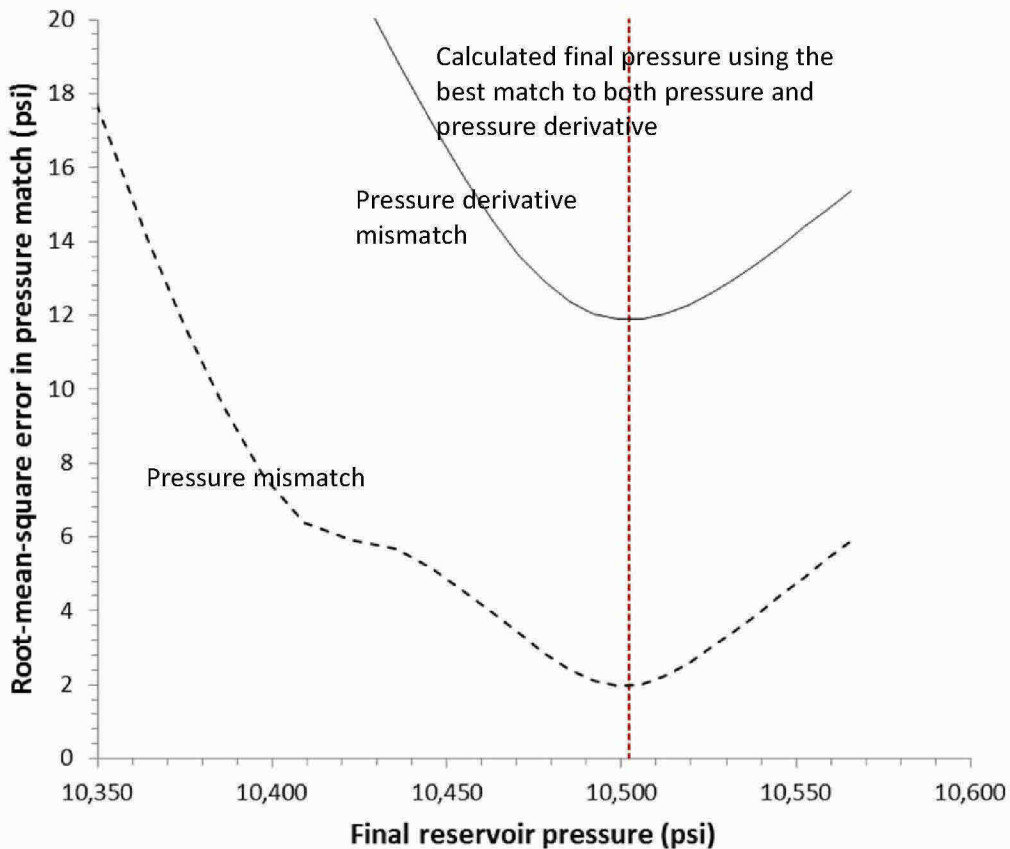
Figure D.3. The average absolute mismatch in pressure and pressure derivative for different assumed values of the final reservoir pressure. The vertical line is the best match – presented in Table D.2 – that uses the best fit to both pressure and its derivative. Here we use Intertek fluid properties.

D.1.4 Finding lengths from times. In Section 5 we use the times to reach boundaries presented in Tables D.1 and D.2 to estimate the size of the connected reservoir. The distances are found as follows. Width, $W = 4\sqrt{\tau_W/\alpha}$; length to the North (or North-West), $L_1 = \sqrt{\tau_1/\alpha}$; and length to the South (or South-East), $L_2 = \sqrt{\tau_2/\alpha}$. α is the inverse diffusivity defined by Eq. (C.4): $\alpha = \frac{\phi\mu c_t}{K}$. The viscosity, μ=0.2197 mPa.s, is taken at the final reservoir pressure (see Table A.1). ϕc_t is tabulated in Table A.8 and I take the entire range of values. The (connected) area $A_c=W(L_1+L_2)$. I take the average area for a given permeability K for the three sets of fluid data. I consider the upper bound $K = 329$ mD from the Gringarten report.

108

D.1.5 Finding sinuosity. In Section 5 we also derive a sinuosity to deduce the flow path in the reservoir. The sine wave shown in Figure 5.1 has a dimensionless amplitude times frequency ε=0.75. Mathematically, the path (arc) length is the straight-line path multiplied a factor $^2/_\pi \sqrt{1 + \varepsilon^2} E(\varepsilon^2/(1 + \varepsilon^2))$ whose value is around 1.14. E is the complete elliptic integral of the second kind (Abramovich and Stegun, 1970). The tortuosity I find is at the lower end of values computed for other channel turbidites (Dykstra and Kneller, 2008).

D.1.6 Finding the connectivity. I have found the connected area A_c from the pressure analysis (Section D.1.4 above). I also know the gross rock volume $V=Ah$ from the BP seismic analysis (see Table A.6). I assume that the disconnected area is resolved at the limit of the seismic interpretation with an average thickness h_L = 10 ft (see Section 5). Then the connected volume is: $V_c = Ah - (A - A_c)h_L$. The connectivity is $V_c/Ah = 1-(1-A/A_c)(h_L/h)$. I find the values shown in Table D.4.

This is an upper bound on connectivity: I take the upper bound on permeability and the lower possible bound on thickness at the peripheries of the field. The average thickness in the connected region varies between 69 and 89 ft, see Table D.5, close to that encountered at the well (93 ft). Technically, the pressure analysis finds a mobility, or a permeability times thickness. In my analysis and that of Dr. Gringarten, this is assumed to be the height near the well (93 ft) in the radial flow period. However, as evident from the seismic interpretation, Figure 4.5, the height away from the well is lower. In our connected domain, this means that the mobility is slightly lower away from the well. However, this value still exceeds the base case mobility determined in the Gringarten report, using a mid-range permeability of 238 mD.

██

██

██████████████████████████████ [223]
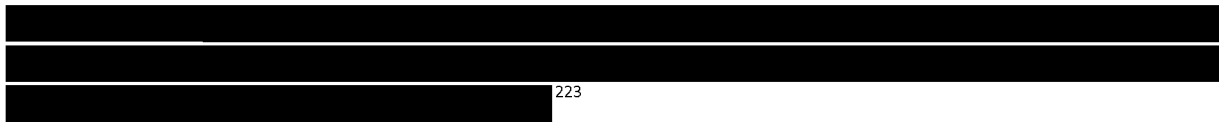
Connectivity (%)	Fluid properties		
	High (Intertek)	**Middle** (Schlumberger)	**Low** (Core Labs)
High case rock compressibility	88	88	87
Mid case rock compressibility	89	89	88
Low case rock compressibility	90	90	89

Table D.4. The connectivity for the full range of fluid and rock compressibilities. Note that a high compressibility leads to lower connectivity, since the pressure response moves slower.

Connected thickness (ft)	Fluid properties		
	High (Core Labs)	**Middle** (Schlumberger)	**Low** (Intertek)
High case rock compressibility	89	84	84
Mid case rock compressibility	81	76	76
Low case rock compressibility	74	69	69

Table D.5. The connected thickness for the different ranges of fluid compressibilities.

---

[223] ████████████████████████████

D.1.7 Discussion of the linear model. The principal reason for employing the linear flow model for my quantitative analysis is that it decouples the uncertainties of flow rate and well cooling in the first day from the key assessment of pressure decline and the overall extent of the field.

For example, consider the radial flow analysis in Section 4.3 used to determine permeability. Here, as evident from the equation in Table D.1 the constant derivative value found (around 55 psi) is a ratio of flow rate to a product of permeability and thickness. The flow rate is the flow rate just before well closure – in the final day of the spill. I have assumed a value of 45,000 stb/day. The thickness is typically assumed to be the thickness encountered at the well, 93 ft. The permeability is the permeability averaged over the distance the pressure wave encounters in the radial flow period – up to a radius of around 750 m (half the reservoir width).

What about channel or linear flow? Here the overall draw-down is given by β (Table D.1). Here we find again a ratio of flow rate to permeability times thickness. But the flow rate is now the average during the spill period, since this is the late-time behaviour, the thickness we assume is lower (see Table D.5) and the permeability is the flow-based average across the whole field. My assessment is that the ratio is the same as in the radial flow period: the thickness is lower, as is the average flow rate (compared to the final value) and the two things broadly cancel. The ratio of the well-thickness to an average value of 78 ft (Table D.5) is around 1.2, equal to the ratio of the final flow rate to the average (taken to be around 37,000 stb/day). The permeability is more-or-less the same as deduced in the radial flow regime.

This explains why a constant rate rectangular model matches the data very well – see Table D.3. Even through the flow rates for the radial and linear flow regimes are likely to be different and the reservoir thickness likely decreases away from the well, consistent with the seismic interpretation (Figure 4.5), a model that assumes constant thickness, rate and permeability fits the pressure response accurately.

However, using a rectangular flow model for all the analysis involves some complexities, as we would need to make assumptions on flow rate history and thickness (which varies) to make a quantitative assessment for the whole build-up period. The use of the linear model avoids these problems: all I take from radial flow is the value of the derivative and the time to see channel flow, both of which are evident from the data itself (Figure 4.12).

D.2. Pressure derivatives

Here we present the equations for the pressure derivatives mentioned in Section 4.3.

D.2.1. Radial flow. From Eq. (C.20), for radial flow and for $\Delta t \ll t_p$ we find the derivative:

$$\frac{dp_w}{d\ln\Delta t} = \frac{dp_w}{d\Delta t} = \eta \left(1 - \frac{1}{1 + t_p/\Delta t} \right) \approx \eta$$

(D.4)

The pressure derivative is constant for radial flow.

D.2.2 Channel flow. From (C.33) the pressure derivative for channel flow (at early time – before the presence of any boundaries is observed) is given by:

$$\Delta t \frac{dp_w}{d\Delta t} = \frac{\beta \sqrt{t}}{2} \left(1 - \frac{1}{\sqrt{1 + t_p/\Delta t}} \right) \approx \frac{\beta \sqrt{t}}{2}$$

(D.5)

for $\Delta t \ll t_p$.

D.3 Pressure match for channel flow.

A direct test of channel flow is – from Eq. (C.53) – to plot the pressure as a function of so-called channel time: $\sqrt{\Delta t + t_p} - \sqrt{\Delta t}$. For an infinite channel, this plot should be a straight line with an intercept at the initial reservoir pressure. Figure D.4 presents this plot: there is a convincing and unambiguous straight line. There is no doubt that the pressure response in Macondo indicates channel flow. This is also consistent with the reservoir geology (Section 5) and provides confidence that we have interpreted the pressure behaviour correctly.

The best linear fit through the data gives a gradient $\beta \approx 0.5$ psi s$^{-1/2}$ with $p_i \approx 11{,}100$ psi (see Table D.1 for an explanation of terms). But the measured $p_i = 11{,}856$ psi; the fitted value is too low by more than 700 psi: this indicates some additional draw-down in the system and demonstrates that despite the good linear fit, Macondo cannot be modelled as an infinite channel: the pressure must have seen one or more barriers to flow at the ends of the channel.

Shown in Figure D.5 is the best fit to the data using the linear and rectangular models.[224] The parameters used to obtain this prediction are provided in Tables D.2 and D.3. The match is excellent: the pressure signal detects one end of the channel during both draw-down and build-up, but the influence of the other, farther, end is somewhat weaker. τ_1 is the time taken for the pressure to reach the farthest reservoir boundary, while τ_2 is the time to reach the nearer end of the channel. t_p is the production time (the length of the spill period). We find $\tau_1 > t_p > \tau_2$. We can tell the presence of the far

---

[224] Mathematically the linear model prediction is made using Eq. (C.64) – see Appendix C for the derivation.

boundary, since it makes a detectable perturbation to the pressure response. On the other hand, τ_1 is larger than t_p, the flow period, meaning that the influence of the far boundary does not dominate the pressure: if t_p were greater than τ_1, we would see a noticeable and sharp decrease in the pressure derivative during the build-up; this is not observed (Section 4.3).
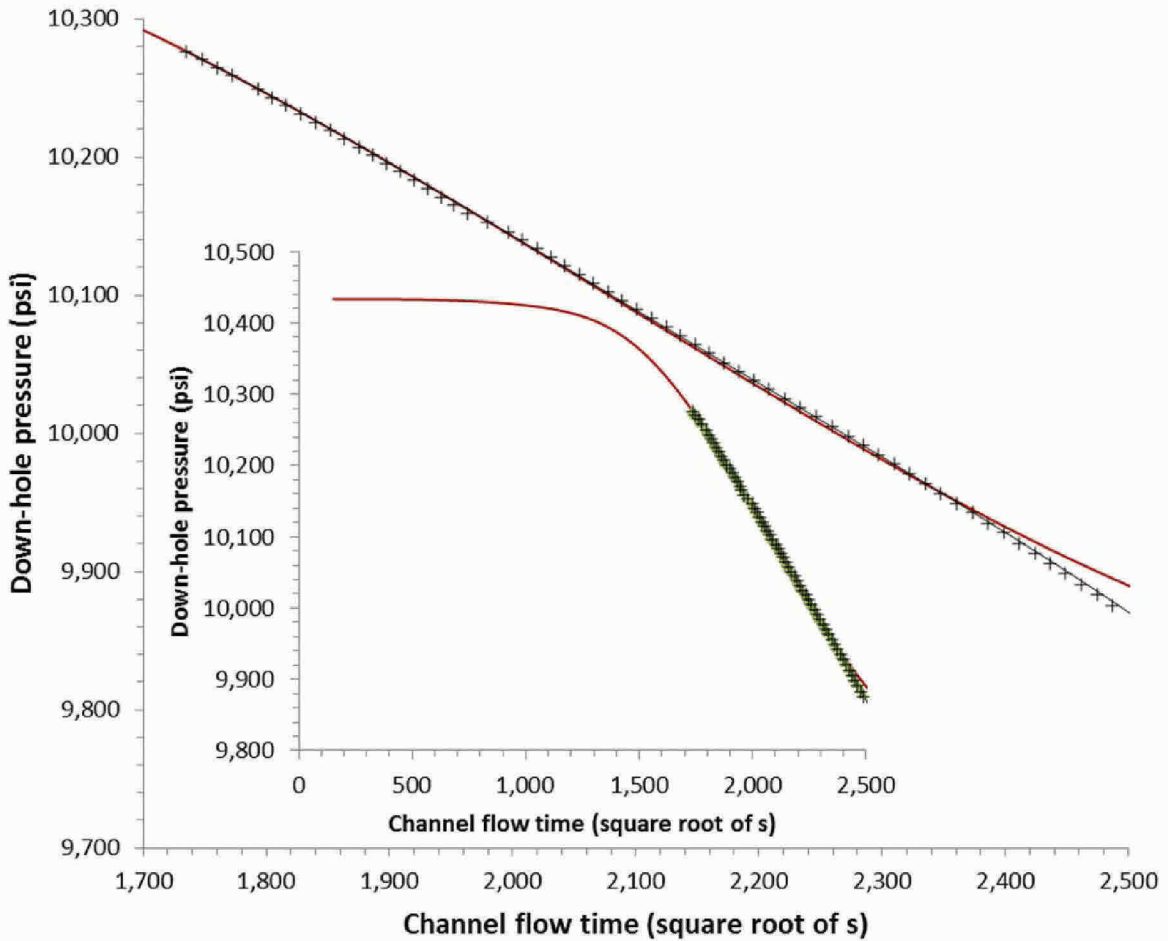
Figure D.4. The reservoir pressure as a function of channel time $\sqrt{\Delta t + t_p} - \sqrt{\Delta t}$. Note the almost exact straight line indicating channel flow. The red line is the best fit using the linear flow model presented in Appendix C and the parameters listed in Table D.2, while the black line is the rectangular model fit (Table D,3): they almost exactly reproduce the measured pressures (crosses – corrected to down-hole conditions). The inset shows the prediction for later time (channel time close to zero) showing that the pressure reaches final value of 10,433 psi. [225]

---

[225] This is the final reservoir pressure computed using Core Labs fluid properties. I have performed the same analysis for all three sets of fluid properties.

112

D.4   Horner analysis and capping stack pressure

A standard method to study radial flow – once it has been identified on the pressure derivative – is through the use of the Horner plot. The Horner plot was also employed in the work of Dr. Hsieh (2010, 2011). For completeness, this is shown here.

Figure D.5 shows the pressure as a function of Horner time: from Eq. (C.19) the pressure build-up should be a straight line for radial flow when plotted as a function of $(t_p+\Delta t)/\Delta t$. The onset of channel flow – a deviation from approximate straight-line behaviour – is at around 60,000 s.

Figure D.6 shows the predicted and measured capping stack pressures for reference. Notice that I predict that the pressure reaches a maximum and then declines: this is at very late times (around 3 months after choke closure) when the cooling of the well-bore has a more significant impact on the pressure than the rise in pressure in the reservoir.
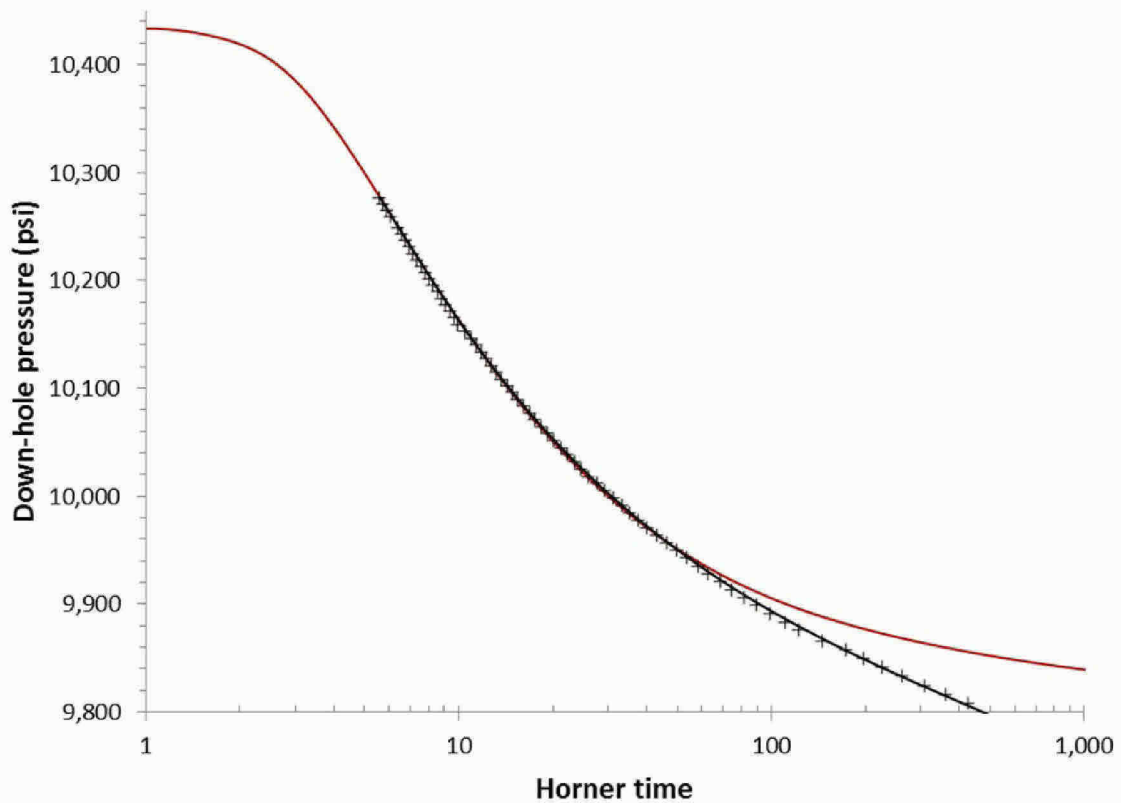
Figure D.5. Horner plot of the pressure response: here pressure is plotted against the logarithm of $(t_p+\Delta t)/\Delta t$: a straight line indicates radial flow. The red line uses a linear model, which deviates from the data at early times – large Horner time, while the black line uses a rectangular model, which provides an excellent fit to the data (crosses) at all times.

113

TREX-011553-R.0113
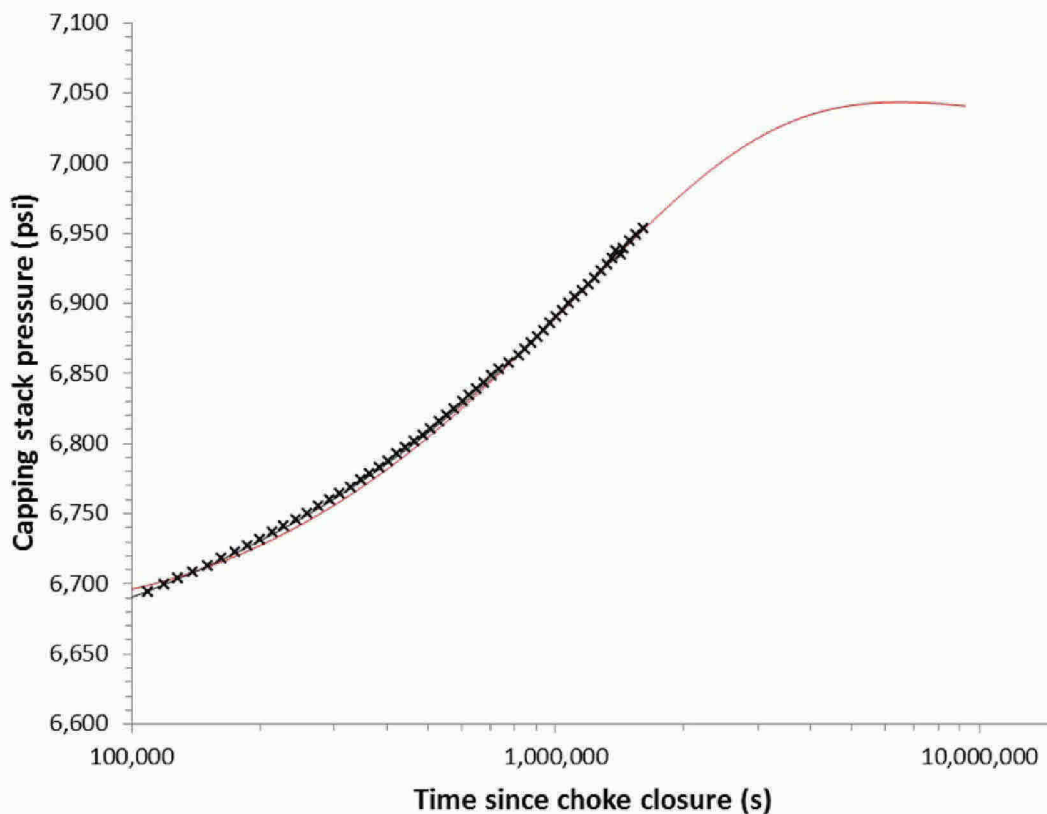
Figure D.6. Predicted and measured capping stack pressure. The red line uses a linear model, the black line the rectangular model, while the data is shown as crosses. Note that I predict that the capping stack pressure reaches a maximum and then declines at late time – well beyond when the well was cemented – to a final value around 7,040 psi: the effects of well-bore cooling over-take the effects of the pressure increase in the reservoir.

114

Appendix E.   Consideration of variable flow rates

My pressure analysis has assumed a constant flow rate, followed by an instant stopping of the flow. In contrast, in Macondo, there was a complex sequence of changes in flow rate as the choke was closed. Furthermore, the flow rate most likely varied throughout the whole spill period as a consequence of alterations in the flow resistance near the well-bore and in the surface equipment.

In this Section we consider – again using standard petroleum engineering techniques – the impact of a variable flow rate. We do this for two reasons. Firstly, we study the flow rate at the time of choke closure. This should, in theory, give us a more refined estimate of permeability. We find in this case though that it has no impact on our calculations. Secondly, we will examine how variable flow rates could affect our later-time pressure analysis and estimates of oil released. Then I provide an analysis of flow resistance (skin) between the reservoir and the well-bore to study the evidence for a flow rate that increased during the spill.

E.1   Superposition method to find permeability

In this Section we study the pressure behaviour shortly after choke closure. To perform this analysis we do need an estimate of flow rate – particularly flow rate as the well was closed. I have digitized the figures in the Ratzel report [3; Figure 9] that show flow rate as a function of time, and as a function of choke closure, using the LANL data. While this gives slightly lower flow rates than the other values considered, it appears to be most consistent with the Griffiths report [2; SKG]. I am not suggesting that this is correct – it is simply used for my calculations as I do not have another independent assessment of flow rate history: indeed I consider its cumulative – the total flow – to be incorrect.

For completeness we repeat the radial flow analysis from Appendix C for a variable flow rate. The pressure response for unit rate is given by Eq. (C.17):

$$p_D(t) = \frac{\mu}{4\pi Kh} \ln\left(\frac{4t}{\alpha\gamma r_w^2}\right)$$

(E.1)

Then using Duhamel's principle the well pressure can be written from Eq. (C.18):

$$p_w = p_i - \delta(t)Q(t) + \int_0^t \frac{\partial Q(\tau)}{\partial \tau} p_D(t-\tau)d\tau$$

(E.2)

Now consider the flow rate to be a series of constant flow periods separated by jumps in rate. We take $Q(t=0)=0$ and then at times t_i there is a change in flow rate ΔQ_i, leading, eventually, to a rate of zero at time $t=t_p$; Δt is the time since flow ceased. ΔQ_i is positive if the flow rate increases and negative if it decreases. From Eqs. (E.1) and (E.2) in the build-up period:

$$p_w = p_i - \frac{\mu}{4\pi Kh}\sum_i \Delta Q_i \ln\left(\frac{4(t_p + \Delta t - t_i)}{\alpha\gamma r_w^2}\right) = p_i - \frac{\mu}{4\pi Kh}\sum_i \Delta Q_i \ln(t_p + \Delta t - t_i)$$

(E.3)

since $\sum_i \Delta Q_i = 0$, the sum of all the rate changes is zero (the flow rate starts and ends at zero).

If we define a reference flow rate Q_o, we can write Eq. (E.3) as follows:

$$p_w = p_i - \frac{\mu Q_o}{4\pi Kh}\sum_i \frac{\Delta Q_i}{Q_o}\ln(t_p + \Delta t - t_i) = p_i + \eta\ln\tau$$

(E.4)

where η is defined in Table D.1 and we have defined a superposition time τ:

$$\ln(\tau) = -\sum_{i=1}^{f} \frac{\Delta Q_i}{Q_o}\ln(t_p + \Delta t - t_i)$$

(E.5)

The reference flow rate can be either the final flow rate (just before well closure) or some average flow rate. In this analysis I take Q_o = 53,000 stb/day, which is the flow rate estimated before the beginning of choke closure for the flow rate history we have assumed [2,3].

E.2.1 Pressure derivative. The pressure derivative, Eq. (D.1) is found as a function of τ rather than time t:

$$\tau\frac{dp_w}{d\tau} = \eta$$

(E.6)

Very simply – variable rates in the radial flow regime become a constant derivative.

If we do not have radial flow, we follow the same procedure: we simply treat the derivative computed using the superposition time as a normal derivative for interpretation.

Figure E.1 shows the reservoir pressure derivative, but using the superposition time τ rather than normal time t. The results are very similar, giving essentially identical assessments of permeability and channel flow. Hence, for simplicity, in the main text (Section 4.3) I only present a constant flow rate case. We see a radial flow stabilization at around η = 55 psi and a transition to channel flow τ_w at 60,000 s, consistent with the best-match rectangular flow models presented in Appendix D. Using the equation in Table D.1 we find, as in Section 4.3, a permeability of around 300 mD. This is close to the average of the core measurements (Appendix A.5), while representing a flow-based average over around 750 m from the well. However, before a day, the conversion from capping stack to reservoir pressures is uncertain (Appendix B) and so I do not consider this estimate of permeability to be as robust as the determination of 238 mD by Dr. Gringarten. He also finds a flow-based average, but from pressure measurements made down-hole shortly after drilling the well, which avoids the problem of the pressure conversion.

116

E.2   Effect of variable flow rates on the linear flow regime

My analysis of the late-time pressure response, used to determine the final reservoir pressure, assumes a constant flow rate. This represents the average flow rate during the incident and I have implied that the results of my calculations are insensitive to the flow rate history.

However, the flow rate history does have some impact on the pressure response. In this section I will match my linear model to different hypothetical flow rate histories. I must emphasize though that the flow rates I have used are for illustrative purposes only; I am not claiming that they are correct, or even possible. In particular I am not necessarily suggesting that the initial flow rate was zero (see below) – my conclusions depend only on the average flow rate in the earlier half of the spill relative to that in the latter half.
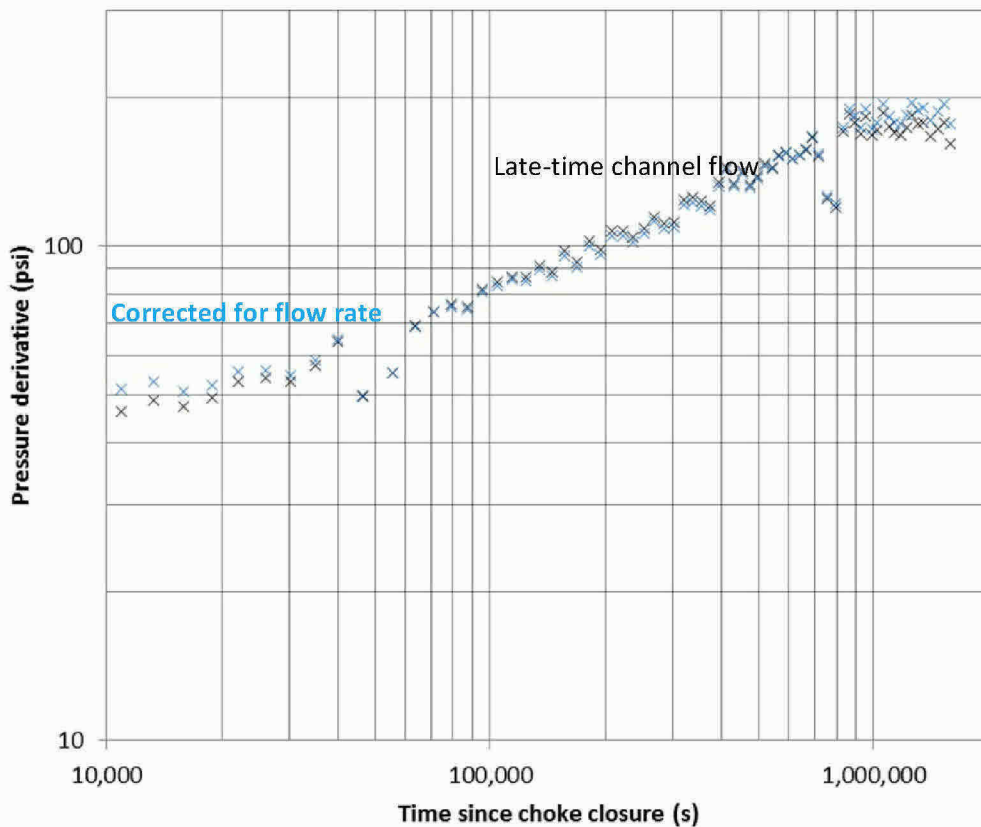
Figure E.1. Reservoir pressure derivative using the superposition time, Eq. (E.5) (blue crosses) compared to the data uncorrected for flow rate changes (black crosses). Accounting for flow rate makes little difference to the derivative after 10,000 s and so has no impact on the analysis. There is evidence of radial flow with a best-match η of around 55 psi and a transition to channel flow at τ_w = 60,000 s.

Table E.1 presents the results of a pressure match using different purely hypothetical flow rate histories. We assume that at early times the flow rate increases from zero to a maximum value, caused by some unspecified erosion in the surface equipment or down-hole. When this erosion ceases, we apply flow

117

conditions consistent with the Government reports where the flow rate declines slowly over time as the reservoir pressure falls. We assume a 6% decrease in flow rate when the capping stack was installed, and a 4% increase when the riser was cut.

The pressure response is computed using Eq. (C.67) – the linear flow model. We find the reservoir parameters that give the best fit to the measured capping stack pressure and pressure derivative. We have used the Core Labs fluid properties.

Relative oil released	τ_1 (s)	τ_2 (s)	Δp (psi)
1 (Constant)	**11,270,444**	**115,079**	**1,433**
1.099 (Govt.)	**11,585,238**	**90,289**	**1,423**
1.081	11,426,063	96,378	1,423
1.059	11,244,226	103,939	1,424
1.039	11,069,093	111,934	1,425
1.018	10,899,775	120,447	1,426
0.997	10,736,090	129,546	1,427
0.976	10,578,211	139,301	1,427
0.956	10,426,536	149,781	1,428
0.935	10,281,669	161,062	1,429
0.915	10,144,414	173,217	1,429
0.895	10,018,331	186,038	1,429
0.875	9,903,928	199,569	1,430
0.855	9,800,620	214,040	1,430
0.835	9,711,066	229,298	1,430
0.815	9,638,577	244,985	1,430
0.794	9,587,229	260,369	1,429
0.774	9,561,033	273,907	1,429

Table E.1. The results of matching the analytical linear reservoir model to the pressure data, assuming different flow rate histories and cumulative flows relative to a constant rate case. The first row in red has a constant flow rate (presented in the main body of the report), while the second row (black) uses the Government's assumed flow rate history. In green is a case consistent with a final flow rates of 45,000 – 55,000 stb/day and my material balance calculations. The relative oil released is the cumulative flow relative to a constant flow-rate case with the same final flow rate.

In all cases we have an acceptable pressure match: this analysis cannot discriminate between possible flow histories. Figure E.2 shows these hypothetical flow rate histories, illustrating one that matches – broadly – that assumed in the Ratzel and Griffiths reports, a constant rate, and another case where the cumulative release is approximately 80% of the constant rate case. Figure E.3 shows the corresponding predictions of pressure increase and derivative – by eye the different cases are identical at late time: in all cases the predicted pressure drop varies by less than 10 psi from the constant rate case (less than 1%), while the pressure is matched to 2.7 psi or better.
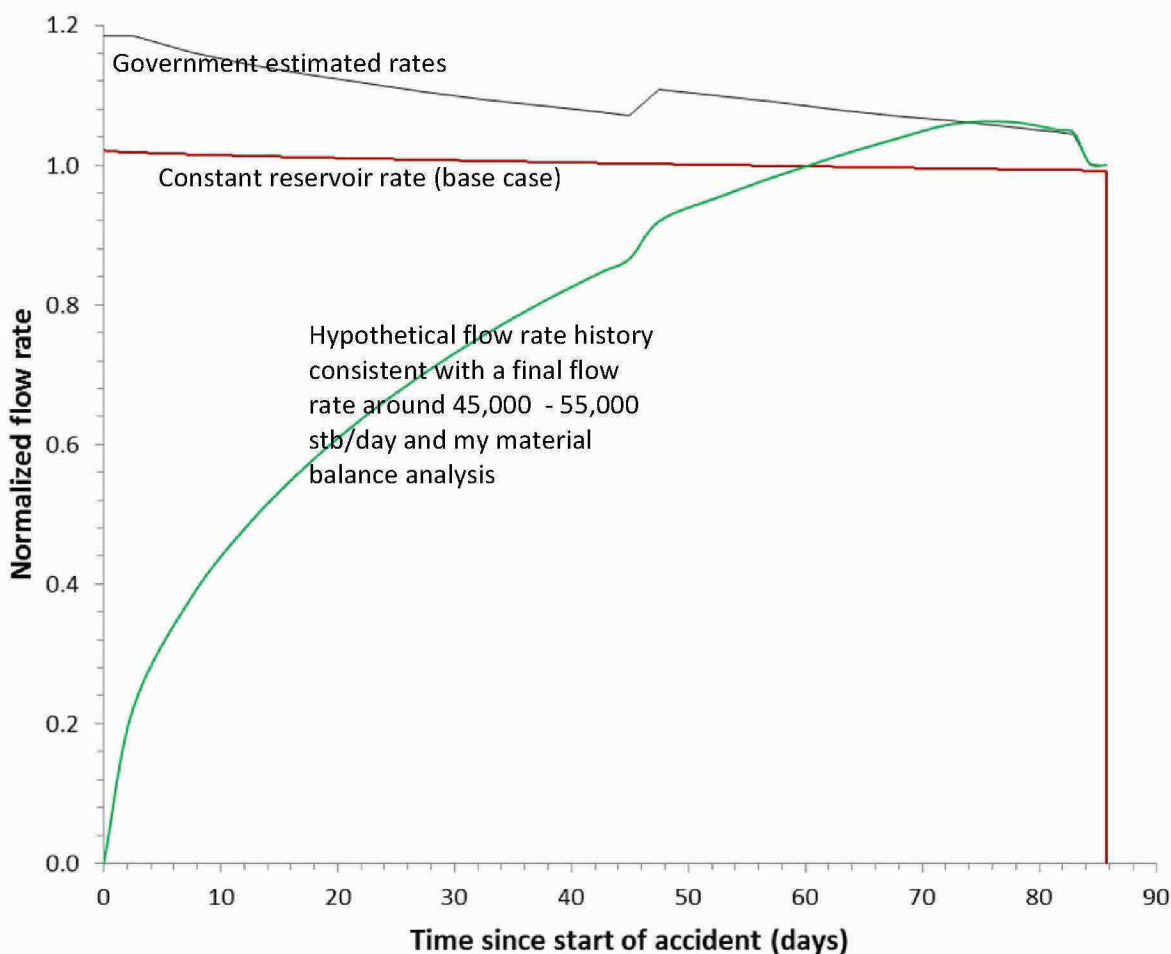
Figure E.2. Different putative flow rate histories. The rate is shown normalized by the rate at the end of the spill. In red is the base case in this report – a constant reservoir rate.[226] In black is a rate history that corresponds to that – approximately – assumed in the Government reports. In green is an increasing flow rate at early time, which will give a cumulative release consistent with my material balance calculations and a final flow rate around 45,000 – 55,000 stb/day.

The case shown in green in Figures E.2 and E.3 gives a cumulative release of between 3.1 and 3.6 MMstb for final flow rates between 45,000 and 55,000 stb/day. This is now consistent with all the reservoir data, the estimated final flow rates from Government investigators, while providing a better pressure match than all of Dr. Pooladi-Darvish's simulation runs (Appendix F.4). The estimated locations of the reservoir boundaries (Section 5) are also consistent with the geology – indeed a rather better agreement is found, since the pressure analysis now allows the connected reservoir to be slightly longer to the South (τ_2 is larger than the constant-rate case), closer to the location of the boundaries of the field identified in the seismic survey. τ_1 is slightly smaller, although still consistent with the boundaries of the field to the North-West.

---

[226] Technically, the base case is a constant *reservoir* rate (Appendix C). Since the reservoir pressure varies over time, so does the oil formation volume factor (measured at the well-bore pressure, ignoring skin), and hence the *surface* rate (measured in stb/day) changes slightly. I have made this correction on the graph, showing a slight decrease in surface rate with time for the base case. The average normalized rate is defined to be 1.

This is an important analysis, as it demonstrates that it is possible to honour the final flow rates proffered by the Government investigators, while being consistent with all the reservoir data and my material balance calculation.
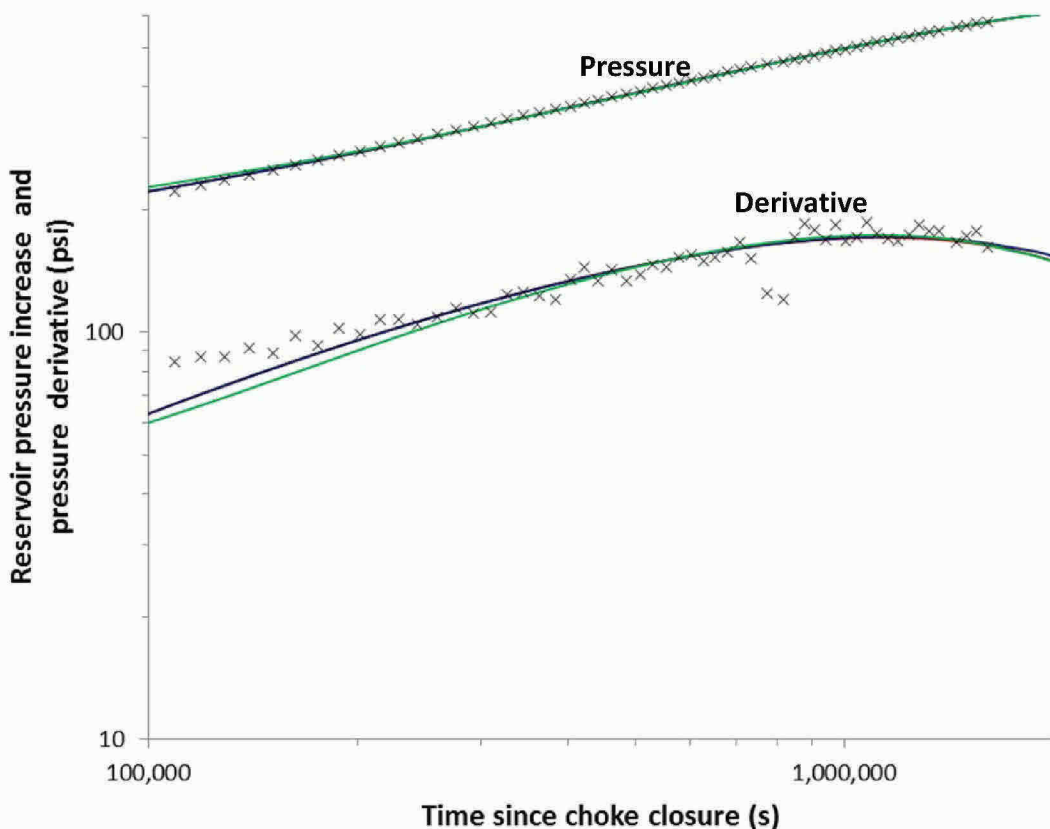
Figure E.3. The capping stack pressure and pressure derivative matches using the linear flow model with the flow rate histories shown in Figure E.2. Crosses are the data, the black line assumes a decreasing (Government) flow rate, the red lines a constant rate (the base case) while green is an increasing rate at early time. In all cases the predictions are indistinguishable at late time.

E.3 Analysis of skin and down-hole pressure

An increasing flow rate requires some opening of flow paths, either down-hole or through erosion of the blow-out preventer and/or other surface equipment. My expertise is in reservoir engineering and so I will ignore – for the sake of argument – any erosion in the surface equipment. In this Section I will demonstrate that it is possible that changes in the flow resistance from the reservoir to the well-bore at reservoir depth alone are sufficient to allow an increasing flow rate.

It is usual in normal oilfield operations for the flow path of oil to be impeded in the near well-bore region. This extra resistance to flow is accounted empirically by a so-called skin factor, introduced mathematically in Appendix C. In Macondo this skin has three components: partial penetration skin, because the oil entered the well-bore over a restricted interval of the reservoir; reduced permeability

120

TREX-011553-R.0120

near the well, since the rock may be clogged with drilling mud and cuttings (sand) forced into the formation during drilling; and any additional resistance to flow due to cement and other material in or near the well-bore at reservoir depth.

E.3.1. Estimate of the skin at the time of the blowout. The Emilsen report in its analysis of the accident,[227] estimates that the oil flow was initially coming from between only 13 to 16.5 ft of the reservoir thickness. We can use this information to estimate the skin factor.[228]

$$ S = \left(\frac{h}{h_f} - 1 \right) ln \left(\frac{h}{r_w} \sqrt{\frac{K_h}{K_v}} - 2 \right) $$

(E.7)

where h is the thickness of the reservoir (I will use 93 ft[229]); h_f is the thickness of the flowing interval (I take a mid-range value of 15 ft); r_w is the well radius (4.25 inches) while K_h and K_v are the horizontal and vertical permeabilities respectively. Typically K_h is greater than K_v due to the presence of thin, horizontal layers of shale or other low permeability rock that restricts vertical flow: I will assume $K_h/K_v=10$, taken from the pressure analysis in the Gringarten report. Then from Eq. (E.7) I find than $S=35$.

I note that the permeability of core samples taken directly from the well had an average permeability to oil of 75 mD (Appendix A.5); in contrast Dr. Gringarten's estimate of the field-average permeability is around 240 mD. This suggests that the rock near the well-bore could have been clogged with drilling mud and cuttings (sand) dislodged during drilling. On the other hand, the pressure analysis in the Gringarten report sees no skin due to permeability reductions in the near well-bore region before cementing.

Last, it is also difficult to quantify the impact of other restrictions to flow from the reservoir to the well-bore, through the cement and other material present down-hole.

Overall, the estimated skin factor of 35 must be considered a lower bound: I will consider a likely range of 35-50 in the discussion that follows – the upper end being used (as a fixed value) by Dr. Pooladi-Darvish.[230]

The skin introduces an additional pressure drop from the reservoir to the well-bore that is given, from Eq. (C.16) as:

$$ \Delta p = 2\eta S = \frac{\mu Q_0}{2\pi K h} S $$

(E.8)

---

[227] Final Emilson report [27], Section 2, page 7.
[228] A determination of the partial penetration skin requires knowledge of the reservoir geometry and several different correlations have been proposed in the literature. Here I use a standard and simple expression derived by Saidikowski (1979).
[229] The Emilson report uses 86 ft [27].
[230] The Pooladi-Darvish report considers a range of 0-50 for skin; [PD], Appendix III, slide 8. However, the skin factor is assumed to be constant during the spill period.

From Section E.1, a representative value of η is around 55 psi for a given final flow rate final rate Q_f. This enables me to write the following equation to find Δp in psi:

$$\Delta p = 110\, S \frac{Q_i}{Q_f} S$$

<div align="right">(E.9)</div>

where Q_i is the initial flow rate, or at least the flow rate in the early part of the spill period, and Q_f is the final flow rate.

Let us now estimate the magnitude of this pressure drop. If we assume that the initial flow rate is around half that at the end (see the previous Section E.2) and a skin of 35, the pressure drop is 1,925 psi; with a skin of 50 it is 2,759 psi. Note that this is larger than the overall decline in reservoir pressure (around 1,400 psi – Section 4.3). We can use Eq. (E.9) to put in different hypothetical skin factors and flow rates – neither of which we know with certainty at the beginning of the spill period – but it is likely that the skin introduced a pressure drop larger than the decline in average reservoir pressure.

E.3.2 The skin at the end of the spill. We have two pieces of evidence to help estimate the final skin: the pressure increase measured at the capping stack when the well was closed, and the flow test with base oil preformed just before the well was cemented. I will consider each in turn.

The skin factor is normally estimated from the rapid rise in pressure when a well is shut-in: the more-or-less instantaneous pressure rise allows us to estimate the skin from Eq. (E.9).[231]

The pressure rose by around 4,000 psi during choke closure. The Government investigators[232] have modelled this successfully assuming no skin; they assigned no additional resistance between the well-bore and the reservoir: all this pressure rise is accounted for by the ending of flow in the well-bore and surface equipment. This would suggest that only small, or even negligible, portion of this pressure rise is due to the reservoir skin.

The pressure increase due to skin alone, from Eq. (E.9), is $110S$. If S is in the range 35-50, this gives values between 3,850 and 5,500 psi. If only a small fraction of the 4,000 psi pressure rise is due to skin, then this suggests that the skin at the end of the spill is much lower – and may indeed be zero – but it is impossible to be more precise.

The other, more definitive, determination of skin comes from the injection of base oil into the capped well prior to mud injection and cementing. This oil was injected through the capping stack at rates between 1 and 7 barrels per minute.[233] The pressure increase on oil injection was very low, around 15

---

[231] In standard petroleum practice, when the down-hole pressure is measured, the skin is determined from pressure transient analysis – see Section 4.3.

[232] The revised Ratzel [3] and revised Griffiths [2] reports and the work of Hsieh (2010, 2011) [11, 44].

[233] http://www.bp.com/liveassets/bp_internet/globalbp/globalbp_uk_english/incident_response/STAGING/local_assets/downloads_pdfs/BP_technical_audio_08032010.pdf

psi on average – bearing in mind the gauge precision of only 5 psi, it is difficult to say more than the pressure increased slightly.[234]

In this test, we have much slower flows than during the spill – these injection rates are 1,440 to 10,080 stb/day – and the fluid is a single (oil) phase in the well-bore. We can assume that, unlike during choke closure, the principal pressure drop is due to skin and flow in the reservoir itself. In this case, the pressure increase can be calculated assuming that for the minutes to hour-long duration of the test, we are in the radial flow period. Then, from Eq. (C.16):

$$\Delta p = \eta \left(\ln \left(\frac{4t}{\alpha \gamma r_w^2} \right) + 2S \right)$$

(E.10)

Let us first estimate the magnitude of the logarithmic term. $\alpha \gamma r_w^2$ has a value of approximately 0.0038 s.[235] The duration of the injectivity test was around 1 hour, while the pressure reached 6,976 psi – its highest consistent reading – after only 10 minutes (600 s): this is a Δp of 24 psi. Since we find a logarithm, the magnitude of the term is relatively insensitive to the precise time used, but to avoid over-estimating the reservoir pressure change, I will take the lower time t = 600 s: the logarithmic term then has a value of 13.4.

To find the pressure drop, I need to correct η for different flow rates – its value is 55 psi times the ratio of the mud injection rate to the estimated final flow rate during the spill, measured at *reservoir* conditions. This is an approximate calculation, so let's assume that the highest mud injection rate is around one tenth of the final flow rate.

Had the skin factor been around 35-50, pressure changes of over 250-350 psi would have been seen (Eq. (E.10)): this is an order of magnitude higher than what was observed. Even with no skin, the maximum pressure rise is predicted to be around 70 psi, so – if anything – there is a negative skin, implying enhanced flow near the well at the end of the spill. This suggests limited resistance to flow between the reservoir and the well-bore down-hole at the end of the incident

I have ignored any pressure drop in the capping stack and well-bore, I have not accounted for the changing gravitational head between the capping stack and the reservoir during injection, while the measured the capping stack pressures only have a precision of 5 psi and I have taken one – relatively high – pressure drop for my calculations. The skin at the end of the spill is lower than its likely value at the beginning. It is reasonable to assume – as did all the Government investigators – that the skin was zero at the end of the spill.

---

[234] Trusler report [T], from a study of the capping stack pressures (PT-3K-2) from 13:00 on August 3 2010 (line 120,951 on the spreadsheet provided). The pressure before base oil injection is between 6,952 psi, rising to at most 6,976 psi on injection, except for one reading that spikes just over 7,000 psi.
[235] α = 0.5633 s/m^2, using Core Labs properties and the mid-range compressibility, the Euler constant γ is 0.57722, and the well diameter is 8.5 inches, giving r_w = 0.108 m.

E.3.3 Likely change in skin during the spill period and implications for flow rate. We cannot draw any definitive conclusions concerning the skin, or flow resistance from the reservoir to well-bore, or how it changed over time. However, the available evidence does suggest that the skin was initially high and declined during the flow period. This change would increase the pressure in the well-bore at reservoir depths by an amount that is of the same magnitude, or greater than, the reservoir pressure decline. The net effect is a down-hole pressure that may have *increased* over time, leading to an increasing flow rate, even if we ignore any erosion of the surface facilities. The work of Oldenburg *et al.* (2012) that studied flow through the well-bore and blow-out preventer, implies that small changes in this pressure could have a large impact on flow rate.

The imprecision of this analysis, however, demonstrates that it is very difficult to determine flow rates at the beginning of the flow period. Rather than make unsupported assertions concerning pressure drops and flow resistance, it is preferable to employ an approach that avoids this problem completely, namely a material balance analysis that determines the cumulative oil flow directly.

Appendix F.   Critique of Government expert reports

This Appendix provides a detailed critique of the three Government expert reports which include a study of reservoir flow, or fluid properties. These are the reports prepared by Dr. Zick (the Zick report [Z]), Drs. Kelkar & Raghavan (the Kelkar & Raghavan report [KR]), and Dr. Pooladi-Darvish (the Pooladi-Darvish report [PD]). Dr. Zick developed an equation-of-state model to predict fluid properties. Drs. Kelkar & Raghavan presented a material balance calculation of oil released, following, conceptually, a similar approach to mine. As we show below, however, the details – and the final answers – are different. Dr. Pooladi-Darvish linked a model of outflow performance to a reservoir simulator to deduce cumulative release. His approach is most similar to the Sandia researchers Drs. Griffiths and Ratzel, albeit with a more sophisticated reservoir model.

F.1   How the calculations were performed and what parameters they used

My analysis multiplies three quantities together to determine the volume of oil released: (1) the oil volume connected to the well; (2) the compressibility of the rock and fluids; and (3) the pressure drop. This is simply a statement of conservation of mass: any estimate of oil released – however it is presented – must obey material balance. Therefore, regardless of the complexity of a reservoir analysis, the total amount of oil released can be determined simply from these three quantities. In this Section, expanding on the discussion in Sections 2 and 3, I discuss *how* these quantities were determined, to assess the quality of the analysis, and *what* values were assigned, to determine the effect on the estimate of oil released.

F.1.1 Methodology, or *how* key parameters were determined.

1. **Connected oil volume**.   Neither the Kelkar & Raghavan nor the Pooladi-Darvish reports mentioned the possibility that not all the oil in the field is connected to the well. There was no independent discussion of geology and the seismic survey as part of a quantitative consistency check with the results of the pressure analysis (my Section 5). The conversion from reservoir to surface volumes was performed inconsistently and was not based on measured data.

2. **Rock and fluid compressibility.** The Kelkar & Raghavan report did not take a value of pore volume compressibility from direct measurements, relying instead on an incorrect inference as to what BP considered a "most likely" value. However, Dr. Kelkar, when he consulted for the US Government Flow Rate Technical Group, did use values based on the measurements. And when Kelkar & Raghavan used a rock compressibility closer to the measured value, they calculate a cumulative flow consistent with my own.

3. **Pressure drop**. The Pooladi-Darvish report's base case numerical match to the pressure data had a pressure difference between the capping stack and the reservoir that was unfeasibly low: during the 19 days that the oil remained motionless in the capping stack, surrounded by the cold, deep ocean, it was assumed that this oil maintained a near-reservoir-condition temperature of 220°F.

125

F.1.2 Results, or *what* values were assumed. At the end of this Appendix, I provide a table that quantifies the impact of different assumptions on the calculated volume of oil released, and shows how by correcting these errors my values are recovered. Here I mention the key points.

1. **Connected oil volume.** The Zick report provided values of oil formation volume factor that lie outside the range of direct measurements.[236] An inappropriate value of formation volume factor led to a biased over-statement of oil volume measured at surface conditions in the Raghavan & Kelkar report. Furthermore, they assumed 100% connectivity of the reservoir, or at least never discussed connectivity explicitly. The result was an over-statement of oil volume, compared to my determination, of up to 30% or more.

2. **Rock and fluid compressibility**. The Raghavan & Kelkar report assumed a pore volume compressibility of 12 microsips – a value that is about twice the average of direct measurements. The only analytical pressure transient analysis presented by Pooladi-Darvish used an oil compressibility that is also twice the measured value.

3. **Pressure drop.** The Raghavan & Kelkar report uses a very different approach to mine to find the final reservoir pressure and it understates the weight of the oil between the capping stack and the reservoir. The Pooladi-Darvish report under-states the final reservoir pressure by at least 200 psi, again due principally to the under-statement of the pressure difference between the capping stack and the reservoir (see Appendix B.4).

The Kelkar & Raghavan and Pooladi-Darvish reports, despite using different assumptions and values for these key quantities, reach the same conclusion: that the oil released was approximately 5 MMstb. My report demonstrates that it is not possible to arrive at this volume while also honouring the pressure data, the measured fluid and rock properties, and the most-likely estimates of reservoir size. If you assert that 5 MMstb was released, then you have to demonstrate why the data is wrong, or unrepresentative of the field. While this was not admitted in the expert reports, it is evident on careful reading and close examination of the assumptions made. The authors of these reports cannot arrive at a cumulative release of 5 MMstb without ignoring the data.

F.2   The Zick report

Dr. Zick took the measured fluid properties and composition to construct an equation-of-state model of the Macondo hydrocarbons. He used this equation-of-state to construct fluid property tables. This is a standard approach in the oil industry, and allows fluid properties – such as density, viscosity and the ratio of oil to gas – to be computed at any temperature and pressure and for any combination of oil and gas phases. Dr. Zick provided his model to the other experts providing analyses of flow rate for the Government. As stated in the Zick report, it is reasonable to construct a model that is thoroughly checked for consistency against the experimental data.

F.2.1 Conversion from reservoir to surface volumes. In petroleum engineering it is standard practice to refer to oil volumes in stock tank barrels. This is the volume of oil measured at surface conditions of

---

[236] Dr. Zick [Z] also used a different definition for this conversion, which I discuss later. Here I simply note that his model gives predictions that lie outside the range of the measurements in a manner that will consistently over-state the volume of oil released.

60°F and 1 atmosphere pressure (15 psi). The analyses of flow rate presented in the public domain,[237] and in the expert reports discussed in this Section, have followed this convention, as have I.

The oil formation volume factor, B_o, is the ratio of reservoir volume to surface volume. My analysis determines the reservoir volume of oil that was released. I divide by the oil formation volume factor to find the surface volume – at 60°F and 1 atm pressure. A related quantity is the gas/oil ratio, R_s, which is the ratio of the surface volume to the surface volume of oil.

F.2.2 Bias in the Zick model that will over-state the oil volume. Unfortunately, Dr. Zick's model predicts oil formation volume factors and gas/oil ratios that lie outside the range of the measurements, introducing a bias that will over-state the volume of oil released by between 3 and 4 %. This comparison is presented in Table F.1. As with the BP tables, I will not use these values but reply instead on using the measured values in my analysis.

Quantity	Core labs[238]	Schlumberger[239]	Intertek[240]	Average of the measurements	Zick report value	% deviation between Zick and measured average
Formation volume factor (single-stage separation)[241]	2.618	2.539	2.5104	2.556	2.473	**3.2**
Formation volume factor (multistage separation)[242]	2.339	2.262	2.3875	2.330	2.227	**4.4**
Gas/oil ratio, scf/stb (single-stage separation)	2,906	2,945	2,831	2,894	2,826	**2.3**
Gas/oil ratio, scf/stb (multistage separation)	2,485	2,442	2,747	2,558	2,418	**5.5**

Table F.1. Table comparing measured formation volume factors and gas/oil ratios to the values presented in the Zick report.[243] The values in the Zick report lie outside the range of the measured data and lead to an over-statement of oil volume at surface conditions.

F.2.3 Single-stage separation. There is a subtlety in how the conversion from the reservoir to the surface is defined; this explains why two sets of formation volume factors and gas/oil ratios are presented in Table F.1.

The single-stage flash or separation occurs when oil from the reservoir is taken to the surface while remaining in contact with the exsolved gas. In this case B_o and R_s do not depend on the exact sequence of temperature and pressure changes as the oil was brought to the surface. The single-stage separation occurs for flow up the well-bore to collection at the surface, as discussed in Appendix A.2.

---

[237] See, for instance, McNutt *et al.* (2012b).

[238] BP-HZN-2179MDL00063084 (Core Labs fluid property report) [20].

[239] BP-HZN-2179MDL01608973 (Schlumberger fluid analysis on Macondo Samples) [34].

[240] BP-HZN-2179MDL04440732 (Intertek fluid property report) [18].

[241] This is the formation volume factor measured at the saturation pressure – its maximum value. Here taken for a single-stage separation to surface conditions.

[242] This is the formation volume factor measured at the saturation pressure measured for a multistage separation to surface conditions.

[243] Zick report [Z], Table 3, page 15.

127

F.2.4 Multistage separation. The Zick report suggests that it is more representative to use values of B_o and R_s from a multistage separation. Let me explain the reasoning in my own words, and I will then provide my own assessment. Oil is more valuable than gas, and so companies design their facilities to capture as much oil as possible. While most of the methane in the reservoir oil forms a gas at the surface, some of the other, lighter hydrocarbon components (so-called intermediates, such as ethane, butane and propane) can be present in significant quantities in either the gas or liquid phases. To produce as much valuable liquid as possible, oil companies want to ensure that as most of the intermediate components remain in the liquid (oil) phase at the surface. This is achieved by separating the gas from the oil at high pressure. The remaining hydrocarbon then evolves less gas, containing fewer intermediates and giving a larger oil volume than for a single-stage separation. The hydrocarbon may go through several stages of separation at progressively lower pressures until stock tank conditions are reached.

The fluid property reports contain details of a four-stage separation. The Zick report assumed that this represents the separator conditions had the accident not occurred and BP had produced the oil normally. So, in a hypothetical scenario, with no accident and with BP applying the separator conditions studied in the fluid property reports, the conversion from surface to stock tank conditions would be performed using B_o from this four-stage separation. This conversion produces more oil for the same volume released from the reservoir compared to a single-phase flash, by design. The Zick report states that the oil volume is 11% higher if the multistage values are employed.

The Zick report describes single-stage separation[244] *"as though the oil that spilled into the Gulf of Mexico went immediately from reservoir temperatures and pressures to ambient surface conditions."* This could be misinterpreted: single-stage separation is independent of the speed of the process or the sequence of temperature and pressure changes, as long as the oil and gas remain in contact (the gas is not separated from the oil). The report then recommends using values from a *"multistage separation process that would more accurately reflect the way stock tank oil is normally produced."*

F.2.5 Ambiguities in the definition of multistage separation. The use of a multistage separation process introduces ambiguities, as the exact value of B_o depends on the temperature and pressure of each stage, as well as the number of stages: there are an infinite number of possibilities to choose from. It is correct that one particular sequence was studied in the fluid property reports. However, armed with a good equation-of-state model, BP engineers may have been able to design a better process to capture even more oil, or – on cost grounds – chosen instead to use fewer stages, or have been forced to combine the production with that from other wells and use existing separators that were not designed for the Macondo fluids, and so were less efficient.

Its premise rests on determining what BP would have produced (and sold) had a given reservoir volume of oil been extracted. This involves a consideration of BP's production plans, or design criteria for the field, which have no direct bearing on a calculation of oil released. While the Zick report asserts that the

---

[244] Zick report [Z], page 16.

four-stage separation process represents these likely conditions, there may be evidence to the contrary, adding a layer of unnecessary complexity and potential uncertainty to an already involved calculation.

I use values from a single-stage separation in my report, based on the experimental measurements. The oil that was released to the ocean also underwent a separation, but at the temperatures and pressures at the sea bed, followed by further separations as it rose to the surface.

F.3   The Kelkar & Raghavan report

The Kelkar & Raghavan report has three distinct components: (1) a calculation of the flow rate near the end of the spill; (2) an analysis of the capping stack pressures after choke closure to determine the final reservoir pressure; and (3) the use of a material balance analysis to estimate the cumulative volume of oil released. I will discuss the latter two analyses.

F.3.1 Pressure build-up analysis.   Kelkar & Raghavan state:[245] "*We use the data gathered during the shut-in to assess certain characteristics of the reservoir, including the shape and well location.*"   They then present the standard pressure build-up and derivative plots[246] and say:[247] *Our analysis of the data also suggests that the Macondo well is in the corner of a reservoir with a rectangular shape. Both of these observations are consistent with the BP pre-drill report, which suggests that the well is indeed located at the corner of a reservoir with a rectangle shape*"   They then show a figure[248] – a seismic depth map – that purports to support this conclusion.

The seismic depth map is of such poor quality that I cannot decipher the well location unambiguously on it, nor does it appear to indicate the extent of the field. While indeed it is correct to model the reservoir as a rectangle for the pressure analysis, the well was not drilled at one corner of the field (see, for instance, Figure 4.5). No direct evidence to support this assertion is given; it contradicts the pressure analysis of Dr. Hsieh, BP engineers and the Pooladi-Darvish report (see later).

The standard practice in pressure transient analysis is to compare the measured pressure and its derivative with the output of an analytical model of the pressure response for linear flow (as I have done) or for a rectangle (as Dr. Pooladi-Darvish and I have done as well). Instead, Drs, Kelkar & Raghavan simply fit a curve to the pressure build-up.[249] The authors state that this curve is a "*rectangular hyperbola*" which may lead the non-expert to consider this is an appropriate methodology for a rectangular reservoir. It is not: the functional form for the pressure build-up is inconsistent with the rigorously derived equations for flow in a channel (see Appendix C).

The Kelkar & Raghavan report provides a reference (Haugland *et al.,* 1984) to justify this approach. This paper states: "*If nothing is known about the reservoir, then the hyperbola method can be used to get a rough estimate of the pressure.*"   But Drs. Kelkar & Raghavan – and everyone else who has studied

---

[245] Kelkar-Raghavan report [KR], page 21.
[246] Kelkar-Raghavan report [KR], figure 7, page 22.
[247] Kelkar-Raghavan report [KR], page 22.
[248] Kelkar-Raghavan report [KR], figure 8, page 23.
[249] Kelkar-Raghavan report [KR], figure 9, page 24.

Macondo – do know something about the reservoir – it has an approximately rectangular shape, while the seismic survey indicates its likely size.

Drs. Kelkar & Raghavan then mention a series of other curve-fit approaches to find the average pressure that provide lower numbers. Again these are methods of poor reliability – "*rough estimates*" – that are normally only be applied to cases where the reservoir geometry is unknown.

In the Appendices they discuss standard petroleum engineering methods. For pressure transient analysis they say that it can be used to find[250] "*the location of boundaries or barriers.*" However, they did not do this for Macondo.

F.3.2 Conversion from capping stack to reservoir pressures. Drs. Kelkar & Raghavan used a constant head of 3,220 psi to convert the capping stack pressure to down-hole conditions.[251] As discussed in Appendix B, this approach is incorrect, as it ignores the compressibility of the oil: the pressure difference changes with pressure and temperature, and is higher than they assumed. The data reported in Figure 8 show a non-monotonic trend (one point above the others) at late time – this is not seen in the data I have used and is not evident in their Figure 7 either.

In conclusion, the authors report a series of final pressures between 10,235 and 10,396 psi. They took the highest number for their material balance calculation. My range of final pressure – using rigorous methods – is between 10,433 and 10,531 psi – with the last recorded capping stack pressure corresponding to a down-hole value between 10,276 and 10,371 psi, dependent on what set of fluid measurements is used.[252] I consider Drs. Kelkar & Raghavan's final value – 10,396 psi – too low.

F.3.3 Material balance analysis. This is similar, conceptually, to the work presented in this report. Kelkar & Raghavan correctly stated that they are[253] "*using an industry standard material balance methodology.*" I agree with them that material balance is indeed the correct approach to determine the total volume of oil released.

They followed the same approach as I do in Section 4: determining the original oil in place, the total compressibility and the pressure drop, before multiplying these three quantities together to obtain the oil released.

There is a difference, though, in how we do the analysis. Drs. Kelkar & Raghavan did not – at any stage – use fluid or rock data taken from a critical and independent review of the direct measurements, despite this data being made available to them. Instead, they picked data from secondary sources, with scant justification.

F.3.4 Inappropriate value of the oil formation volume factor. The Kelkar & Raghavan report estimated the STOIIP (stock tank oil initially in place) as 137 MMstb. This is higher than my estimates of between

---

[250] Kelkar-Raghavan report [KR], page 32.
[251] Kelkar-Raghavan report [KR], page 19.
[252] Table D.2.
[253] Kelkar-Raghavan report [KR], page 8.

122 and 127 MMstb (with 100% connectivity). However, this is a consequence of the use of an oil formation volume factor of 2.14. The authors appear to have taken a value from a BP property table.[254] The value of B_o is inconsistent with the data, as I discuss in Section 4.1. They assumed a reservoir volume of oil that is 293 MMrb, which is very close to my value of 291 MMrb (see Table A.3). Hence, the over-statement of oil volume is simply a consequence of a poor value of B_o employed – something that would have been evident had the authors studied the fluid property reports.

Drs. Kelkar & Raghavan present various sensitivities, including a lower STOIIP of 110 MMstb, a value that they say was reported by BP. In the end, the range of STOIIP is not linked to a proper assessment of the oil volume underground, but arises from a selection of various incorrect conversions from reservoir to surface volumes.

Drs. Kelkar & Raghavan used an oil compressibility of 14.3 microsips. This is in my range of values – see Table A.5. However, they did not review the fluid data directly, but again relied on an average value from BP's fluid property tables.

F.3.5 Exaggerated pore volume compressibility of 12 microsips. The report states:[255] *"Our calculation uses a formation compressibility is 12×10^{-6} psi^{-1}. According to BP, this is the most likely value of formation compressibility."* This is the single most significant error in their analysis. There is no scientific evidence to support the use of this value. It is not the most likely value according to BP. This value was employed during the well integrity test as a worst case scenario: BP considered 6 microsips to be the most likely formation (or pore volume) compressibility, and this number was used after choke closure in their analysis of the pressure response.[256] I consider the fact that Drs. Kelkar & Raghavan have ignored the directly-measured data, which gives an average compressibility of approximately 6 microsips – presented in Section 4.2 – to be a serious shortcoming in their analysis.

F.3.6 Dr. Kelkar had earlier used 5.61 microsips for his work on Macondo. The insistence on 12 microsips is all the more baffling, when compared to the analysis that Dr. Kelkar performed as a consultant for the US Government's Flow Rate Technical Group. During the spill his team estimated most likely flow rates of between 27,000 and 32,000 stb/day.[257] However, it is not the flow rates that I will comment on – I agree with Drs. Kelkar & Raghavan that the appropriate method to determine cumulative release is a material balance analysis – but on the data that were employed.

Dr. Kelkar used a base case pore volume compressibility of 5.61 microsips[258] and a high case of 8.29 microsips.[259] These values are taken directly from Weatherford's reports of core measurements.[260]

---

[254] *See* the value of B_{oi} for the BP tables quoted in Table A.4: 2.1431.
[255] Kelkar-Raghavan report [KR], page 28.
[256] *See*, for instance, Pinky Vinson's deposition [47], page 300, line 15. Also Dr. Merrill's deposition [54], page 192, line 5; page 214, line 23; and page 216, line 15 onwards.
[257] *See* McNutt *et al.* (2012b), Table 3.
[258] *See* Don Maclay's deposition [62], page 393, lines 10-13; ; Exhibit 9859 (Kelkar FRTG Report).
[259] *See* Don Maclay's deposition [62], page 413, line 25 and page 414, line 1; ; Exhibit 9859 (Kelkar FRTG Report).
[260] BP-HZN-2179MDL02393883 (Weatherford summary of pore volume compressibility, "UPVC" tab, cells B17 and D17 [26].

Looking at the measured data, is, of course, the appropriate approach which I have followed.[261] The Kelkar & Raghavan report, however, did not discuss the measured data at all.

F.3.7 Calculated oil released of 3.4 MMstb if a compressibility of 6 microsips is used. In Appendix C,[262] the Kelkar & Raghavan report considered a formation compressibility of 6 microsips (close to the measured value), for which the calculated oil released had a lower range of 3.4 MMstb. This is similar to the mid-range of my calculations; this demonstrates that when Drs. Kelkar & Raghavan admitted the measured values they arrived at a similar determination of oil released to mine.

However, they concluded the main text with a range of oil released between 4.5 and 5.5 MMstb, using a range of STOIIP between 110 and 137 MMstb. They did not discuss the likely connectivity of the field, nor did they provide any analysis of the reservoir geology, which is a vital – and standard – consistency check in any reservoir engineering calculation.

F.4   The Pooladi-Darvish report

Dr. Pooladi-Darvish also simulated flow through the well-bore, capping stack and other surface equipment to estimate the flow rate near the end of the spill. Assuming fixed outflow conditions, the model was run for the entire period of the spill to find the cumulative volume of oil released. In a second stage of the work, a well-flow model was coupled to a reservoir simulation model and run with different sets of assumed parameters. The models matched the pressure response at the capping stack after choke closure with an average error of better than 0.1% and predicted the collected volumes of oil within 25%. These good match models had a cumulative oil released of between 5 and 5.3 MMstb.

The report contains a long series of Appendices prepared as slides, rather than text. However, it is possible to disentangle the analysis and explain how different conclusions are reached from my analysis. One thing I will also emphasize is that although the final numbers appear consistent with the Kelkar & Raghavan report, the input data are significantly different.

F.4.1 Analytical method with fixed outflow performance. The Pooladi-Darvish report first presents an analytical estimate of oil released. This work is akin to the Ratzel and Griffiths Sandia reports, using an estimate of the final flow rate and fixed outflow conditions to extrapolate the flow throughout the spill period. This method made unsupported assumptions concerning the flow resistance in the early part of the spill and essentially fixed the cumulative once the final flow rate was determined.

F.4.2 Well test analysis and an exaggerated oil compressibility. In the analytical model, Pooladi-Darvish coupled his well-bore flow model to a prediction of the pressure build-up. I presume that this is a conventional well test analysis. The results are shown in Appendix II.[263] As is standard in the petroleum community, the data and a model match to the pressure and pressure derivative are shown.

---

[261] These values are the pore volume compressibilities at a fluid pressure of 11,000 psi. The pore volume compressibility decreases as the pressure drops: as explained in Appendix A, I use values that exactly reproduce the change in pore volume for a pressure drop from initial to final reservoir pressures.
[262] Kelkar-Raghavan report [KR], page 45.
[263] Pooladi-Darvish report [PD], Appendix II, slides 30 and 31.

The inputs to Pooladi-Darvish's model lack foundation. First, the pressure derivative data are very noisy – much more noisy than the data I present in Section 4.3. It is not clear how the data were selected or the derivatives computed. The derivative data shows a rapid drop to close to zero near the end of the build-up period. This is not evident in my analysis, or in the data shown by Drs. Kelkar & Raghavan or Dr. Hsieh. As a result, the match is unlikely to be precise (as the data are noisy) and under-estimate the final pressure (because the final derivative values are too low). The estimated final pressure is 10,336 psi – indeed this is too low. A fixed pressure difference of 3,282 psi[264] was applied between the capping stack and reservoir. Using a fixed value introduced a systematic error, as discussed in Appendix B. However, at least the value itself is in the range I consider.

More significant though is the assumed oil compressibility in one case: 28.5 microsips, which is twice the measured value (see Table A.5). The pore volume compressibility is under-estimated at 2 microsips, but the total compressibility, Eq. (A.7), is exaggerated at 26.6 microsips. The total compressibility times porosity is 5.85 microsips: this is far outside the measured range 3.4-4.5 microsips (see Table A.8).

Why did Dr. Pooladi-Darvish do this? He cannot match the pressure data otherwise. He has hooked his model to a well-bore simulator and assumed constant outflow conditions. Hence, if he estimates a final flow rate of 51,000-54,000 stb/day, he has to have a cumulative release of around 5 MMstb. His model is not predictive: once the final flow rate is determined, so is the cumulative to within tight bounds. This is why all his good match models have more-or-less the same total flow – they can do nothing else, unless he relaxes the constraint of a fixed outflow. But, he also has to obey material balance. He has fixed his reservoir volume to around 109 MMstb. His (poor) match to the pressure data gives a pressure drop of 1,515 psi. His cumulative is – for this case – 5.20 MMstb. Hence, from Eqs. (A5) and (4.2), he has to have a total compressibility of around 26 microsips. If he assumed a compressibility that was consistent with the measurements, he would not have been able to match the pressure. This would have indicated that some of his underlying assumptions – specifically the assumption of a cumulative flow around 5 MMstb – were wrong.

There is a fundamental point here that lies at the heart of my analysis, and which is ignored – in different ways – by all the Government investigators:

It is not possible to match the pressure build-up with a cumulative release of 5 MMstb while honouring the measured reservoir rock and fluid properties.

Either 5 MMstb is wrong, or the measured reservoir properties are wrong. You cannot have both. Drs. Kelkar & Raghavan (and Dr. Hsieh) avoided this problem by using a pore volume compressibility that is more than twice the measured value, while Dr. Pooladi-Darvish adjusted the oil compressibility to obtain a fit. Later – as we discuss – Dr. Pooladi-Darvish did take representative reservoir properties, but used a new trick to hide the discrepancy by allowing unfeasibly low final pressures and growing his reservoir.

---

[264] Pooladi-Darvish report [PD], Appendix II, slide 15.

F.4.3 Confusion over fluid properties. The Pooladi-Darvish report states that it uses:[265] *"The measured Pencor data obtained from the single stage flash test."* Again, multistage values are not used, contradicting the assertions in the Zick report. However, as with Drs. Kelkar & Raghavan, the value of B_o is not representative of the measurements. A graph of B_o as a function of pressure is shown, displaying values that − above the bubble point − are all greater than 2.3. However, in the well test analysis (see above), B_o is assumed to be 2.131. This lower value would appear to be from the separator test.[266] But then later, it is stated that single-stage values are used for the outflow performance simulation − which is correct, as these are the conditions that pertain in the well-bore.[267] But, I don't see how different sets of data can be used in different parts of the simulation − you have to be consistent. This is one of several examples, where different properties are used for different calculations, with a significant shift between the analytical and numerical models.

F.4.4 Assumed oil volume is too large. Dr. Pooladi-Darvish then coupled the outflow simulation to a reservoir simulator. A base-case reservoir model is described. This has a rectangular geometry with an oil volume of 137 MMstb. This value is the same as reported by Drs. Kelkar & Raghavan, but higher than used in the analytical model. The justification appears to come from BP's estimates before drilling.[268] It is not clear why the reservoir size has increased from the analytical model, and if any independent assessment of reservoir volume was undertaken

F.4.5 Correct assignment of pore volume compressibility. The Pooladi-Darvish report then presents 25 different simulations with parameters presented in Table 2.[269] I will note one significant difference with the work of Drs. Kelkar & Raghavan: the base case pore volume compressibility is 6 microsips, as assumed by BP and close to my mid-range value. This value is based − as it should be − on the measurements.

F.4.6 Exaggerated range of data. Dr. Pooladi-Darvish presented tables giving ranges of parameter values.[270] In many cases the range was over-stated and not supported by the available data. He then allowed his reservoir model to have properties within these ranges, outside the values from direct measurement.

- **Permeability.** The range is 170 − 850 mD with a best estimate of 550 mD. The best case does not correspond to the average of the core measurements or from pressure analysis (Section 4.3), while the high case lies outside the range of measured values (Appendix A.5). Overall there is a bias to over-estimate permeability. The average permeability is twice as high as the most robust determination from pressure analysis (238 mD in the Gringarten report). This leads to a doubling of predicted flow rate.

---

[265] See Pooladi-Darvish report [PD], Appendix II, slide 45.
[266] See Pooladi-Darvish report [PD], Appendix III, slide 8.
[267] See Pooladi-Darvish report [PD], Appendix III, slide 9.
[268] See Pooladi-Darvish report [PD], Appendix III, slide 8.
[269] See Pooladi-Darvish report [PD], page 14.
[270] See Pooladi-Darvish report [PD], Appendix III, slides 8 and 9.

- **Porosity.** The base case value is 0.23 with a range 0.17-0.28 – the values are taken from BP's assessment before drilling and direct data was available. Once porosity had been measured, the best estimate of the average value is lower – 0.217 – and the range of values considerably narrower (see Section 4.1).

- **Oil compressibility.** A base case value of 12.3 microsips is given. This is below the range of the measurements: 13.7-14.8 microsips (see Table A.5). However, Dr. Pooladi-Darvish allows a range from 6 to 32.3 microsips. This range is far too wide: his high value is the compressibility at the bubble point.[271] However, the reservoir pressure is – at all times – much higher and so these values are unrepresentative and have no relevance for calculating oil expansion. In the simulation runs, it appears that the oil compressibility was adjusted to match the data: the value he used was around 15.3 microsips, above the measured values.[272]

- **Pore volume compressibility.** As mentioned above, Dr. Pooladi-Darvish took a representative base estimate of 6 microsips. However, his high estimate is the all-too-familiar value of 12 microsips. He states that both values are taken from the *"test conducted by Weatherford."* While 6 microsips can indeed be justified, 12 microsips is not a value that was measured (see Section 4.2).

- **Oil volume.** Dr. Pooladi-Darvish quotes a range from 75-200 MMstb with a base estimate of 137 MMstb. He based this on BP's pre-drill range of 138-239 MMstb. However, the value of B_o used by BP in their calculations was far below what was later measured. He needs to correct for this. It is not clear if or how this was done. Moreover, as I state in Section 5, the consistency of the predicted and measured height of oil-bearing sandstone at the well, combined with the results of the pressure analysis, considerably reduce the uncertainty in connected oil volume. Instead Dr. Pooladi-Darvish suggests a wider range, even though we now have additional information: his range is approximately ±39%, as opposed to BP's ±27%. In any event, the base case is too high – as mentioned above.

- **Oil formation volume factor, B_{oi}.** The range of B_{oi} from 2.0-2.35 with a base case of 2.1 has a bias that leads to an over-statement of oil released. The measured range (Table A.4) is from 2.27-2.36.

Dr. Pooladi-Darvish's considered a range of values, anchoring the range on measurements. However, in most cases, the justification for his choices was somewhat flimsy with a tendency to over-state the uncertainty and – in some cases – to bias the estimates.

F.4.7 Poor pressure match using a numerical simulator. Figure 7[273] of the Pooladi-Darvish report shows the match to the pressure after choke closure and the associated error. By eye the match appears impressive and similar to the matches presented in this report and by Dr. Hsieh. However, as I have

---

[271] As a technical point, the fluid compressibility at the critical point of a fluid is infinite. In a near-critical fluid, such as the Macondo hydrocarbon, the bubble point is close to the critical point and hence very large values of compressibility are expected. This is fascinating thermodynamically but has no bearing on the calculation of oil released.

[272] I have deduced this value to be consistent with material balance. While Dr. Pooladi-Darvish has made all his computer files available, I have not been able to deduce the oil compressibility directly from his data.

[273] See Pooladi-Darvish report [PD], page 16.

emphasized, close scrutiny is required. I have matched the reservoir pressure with an average (root-mean-square) error of 2 psi or less.[274] This is a fractional error of 0.02%. This is superior to any of the pressure matches achieved by Dr. Pooladi-Darvish.[275] Furthermore, Figure 7 shows that at late time – just the period when we need to match the pressure as precisely as possible to find the correct final value – the mismatch increases to almost 0.1%, or 10 psi.[276] This is significant by the standards of pressure transient analysis. I do note, however, that some of the other matches shown are better at late time, although the overall error is always 0.03% (3 psi) or greater. The problem here is that numerical simulation is not the best way to match pressure – the use of analytical well test analysis tools provides a superior determination of reservoir properties.

F.4.8 Incorrect pressure difference between the capping stack and the reservoir. The Pooladi-Darvish report presents a detailed analysis of this pressure difference, quantifying its value with a linear function of temperature and pressure.[277] This approach mirrors that in Appendix B of this report. He demonstrates, correctly, that variations in pressure and temperature lead to a change of ±150 psi in the pressure difference. However, Dr. Pooladi-Darvish kept this difference fixed during the simulation of the pressure build-up: this is incorrect, it increases with the rising capping stack pressure and as the well-bore cools. This is important, as it affects the shape of the pressure build-up in the reservoir and the derivative.

For the simulations, he assumed a pressure difference of 3,157 psi.[278] This is significantly lower than the value he used in the analytical model (3,282 psi) and is well below the range of my values. This led to final reservoir pressures that were far too low, and an exaggerated pressure drop. With the numerical simulation, mismatches in the final pressure were hidden, allowing a cumulative release of 5 MMstb, obeying material balance and using otherwise representative fluid and rock properties.

I quote from the report:[279] *"The fluid at wellhead is expected to be between 243 and 40 F (with the high and low limits corresponding to fluid velocities of infinity and zero). Here, the uncertainty in hydrostatic pressure is evaluated if the wellhead pressure was uncertain between 140 and 220 F. (Note that the "Base Model" considered in this study assumes a wellhead temperature of 220 F."* But, during the build-up period – when the pressure is matched – there is no flow. So, the temperature should be nearer 40°F, according to Dr. Pooladi-Darvish. Later, a detailed sensitivity analysis is presented: every value for the pressure drop that is calculated using measured fluid properties lies above his base case.[280] This introduces a bias into the model. The pressure change is significantly under-stated and is the key error in this analysis, giving final reservoir pressures that are typically more than 200 psi lower than the values I determine.

---

[274] See Appendix D, Tables D.2 and D.3.
[275] See Pooladi-Darvish report [PD], Table 1, page 3.
[276] Note that the figure uses a logarithmic time axis, so a small increment in the logarithm of time at the end represents a significant fraction of the build-up period.
[277] See Pooladi-Darvish report [PD], Appendix III, slide 3.
[278] Pooladi-Darvish report See [PD], Appendix III, slide 5; see also Appendix IV, slide 6.
[279] Pooladi-Darvish report [PD], Appendix III, slide 18.
[280] Pooladi-Darvish report [PD], Appendix III, slide 23.

As an example, I take Dr. Pooladi-Darvish's base case model that has a final reservoir pressure of 10,202 psi.[281] I consider this value implausible: as stated in Section F.3, at the end of the build-up period the down-hole pressure lies between 10,276 and 10,371 psi dependent on the fluid properties used. The final pressure cannot be below this. Indeed, using rigorous methods, I find a final pressure between 10,433 and 10,531 psi (Section 4.3). Since – from material balance – the cumulative release is proportional to the pressure drop – the difference between the initial and final pressures – this introduces a significant bias in the analysis, consistently over-stating the oil released.

For the "good match" cases the final reservoir pressures lie between 10,053 and 10,239 psi.[282] I consider all these values implausible. They all lie below the likely down-hole pressure when the well was cemented and the well test analysis fit by Dr. Pooladi-Darvish of 10,336 psi.

F.4.9 An increasing initial flow rate allows a lower estimate of cumulative release. Dr. Pooladi-Darvish also considered a case where the flow rate increases initially before reaching a maximum and then declining. This scenario is not dissimilar to the ones I explore in Appendix E.3. The cumulative flow in this case is 4.7 MMstb, with a possible 4.5 MMstb discussed in a footnote.[283] Dr. Pooladi-Darvish does not explore, however, the full range of possible flow rate histories, some of which may have much lower cumulative releases of oil. The quoted range cumulative release 5.0-5.3 MMstb was based on the unsupported assumption that the outflow conditions remain constant during the spill period.

Imagine that Dr. Pooladi-Darvish done the following: considered a wider range of flow rate histories; kept the (correct) fluid and rock compressibility; adjusted the oil volume to be consistent with BP's mid-range estimate and the likely connectivity of the field, while using the correct conversion from reservoir to surface volumes; and used a more representative value of the pressure difference from the capping stack to the reservoir (as he presents in his Appendix III). If he had done all this, then I suggest that he would have obtained similar values of oil released to mine.

F.4.10 Final discussion – taking a fixed outflow pre-determines the cumulative. The Pooladi-Darvish report suffers from the same problem as the Ratzel and Griffiths reports, even though the reservoir models employed are more sophisticated. Dr. Pooladi-Darvish linked a reservoir model to the outflow performance, found a final flow rate of around 50,000 stb/day and then assumed a fixed outflow performance over the period of the spill. This pre-determined – within narrow bands – the cumulative flow. This explains that even with very different assumed reservoir properties, the total flow remained between 5.0 and 5.3 MMstb in all cases. Only a limited investigation of changing outflow performance was provided, and so the full range of possible cumulative release was not considered.

In order to match the capping stack pressure build-up, while allowing the reservoir model to release 5 MMstb, the report made two errors. First, the connected reservoir volume in the simulations was too large – 137 MMstb or more. The possibility that the reservoir is not completely connected was not considered. As in the Kelkar & Raghavan report, there was no discussion of reservoir geology at all.

---

[281] Pooladi-Darvish report [PD], Appendix IV, slide 17.
[282] Pooladi-Darvish report [PD], Appendix V, slides 4 and 5.
[283] Pooladi-Darvish report [PD], page 26 n.10.

Second, the pressure difference between the capping stack and the reservoir was under-estimated during the build-up period, giving reservoir pressures that were too low, over-stating the pressure drop and the oil released.

F.5 Overview of estimates of cumulative oil released

I conclude this Appendix with an overview of the estimates provided by Drs. Kelkar & Raghavan, Dr. Pooladi-Darvish and Dr. Hsieh (see Appendix G). In Table F.2 I show how, by correcting for the pressure drop, compressibility and connected oil volume, my calculation of oil released can be recovered. While the methodology is – in places – correct, such as the use of pressure transient analysis and material balance, they all contain flaws in the application of these methods and in the use of measured data.

Investigator	Estimated oil released	Using my connected volume	Correcting the compressibility	Correcting the pressure drop	Corrected calculation of oil released
Drs. Kelkar & Raghavan	5 MMstb[284]	-0.48 MMstb	-1.04 MMstb	-0.22 MMstb	3.26 MMstb
Dr. Hsieh	4.92 MMstb	+0.07 MMstb	-1.22 MMstb	-0.51 MMstb	3.26 MMstb
Dr. Pooladi-Darvish	5.03 MMstb[285]	-0.93 MMstb	-0.16 MMstb	-0.68 MMstb	3.26 MMstb

Table F.2. Table illustrating the impact of the different assumptions in the analyses presented by Dr. Hsieh, Drs. Kelkar & Raghavan, and Dr. Pooladi-Darvish. The table shows by how much the estimates presented by these investigators changes if we use the connected oil volume, compressibility and pressure drop, compressibility values presented in this report. The final column provides my determinations of oil released. I have taken the mid-case pore volume compressibility of 6.35 microsips to correct the compressibility and have taken the average of my calculation for the three sets of fluid data. These results are also shown in the summary table in Section 2.

---

[284] Their mid-range value, which requires an assumption of a connected oil volume of 123.5 MMstb. Kelkar & Raghavan report [KR], page 28.
[285] The base case Pooladi-Darvish simulation model [PD], Appendix IV, slide 14.

Appendix G.   Further critique of the Hsieh analysis

This Appendix provides a detailed critique and analysis of the reservoir modelling work of Dr. Hsieh reported in the open literature (Hsieh, 2010, 2011), and in reports and presentations [11,12]. I will also refer to his deposition in September 2012 [42,43] and use data provided to me in spreadsheet form [44]. Further information is also contained in McNutt *et al.* (2012a,b) and Hickman *et al.* (2012).

G.1   Comparison of pressure data and analysis

G.1.1 Comparison of the data used by me and Dr. Hsieh. Both Dr. Hsieh and I match the pressure data, so this critique starts with a presentation of the data that we used. Figure G.1 shows the capping stack pressure that formed the basis of both our analyses.[286] As mentioned in Section 4.3, I have used all the distinct pressure readings and taken the average time for consecutive readings of the same pressure value. Dr. Hsieh has stated that he selected data values that had an approximately even spacing in Horner time.[287] Since the pressure gauge only had a sensitivity of 5 psi, selecting data at predetermined times immediately introduces an error, whereas averaging the time for a given reading – as I have done – preserves all the information. It is evident, moreover, that the data we use are quite different. While at late time (after around 1 day or 100,000 s) the trend is similar, my values are lower by an approximately constant offset of almost 40 psi. Note that I have more pressure points at late time. This means that in matching my model to the data, I give more weight to later times. This allows me to represent better the end of the build-up period and hence the final reservoir pressure. At early time, not only the pressure values, but their trend is very different. Dr. Hsieh uses data that display a much steeper rise in pressure at around 20,000 s.

I also show the match to the pressure provided by Dr. Hsieh's rectangular simulation model and my analytical rectangular model using a constant flow rate. In my rectangular model I have applied the temperature-dependent conversion from capping stack to reservoir pressures presented in Appendix B using Core Labs fluid properties. Dr. Hsieh appears to obtain – overall – a good match to the pressure. However, it is the late-time behaviour that is most significant in determining reservoir boundaries and the final pressure, as we will see later: we see a slight under-shoot of the final pressure measurement.

G.1.2 Comparison of pressure derivatives. Figure G.2 shows the pressure derivative for the two datasets. At late time, we see roughly similar values with a signature of channel flow. At early time Dr. Hsieh's data indicate a higher derivative of a roughly constant value, suggesting radial flow.

The sampling of the data does have a significant bearing on the pressure match. The presence of the far reservoir boundary, which determines the final reservoir pressure, is only seen at the latest times. If you have few data points to match in this time period, then, when you fit the data, you may allow a mismatch of these few points in favour of a better fit to an earlier time period, where there are more

---

[286] The data from Dr. Hsieh comes directly from a spreadsheet provided (*see* Exhibit 8617 (Hsieh pressure analysis)) [44]. This is presented as pressure as a function of Horner time. I have converted to time since choke closure using his assumed flow period t_p of 86 days.

[287] Dr. Hsieh's deposition [43], page 363, line 13.

data. However, this earlier time period is unaffected by the presence of the far boundary and so does not help specify the final reservoir pressure. This is where Dr. Hsieh introduces a source of inaccuracy in his analysis: he has few data points at late time and so does not steer his pressure match to fit this vital late-time behaviour.
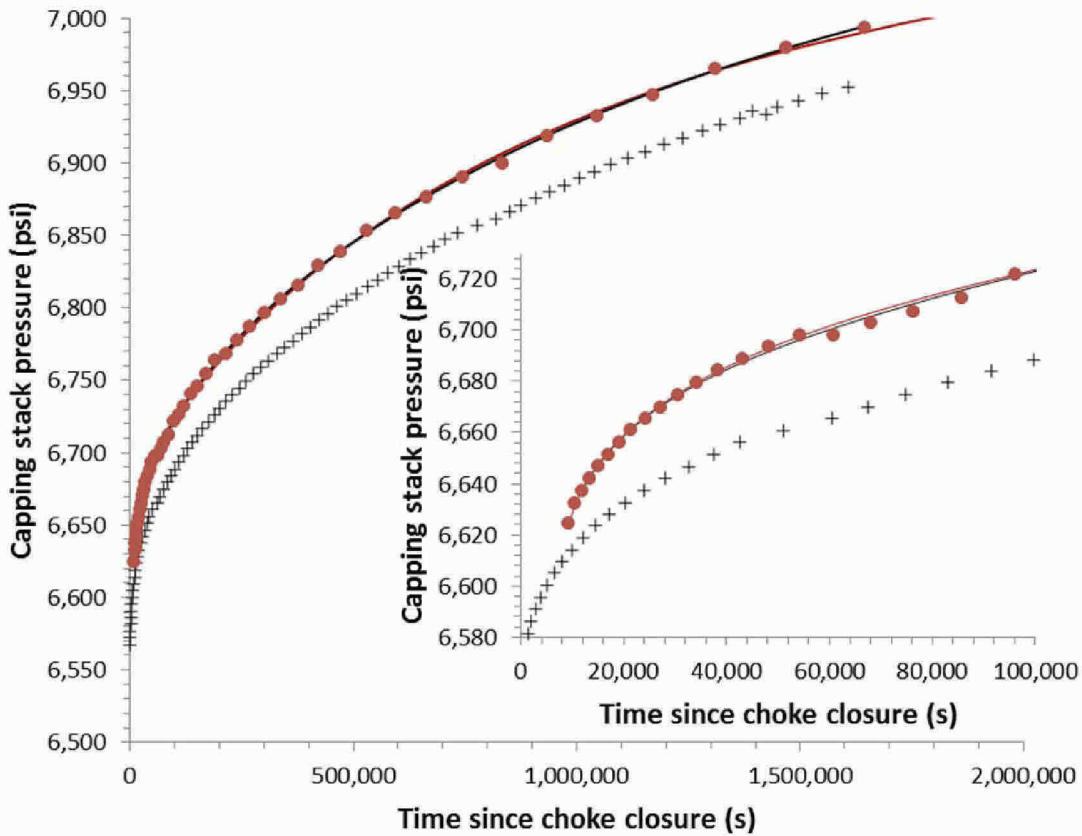
Figure G.1. Comparison of the pressure data used by me (crosses) and Dr. Hsieh [44] (circles). The inset shows the early-time behaviour in more detail. Note an offset at late time, due to an expert reassessment of the raw pressure recordings [T] made after Dr. Hsieh published his analysis. Also shown are Dr. Hsieh's match to the pressure (the red line) and my match to his data using a constant-flow-rate rectangular model (black line).

Dr. Hsieh used an optimization package, linked to a numerical reservoir simulator, to find the reservoir shape, well location and permeability that led to the best match of pressure. Like Dr. Hsieh, I too have used an optimization routine to find the best-fit parameters. However, in the optimization – as described in Appendix D – I use an analytical model whose results can be evaluated to arbitrary accuracy. Table G.1 provides my best-match parameters for the three sets of fluid data studied: this Table conveys the same information as Table D.2, except that I have matched to Dr. Hsieh's pressure data in this Section.

140
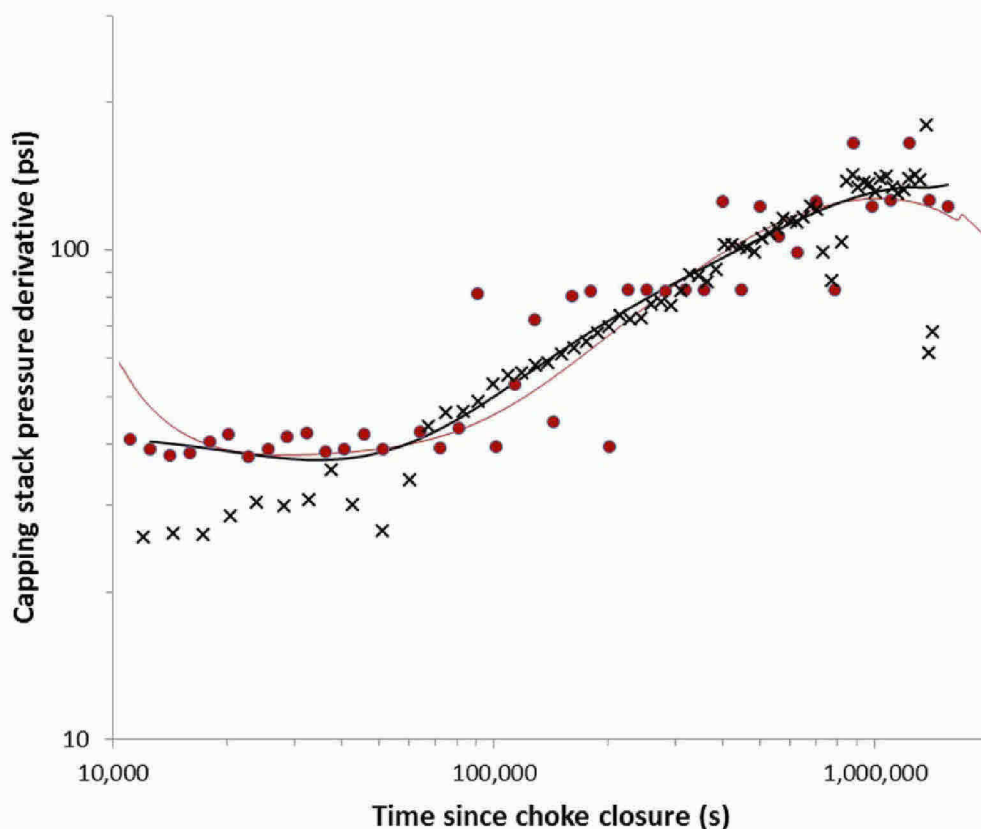
Figure G.2. Comparison of the pressure derivative computed from the data used by me (crosses) and Dr. Hsieh (red circles). At late time the derivatives are broadly similar, although my final few values lie above those of Dr. Hsieh. The best-match models from Dr. Hsieh (red line) and my analysis (black line) are also shown. Note that Dr. Hsieh tends to under-estimate the derivative at late time, leading to too low a final reservoir pressure.

G.1.3 Comparison of pressure matches. Dr. Hsieh's model under-states the pressure derivative at late time, just before the well was cemented. He predicts a decrease in the derivative when this is not apparent in the data. My best matches to his data, shown in Table G.1, indicate a higher final reservoir pressure than when I use my own data (compare with Table D.2) and so – had I used his pressure data – I would predict less oil released than reported here, not more. Since Dr. Hsieh only considered pressure and the readings were only accurate to only 5 psi, his matches are somewhat insensitive to the final estimated reservoir pressure, as discussed in Appendix D. Overall, Dr. Hsieh matches his pressure data with a root-mean-square-error of 2.2 psi; I do better with an error of only 1.5 psi. However, I also match to the pressure derivative with a root-mean-square error of 8.5 psi; Dr. Hsieh's error is 16.7 psi. This is outside the range of acceptable matches shown in graphs D.1 to D.3.

Parameter	τ_1	τ_2	Δp	p_f	Pressure error	Derivative error
Using proper conversion from capping stack to reservoir[288]	10,734,170	209,361	1,392	10,458	1.46	8.53
Fixed pressure difference between capping stack and reservoir	11,300,000	775,000	1,499	10,351	1.81	6.47
Dr. Hsieh's analysis			1,583	10,267	2.22	16.72
Unit	s	s	psi	psi	psi	psi

Table G.1. Parameters determined from the pressure match to Dr. Hsieh's data. Table D.1 provides definitions and descriptions of each of these terms. I have used an initial reservoir pressure of 11,850 psi to find p_f, since this was the value used by Dr. Hsieh. Dr. Hsieh's estimates of final pressure and pressure drop are also shown for comparison.

Dr. Hsieh selected too few pressure points at late time and so tolerated an error in their trend in favour of a better fit to the early-time data. This makes his analysis insensitive to his assumed final reservoir pressure. Instead, I have focussed my attention on the important parameter in this analysis: the final reservoir pressure. To determine this precisely, I have ensured that I match the measured pressures and their trend accurately at the end of the build-up period. I place less emphasis on the early-time transient (although I also match this well), since this has less impact on the material balance calculation.

G.1.4 Fixed pressure conversion from capping stack to reservoir. There is another significant difference between my analysis and that of Dr. Hsieh. Dr. Hsieh assumed that the reservoir pressure was a fixed 3,199 psi larger than the capping stack pressure.[289] In contrast, since the oil is compressible, the pressure difference is itself a function of temperature and pressure, as described in Appendix B: my pressure differences are larger and vary from around 3,200 to 3,400 psi dependent on the capping stack pressure and fluid properties used. This discrepancy also leads Dr. Hsieh to estimate lower reservoir pressures than in my analysis: for the same capping stack pressure, he under-estimates the reservoir pressure and the reservoir pressure derivative. In Table G.1, I also show the best match to pressure if I retain Dr. Hsieh's fixed pressure difference: this isolates the impact of the poor match to the pressure derivative from the effect of his simplification of the pressure difference between the capping stack and the reservoir. I find a final reservoir pressure of 10,351 psi if I match Dr. Hsieh's data using his assumed pressure drop from reservoir to capping stack.

Dr. Hsieh predicted a final reservoir pressure of 10,267 psi,[290] while I obtain 10,458 psi using his data. This discrepancy can be broken down into two contributions. First, correcting Dr. Hsieh's poor match to the late-time pressure derivative increases the predicted final reservoir pressure by 84 psi (the difference between his estimated final pressure of 10,267 psi and the best-match using his properties of 10,351 psi). Second, introducing my calculated pressure change from capping stack to reservoir, based on the measured fluid properties, leads to a further increase of 107 psi in the predicted final pressure.

---

[288] Computed using the conversion from capping stack to reservoir pressures for Core Labs properties presented in Appendix B, a rectangular flow model and a constant flow rate. The case with a fixed pressure conversion uses a linear flow model.

[289] This is taken directly from the spreadsheet values (see Exhibit 8617 (Hsieh pressure analysis)) [44].

[290] This value is taken directly from his spreadsheet (see Exhibit 8617 (Hsieh pressure analysis)) [44]; in his report, IGS642-000215 (10/13/2010 Draft Hsieh report) [11], he rounds this number to quote a value of 10,300 psi.

I suggest that through neglecting the late-time pressure derivative, combined with the assumption of a fixed pressure drop from capping stack to the reservoir, Dr. Hsieh obtained a final reservoir pressure that was significantly too low.

G.1.5 Radial flow period to find permeability. The final part of the pressure analysis is to study – separately – the early-time radial flow. The constant value of the derivative indicates radial flow, from which the permeability can be calculated (Table D.1). The transition to channel flow occurs at around 60,000 s from my model match. From Figure G.3, the constant derivative value in the first day (times from 10,000 – 80,000 s) is around 40 psi. Before proceeding, I will now assume that this represents the reservoir pressure derivative. As discussed in Section 4.3, this is an error, due to the neglect of oil compressibility and leads, in any event, to an over-estimate of permeability. Let us ignore this for now, and simply analyse Dr. Hsieh's data using his assumptions. I employ his viscosity of 0.168 mPa.s and a reservoir height of 90 ft (see Table G.2 for a full listing and comparison of reservoir properties). I also need to use the final flow rate. To be strictly consistent, I will take the value that Dr. Hsieh computes for the final day of the spill [44]: 52,603 stb/day and convert to reservoir conditions using his assumed value of B_o, 2.35.

I obtain a permeability of 407 mD. Dr. Hsieh's best matched permeability value is 593 mD.[291] In his deposition he explains how his estimates of best-matched parameters varied as he used smaller time-steps and a more refined grid in his numerical model.[292] His estimate of permeability increased from 515 mD to 570 mD and then 593 mD and his final pressure decreased from 10,400 psi to below 10,300 psi as he refined his model. His estimate of oil released changed from 4.6 MMstb to 4.76 MMstb and then finally to 4.92 MMstb.

Simulation models solve the governing equations for flow – those presented in Appendix C – numerically. It is well known that the simulation results are sensitive to the time-step and grid size, as is the case for Dr. Hsieh's model. I have not seen any evidence that the final results presented by Dr. Hsieh are converged – that is, that they represent the true solutions of the governing equations where the numerical errors are insignificant.

To avoid numerical problems, it is standard practice in the oil industry to match the pressure response to analytical mathematical expressions, where computational errors are eliminated, and to use optimization to find the best-fit parameters in these mathematical models. This is the approach I follow in this report.

Dr. Hsieh's model – if correct – must give an exactly constant derivative at early time. Instead we see a high initial value (see Figure F.2) followed by a decline to a roughly fixed value. Analytically this value must be consistent with the permeability, but it is not. He is – in effect – matching the data with numerical errors in his simulation; the results do not provide a valid representation of the reservoir.

---

[291] Exhibit 8615 (10/22/2010 Hsieh Draft Report, Table 2) [67].
[292] Dr. Hsieh's deposition [43], pages 410-420.

Dr. Hsieh did not follow standard practice in the oil industry in his analysis. The data that he considered were different from mine; he neglected to examine the match to the derivative; he assumed a fixed pressure difference between the capping stack and the reservoir; and his results were affected by numerical errors, leading to an inconsistent and over-stated value of permeability, even in the context of his other assumptions.

G.2   Comparison of reservoir properties

Dr. Hsieh assumed a fixed initial oil in place, and full connectivity, and assumed values for the compressibilities of the rock and fluids. Once the final reservoir pressure was determined, it would be possible to calculate the oil released using material balance, Eq. (3.1). This was not done by Dr. Hsieh – instead he used his simulation model with a fixed outflow performance to predict flow rate as a function of time. However, since his model – despite the problems outlined above – does strictly conserve mass, the results are consistent with a material balance analysis.

I start from Tables 1 and 2 of Dr. Hsieh's draft report.[293] Table G.2 compares his data with my calculations based on the analysis I have presented.[294] Those properties emphasized in italics display significant discrepancies, which I will discuss below.

Many of the assumptions made in Dr. Hsieh's modelling work seem perfectly reasonable in the light of the detailed analysis presented in this report. However, there is no evidence that he performed a careful scrutiny of all the available rock and fluid property data, or compared his reservoir model with the structure inferred from seismic surveys.

There are, however, some significant discrepancies that help explain why Dr. Hsieh's estimated oil released, around 4.9 MMstb, differ from my values (2.8-3.8 MMstb).

1. His assumed rock compressibility of 12 microsips lies outside the measured range on core samples. There is no direct evidence to support this value. My mid-range value is 6.35 microsips. This is the principal reason why he finds a larger volume of oil released.

2. As mentioned above, he under-states the final reservoir pressure.

3. He assumes a constant reservoir permeability of 593 mD. As discussed above, this is inconsistent with his own data. The most robust determination of permeability from Dr. Gringarten is 238 mD.

4. The reservoir geometry proposed by Dr. Hsieh is shorter, less wide and with a greater height than implied from the geology, indicating – in comparison with the seismic survey – incomplete connectivity of the field. He assumed that BP's calculated gross rock volume was correct. However, the main problem is that the reservoir geometry used by Dr. Hsieh is not consistent

---

[293] IGS642-000215 (10/13/2010 Draft Hsieh report) [11]: this draft report contains all the data used to construct Dr. Hsieh's simulation model, while the material that was published in the public domain has some of this information missing. My understanding is that some information was removed from the public versions since it was based on proprietary BP data (Hsieh, 2011).

[294] For simplicity I only compare the set of properties described in IGS642-000215 (10/13/2010 Draft Hsieh report) [11]. I do note that ranges of possible reservoir parameters were presented in additional work by Dr. Hsieh (see, for instance IGS629-003048 (Hsieh Modeling Presentation) [12]; Hsieh, 2010; this is discussed later.

with the geological interpretation (Section 5). This is illustrated in Figure G.3, which compares BP's seismic map with the reservoir dimensions in Dr. Hsieh's work. He assumes a fixed thickness of 90 ft – close to the value measured at the well. However, as mentioned in Section 5, the reservoir is longer, wider and, on average, less thick that the total height of sandstone encountered at the well. The pressure analysis identifies the boundaries of the field – these do not encompass the entire volume of oil-bearing sandstone identified from the seismic survey. Hence, Dr. Hsieh's connected oil volume could be too high.

Property	Value from Dr. Hsieh's work	Value calculated in this report
Oil volume	110 MMstb	Connected volume 109-114 MMstb
Oil formation volume factor	2.35	Value at final reservoir pressure lies between 2.3 and 2.4
Porosity	0.21	0.217
Pore volume compressibility	*12 microsips*	*6.35 microsips*
Oil viscosity	0.168 mPa.s	0.205 mPa.s
Oil saturation	0.9	0.878
Water compressibility	3 microsips	3 microsips
Oil compressibility	14.6 microsips	13.7 - 14.8 microsips
Permeability	*593 mD*	*300 mD from pressure analysis*
Total length, L	*6,788 m*	*8,178 m*

Table G.2. Comparison of values used in the reservoir modelling of Dr. Hsieh taken from [11, Tables 1 and 2 and Figure 1] compared to calculations presented in this report. The properties indicated in bold italics are significant discrepancies that are discussed in the text.

These discrepancies help explain the differences in our values of oil released. Using the data in Table G.2, I find that Dr. Hsieh assumed an effective compressibility of 28.27 microsips. Note that this is much larger than the values I take (19 to 24 microsips – see Section 4.2). The oil in place is 110 MMstb (coincidentally in my range of calculated connected oil volume). Then, for the final simulation, the pressure drop is 1,583 psi.[295] Multiplying these numbers together – using the material balance equation Eq. (3.1)[296] – gives a total oil released of 4.92 MMstb – exactly Dr. Hsieh's number, as it has to be. The same exercise can be performed for his other simulation runs using different parameters. Instead of multiple optimizations, he only needed to perform one best match to find the final pressure, and then the cumulative oil released could be computed from his assumed reservoir properties directly. Hsieh (2010) quotes an uncertainty of +/- 10% in the estimates of oil released. This is based on assuming a 25% variation in his assumed reservoir properties. In his Table 4, the sensitivities can be determined immediately from their impact on the material balance equation. A 25% change in STOIIP leads, obviously, to a 25% change in oil released, as does a 25% change in total compressibility (obtained by adding the contributions from pore, oil and water compressibility together in his Table 4). This is not a true sensitivity analysis, since with arbitrary reservoir properties, any value of oil released could be

---

[295] Using Dr. Hsieh's assumed initial pressure of 11,850 psi and a final reservoir pressure of 10,267psi.

[296] While Dr. Hsieh did not explicitly perform a material balance calculation, material balance is simply a statement of conservation of volume and so Dr. Hsieh's results are consistent – indeed have to be consistent – with a material balance analysis.

145

obtained. Furthermore, it is not clear how 10% can be quoted as the uncertainty, when based on variations that are considerably larger. The exercise only makes sense if based on a careful study of available experimental data.
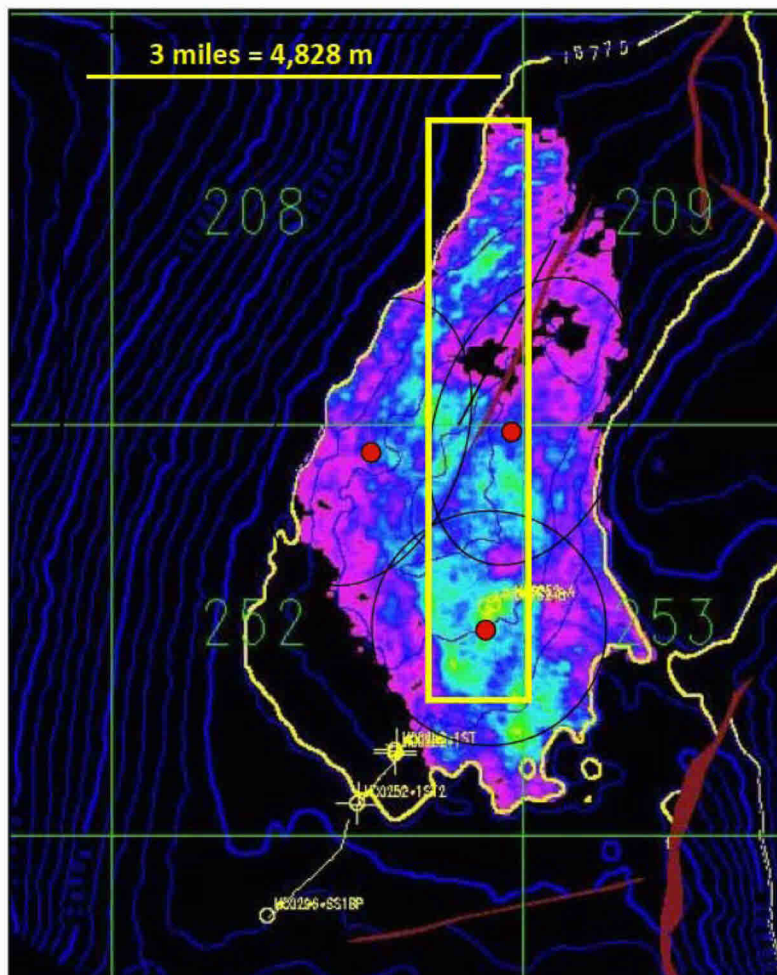
Figure G.6. Map of the Macondo field (see Figure 4.4). The bright colours indicate likely oil-bearing sandstone. The yellow box is Dr. Hsieh's reservoir model. The overall size of Dr. Hsieh's model is too small, indicating that the entire reservoir volume is not connected to the Macondo well.

I conclude by illustrating the effects of the different assumptions in Dr. Hsieh's analysis. These are presented in Table G.3, where the impact of correcting the pressure drop and compressibility on the calculated amount of oil released is determined using the material balance equation. Overall, the biggest impact on the calculations is the over-estimate of compressibility, based on a value of pore volume compressibility that lies outside the range of the measured data: the same mistake as was made by Drs. Kelkar & Raghavan.

The seismic image in Figure G.6 above is HIGHLY CONFIDENTIAL

TREX-011553-R.0146

Dr. Hsieh estimated oil released: 4.92 MMstb	Using my connected volume	Correcting for compressibility	Correcting for the pressure drop	Corrected calculation of oil released
Core Labs data	-0.04 MMstb	-1.08 MMstb	-0.39 MMstb	**3.41 MMstb**
Schlumberger data	+0.10 MMstb	-1.26 MMstb	-0.61 MMstb	**3.15 MMstb**
Intertek data	+0.16 MMstb	-1.31 MMstb	-0.55 MMstb	**3.22 MMstb**

Table G.3. Table quantifying the impact of the different assumptions in Dr. Hsieh's analysis on the calculated oil released, using the material balance equation. Dr. Hsieh estimated an oil release of 4.92 MMstb: the table shows by how much this value changes if we use the connected oil volume, compressibility and pressure drop values presented in this report. The final column provides my determinations of oil released. I have used the mid-case pore volume compressibility of 6.35 microsips to correct the compressibility. For completeness I present the calculations for all three sets of measured fluid data. The corrections averaged for all three sets of fluid data are shown in the summary table in Section 2 and F.2.

Appendix H. Critique of published flow rate estimates

H.1   Overview

The *Proceedings of the National Academy of Sciences* (PNAS) published a special feature on December 11th 2012 entitled "Science applications in the *Deepwater Horizon* oil spill."   This is a collection of research articles outlining the scientific endeavours of Government, academia and industry in response to this accident. This special issue was mentioned by Secretary Chu in his deposition as containing the most recent, peer-reviewed, published estimates of flow rate.[297] In this Appendix, I will briefly review the papers relevant to my work.

Three independent approaches to estimate flow rate are presented.

1. *In situ* **measurements of oil flow** into the ocean.
2. The use of **pressure differences across the capping stack** to calculate the flow rate near the end of the spill.[298]
3. **Reservoir analysis**, using the capping stack pressure build-up and estimated reservoir properties to determine flow rates and oil released. This is the work of Dr. Hsieh at the USGS and is, conceptually, most similar to the calculation presented in this report.

In brief my critique of the three methods above is as follows.

1. **Over-estimate of the flow of oil relative to gas.** The *in situ* measurements found the combined flow oil, gas (or gas hydrate) and entrained sea water. To convert this to an oil volume alone, the relative proportions of gas and oil in the flow need to be known. This can be determined from the gas/oil ratio, a standard quantity in petroleum engineering (see Appendix J); it is the ratio of the volume of gas to the volume of oil of the produced fluid, measured at surface conditions. This was done for Macondo: the value, measured independently at three laboratories, lies between 2,831 and 2,945 scf/stb, with an average of 2,894 scf/stb (Table A.7).[299] Down-hole the fluid is a single (oil) phase making it possible to take a representative sample; at the surface we have gas and oil flowing together and it is extremely difficult to collect the correct overall proportion of the two phases.[300] Many of the papers contain flow rate estimates used a gas/oil ratio of 1,600 scf/stb.[301] This was measured on a mixture of oil and gas collected in the deep ocean directly above the Macondo well from a remotely-controlled

---

[297] Secretary Steven Chu's deposition [58]; page 293, line 17 onwards.

[298] Described in further detail in the Sandia reports (revised Griffiths report [2] and revised Ratzel report [3]).

[299] BP-HZN-2179MDL03290054 (BP Post-Well Subsurface Technical Memorandum) also quotes gas/oil ratios measured on additional samples taken at different depths in the reservoir: these values are 2,840, 2,909 and 3,017 scf/stb for samples tested offshore as a quality control ([6], page 40); and service company measurements between 2,890 and 3,096 scf/stb ([6], page 41).

[300] To quote from a standard reservoir engineering textbook referring to the collection of oil and gas, as opposed to a single-phase sample (Dake, 2001; page 35): "*No matter how carefully the sampling is conducted, however, it is often very difficult to obtain the oil and gas mixed in the required ratio.*"

[301] *See, e.g.,* Ryerson *et al.* (2012) "Chemical data quantify *Deepwater Horizon* hydrocarbon flow rate and environmental distribution."

vehicle. While I do not know why there is such a discrepancy, the use of down-hole samples is the industry-standard benchmark and should be accepted as being accurate. The papers under-state the gas/oil ratio, leading to an over-estimate of oil flow.

2. **Unsupported assumption of a declining flow rate.** McNutt *et al.* (2012a) state *"the most definitive measurement of the flow occurred just before the well was shut in,"* referring to the use of differential pressure measurements across the capping stack to determine flow rate. However, even if we accept the determination of final flow rate, this does not allow a quantification of total oil released: to know this, we need to know the flow rates during the entire period of the spill. It has been assumed by all the Government investigators that the pressure difference between the well-bore (at reservoir depth) and the blow-out preventer decreased over time, as the average reservoir pressure declined. This leads to a flow rate that also declines with time, if we neglect the impact of any possible erosion of the blow-out preventer and other surface equipment. The pressure decline is consistently over-stated (point 3 below), but this is not the fundamental problem. To reach the well-bore, the oil has to find a tortuous pathway to enter the damaged well; it is implausible to suggest that – for the entire period of the spill – the oil flow was completely unimpeded over the full 93 ft height of the reservoir. The Emilsen report states that at the beginning of the incident, the likely length of reservoir open to flow was between 13 and 16.5 ft.[302] Furthermore the rock near the well-bore could have been clogged with cuttings from drilling: core samples taken from the well had permeabilities around five times lower than measured after cleaning (Appendix A.5). These effects, plus any further resistance to flow in the well-bore itself at reservoir depths, lead to an additional pressure drop between the reservoir and the well. As discussed in Appendix E.3, this pressure drop is likely to be larger than the reservoir depletion. At the end of the spill, the injectivity test indicated, however, that this flow resistance was negligible. This implies that the flow became less restricted during the spill period, leading to a pressure difference between the well down-hole and the blow-out preventer that increased over time, giving an increasing flow rate. It is impossible to quantify this effect with any certainty, but this discussion serves to illustrate how it is problematic to quantify the flow rate during the spill from a measurement at any one time. It is necessary to find a methodology that addresses the cumulative flow directly – namely the material balance analysis presented in this report.

3. **Flaws in the reservoir analysis.** The reservoir analysis of Dr. Hsieh used properties, specifically pore volume compressibility, that lay far outside the range of the measured data and did not use the best approach to analyse the capping stack pressure data and so over-estimated the pressure decline. As a consequence he over-estimated the volume of oil released. Since this work is most aligned to my own calculations, it requires a separate and more detailed critique which is provided in Appendix G.

---

[302] See Appendix E.6: taken from Emilsen report on the well failure [27], Section 2, page 7.

H.2   Details of selected papers

I will now briefly review several papers in the PNAS special issue, relevant to my work.

H.2.1. Lubchenco *et al.* (2012) "Science in support of the *Deepwater Horizon* response." This is the introduction to the special issue and presents the context for science during the spill response. The paper states *".. a final estimate derived from pressure measurements of 62,000 bpd at the outset and 53,000 bpd at well shut in for a total of 4.9 ± 10% million barrels."* The paper mentions that the (capping stack) pressure measurements allow the most reliable determination of final flow rate. However, the flow rate may have increased during the earlier part of the spill period (see Appendix E.3); to quantify the total flow, a reservoir analysis is required – it cannot be inferred from a flow rate at the end of the spill.

H.2.2. McNutt *et al.* (2012a) "Applications of science and engineering to quantify and control the *Deepwater Horizon* oil spill." This paper provides an overview of the different scientific and technical assessments made by different agencies in support of the oil spill response. The paper quotes a final flow rate of 53,000 stb/day ± 10%. Note that the uncertainty in final flow rate is the same as the uncertainty in total flow: no additional uncertainty is associated with the extrapolation of the flow rate at one time to the whole spill period. This is an unsupported assumption for the reasons given above.

The paper also addresses the reservoir modelling work of Dr. Hsieh. It states *"Both Hsieh and BP plotted the time dependence of the pressure in a Horner plot,"* which is provided in Figure 3 of the paper, while the diagnostics of radial and linear (channel) flow are discussed in the text. My understanding is that BP initially used a Horner plot simply because it could be provided rapidly without having to specify a flow rate in their proprietary software.[303] However, the industry standard to identify flow regimes is the pressure derivative, as used later by BP's engineers who studied the capping stack pressure.[304] The presentation of the plot indicates a poor understanding of pressure transient analysis. A flow rate of 50,000 stb/day is mentioned even though the plot does not require a flow rate to be specified. Second, different matches to the data are shown for varying reservoir widths. Fundamentally this is not correct: the changing shape of the curve is determined from the pressure wave hitting a far boundary, indicating the length of the field. The width is determined from the earlier-time response when the pressure wave hits the side of the channel. The only reason why width appears to vary is the unnecessary constraint in Dr. Hsieh's model that the total reservoir volume is fixed; therefore a longer reservoir has to be thinner. The paper mentions a *"1,800 psi"* pressure decline. The reservoir pressure decline is in fact around 1,400 psi (see Section 4.3); Dr. Hsieh found a value closer to 1,600 psi (Appendix G). This is an example of the persistent over-statement of pressure decline in Government reports and papers. Moreover, the use of this value – outside an explicit reservoir engineering calculation – is to estimate the down-hole pressure driving flow up the well-bore and through the surface equipment. This pressure instead may have increased, because of the changing flow resistance in the near-well region, as mentioned above. Hence, quoting this value of pressure decline is misleading in the wider context of flow rate estimates.

---

[303] Dr. Merrill's deposition [54], page 34, line 1.
[304] See Section 4.3 and Dr. Merrill's deposition [55], page 344, line 18.

The paper also says *"On August 3 (day 106), base oil was injected into the well as the first part of the injectivity test. The pressure rise was only 35 psi, hundreds of psi below the most optimistic expectations of the lowest pressure rise needed to stop and then reverse the hydrocarbon flow..... The impedance to flow at the well-reservoir interface or elsewhere in the lower rock formation was very small."* Why was the pressure rise expected to be hundreds of psi, and what are the implications of this test? As I discuss in Section E.3, analysis of the pressure at the time of the blow-out indicates highly restricted flow into the well-bore from the reservoir. Had this flow resistance persisted throughout the incident, then, when oil was injected back into the formation, a pressure rise of at least 250-350 psi would be anticipated. Instead, the pressure rise was an order of magnitude lower. This demonstrates that the resistance to flow probably decreased during the incident, and the pressure in the well-bore at reservoir depths could have risen, giving an increasing flow rate, even if any erosion of the surface equipment is ignored. This is a vital piece of evidence indicating an increasing flow rate, contradicting Government assertions to the contrary.

H.2.3. McNutt *et al.* (2012b) "Review of flow rate estimates of the *Deepwater Horizon* oil spill." This paper presents an overview of the different flow rate estimates. The paper reviews several methods for calculating flow, including the reservoir analysis of Dr. Hsieh. Dr. Hsieh's work is discussed in Appendix G: it is not based on an independent scrutiny of the measured fluid and rock data, and over-states the overall pressure drop. In the supplementary material, Figure S4 shows the Horner plot again: close scrutiny suggests that a better match to the final pressure measurements would give a higher estimated final pressure – something that is more evident if the best diagnostic method – the pressure derivative – is employed. Figure S5 shows the simulated flow rate as a function of time: this makes the unsupported assumption that there is no resistance to flow in the near well-bore region and fixed outflow conditions.

The flow rate estimates using reservoir modelling by consultants to the Flow Rate Technical Group are presented in Table 3 of the paper. These show a wide range consistent with values above and below my average flow rates. However, these estimates were made before the well was closed, and the pressure data was available. Hence, these somewhat unconstrained calculations will be much less certain than those informed by the reservoir pressure behaviour after shut-in.

H.2.4. Hickman *et al.* (2012) "Scientific basis for safely shutting in the Macondo well after the April 20, 2010 *Deepwater Horizon* blowout. This paper describes the analysis used to conclude that the well could remain safely closed after shut-in. Figure 3 shows the Horner plot of the capping stack pressure – the third time in the special issue this plot is shown. The directly-measured pressure (rather than public-domain reports of the pressure) is shown. The repeated presentation of this plot implies that is a particularly useful tool in this pressure analysis: it is not. As discussed in Section 4.3, no competent reservoir engineer would present a pressure analysis without showing the pressure derivative; the Horner plot has very poor diagnostic ability. Had the standard derivative plot been shown, the under-estimate of the final reservoir pressure, leading to an over-statement of oil released, would have been apparent.

The paper states *"The reservoir permeability and formation compressibility were also adjusted, but these measurements remained within ranges typical of reservoir sands."* What is not reported is that the

151

authors did not perform any independent analysis of rock and fluid data for Macondo; their values lay outside the range of these measurements.

The final comment of the paper mentions *"Excellent access to company data ...... for use by government oversight teams and their collaborators."* This may have been the case, but the selective use of this data is concerning. To recap: much of the analysis used a gas/oil ratio relied on data from a subsea sample with too low a value compared to measurements on a down-hole sample; Dr. Hsieh's reservoir analysis did not use reservoir properties consistent with the measured data; and last, there was no holistic approach to all the facts – for instance, the significance of the low pressures needed to flow oil once the well was capped, compared to the likely flow resistance at the time of the accident, was ignored.

Appendix I. Note on units

Traditionally, in the US oil industry, quantities are measured in field units. The data I use in this report is – generally – given in these units. However, most scientific calculations are performed in SI (metric) units, at least outside the US and the oil industry. The advantage of using SI units is that quantities can be computed directly from equations without having to account for unit conversion factors to make the calculations consistent.

To allow easy comparisons with other work on Macondo, I will present my main results in field units. However, I will also quote SI units where appropriate, and all scientific computations will be performed using SI units for consistency.

Unfortunately, this does introduce some confusion, as I will tend to quote quantities for my calculations in SI units (m, and s) while using traditional units in many places – ft, psi, stb and mD – for readability.

As a guide, below I provide a table of units and conversion factors.

Quantity	Length	Area	Oil volume	Permeability	Pressure	Time
Field or customary unit	ft (feet)	Acres	bbl (barrels); stb, rb	mD (milliDarcy)	psi (pounds per square inch)	Days
SI unit	m (metres)	m^2	m^3	m^2	Pa	s (seconds)
Conversion: field to SI	0.3048	4,046.85642	6.2898	9.869233×10^{-16}	6,895	86,400

As is evident in the analysis, it is crucial in any discussion of oil volumes to clarify if the oil is at reservoir or surface conditions. This is displayed in the unit used. So, for instance, stb (stock tank barrels) refers to a barrel of oil at surface conditions whereas rb (reservoir barrel) refers to a barrel at reservoir conditions. Now, the volume of this barrel is the same in both cases – the apparently different unit is given to clarify the condition at which the volume is measured.

Appendix J.   Nomenclature

Symbol	Meaning	Units (field)	Units (SI)
A	Area	Acres	m^2
B_o	Oil formation volume factor	rb/stb	Dimensionless
c	Compressibility	psi^{-1}	Pa^{-1}
c_t	Total compressibility	psi^{-1}	Pa^{-1}
C	Heat capacity		$Jkg^{-1}K^{-1}$
g	Acceleration due to gravity		ms^{-2}
h	Reservoir thickness	ft	m
H	Well-bore height	ft	m
K	Permeability	mD	m^2
L	Length of channel	ft	m
N	STOIIP, oil initially in the reservoir	stb	m^3
N_p	Oil produced at surface	stb	m^3
p	Pressure	psi	Pa
Q	Flow rate	rb/day	m^3/s
r	Radial coordinate	ft	m
R_s	Solution gas/oil ratio	scf/stb	dimensionless
S	Skin	dimensionless	dimensionless
S_o	Oil saturation	dimensionless	dimensionless
S_w	Water saturation	dimensionless	dimensionless
t	Time	days	s
t_p	Duration well was producing	days	s
T	Temperature	$^\circ$F	K
V	Volume	stb or rb	m^3
W	Width from pressure analysis	ft	m
W_{max}	Total reservoir width	ft	m
x	Distance coordinate	ft	m
y	Coordinate for radial flow	dimensionless	dimensionless
z	Depth coordinate	ft	m

Greek symbols

Symbol	Meaning	Units (field)	Units (SI)
α	Inverse diffusivity		s/m^2
β	Draw-down in channel flow	$psi.day^{-1/2}$	$Pa.s^{-1/2}$
γ	Euler's constant	dimensionless	dimensionless
δ	Draw-down from skin	psi.day/rb	$Pa.s/m^3$
ε	Strain	dimensionless	dimensionless
Δp	Pressure drop	psi	Pa
Δt	Time since well closure	day	s

ϕ	Porosity	dimensionless	dimensionless
κ	Turbulent resistance factor	$psi.day^2/rb^2$	$Pa.s^2/m^6$
	Thermal conductivity (Appendix B)		$Wm^{-1}K^{-1}$
μ	Viscosity	cp	Pa.s
η	Draw-down in radial flow	psi	Pa
ρ	Density		$kg.m^{-3}$
ξ	Weight of fluid	psi	Pa
τ	Time in Duhamel integration	day	s
τ_W	Time for pressure to traverse the width of the reservoir	day	s
τ_L	Time for pressure to reach the End of the channel	day	s
τ_1	Time for pressure to reach one end of the channel	day	s
τ_2	Time for pressure to reach the other end of the channel	day	s

Subscripts

cs	Capping stack
c	Cement (Appendix B), connected (Appendix D)
D	For unit flow rate
f	Final or formation (rock)
o	Oil
p	Produced
i	Initial
L	Length
r	Reservoir
s	Surface (or sediment – Appendix B)
t	Theoretical (model)
T	Thermal
w	Water or well
W	Width
0	At the well-bore
1	Channel on one side of well
2	Channel on other side of well

TREX-011553-R.0155

Appendix K.   Glossary of oilfield terms

Every scientific field has its own unique jargon and terminology. Below, I explain some of the terms used in my report. The petroleum industry, unlike many other disciplines, such as medicine, tends to use short, evocative words for technical terms, rather than elaborate Latinate expressions.

Black oil While crude oil is indeed black in colour, this term is used to refer to how we describe the properties of oil as a function of temperature and pressure. In particular, it describes an oil containing dissolved gas that comes out of solution as the pressure drops. BP prepared 'black oil' tables that presented the properties of the oil as a function of temperature and pressure, matched to measured data.

Build-up This refers to the period once a well is closed. The pressure build-up is the increase in pressure measured at the well after flow has ceased. After very long times a final equilibrium value is reached – the final reservoir pressure. The nature of the build-up provides valuable information on the reservoir structure and properties (Section 4.3).

Compressibility This is the fractional change in volume with a change in pressure. We use this to describe the compression (shrinkage) of the rock. It is also used – in reverse – to describe the expansion of fluid as pressure drops.

Down-hole This refers to conditions in the well where it contacts the reservoir. Sometimes this condition is called bottom-hole. Down-hole or bottom-hole pressure refers to the pressure in the well at reservoir depth. I have not used the phrase bottom-hole pressure as this can be shortened to BHP, which inevitably causes confusion, even for experts, with the blow-out preventer (BOP).

Gas/oil ratio This is the ratio of the volume of gas to the volume of oil for a reservoir sample of hydrocarbon that is brought to the surface. It is measured in units of scf (standard cubic feet) per stb (stock tank barrels). The use of the words 'standard' and 'stock tank' emphasize that the volumes are measured at surface conditions of 60°F and 1 atmosphere pressure. In this report, the values I quote are for a single-stage flash, where the gas and oil are kept in equilibrium as the pressure and temperature are dropped from reservoir to surface conditions. In the oil industry it is standard practice to measure the gas/oil ratio on fluid samples collected down-hole and taken to the laboratories of service companies who specialize in making these measurements, as was done for Macondo.

Logs These are measurements of electrical resistance and rock density taken using sophisticated instruments in the well-bore before the well casing and cement is

156

put in place. These logs are used to infer water (and hence oil) saturation and porosity.

Outflow performance   This is the relationship between flow rate and pressure drop through the well-bore, blow-out preventer and other equipment. A full quantitative analysis of oilfield flow rates couples the reservoir behaviour (the inflow performance or relationship between flow rate and pressure drop in the reservoir) to the outflow performance: the flow into the well from the reservoir must be equal to the flow through the well.

Skin   This is an additional pressure drop near the well, because of a restricted flow path or a lowered permeability. During drilling, rock fragments can be forced into the rock itself around the well-bore clogging the pore space and reducing permeability. It is very difficult to predict the magnitude of this effect. It is modelled as an additional pressure drop with a skin factor that is adjusted to match the observed behaviour. In Macondo, it is likely that oil initially could not flow into the well over the whole 93 ft section of oil-bearing sandstone, but followed a tortuous path to reach the damaged sections of the well. This also results in an additional pressure drop called the partial penetration skin. At the end of the spill, the flow rate tests with oil before the well was cemented indicated that the skin was very low, suggesting opening of the flow paths during the incident and a skin that decreased over time.

STOIIP   This stands for stock tank oil initially in place and is the volume of oil initially in the reservoir measured at surface, or stock tank, conditions.

Appendix L.   Biography of M J Blunt

Martin J. Blunt
Professor of Petroleum Engineering
Department of Earth Science & Engineering, Imperial College London SW7 2AZ, UK
Tel. +44(0) 20 75946500, E-mail: m.blunt@imperial.ac.uk

Education

1985	BA Natural Sciences, Cambridge University (First Class Honours)
1988	PhD, Theoretical Physics, Cambridge University. "The Growth and Properties of Fractal Boundaries."

Employment

1988-1992	Research Physicist, BP Research, Sunbury-on-Thames
1992-1999	Faculty member, Department of Petroleum Engineering, Stanford University: Assistant Professor 1992-1995; Associate Professor 1995-1999
1999-date	Professor of Petroleum Engineering Imperial College London: Head of the Petroleum Engineering and Rock Mechanics research group (PERM) 1999-2006; Head of the Department of Earth Science and Engineering 2006-2011; visiting professor, Politecnico di Milano, Italy, 2012-date

Honours and Awards

1985	Research Scholarship, Trinity College Cambridge
1985	Clerk Maxwell and ver Heyden de Lancey Prizes, Cambridge University
1991	Tallow Chandlers Prize, BP
1996	Teaching award, School of Earth Sciences, Stanford University
1996	Cedric Ferguson Medal, Society of Petroleum Engineers
2001	Distinguished Lecturer, Society of Petroleum Engineers
2011	Lester Uren Award and Distinguished Member, Society of Petroleum Engineers
2012	Darcy Award for lifetime achievement, Society of Core Analysts

Professor Blunt's research interests are in multiphase flow in porous media with applications to oil and gas recovery, contaminant transport and clean-up in polluted aquifers, and geological carbon storage. He performs experimental, theoretical and numerical research into many aspects of flow and transport in porous systems, including pore-scale modelling of displacement processes, and large-scale simulation using streamline-based methods. He has written over 150 scientific journal papers and is Editor in Chief of the journal *Transport in Porous Media*. He is a director of two start-up companies – Streamsim Technologies and iRock Technologies – founded by his former PhD students. In 2011 he was awarded the Uren Award from the Society of Petroleum Engineers for outstanding contributions to the technology of petroleum engineering made before the age of 45. In 2012 he was awarded the Darcy Award from the Society of Core Analysts for lifetime achievement. Prof. Blunt is a Fellow of the Energy Institute and a Chartered Petroleum Engineer.

Appendix M.   M J Blunt's Publications list

M.1   Journal papers

1. M J Blunt and R C Ball, "A family of exponents from a fractal model of viscous fingering and DLA," J Phys A: Math Gen, **20** 5961-5969 (1987).

2. M Blunt and P King, "Scaling structure of viscous fingering," Physical Review A **37**(10) 3935-3941 (1988).

3. R Ball and M Blunt, "A fractal model for the impedance of a rough surface," J Phys A: Math Gen, **21** 197-204 (1988).

4. M Blunt, "The impedance of a self-affine surface," J Phys A: Math Gen, **22** 1179-1192 (1989).

5. R C Ball, M Blunt and W Barford,"Can surface states be induced by interfacial roughness?" J Phys A: Math Gen, **22** 2587-2595 (1989).

6. R C Ball, M J Blunt and O Rath Spivak, "Diffusion-controlled growth," Proceedings of the Royal Society of London A, **423** 123-132 (1989).

7. M Blunt, "Hydrodynamic force distribution on a fractal cluster," Physical Review A, **39** 5801-5806 (1989).

8. M Blunt, W Barford and R Ball, "Polymer Adsorption and Electron Binding on Rough and Fractal Surfaces," Macromolecules, **22** 1458-1466 (1989).

9. R Ball and M Blunt, "Screening in multifractal growth," Physical Review A, **39**(7) 3591-3596 (1989).

10. M Blunt, "Geometry of multifractal systems," Physical Review A **39**(5) 2780-2782. (1989).

11. R Ball and M Blunt, "Dynamics of screening in multifractal growth," Physical Review A, **41**(2) 582-589 (1990).

12. M Blunt and P King, "Macroscopic parameters from simulations of pore scale flow," Physical Review A, **42**(8) 4780-4787 (1990).

13. F J Fayers, M J Blunt and M A Christie, "Accurate calibration of empirical viscous fingering models," Revue de L'Institut Francais du Petrole, **46**(3) 311-324 (1991).

14. M Blunt and P King, "Relative Permeabilities from Two- and Three-Dimensional Pore-Scale Network Modelling," Transport in Porous Media, **6** 407-433 (1991).

15. M J Blunt, P R King and J A Goshawk, "Simulations of Viscous Fingering in a Random Network," in "The Mathematics of Oil Recovery," Ed. P R King, The Institute of Mathematics and its Applications Conference Series, no 31, Clarendon Pres, Oxford (1992).

16. S Bryant and M Blunt, "Prediction of relative permeability in simple porous media," Physical Review A, **46** 2004-2011 (1992).

17. M Blunt and B Rubin, "Implicit Flux Limiting Schemes for Petroleum Reservoir Simulation," Journal of Computational Physics, **102**(1) 194-210 (1992).

18. M Blunt, M J King and H Scher, "Simulation and theory of two-phase flow in porous media," Physical Review A, **46**(12) 7680-7699 (1992).

19. F J Fayers, M J Blunt and M A Christie, "Comparisons of Empirical Viscous-Fingering Models and Their Calibration for Heterogeneous Problems," SPE Reservoir Engineering, **7**(May) 195-203 (1992).

20. M Blunt, F J Fayers and F M Orr, "Carbon Dioxide in Enhanced Oil Recovery," Energy Conversion Management, **34** 1197-1204 (1993).

21. M Blunt and M Christie, "How to Predict Viscous Fingering in Three Component Flow," Transport in Porous Media, **12** 207-236 (1993).

22. M J Blunt, J W Barker, B Rubin, M Mansfield, I D Culverwell and M A Christie, "Predictive Theory for Viscous Fingering in Compositional Displacement," SPE Reservoir Engineering, **9**(1) 73-80 (1994).

23. M Blunt and M Christie, "Theory of Viscous Fingering in Two Phase, Three Component Flow," SPE Advanced Technology Series, **2**(2), 52-60 (1994).

24. M J Blunt, D Zhou and D H Fenwick, "Three Phase Flow and Gravity Drainage in Porous Media," Transport in Porous Media **20** 77-103 (1995).

25. M R Thiele, M J Blunt and F M Orr, "Modeling flow in heterogeneous media using streamtubes: I miscible and immiscible displacements," In Situ, **19**(3), 299-339 (1995).

26. M R Thiele, M J Blunt and F M Orr, "Modeling flow in heterogeneous media using streamtubes: II compositional displacements," In Situ, **19**(4), 367-391 (1995).

27. M J Blunt and H Scher, "Pore Level Modeling of Wetting," Physical Review E, **52** 6387-6403 (1995).

28. M R Thiele, R P Batycky, M J Blunt and F M Orr, "Simulating Flow in Heterogeneous Systems Using Streamtubes and Streamlines" SPE Reservoir Engineering, **11** 5-12 February (1996).

29. M J Blunt, K Liu and M R Thiele, "A Generalized Streamline Method to Predict Reservoir Flow" Petroleum Geoscience, **2** 259-269 (1996).

30. M R Thiele, S E Rao and M J Blunt, "Quantifying Uncertainty in Reservoir Performance Using Streamtubes" Mathematical Geology, **28** 843-856 (1996).

159

31.   D Zhou and M J Blunt, "Effect of Spreading Coefficient on the Distribution of Light Non-Aqueous Phase Liquid in the Subsurface" J Contaminant Hydrology, **25** 1-19 (1997).

32.   M J Blunt, "Effects of Heterogeneity and Wetting on Relative Permeability using Pore Level Modeling" SPE Journal, **2** 70-87 March (1997).

33.   A A Keller, M J Blunt and P V Roberts, "Micromodel Observation of the Role of Oil Layers in Three Phase Flow" Transport in Porous Media, **26** 277-297 (1997).

34.   D Zhou, M J Blunt and F M Orr, "Hydrocarbon Drainage Along Corners of Noncircular Capillaries" J Colloid Interface Sci, **187** 11-21 (1997).

35.   D Ronen, H Scher and M J Blunt, "On the Structure and Transport Properties in the Capillary Fringe of Phreatic Aquifers" Transport in Porous Media, **28** 159-180 (1997).

36.   R P Batycky, M J Blunt and M R Thiele, "A 3D Field-Scale Streamline-Based Reservoir Simulator" SPE Reservoir Engineering, **12** 246-254 November (1997).

37.   M J Blunt, "Pore Level Modeling of the Effects of Wettability" SPE Journal, **2** 494-510 December (1997).

38.   D H Fenwick and M J Blunt, "Three dimensional, Three Phase Network Modeling of Drainage and Imbibition" Advances in Water Resources, **21**(2) 121-143 (1998).

39.   D H Fenwick and M J Blunt, "Network Modeling of Three Phase Flow in Porous Media" SPE Journal, **3** 86-97 March (1998).

40.   M J Blunt, "Physically Based Network Modeling of Multiphase Flow in Intermediate-Wet Media" Journal of Petroleum Science and Engineering, **20** 117-125 June (1998).

41.   D Zhou and M J Blunt, "Wettability Effects in Three-Phase Gravity Drainage" Journal of Petroleum Science and Engineering, **20** 203-211 June (1998).

42.   A A Keller, P V Roberts, and M J Blunt, "Effect of Fracture Aperture Variations on the Dispersion of Contaminants" Water Resources Research, **35**(1) 55-63 (1999).

43.   T Firincioglu, M J Blunt and D Zhou, "Three-Phase Flow and Wettability Effects in Triangular Capillaries" Colloids and Surfaces A, **155** 259-276 (1999).

44.   C E Schaefer, P V Roberts and M J Blunt, "Measurement and Prediction of Effective Diffusivities through Spreading and Nonspreading Oils in Unsaturated Porous Media" Environmental Science and Technology, **33**(17) 2879-2884 (1999).

45.   M J Crane and M J Blunt, "Streamline-based Simulation of Solute Transport" Water Resources Research, **35**(10) 3061-3078 (1999).

46.   Y Gautier, M J Blunt and M A Christie, "Nested gridding and streamline-based simulation for fast reservoir performance prediction" Computational Geosciences **3** 295-320 (1999).

47.   A A Keller, M J Blunt and P V Roberts, "Behavior of Nonaqueous Phase Liquids in Fractured Porous Media under Two-Phase Flow Conditions" Transport in Porous Media, **38**(1/2) 189-203, (2000).

48.   L A Dillard and M J Blunt, "Development of a pore network simulation model to study nonaqueous phase liquid dissolution" Water Resources Research **36**(2) 439-454 February (2000).

49.   D A DiCarlo, A Sahni and M J Blunt, "Three-Phase Relative permeability of Water-Wet, Oil-Wet and Mixed-Wet Sandpacks" SPE Journal **5** 82-91 March (2000).

50.   D Zhou, L A Dillard and M J Blunt, "A Physically Based Model of Dissolution of Nonaqueous Phase Liquids in the Saturated Zone" Transport in Porous Media **39**(2) 227-255 May (2000).

51.   D A DiCarlo, A Sahni and M J Blunt, "The Effect of Wettability on Three-Phase Relative Permeability," Transport in Porous Media, **39** 347-366 (2000).

52.   C E Schaefer, D A DiCarlo and M J Blunt, "Determination of water-oil interfacial area during 3-phase gravity drainage in porous media," Journal of Colloid and Interface Science, **221** 308-312 (2000).

53.   M-H Hui and M J Blunt, "Effects of Wettability on Three-Phase Flow in Porous Media," J. Phys. Chem. B, **104** 3833-3845 (2000).

54.   C E Schaefer, D A DiCarlo, and M J Blunt, "Experimental Measurement of Air-Water Interfacial Area During Gravity Drainage and Secondary Imbibition in Porous Media," Water Resources Research, **36** 885-890, (2000).

55.   R G Hughes and M J Blunt, "Pore Scale Modeling of Rate Effects in Imbibition," Transport in Porous Media, **40**(3), 295-322 (2000).

56.   D Ronen, H Scher and M Blunt, "Field observations of a capillary fringe before and after a rainy season," Journal of Contaminant Hydrology, **44** 103-118 (2000).

57.   D A DiCarlo and M J Blunt, "Determination of finger shape using the dynamic capillary pressure," Water Resources Research, **36** 2781-2785 (2000).

58.   M J Blunt, "An Empirical Model for Three-Phase Relative Permeability" SPE Journal **5** 435-445 December (2000).

59.   R G Hughes and M J Blunt, "Network modeling of multiphase flow in fractures," Advances in Water Resources **24** 409-421 (2001).

60.   L A Dillard, H I Essaid and M J Blunt, "A functional relationship for field-scale nonaqueous phase liquid dissolution developed using a pore network model," Journal of Contaminant Hydrology **48** 189-199 (2001).

61.   S P Bertels, D A DiCarlo and M J Blunt, "Measurement of aperture distribution, capillary pressure, relative permeability, and in situ saturation in a rock fracture using computed tomography scanning," Water Resources Research, **37**(3) 649-662 (2001).

62.   M J Blunt, "Flow in porous media – pore-network models and multiphase flow," Current Opinion in Colloid and Interface Science, **6**(3) 197-207 (2001).

63.   M J Blunt, "Constraints on contact angles for multiple phases in thermodynamic equilibrium," Journal of Colloid and Interface Science, **239** 281-282 (2001).

64.   H S Al-Hadhrami and M J Blunt, "Thermally Induced Wettability Alteration to Improve Oil Recovery in Fractured Reservoirs" SPE Reservoir Engineering and Evaluation, **4** 179-186 June (2001).

65.   R G Hughes and M J Blunt, "Pore-Scale Modeling of Multiphase Flow in Fractures and Matrix/Fracture Transfer" SPE Journal, **6**(2) 126-136 June (2001).

66.   M A Christie and M J Blunt, "Tenth SPE Comparative Solution Project: A Comparison of Upscaling Techniques," SPE Reservoir Engineering and Evaluation, **4**(4) 308-317 August (2001).

67.   M D Jackson and M J Blunt, "Elliptic Regions and Stable Solutions for Three-Phase flow in Porous Media" Transport in Porous Media, **48**(3) 249-269, September (2002).

68.   M J Blunt, M D Jackson, M Piri and P H Valvatne, "Detailed physics, predictive capabilities and macroscopic consequences for pore-network models of multiphase flow,"
Advances in Water Resources, **25** 1069–1089, (2002).

69.   M Prévost, M G Edwards and M J Blunt, "Streamline Tracing on Curvilinear Structured and Unstructured Grids," SPE Journal **7**(2) 139-148, June (2002).

70.   J J Hastings, A H Muggeridge and M J Blunt, "A New Streamline Method for Evaluating Uncertainty in Small-Scale, Two-Phase Flow Properties," SPE Journal **8**(1) 32-40, March (2003).

71.   B Bijeljic, A H Muggeridge and M J Blunt, "Multicomponent Mass Transfer across Water Films During Hydrocarbon Gas Injection," Chem. Eng. Sci. **58**(11) 2377-2388, June (2003).

72.   G Di Donato, E I Obi and M J Blunt, "Anomalous transport in heterogeneous media demonstrated by streamline-based simulation," Geophysics Research Letters **30**(12) 1608-1612, June (2003).

73.   B Agarwal and M J Blunt, "Streamline-Based Method with Full-Physics Forward Simulation for History Matching Performance Data of a North Sea Field," SPE Journal **8**(2) 171-180, June (2003).

74.   X Lopez, P H Valvatne, and M J Blunt, "Predictive network modeling of single-phase non-Newtonian flow in porous media," Journal of Colloid and Interface Science, **264**(1) 256-265, August (2003).

75.   M D Jackson, P H Valvatne and M J Blunt, "Prediction of wettability variation and its impact on flow using pore- to reservoir-scale simulations," Journal of Petroleum Science and Engineering, **39** 231– 246, (2003).

76.   P Audigane and M J Blunt, "Dual Mesh Method for Upscaling in Waterflood Simulation," Transport in Porous Media, **55** 71-89, (2004).

77.   G Di Donato and M J Blunt, "Streamline-based dual-porosity simulation of reactive transport and flow in fractured reservoirs," Water Resources Research, **40**, W04203, doi:10.1029/2003WR002772 (2004).

78.   W Huang, G Di Donato and M J Blunt, "Comparison of streamline-based and grid-based dual porosity simulation," Journal of Petroleum Science and Engineering, **43**, 129-137 (2004).

79.   P H Valvatne and M J Blunt, "Predictive pore-scale modeling of two-phase flow in mixed wet media," Water Resources Research, **40**, W07406, doi:10.1029/2003WR002627 (2004).

80.   E-O Obi and M J Blunt, "Streamline-based simulation of advective–dispersive solute transport," Advances in Water Resources, **27** 913–924, (2004).

81.   B Bijeljic, A H Muggeridge and M J Blunt, "Pore-scale modeling of longitudinal dispersion," Water Resources Research, **40**, W11501, doi:10.1029/2004WR003567 (2004).

82.   M Piri and M J Blunt, "Three-phase threshold capillary pressures in noncircular capillary tubes with different wettabilities including contact angle hysteresis," Physical Review E **70**, 061603 (2004).

83.   H Okabe and M J Blunt, "Prediction of permeability for porous media reconstructed using multiple-point statistics," Physical Review E **70**, 066135 (2004).

84.   B Agarwal and M J Blunt, "A Streamline-Based Method for Assisted History Matching Applied to an Arabian Gulf Field," SPE Journal **9**, 437-449, December (2004).

85.   M S Al-Gharbi and M J Blunt, "Dynamic network modeling of two-phase drainage in porous media," Physical Review E **71**, 016308 (2005).

86.   H Okabe and M J Blunt, "Pore space reconstruction using multiple-point statistics," Journal of Petroleum Science and Engineering **46** 121– 137 (2005).

87.   M Piri and M J Blunt, "Three-dimensional mixed-wet random pore-scale network modeling of two- and three-phase flow in porous media. I. Model description," Physical Review E **71**, 026301 (2005).

88.   M Piri and M J Blunt, "Three-dimensional mixed-wet random pore-scale network modeling of two- and three-phase flow in porous media. II. Results," Physical Review E **71**, 026302 (2005).

161

TREX-011553-R.0161

89.   P H Valvatne, M Piri, X Lopez and M J Blunt, "Predictive Pore-Scale Modeling of Single and Multiphase Flow," Transport in Porous Media **58**, 23–41, doi:10.1007/s11242-004-5468-2 (2005).

90.   Z Tavassoli, R W Zimmerman and M J Blunt, "Analytic Analysis for Oil Recovery During Counter-Current Imbibition in Strongly Water-Wet Systems," Transport in Porous Media **58**, 173–189, doi:10.1007/s11242-004-5474-4 (2005).

91.   M D Jackson, P H Valvatne and M J Blunt, "Prediction of Wettability Variation Within an Oil/Water Transition Zone and Its Impact on Production," SPE Journal **10**(2), 184-195, June (2005).

92.   Z Tavassoli, R W Zimmerman and M J Blunt, "Analysis of counter-current imbibition with gravity in weakly water-wet Systems," Journal of Petroleum Science and Engineering **48**, 94– 104 (2005).

93.   H Behbahani and M J Blunt, "Analysis of Imbibition in Mixed-Wet Rocks Using Pore-Scale Modeling," SPE Journal, **10**(4) 466-474, December (2005).

94.   H Behbahani, G Di Donato and M J Blunt , "Simulation of counter-current imbibition in water-wet fractured reservoirs," Journal of Petroleum Science and Engineering **50**, 21– 39 (2006).

95.   B Bijeljic and M J Blunt, "Pore-scale modeling and continuous time random walk analysis of dispersion in porous media," Water Resources Research **42**, W01202, doi:10.1029/2005WR004578 (2006).

96.   E I Obi and M J Blunt, "Streamline-based simulation of carbon dioxide storage in a North Sea aquifer," Water Resources Research **42**, W03414, doi:10.1029/2004WR003347 (2006).

97.   M E Rhodes and M J Blunt, "An exact particle tracking algorithm for advective-dispersive transport in networks with complete mixing at nodes," Water Resources Research **42**, W04501, doi:10.1029/2005WR004504 (2006).

98.   R Juanes and M J Blunt, "Analytical Solutions to Multiphase First-Contact Miscible Models with Viscous Fingering," Transport in Porous Media **64**(3), 339 - 373, doi:10.1007/s11242-005-5049-z (2006).

99.   G Di Donato, Z Tavassoli and M J Blunt, "Analytical and numerical analysis of oil recovery by gravity drainage," Journal of Petroleum Science and Engineering **54**, 55–69 (2006).

100.   R Juanes, E J Spiteri, F M Orr, Jr. and M J Blunt, "Impact of relative permeability hysteresis on geological CO_2 storage," Water Resources Research, **42**, W12418, doi:10.1029/2005WR004806 (2006).

101.   V S Suicmez, M Piri and M J Blunt, "Pore-scale Simulation of Water Alternate Gas Injection," Transport in Porous Media, **66**, 259–286 doi:10.1007/s11242-006-0017-9 (2007).

102.   M E Rhodes and M J Blunt, "Advective transport in percolation clusters," Physical Review E, **75,** 011124, doi:10.1103/PhysRevE.75.011124 (2007).

103.   G Di Donato, H Lu, Z Tavassoli and M J Blunt, "Multirate-transfer dual-porosity modelling of gravity drainage and imbibition," SPE Journal **12**, 77-88 (2007).

104.   A S Al-Kharusi and M J Blunt, "Network extraction from sandstone and carbonate pore space images," Journal of Petroleum Science and Engineering **56**, 219–231 (2007).

105.   B Bijeljic and M J Blunt, "Pore-scale modeling of transverse dispersion in porous media," Water Resources Research, **43**, W12S11, doi:10.1029/2006WR005700 (2007).

106.   H Okabe and M J Blunt "Pore space reconstruction of vuggy carbonates using microtomography and multiple-point statistics," Water Resources Research, **43**, W12S02, doi:10.1029/2006WR005680 (2007).

107.   M I J van Dijke, M Piri, J O Helland, K S Sorbie, M J Blunt, and S M Skjæveland, "Criteria for three-fluid configurations including layers in a pore with nonuniform wettability," Water Resources Research, **43**, W12S05, doi:10.1029/2006WR005761 (2007).

108.   R Juanes and M J Blunt, "Impact of Viscous Fingering on the Prediction of Optimum WAG Ratio," SPE Journal **12**(4), 486-495 (2007).

109.   T Sochi and M J Blunt, "Pore-scale network modeling of Ellis and Herschel–Bulkley fluids," Journal of Petroleum Science and Engineering **60**, 105-124 (2008).

110.   V S Suicmez, M Piri and M J Blunt, "Effects of wettability and pore-level displacement on hydrocarbon trapping," Advances in Water Resources **31**, 503–512 (2008).

111.   E J Spiteri, R Juanes, M J Blunt and F M Orr, Jr., "A New Model of Trapping and Relative Permeability Hysteresis for All Wettability Characteristics," SPE Journal **13**(3), 277-288 (2008).

112.   M E Rhodes, B Bijeljic and M J Blunt, "Pore-to-field simulation of single-phase transport using continuous time random walks," Advances in Water Resources **31**(2) 1527-1539 (2008).

113.   H Lu, G Di Donato and M J Blunt, "General Transfer Functions for Multiphase Flow in Fractured Reservoirs," SPE Journal **13**(3) 289-297 (2008).

114.   A S Al-Kharusi and M J Blunt, "Multiphase flow predictions from carbonate pore space images using extracted network models," Water Resources Research **44**, W06S01, doi:10.1029/2006WR005695 (2008).

115.   O Talabi, S AlSayari, S Iglauer and M J Blunt, Pore-scale simulation of NMR response, Journal of Petroleum Science and Engineering **67**(3-4), 168-178 (2009).

116.   R Qi, T C LaForce and M J Blunt, "Design of carbon dioxide storage in aquifers," International Journal of Greenhouse Gas Control **3** 195-205 (2009).

117.   M E Rhodes, B Bijeljic and M J Blunt, "A rigorous pore-to-field-scale simulation methodology for single-phase flow based on continuous time random walks," SPE Journal **14**(1) 88-94 (2009).

118.   G Frenkel, R Blumenfled, P R King and M J Blunt, "Topological Analysis of Foams and Tetrahedral Structures," Advanced Engineering Materials **11**(3) 169-176 (2009).

119.   C J Xie, Z L Guan, M Blunt and H Zhou, "Numerical simulation of oil recovery after cross-linked polymer flooding," Journal of Canadian Petroleum Technology **48**(4) 37-41 (2009).

120.   X Garcia, L T Akanji, M J Blunt, S K Matthai and J P Latham, "Numerical study of the effects of particle shape and polydispersity on permeability," Physical Review E **80**, 021304, doi: 10.1103/PhysRevE.80.021304 (2009).

121.   N Al-Bulushi. P R King, M J Blunt and M Kraaijveld, "Development of artificial neural network models for predicting water saturation and fluid distribution," Journal of Petroleum Science and Engineering **68** 197-208 (2009).

122.   H Dong and M J Blunt, "Pore-network extraction from micro-computerized-tomography images," Physical Review E **80**, 036307, doi: 10.1103/PhysRevE.80.036307 (2009).

123.   S K Al Mansoori, S Iglauer, C H Pentland and M J Blunt, "Three-phase measurements of oil and gas trapping in sand packs," Advances in Water Resources **32**, 1535-1542 (2009).

124.   M W Belayneh, S K Matthäi, M J. Blunt and S F Rogers, "Comparison of deterministic with stochastic fracture models in water-flooding numerical simulations," AAPG Bulletin **93**(11) 1633-1648 (2009).

125.   R Qi, T C LaForce and M J Blunt, "A three-phase four-component streamline-based simulator to study carbon dioxide storage," Computational Geoscience **13** 493–509, doi: 10.1007/s10596-009-9139-9 (2009).

126.   V T Beraldo, M J Blunt and D J Schiozer, "Compressible Streamline-Based Simulation With Changes in Oil Composition," SPE Reservoir Engineering and Evaluation **12**(6) 963-973 (2009).

127.   N Muller, R Qi, E Mackie, K Pruess and M J Blunt, "CO_2 injection impairment due to halite precipitation," Energy Procedia **1** 3507-3514 (2009).

128.   S K Al Mansoori, E Itsekiri, S Iglauer, C H Pentland, B Bijeljic and M J Blunt, "Measurements of non-wetting phase trapping applied to carbon dioxide storage," International Journal of Greenhouse Gas Control **4** 283–288 (2010).

129.   N Al-Bulushi, P R King, M J Blunt and M Kraaijveld, "Generating a capillary saturation-height function to predict hydrocarbon saturation using artificial neural networks," Petroleum Geoscience **16** 77–85 (2010).

130.   N A Idowu and M J Blunt, "Pore-Scale Modelling of Rate Effects in Waterflooding," Transport in Porous Media **83** 151–169 (2010).

131.   X Zhao, M J Blunt and J Yao, "Pore-scale modeling: Effects of wettability on waterflood oil recovery," Journal of Petroleum Science and Engineering **71** 169–178 (2010).

132.   C H Pentland, E Itsekiri, S Al-Mansoori, S Iglauer, B Bijeljic and M J Blunt, "Measurement of Non-Wetting Phase Trapping in Sandpacks," SPE Journal **15** 274-281 (2010).

133.   O Talabi and M J Blunt, "Pore-scale network simulation of NMR response in two-phase flow," Journal of Petroleum Science and Engineering **72** 1-9 (2010).

134.   E Unsal, S K Matthäi and M J Blunt, "Simulation of multiphase flow in fractured reservoirs using a fracture-only model with transfer functions," Computational Geosciences **14** 527–538 (2010).

135.   P Gittins, S Iglauer, C H Pentland, S Al-Mansoori, S Al-Sayari, B Bijeljic, and M J Blunt, "Nonwetting phase residual saturation in sand packs," Journal of Porous Media **13**(7), 591–599 (2010).

136.   A J Cavanagh, R S Haszeldine and M J Blunt, "Open or closed? A discussion of the mistaken assumptions in the Economides pressure analysis of carbon sequestration," Journal of Petroleum Science and Engineering **74** 107-110 (2010).

137.   S Iglauer, S Favretto, G Spinelli, G Schena and M J Blunt, "X-ray tomography measurements of power-law cluster size distributions for the nonwetting phase in sandstones," Physical Review E **82** 056315 (2010).

138.   A M AlSofi and M J Blunt, "Streamline-Based Simulation of Non-Newtonian Polymer Flooding," SPE Journal **15**(4) 901-911 (2010).

139.   C H Pentland, R El-Maghraby, S Iglauer and M J Blunt, "Measurements of the capillary trapping of super-critical carbon dioxide in Berea sandstone," Geophysics Research Letters, **38**, L06401, doi:10.1029/2011GL046683 (2011).

140.   H M Nick, A Paluszny, M J Blunt and S K Matthai, "Role of geomechanically grown fractures on dispersive transport in heterogeneous geological formations, Physical Review E **84** 056301 (2011)

141.   B Bijeljic, P Mostaghimi and M J Blunt, "The signature of Non-Fickian Solute Transport in Complex Heterogeneous Porous Media," Physical Review Letters **107** 204502 (2011).

142.   S Iglauer, A Paluszny C H Pentland and M J Blunt, "Residual CO_2 imaged with X-ray micro-tomography," Geophysical Research Letters **38** L21403 (2011).

143.   S Iglauer, W Wülling, C H Pentland, S K Al Mansoori and M J Blunt, "Capillary Trapping Capacity of Rocks and Sandpacks," SPE Journal **16**(4) 778-783 (2011).

144.   R M El-Maghraby, C H Pentland, S. Iglauer and M J Blunt, "A fast method to equilibrate carbon dioxide with brine at high pressure and elevated temperature including solubility measurements," J. of Supercritical Fluids **62** 55-59 (2012).

145.   A M AlSofi and M J Blunt , "A segregated flow scheme to control numerical dispersion for multi-component flow simulations," Computational Geoscience, doi:10.1007/s10596-012-9278-2 (2012).

146.   S Iglauer, M A Fernø, P Shearing and M J Blunt, "Comparison of residual oil cluster size distribution, morphology and saturation in oil-wet and water-wet sandstone," Journal of Colloid and Interface Science **375** 187–192 (2012).

147.   N I Al-Bulushi, P R King, M J Blunt and M Kraaijveld, "Artificial neural networks and its application in the petroleum industry," Neural Computing and Applications **21**(3) 409-421 (2012).

148.   A Q Raeini, M J Blunt and B Bijeljic, "Modelling two-phase flow in porous media at the pore scale using the volume-of-fluid method." Journal of Computational Physics **231**(17) 5653-5668 (2012).

149.   Y Tanino and M J Blunt, "Capillary trapping in sandstones and carbonates: Dependence on pore structure," Water Resources Research **48** W08525, doi:10.1029/2011WR011712 (2012).

150.   J D Paul and M J Blunt, "Wastewater filtration and re-use: An alternative water source for London." Sci Total Environ **437** 173-184 15 (2012).

151.   P Mostaghimi, B Bijeljic and M J Blunt, "Simulation of Flow and Dispersion on Pore-Space Images," SPE Journal **17** 1131-1141 (2012).

152.   P Mostaghimi, M J Blunt and B Bijeljic, "Computations of Absolute Permeability on Micro-CT Images," Mathematical Geosciences, doi: 10.1007/s11004-012-9431-4 (2012).

153.   O Gharbi and M J Blunt, "The impact of wettability and connectivity on relative permeability in carbonates: A pore network modeling analysis," Water Resources Research **48** W12513, doi:10.1029/2012WR011877 (2012).

154.   R M El-Maghraby and M J Blunt, "Residual CO_2 Trapping in Indiana Limestone," Environmental Science and Technology **47** 227–233, doi:10.1021/es304166u (2013).

155.   J-P Latham, J Xiang, M Belayneh, H M Nick, C-F Tsang and M J Blunt, "Modelling stress-dependent permeability in fractured rock including effects of propagating and bending fractures," International Journal of Rock Mechanics & Mining Sciences **57** 100–112 (2013).

156.   S Iglauer, A Paluszny and M J Blunt, "Simultaneous oil recovery and residual gas storage: A pore-level analysis using in situ X-ray micro-tomography," Fuel **103** 905–914 (2013).

157.   B Bijeljic, A Raeini, P Mostaghimi and M J Blunt, "Predictions of non-Fickian solute transport in different classes of porous media using direct simulation on pore-scale images," Physical Review E **87**, 013011 (2013).

158.   M J Blunt, B Bijeljic, H Dong, O Gharbi, S Iglauer, P Mostaghimi, A Paluszny and C Pentland, "Pore-scale imaging and Modelling." Advances in Water Resources, **51** 197–216 (2013).

M.2   Conference proceedings and book chapters

159.   M Blunt and B Rubin, "Implicit Flux Limiting Schemes for Petroleum Reservoir Simulation," SPE 22192, proceedings of the 2nd European Conference on the Mathematics of Oil Recovery, Arles, France, September 1990, Editions Technip, Paris (1990).

160.   B Rubin and M J Blunt, "Higher-Order Implicit Flux Limiting schemes for Black Oil Simulation," SPE 21222, proceedings of the 11th SPE Symposium on Reservoir Simulation, Anaheim, California, February 17-20 (1991).

161.   B Rubin, J. W. Barker, M J Blunt, M A Christie, I D Culverwell and M Mansfield, "Compositional Reservoir Simulation With a Predictive Model for Viscous Fingering," SPE 25234, proceedings of the 12th SPE Symposium on Reservoir Simulation, New Orleans, February 28 – March 3 (1993).

162.   M J King, M J Blunt, M Mansfield and M A Christie, "Rapid Evaluation of the Impact of Heterogeneity on Miscible Gas Injection," SPE 26079, proceedings of the SPE Western Regional Meeting, Anchorage, Alaska, May (1993). Also in "New Developments in Improved Oil Recovery," ed. H J de Haan, Geological Society Special Publication No. 84.

163.   M J Blunt, D H Fenwick and D Zhou, "What Determines Residual Oil Saturation in Three-Phase Flow?" SPE 27816, proceedings of the SPE?DOE Ninth Symposium on Improved Oil Recovery, Tulsa, 17-20 April (1994).

164.   M R Thiele, M J Blunt and F M Orr, "Predicting Multicomponent, Multiphase Flow in Heterogeneous Systems using Streamtubes," proceedings of the 4th European Conference on the Mathematics of Oil Recovery, Roros, Norway, June 7-10 (1994).

165.   D H Fenwick and M J Blunt, "Pore level Modeling of Three Phase Flow in Porous Media," proceedings of the 8th European Symposium on Improved Oil Recovery, Vienna, May 15-17 (1995).

166.   R P Batycky, M R Thiele and M J Blunt, "A Streamline Simulator to Model Field Scale Three-Dimensional Flow" proceedings of the 5th European Conference on the Mathematics of Oil Recovery, Leoben, Austria, September 3-6 (1996).

167.   D H Fenwick and M J Blunt, "Calculating Three-Phase Relative Permeabilities Using Network Modeling" proceedings of the 5th European Conference on the Mathematics of Oil Recovery, Leoben, Austria, September 3-6 (1996).

168.   D Zhou, M J Blunt and F M Orr, "Effect of Wettability and Spreading Coefficient on Three-Phase Distributions" proceedings of the 17th IEA Collaborative Project on Enhanced Oil Recovery Workshop and Symposium, Sydney, Australia, September 30 - October 2 (1996).

169.   R P Batycky, M J Blunt and M R Thiele, "A 3D Multipurpose Streamline Simulator with Gravity and Changing Well Conditions" proceedings of the 17th IEA Collaborative Project on Enhanced Oil Recovery Workshop and Symposium, Sydney, Australia, September 30 - October 2 (1996).

170.   A Sahni, R Guzman and M J Blunt, "Theoretical Analysis of Three Phase Flow Experiments in Porous Media" SPE 36664, proceedings of the SPE Annual Technical Conference and Exhibition, Denver, CO, October 6-9 (1996).

171.   M R Thiele, R P Batycky and M J Blunt, "A Streamline-Based 3D Field-Scale Compositional Reservoir Simulator" SPE 38889, proceedings of the SPE Annual Technical Conference and Exhibition, San Antonio, TX, October 5-8 (1997).

172.   B M Peters, D Zhou and M J Blunt, "Experimental Investigation of Scaling Factors that Describe Miscible Floods in Layered Systems" SPE 39624, proceedings of the SPE/DOE Improved Oil Recovery Symposium, Tulsa, OK, April (1998).

173.   A Sahni, J Burger and M J Blunt, "Measurement of Three Phase Relative Permeability during Gravity Drainage Using CT Scanning" SPE 39655, proceedings of the SPE/DOE Improved Oil Recovery Symposium, Tulsa, OK, April (1998).

174.   D A DiCarlo, A Sahni and M J Blunt, "Three-Phase Relative Permeability for Water-Wet and Oil-Wet Sandpacks" proceedings of the conference on the Evaluation of Reservoir Wettability and its Effect on Oil Recovery, Trondheim, Norway, June (1998).

175.   C E Schaefer, D S Kosson, M J Blunt and P V Roberts, "Diffusive Release of Aromatic Hydrocarbons in the Presence of Immobile NAPL" proceedings of EnviroMEET '98, University of California, Irvine, July 21-23 (1998).

176.   A A Keller, M J Blunt and P V Roberts, "Behavior of Dense Non-Aqueous Phase Liquid in Fractured Media under Two-Phase Flow Conditions" proceedings of EnviroMEET '98, University of California, Irvine, July 21-23 (1998).

177.   R G Hughes and M J Blunt, "Network Modeling of Multiphase Flow in Fractured Porous Media" proceedings of the 6th European Conference on the Mathematics of Oil Recovery, Peebles, Scotland, September 8-11 (1998).

178.   T Kawanishi, Y Hayashi, P V Roberts and M J Blunt, "Fluid-Fluid Interfacial Area during Two and Three phase Fluid Displacement in Porous Media: A Network Model Study" proceedings of the International Conference and Special Seminar on Groundwater Quality: Remediation and Protection, Tubingen, Germany, September IAHS **250** 89-96 (1998).

179.   Y Gautier, M J Blunt and M A Christie, "Nested Gridding and Streamline-Based Simulation for Fast Reservoir Performance Prediction" SPE 51931, proceedings of the SPE Reservoir Simulation Symposium, Houston, February (1999).

180.   M Hui and M J Blunt, "Pore-Scale Modeling of Three-Phase Flow and the Effects of Wettability" SPE 59309, proceedings of the SPE/DOE Improved Oil Recovery Symposium, Tulsa, OK, April (2000).

181.   M D Jackson and M J Blunt, "Dynamic Upscaling from the Pore to the Reservoir Scale," proceedings of the 21st Annual International Energy Agency Workshop, Edinburgh, UK, 19-22 September (2000).

182.   B R Bijeljic, A H Muggeridge and M J Blunt, "Effect of Composition on Waterblocking for Multicomponent Gasfloods," SPE 77697, proceedings of the SPE Annual Meeting, San Antonio, Texas, 29 September – 2 October (2002).

183.   M Piri and M J Blunt, "Pore-scale modeling of three-phase flow in mixed-wet systems," SPE 77726, proceedings of the SPE Annual Meeting, San Antonio, Texas, 29 September – 2 October (2002).

184.   P Audigane and M J Blunt, "Dual Mesh Method in Upscaling," SPE 79681, proceedings of the SPE Reservoir Simulation Symposium, Houston, Texas, 3-5 February 2003.

185.   M Al-Gharbi and M J Blunt, "A 2D dynamic pore-scale model for modeling primary drainage," proceedings of the ESF Workshop on Recent Advances in Multiphase Flow and Transport in Porous Media, European Science Foundation, Delft, 2003.

186.   H Okabe and M J Blunt, "Multiple-point statistics to generate geologically realistic pore-space representations," SCA2003-A33, proceedings of the Society of Core Analysts Annual Meeting, Pau, France, September (2003).

187.   H Okabe and M J Blunt, "Multiple-Point Statistics to Generate Pore Space Representations of Sandstones," proceedings of the International Workshop on X-ray CT for Geomaterials -GeoX2003, Kumamoto, Japan and published in "X-RAY CT For GEOMATERIALS – soil, concrete, rocks", Balkema. p.229-237 (2004).

188.   G Di Donato, W Huang and M J Blunt, "Streamline-Based Dual Porosity Simulation of Fractured Reservoirs," SPE 84036, proceedings of the SPE Annual Meeting, Denver, Colorado, 5-8 October (2003).

189.   P H Valvatne and M J Blunt, "Predictive Pore-Scale Network Modeling," SPE 84550, proceedings of the SPE Annual Meeting, Denver, Colorado, 5-8 October (2003).

190. M R Thiele, R P Batycky, M Iding and M J Blunt, "Extension of streamline-based dual porosity flow simulation to realistic geology," proceedings of the ninth European Conference on the Mathematics of Oil Recovery (ECMOR), Cannes, France, September (2004).

191.   P R Nurafza, M J Blunt and M R Fassihi, "Evaluation of water and gas injection in a carbonate reservoir," SCA2004-A42, proceedings of the Society of Core Analysts Annual Meeting, Abu Dhabi, UAE, September (2004).

192.   H Okabe and M J Blunt, "Predicting permeability through 3D pore-space images reconstructed using multiple-point statistics," SCA2004-A43, proceedings of the Society of Core Analysts Annual Meeting, Abu Dhabi, UAE, September (2004).

193. H Okabe and M J Blunt, "Multiple-point statistics to generate pore space images," proceedings of the Geostatistics Congress, Banff, Canada, September (2004).

194.   X Lopez and M J Blunt, "Predicting the Impact of Non-Newtonian Rheology on Relative Permeability Using Pore-Scale Modeling," SPE 89981, proceedings of the SPE Annual Meeting, Houston, Texas, 26-29 September (2004).

195.   J Bronchalo, R Venkataraman and M J Blunt, "A Multiscale Methodology for Simulating Miscible Gas Injection Projects Applied to the ROD Field in Algeria," SPE 90247, proceedings of the SPE Annual Meeting, Houston, Texas, 26-29 September (2004).

196.   M Barthelemy, D H Fenwick, Y Gautier and M J Blunt, "A Framework for History Matching Using Local Optimization in Streamline Defined Regions," SPE 90137, proceedings of the SPE Annual Meeting, Houston, Texas, 26-29 September (2004).

197.   M Calabrese, F Masserano and M J Blunt, "Simulation of Physical-Chemical Processes during Carbon Dioxide Sequestration in Geological Structures," SPE 95820, proceedings of the SPE Annual Meeting, Dallas, Texas, 9 – 12 October (2005).

198.   E J Spiteri, R Juanes, M J Blunt and F M Orr, Jr., "Relative Permeability Hysteresis: Trapping Models and Application to Geological CO2 Sequestration, SPE 96448, proceedings of the SPE Annual Meeting, Dallas, Texas, 9 – 12 October (2005).

199.   V S Suicmez, M Piri and M J Blunt, "Pore Scale Modeling of Three-Phase WAG Injection: Prediction of Relative Permeabilities and Trapping for Different Displacement Cycles," SPE 95594, proceedings of the SPE/DOE Symposium on Improved Oil Recovery held in Tulsa, Oklahoma, 22–26 April (2006).

200.   A S Al-Kharusi and M J Blunt, "Permeability Prediction and Network Extraction from Pore Space Images," proceedings of CMWRXVI, Copenhagen, June (2006).

201.   B Bijeljic and M J Blunt, "Longitudinal and Transverse Dispersion in Porous Media by Pore-Scale Modeling and Continuous Time Random Walk (CTRW) Theory," proceedings of CMWRXVI, Copenhagen, June (2006).

202.   V S Suicmez, M Piri and M J Blunt, "Pore-scale simulation of water alternate gas injection," proceedings of CMWRXVI, Copenhagen, June (2006).

203.   H Okabe and M J Blunt, "Reconstruction of pore-space images using microtomography and multiple-point statistics," proceedings of CMWRXVI, Copenhagen, June (2006).

204.   M I J van Dijke, M Piri, K S Sorbie and M J Blunt, "Criterion for three-fluid configurations including layers in a pore with non-uniform wettability," proceedings of CMWRXVI, Copenhagen, June (2006).

205.   M Rotondi, G Nicotra, A Godi, F M Contento, M J Blunt and M A Christie, "Hydrocarbon Production Forecast and Uncertainty Quantification: A Field Application," SPE 102135, proceedings of the SPE Annual Meeting, San Antonio, Texas, 24 – 27 September (2006).

206.   B Bijeljic and M J Blunt, "A Physically-Based Description of Dispersion in Porous Media," SPE 102869, proceedings of the SPE Annual Meeting, San Antonio, Texas, 24 – 27 September (2006).

207.   H Dong, M Touati and M J Blunt, "Pore Network Modeling: Analysis of Pore Size Distribution of Arabian Core Samples," SPE 105156, proceedings of the 15th SPE Middle East Oil & Gas Show and Conference, Bahrain, 11–14 March (2007).

208.   F Verre, M J Blunt, A Morrison, T McGarva, "Applicability of Water Shut-Off Treatment for Horizontal Wells in Heavy Oil Reservoirs," SPE 106908, proceedings of the SPE Europec/EAGE Annual Conference and Exhibition in London, UK, 11 - 14 June (2007).

209.   H Lu and M J Blunt, "General Fracture/Matrix Transfer Functions for Mixed-Wet Systems," SPE 107007, proceedings of the SPE Europec/EAGE Annual Conference and Exhibition in London, UK, 11 - 14 June (2007).

210.   V T Beraldo, M J Blunt, D J Schiozer and R Qi, "Streamline Simulation with an API Tracking Option," SPE 107498, proceedings of the SPE Europec/EAGE Annual Conference and Exhibition in London, UK, 11 - 14 June (2007).

211.   G Frenkel, R Blumenfeld, PR King and M J Blunt, "Topological Analysis of Foams and tetrahedral structures," proceedings of MetFoam 2007, Montreal, Canada, 5-7 September (2007).

212.   R Qi, V Beraldo, T LaForce and M J Blunt, "Design of Carbon Dioxide Storage in a North Sea Aquifer Using Streamline-Based Simulation," SPE 109905, proceedings of the SPE Annual Meeting, Anaheim, California, 11-14 November (2007).

213.   A S Al-Rabaani, M J Blunt and A H Muggeridge, "Calculation of a Critical Steam Injection Rate for Thermally-Assisted Gas-Oil Gravity Drainage, SPE 113351, proceedings of the SPE Improved Oil Recovery Symposium, Tulsa, Oklahoma, 19-23 April (2008).

214.   O Talabi, S AlSayari, M J Blunt, H Dong and X Zhao, "Predictive Pore-Scale Modeling: From Three-Dimensional Images to Multiphase Flow Simulations," SPE 115535, proceedings of the SPE Annual Meeting, Denver, Colorado, USA, 21-24 September (2008).

215.   R Qi, T C LaForce and M J Blunt, "Design of Carbon Dioxide Storage in Oilfields," SPE 115663, proceedings of the SPE Annual Meeting, Denver, Colorado, USA, 21-24 September (2008).

216.   N A Idowu and M J Blunt, "Pore-scale modeling of rate effects in waterflooding," IPTC 12292, proceedings of the International Petroleum Technology Conference, Kuala Lumpur, Malaysia, 3-5 December (2008).

217.   A M AlSofi, T C LaForce and M J Blunt, "Sweep Impairment due to Polymers Shear Thinning," SPE 120321, proceedings of the. SPE Middle East Oil and Gas Show and Conference (2009).

218.   W Sifuentes, M J Blunt and M A Giddins, "Modeling CO_2 Storage in Aquifers: Assessing the Key Contributors to Uncertainty," SPE 123582, proceedings of the SPE Offshore Europe Oil & Gas Conference & Exhibition, Aberdeen, UK, 8–11 September (2009).

219.   S K Al Mansoori, S Iglauer, C H Pentland, B Bijeljic, and M J Blunt, "Measurements of Non-Wetting Phase Trapping Applied to Carbon Dioxide Storage," Proceedings of the Greenhouse Gas Controls Technology Conference Washington D.C., U.S.A (2009).

TREX-011553-R.0166

220.		S K Al Mansoori, C H Pentland, S Iglauer and M J Blunt, "Three-Phase Measurements of Non-Wetting Phase Trapping in Unconsolidated Sand Packs," SPE 123994, proceedings of the SPE Annual Meeting, New Orleans, Louisiana, USA, 4–7 October (2009).

221.		M J Blunt, R Qi and T C LaForce, "Carbon dioxide (CO2) injection design to maximise underground reservoir storage and enhanced oil recovery (EOR)" In: Developments and Innovation in carbon dioxide (CO2) capture and storage technology. Volume 2: Carbon dioxide (CO2) storage and utilisation. Edited by M. Mercedes Maroto-Valer, Woodhead Publishing Series in Energy. Pages 169-184 (2010).

222.		C S Lamy, S Iglauer, C H Pentland, M J Blunt and G Maitland, "Capillary Trapping in Carbonate Rocks," SPE 130720, proceedings of SPE EUROPEC/EAGE Annual Conference and Exhibition, Paper, Barcelona, Spain (2010).

223.		H Okabe, Y Tsuchiya, C H Pentland, S Iglauer, and M J Blunt, "Residual CO_2 saturation distributions in rock samples measured by X-ray CT," proceedings of the 3rd International Workshop on X-Ray CT for Geomaterials, New Orleans, Louisiana, USA. (2010).

224.		A M Al-Sofi and M J Blunt, "The Self-flattening Nature of Trailing Shocks in Augmented Waterflooding - Segregation-in-flow Reestablish Self-sharpness," A004, proceedings of ECMOR XII, Oxford (2010).

225.		C H Pentland, Y Tanino, S Iglauer and M J Blunt, "Capillary Trapping in Water-Wet Sandstones: Coreflooding Experiments and Pore-Network Modeling," SPE 133798, proceedings of the SPE Annual Technical Conference and Exhibition, Florence, Italy. (2010).

226.		C H Pentland, R. El-Maghraby, A. Georgiadis, S. Iglauer, M. J. Blunt, Immiscible Displacements and Capillary Trapping in CO2 Storage, proceedings of the Greenhouse Gas Controls Technology Conference, Amsterdam, The Netherlands, September (2010).

227.		C H Pentland, S Iglauer, R El-Maghraby, Y Tsuchiya, H Okabe and M J Blunt, "Measurement of Carbon Dioxide Capillary Trapping in Core Analysis," SPE 138476, proceedings of the SPE International Conference on CO2 Capture, Storage and Utilization, New Orleans, Lousiana, USA, 10-12 November (2010).

228		J Kalunka, T C LaForce and M J Blunt, "Effects of CO2 stroage in Saline Aquifers on Groundwater Supplies,"SPE 139665, proceedings of the SPE International Conference on CO2 Capture, Storage and Utilization, New Orleans, Louisiana, USA, 10-12 November (2010).

229.		M J Blunt, "Carbon Dioxide Storage," Grantham Briefing Paper, No 4, Imperial College London (2010).

230.		M R Thiele, M Gerritsen and M Blunt (Eds.), "Streamline Simulation," Society of Petroleum Engineers, Richardson TX, ISBN:978-1-61399-065-0 (2011).

231.		M J Blunt, Two hundred barrels left: an analysis of population growth, oil reserves and carbon dioxide emissions http://www.decc.gov.uk/en/content/cms/meeting_energy/int_energy/global_oil/cfe_crude_oil/cfe_crude_oil.aspx

232.		A M AlSofi and M J Blunt, "Polymer Flooding Design and Optimization Under Uncertainty," SPE 145110, proceedings of the SPE Enhanced Oil Recovery Conference held in Kuala Lumpur, Malaysia, 19–21 July (2011).

233.		L E Sobers, M J Blunt and T C LaForce, "Design of simultaneous enhanced oil recovery and carbon dioxide storage applied to a heavy oil field offshore Trinidad," SPE 147241, proceedings of the SPE Annual Technical Conference and Exhibition, Denver, Colorado, USA. (2011).

234.		R M El-Maghraby. C H Pentland and M J Blunt, "Coreflood measurements of CO_2 trapping," SPE 147373, proceedings of the SPE Annual Technical Conference and Exhibition, Denver, Colorado, USA. (2011).

235.		A S Abushaikha, M J Blunt, T C LaForce and O R Gosselin, "Improved Mobility Calculation for Finite Element Simulation," SPE 154480, proceedings of the EAGE Annual Conference and Exhibition incorporating SPE Europec, Copenhagen, Denmark, 4-7 June (2012).

236.		B Bijeljic, M J Blunt, H Dong, P Mostaghimi, A Raeini, O Gharbi and M Andrew, "Pore-scale Imaging and Modelling of Transport and Flow in Complex Porous Media," Proceedings of the Energy and Storage Materials Workshop, Diamond Light Source (DLS) Synchrotron Users Meeting, Didcot, UK, 5-6 September (2012).

237.		O Gharbi, B Bijeljic, E Boek E and M J Blunt, "Changes in Pore Structure and Connectivity Induced by CO_2 Injection in Carbonates: a Combined Pore-scale Approach," Proceedings of the International Conference on Greenhouse Gas Technologies (GHGT) 11, Energy Procedia, Kyoto, Japan, 18-22 November (2012).

238.		A Al-Qattan, M J Blunt, O Gharbi, A Badamchizadeh, J M Al-Kanderi, M Al-Jadi, H H Dashti, V Chimmalgi, D J Bond and F Skoreyko, "Evaluation of the Effect of Asphaltene Deposition in the Reservoir for the Development of the Magwa Marrat Reservoir," SPE 163331, proceedings of the SPE Kuwait International Petroleum Conference and Exhibition, Kuwait City, Kuwait, 10-12 December (2012).

239.		M D Jackson, J L M A Gomes, P Mostaghimi, J R Percival, B S Tollit, D Pavlidis, C C Pain, A H El-Sheikh, A H Muggeridge and M J Blunt, "Reservoir Modeling for Flow Simulation Using Surfaces, Adaptive Unstructured Meshes and Control-Volume-Finite-Element Methods," SPE 163633, proceedings of the SPE Reservoir Simulation Symposium, The Woodlands, Texas USA, 18–20 February (2013).

Appendix N. Facts and data considered in forming my opinion

N.1 US Government and BP expert reports

Letter	Date posted	Name	File type	Description of contents
Z	2013-03-22	Expert report, "Equation-of-state fluid characterization and analysis of the Macondo reservoir fluids," prepared by Aaron A. Zick	Pdf	The Zick report
KR	2013-03-22	Expert report, "Rate prediction from the Macondo Well," prepared by Mohan Kelkar and Rajagopal Raghavan	Pdf	The Kelkar & Raghavan report
PD	2013-03-22	Expert report, "Estimate of the cumulative volume of oil released from the MC252 Macondo well," prepared by Mehran Pooladi-Darvish	Pdf	The Pooladi-Darvish report
SKG	2013-03-22	Expert report, "Oil Release from the MC252 Macondo Well," prepared by Stuart Griffiths	Pdf	The Griffiths report
ACG	2013-01-05	Expert report prepared by Alain Gringarten	Pdf	The Gringarten report
T	2013-01-05	Expert report prepared by Martin Trusler	Pdf/Excel	The Trusler report and asscociated pressure data
W	2013-01-05	Expert report prepared by Curtis Whitson	Pdf/Excel	The Whitson report and associated fluid property tables
RWZ	2013-01-05	Expert report prepared by Robert Zimmerman	Pdf	The Zimmerman report
█	███	████████	█	████

N.2 Confidential reports, deposition transcripts and other material

Number	Date posted	Name	File type	Description of contents
1	2012-02-24	Weatherford – Summary of Effective Permeability to Oil Measurements BP-HZN-2179MDL05223139	Excel	Weatherford permeability measurements to oil
2	2011-11-14	Griffiths_Revised_6_2011	Pdf	Revised Griffiths Report
3	2011-11-14	Revised_Ratzel_9_2011	Pdf	Revised Ratzel Report
4	2011-11-11	BP-HZN-2179MDL05223139	Pdf	BP internal email confirming water depth and depth of capping stack HC connector
5	2011-10-18	(6d16a1d913363e181102bbfc06f0b9a0) Black Oil Tables from EoS for All Temps 11June2010; BP-HZN-2179MDL04578104	Excel	BP fluid property tables
6	2011-10-12	Post-Well Subsurface Technical Memorandum BP-HZN-2179MDL03290054	Word	BP's seismic and log interpretation
7	2011-10-06	BP-HZN-2179MDL04549798	Excel	Description of capping stack closure
8	2011-09-27	Macondo OOIP (ff9a70a171043e7d458cae0765f5aa5c); BP-HZN-2179MDL04440267	Excel	Summary of Macondo oil-in-place
9	2011-09-27	TAM Chapter 1 (BP-HZN-2179MDL02900640)	Excel	Technical assurance memorandum: drilling plan and reservoir description pre-drill
10	2011-09-27	Technical Assurance Memorandum - Sections 2, 3 and 4 (BP-HZN-2179MDL02107723)	Excel	As above – sections 2-4
11	2012-03-06	10-13-2010 Pre-decisional draft, Hsieh, Computer simulation of Reservoir Depletion and Oil Flow (IGS642-000215)	Pdf	Draft of Hsieh report with all reservoir parameters listed
12	2012-03-06	Hsieh Modeling Presentation (IGS629-003048)	Powerpoint	Dr. Hsieh presentation with sensitivities
13	2011-09-20	DataDump_MC252_K_303.csv	Excel	Capping stack pressure

		BP-HZN-2179MDL04440614 and others; BP-HZN-2179MDL04440614; BP-HZN-2179MDL04440804; BP-HZN-2179MDL04440775; BP-HZN-2179MDL04440733; BP-HZN-2179MDL04440614; BP-HZN-2179MDL04440613; BP-HZN-2179MDL04440584; BP-HZN-2179MDL04440466; BP-HZN-2179MDL04440382; BP-HZN-2179MDL04440263; BP-HZN-2179MDL04440262; BP-HZN-2179MDL04440249; BP-HZN-2179MDL04440192; BP-HZN-2179MDL04440168; BP-HZN-2179MDL04440100		measurements
14	2011-09-20	Macondo Technical Note (Preliminary Draft) – Well Integrity Test (601555a84d8d77a9bf7fbd119604ca45); BP-HZN-2179MDL04440249	Pdf	Discussion of capping stack pressure measurements with location of transducer (Figure 4)
15	2011-09-01	BP-HZN-2179MDL04440691	Powerpoint	BP summary of log analysis
16	2011-09-01	BP-HZN-BLY00120160	Excel	BP summary of permeability, porosity and saturation
17	2011-09-01	BP-HZN-2179MDL04440238	Powerpoint	BP seismic summary
18	2011-08-23	BP-HZN-2179MDL04440732; see also Exhibits 9734, 10423	Excel	Intertek fluid property report
19	2011-08-23	BP-HZN-2179MDL00063016	Excel	Core Labs fluid property report
20	2011-08-23	BP-HZN-2179MDL00063084; see also Exhibits 8583, 8584, 8585	Excel	Core Labs fluid property report with cover page
21	2011-08-23	BP-HZN-2179MDL00470598	Excel	Weatherford summary of cores collected
22	2011-08-23	BP-HZN-2179MDL00470599	Excel	Weatherford core summary
23	2011-08-23	BP-HZN-2179MDL02394182; see also Exhibit 9070	Excel	Weatherford permeability measurements
24	2011-08-23	BP-HZN-2179MDL02394185; see also Exhibit 9067	Excel	Weatherford pore volume compressibility – raw data
25	2011-08-23	BP-HZN-2179MDL02394186; see also Exhibit 9066	Excel	Weatherford grain size analysis
26	2011-08-19	BP-HZN-2179MDL02393883; see also Exhibit 9053	Excel	Weatherford summary of pore volume compressibility
27	2012-03-06	Final Emilsen Report	Pdf	Emilsen report on the well failure
28	2011-08-25	BP-HZN-2179MDL00477088	Excel	BP drilling report and well description
29	2012-05-11	BP-HZN-2179MDL00059145	Powerpoint	BP Shallow Hazards presentation
30	2012-05-11	BP-HZN-2179MDL05173765	Powerpoint	BP gross rock volume assessment
31	2012-05-11	BP-HZN-2179MDL06566208	Powerpoint	BP Pre-drill review
32	2011-08-19	BP-HZN-2179MDL04440977	Excel	Intertek multistage separator tests and compositions
33	2011-08-19	BP-HZN-2179MDL04440978	Pdf	Intertek multistage separator test results
34	2011-08-02	BP-HZN-2179MDL01608973; see also Exhibits 10452, 10459	Pdf	Schlumberger Fluid Analysis on Macondo Samples
35	2011-08-02	BP-HZN-2179MDL01872218	Excel	Core Labs fluid properties report
36	2011-05-23	June 22 2010 Macondo Review (BP-HZN-2179MDL05181294)	Powerpoint	Macondo review with data from analogue fields
37	2011-08-23	BP-HZN-2179MDL02394187; see also Exhibit 9068	Excel	Weatherford rock composition analysis

38	2011-08-02	BP-HZN-BLY00000526	Pdf	BP Deepwater Horizon Accident Investigation Report, Appendix W Dynamic Simulations
39	2012-07-03	Unconfined Low Relief Slope Channel System BPHZN2179MDL06604338 – 52	Powerpoint	BP presentation of reservoir geology in channel systems
40	2012- 07-16	08-MC252_PT_3K_2-CORR2-Calculated-1 (BP-HZN-2179MDL07279441) and 08-MC252_PT_3K_2-CORR2-Calculated-2 (BP-HZN-2179MDL07279439)	Excel	Corrected capping stack pressure measurements used in this report
41	2012- 07-16	Equation_Corr (BP-HZN-2179MDL07279440)	Excel	Equation used to compute pressure from the raw data
42	2012-09-11	30(b)(6) deposition of Paul Anthony Hsieh, PhD, USGS, taken at the Pan-American Building, 601 Poydras Street, 11th Floor, New Orleans, Louisiana, 70130, on the 11th day of September, 2012.	Pdf	Transcript of Dr. Hsieh's (USGS) deposition: first day
43	2012-09-11	Continuation of the 30(b)(6) deposition of Paul Anthony Hsieh, Ph.D., USGS, taken at the Pan-American Building, 601 Poydras Street, 11th Floor, New Orleans, Louisiana, 70130, on the 12th day of September, 2012.	Pdf	Transcript of Dr. Hsieh's (USGS) deposition: second day
44		Hsieh pressure analysis; EXHIBIT 8617, BATES IGS770-000026	Excel	Data used in Dr. Hsieh's analysis. Provided by email September 2012
45	2012-10-04	30(b)(6) deposition of Bryan David Ritchie, BP, PhD, taken at the Pan-American Building, 601 Poydras Street, 11th Floor, New Orleans, Louisiana, 70130, on the 4th day of October, 2012.	Pdf	Transcript of Dr. Ritchie's (BP) deposition: first day
46	2012-10-05	Continuation of the 30(b)(6) deposition of Bryan David Ritchie, BP, taken at the Pan-American Building, 601 Poydras Street, 11th Floor, New Orleans, Louisiana, 70130, on the 5th day of October, 2012.	Pdf	Transcript of Dr. Ritchie's (BP) deposition: second day
47	2012-09-18	30(b)(6) deposition of Graham 'Pinky' Vinson, BP, PhD, taken at the Pan-American Building, 601 Poydras Street, 11th Floor, New Orleans, Louisiana, 70130, on the 18th day of September, 2012.	Pdf	Transcript of Pinky Vinson's (BP) deposition: first day
48	2012-09-19	Continuation of the 30(b)(6) deposition of Graham 'Pinky' Vinson, BP, taken at the Pan-American Building, 601 Poydras Street, 11th Floor, New Orleans, Louisiana, 70130, on the 19th day of September, 2012.	Pdf	Transcript of Pinky Vinson's (BP) deposition: second day
49	2012-09-20	30(b)(6) deposition of Jaime Loos, taken at the Pan-American Building, 601 Poydras Street, 11th Floor, New Orleans, Louisiana, 70130, on the 20th day of September, 2012.	Pdf	Transcript of Jaime Loos' (Weatherford) deposition
50	2010-10-23	PresComm - BP Comments to Oct 6 Working Paper No 3 - Amount and Fate of Oil	Pdf	BP's response to flow rate estimates
51	2012-11-12	WFT-MDL-00039271; WFT-MDL-00039272; WFT-MDL-00039273; WFT-MDL-00039274; WFT-MDL-00039275; WFT-MDL-00039276; WFT-MDL-00039277; WFT-MDL-00039278; WFT-MDL-00039279; WFT-MDL-00039280; WFT-MDL-00039281; WFT-MDL-00039282; WFT-MDL-00039283; WFT-MDL-00039284; WFT-MDL-00039285; WFT-MDL-00039286; WFT-MDL-00039287; WFT-MDL-00039288;	JPEG	Weatherford's core photographs

		WFT-MDL-00039289; WFT-MDL-00039290; WFT-MDL-00039291; WFT-MDL-00039292; WFT-MDL-00039293; WFT-MDL-00039294; WFT-MDL-00039295; WFT-MDL-00039296; WFT-MDL-00039297; WFT-MDL-00039298; WFT-MDL-00039299; WFT-MDL-00039300; WFT-MDL-00039301; WFT-MDL-00039302; WFT-MDL-00039303; WFT-MDL-00039304; WFT-MDL-00039305; WFT-MDL-00039306; WFT-MDL-00039307; WFT-MDL-00039308; WFT-MDL-00039309; WFT-MDL-00039310; WFT-MDL-00039311; WFT-MDL-00039312; WFT-MDL-00039313; WFT-MDL-00039314; WFT-MDL-00039315; WFT-MDL-00039316; WFT-MDL-00039317; WFT-MDL-00039318; WFT-MDL-00039319; WFT-MDL-00039320; WFT-MDL-00039321; WFT-MDL-00039322; WFT-MDL-00039323; WFT-MDL-00039324; WFT-MDL-00039325; WFT-MDL-00039326; WFT-MDL-00039327; WFT-MDL-00039328; WFT-MDL-00039329; WFT-MDL-00039330; WFT-MDL-00039331; WFT-MDL-00039332; WFT-MDL-00039333; WFT-MDL-00039334; WFT-MDL-00039335; WFT-MDL-00039336; WFT-MDL-00039337; WFT-MDL-00039338; WFT-MDL-00039339; WFT-MDL-00039340; WFT-MDL-00039341; WFT-MDL-00039342; WFT-MDL-00039615; WFT-MDL-00039616; WFT-MDL-00039617; WFT-MDL-00039618; WFT-MDL-00039619; WFT-MDL-00039620; WFT-MDL-00039621; WFT-MDL-00039622; WFT-MDL-00039623; WFT-MDL-00039624; WFT-MDL-00039625; WFT-MDL-00039695; WFT-MDL-00039696; WFT-MDL-00039697; WFT-MDL-00039698; WFT-MDL-00039699; WFT-MDL-00039700; WFT-MDL-00039701; WFT-MDL-00039702; WFT-MDL-00039703; WFT-MDL-00039704; WFT-MDL-00039705; WFT-MDL-00039706; WFT-MDL-00039707; WFT-MDL-00039708; WFT-MDL-00039709; WFT-MDL-00039710; WFT-MDL-00039711; WFT-MDL-00039712; WFT-MDL-00039713; WFT-MDL-00039714; WFT-MDL-00039715; WFT-MDL-00039716; WFT-MDL-00039717; WFT-MDL-00039718; WFT-MDL-00039719; WFT-MDL-00039720; WFT-MDL-00039721; WFT-MDL-00039722; WFT-MDL-00039723; WFT-MDL-00039724; WFT-MDL-00039725; WFT-MDL-00039726; WFT-MDL-00039727; WFT-MDL-00039728; WFT-MDL-00039729; WFT-MDL-00039730; WFT-MDL-00039731; WFT-MDL-00039732; WFT-MDL-00039733; WFT-MDL-00039734; WFT-MDL-00039735; WFT-MDL-00039736; WFT-MDL-00039737; WFT-MDL-00039738; WFT-MDL-00039739; WFT-MDL-00039740; WFT-MDL-00039741; WFT-MDL-00039742; WFT-MDL-00039743; WFT-MDL-00039744; WFT-MDL-00039745;		

		WFT-MDL-00039746; WFT-MDL-00039747; WFT-MDL-00039748; WFT-MDL-00039838; WFT-MDL-00039839; WFT-MDL-00039840; WFT-MDL-00039841		
52	2012-11-12	WFT-MDL-00039232; WFT-MDL-00039234; WFT-MDL-00039235; WFT-MDL-00039236; WFT-MDL-00039237; WFT-MDL-00039238; WFT-MDL-00039239; WFT-MDL-00039240; WFT-MDL-00039241; WFT-MDL-00039242; WFT-MDL-00039243; WFT-MDL-00039244; WFT-MDL-00039245; WFT-MDL-00039246; WFT-MDL-00039247; WFT-MDL-00039248; WFT-MDL-00039343; WFT-MDL-00039344; WFT-MDL-00039345; WFT-MDL-00039346; WFT-MDL-00039347; WFT-MDL-00039348; WFT-MDL-00039349; WFT-MDL-00039350; WFT-MDL-00039351; WFT-MDL-00039352; WFT-MDL-00039353; WFT-MDL-00039354; WFT-MDL-00039355; WFT-MDL-00039356; WFT-MDL-00039357; WFT-MDL-00039358; WFT-MDL-00039359; WFT-MDL-00039360; WFT-MDL-00039361; WFT-MDL-00039362; WFT-MDL-00039363; WFT-MDL-00039364; WFT-MDL-00039365; WFT-MDL-00039366; WFT-MDL-00039367; WFT-MDL-00039368; WFT-MDL-00039385; WFT-MDL-00054278; WFT-MDL-00054279; WFT-MDL-00054280; WFT-MDL-00054281; WFT-MDL-00054282; WFT-MDL-00054283; see also Exhibits 9063, 9064, 9065	JPEG	Weatherford's CT scans of core samples.
53	2012-11-30	30(b)(6) Deposition of Edmond Shtepani, Ph.D., P.Eng, Intertek, taken at the Pan-American Building, 601 Poydras Street, 11th Floor, New Orleans, Louisiana, 70130, on the 30th day of November, 2012.	Pdf	Transcript of Edmond Shtepani's (Intertek) deposition
54	2013-1-15	30(b)(6) Deposition of Robert C. Merrill, Jr., taken at Pan-American Building, 601 Poydras Street, 11th Floor, New Orleans, Louisiana, 70130, on the 15th day of January, 2013.	Pdf	Transcript of Dr. Merrill's (BP) deposition: first day
55	2013-1-16	Continuation of the 30(b)(6) Deposition of Robert C. Merrill, Jr., taken at Pan-American Building, 601 Poydras Street, 11th Floor, New Orleans, Louisiana, 70130, on the 16th day of January, 2013.	Pdf	Transcript of Dr. Merrill's (BP) deposition: second day
56	2013-1-30	Deposition of Michael M. Levitan, Ph.D., taken at the Pan-American Building, 601 Poydras Street, 11th Floor, New Orleans, Louisiana, 70130, on the 30th day of January, 2013.	Pdf	Transcript of Dr. Levitan's (BP) deposition: first day
57	2013-1-31	Continuation of the deposition of Michael M. Levitan, Ph.D., taken at the Pan-American Building, 601 Poydras Street, 11th Floor, New Orleans, Louisiana, 70130, on the 31st day of January, 2013.	Pdf	Transcript of Dr. Levitan's (BP) deposition: second day
58	2013-1-24	Deposition of SECRETARY OF ENERGY, DR. STEVEN CHU, taken at Department of Energy Headquarters, 1000 Independence Avenue,	Pdf	Transcript of Secretary Steven Chu's deposition

TREX-011553-R.0172

59	2012-10-24	SW, Washington, D.C., 20508, on the 24th day of January, 2013. 30(b)(6) Deposition of Marcia Kemper McNutt, Ph.D., United States of America, taken at the Pan-American Building, 601 Poydras Street, 11th Floor, New Orleans, Louisiana, 70130, on the 24th day of October, 2012.	Pdf	Transcript of Prof. McNutt's (USGS) deposition
60	2012-09-12	Deposition of Anadarko, by and through Brian O'Neill, taken at Pan-American Building, 601 Poydras Street, 11th Floor, New Orleans, Louisiana, 70130, on the 12th day of September, 2012.	Pdf	Transcript of Brian O'Neill's (Anadarko) deposition
61	2012-10-31	Deposition of Don Maclay, taken at Pan-American Building, 601 Poydras Street, 11th Floor, New Orleans, Louisiana, 70130, on the 31st October, 2012.	Pdf	Transcript of Don Maclay's deposition: first day
62	2012-11-01	Continuation of the deposition of Don Maclay, taken at Pan-American Building, 601 Poydras Street, 11th Floor, New Orleans, Louisiana, 70130, on the 1st of November, 2012.	Pdf	Transcript of Don Maclay's deposition: second day
63	2011-10-18	BP-HZN-2179MDL03742328	Pdf	MDT report used to find the datum depth
64	2013-04-11	Exhibit 8624, "Geological evidence for an elongate, heterogeneous reservoir"	Pdf	USGS discussion of connectivity
65	2013-04-21	Exhibit 8635	Powerpoint	Government's Flow Analysis Activities Presentation
66	2012-09-10	Deposition of Pencor, by and through Jason LeBlanc, taken at Pan-American Building, 601 Poydras Street, 11th Floor, New Orleans, Louisiana, 70130, on the 10th day of September, 2012.	Pdf	Transcript of Jason LeBlanc's (Pencor) deposition and associated exhibits 8583 and 8584.
67	2012-09-17	Exhibit 8615	Pdf	Dr. Hsieh October 22nd 2010 draft report

N.3   Books, papers and reports in the public domain

A detailed and frequently updated bibliography of public domain papers and reports on the *Deepwater Horizon* Incident can be accessed at:

http://www.lib.noaa.gov/researchtools/subjectguides/dwh_bibliography.pdf

M Abramovich and I A Stegun, *Handbook of Mathematical Functions*, Dover Publications (1970).

V Abreu, M Sullivan, C Pirmez and D Mohrig, "Lateral accretion packages (LAPs): an important reservoir element in deep water sinuous channels," Marine and Petroleum Geology **20** 631–648 (2003).

F O Alpak, M D Barton, F F van der Vlugt, C Pirmez, B E Prather and S H Tennant, "Simplified Modeling of Turbidite Channel Reservoirs," SPE Journal **15** 480-494 (2010).

F O Alpak, M D Barton and S J Naruk, "The impact of fine-scale turbidite channel architecture on deepwater reservoir performance," AAPG Bulletin **9** 251-286 (2013).

A C Azi, A Gbi, T Whittle and A C Gringarten, "Evaluation of confidence intervals in well test interpretation results," SPE 113888, proceedings of the SPE Europec/EAGE Annual Conference and Exhibition, Rome, Italy 9-12 June (2008).

Bijeljic, H Dong, O Gharbi, S Iglauer, P Mostaghimi, A Paluszny and C Pentland, "Pore-scale imaging and Modelling." Advances in Water Resources, **51** 197–216 (2013).

D Bourdet, *Well Test Analysis: The Use of Advanced Interpretation Models*, Elsevier, Amsterdam, ISBN 0444509682 (2002).

D Bourdet, T M Whittle, A A Douglas and Y M Pirard, "A New Set of Type-Curves Simplifies Well Test Analysis," World Oil **6** 95-106 (1983).

D Bourdet, J A Ayoub and Y M Pirard, "Use of Pressure Derivative in Well-Test Interpretation," SPE Formation Evaluation **4** 293-302 June (1989).

M J Bourgeois, F H Daviau and J-L Boutaud de la Combe, "Pressure Behavior in Finite Channel-Levee Complexes," SPE Formation Evaluation **11** 262-268 September (1996).

GEP Box*, Empirical Model-Building and Response Surfaces*, co-authored with Norman R. Draper, p. 424, ISBN 0471810339 (1987).

BP, "Deepwater Horizon Accident Investigation Report," Houston, TX. http://www.bp.com/liveassets/bp_internet/globalbp/globalbp_uk_english/incident_response/STAGING/local_assets/downloads_pdfs/Deepwater_Horizon_Accident_Investigation_Report.pdf (2010). Also Appendix W, "Report Dynamic Simulations Deppwater Horizon Incident BP (from ae add enenry)."

R Camilli, D Di Iorio, A Bowen, C M Reddy, A H Techet, D R Yoerger, L L Whitcomb, J S Seewald, S P Sylva and J Fenwick, "Acoustic measurement of the *Deepwater Horizon* Macondo well flow rate," Proceedings of the National Academy of Sciences **109**(50) 20235–20239 (2012).

H S Carslaw and J C Jaeger, *Conduction of Heat in Solids*, 2nd Edition, Oxford Science Publications, Clarendon Press, Oxford (1946).

T J Crone and M Tolstoy, "Magnitude of the 2010 Gulf of Mexico Oil Leak," Science **330** 624 (2011) plus supporting material.

L P Dake, *Fundamentals of Reservoir Engineering*, Elsevier Science Publishers, Amsterdam (1978).

L P Dake, *The Practice of Reservoir Engineering*, Revised Edition, Elsevier Science Publishers, Amsterdam (2001).

M Dykstra and B Kneller, "Lateral accretion in a deep-marine channel complex: implications for channellized flow processes in turbidity currents," Sedimentology, doi: 10.1111/j.1365-3091.2008.01040.x (2008).

H Darcy, *The Public Fountains of the City of Dijon*, Kendall/Hunt Publishing Company, Dubuque, Iowa, English translation 2004 by P Bobeck, originally published in French by Victor Dalmont, Paris (1856).

R C Earlougher, Jr., H J Ramey, Jr., F G Miller and T D Mueller, "Pressure Distributions in Rectangular Reservoirs," Journal of Petroleum Technology February 199-208; Trans. AIME **243** (1968).

R C Earlougher, Jr., *Advances in Well Test Analysis,* Henry L. Dougherty Monograph Series, Volume 5, Society of Petroleum Engineers, Dallas, USA, ISBN 0-89520-204-2 (1977).

J Forrest, E Marcucci and P Scott, "Geothermal Gradients and Subsurface Temperatures in the Northern Gulf of Mexico," GCAGS Transactions **55** 233-248 (2005).

A Govan, T Primmer, C Douglas, N Moodie, M Davies and F Nieuland, "Reservoir Management in a Deepwater Subsea Field – The Schiehallion Experience," SPE Reservoir Engineering and Evaluation, SPE 96610-PA, **9** 382-390 (2006).

T Gowers, *Mathematics: A Very Short Introduction*, Oxford University Press, Oxford UK (2002).

A C Gringarten, "From Straight Lines to Deconvolution: The Evolution of the State of the Art in Well Test Analysis," SPE Reservoir Engineering and Evaluation, SPE 102079-PA, **11**(1) 41-62 (2008).

A C Gringarten, *MSc Well-test analysis lecture notes*, Imperial College London (2012).

S K Griffiths, "Oil Release from Macondo Well MC252 Following the Deepwater Horizon Accident," Environmental Science and Technology **46** 5616-5622 (2012).

H N Hall, "Compressibility of Reservoir Rocks," Journal of Petroleum Technology **5**(1) 17-19 (1953).

T Haugland, L Larsen and S M Skaeveland, "Analyzing Pressure Builup Data by the Rectangular Hyperbola Approach," SPE 13079, proceedings of the SPE Annual Technical Conference and Exhibition, Houston, Texas, USA, September 16-19 (1984).

S H Hickman, P A Hsieh, W D. Mooney, C B Enomoto, P H Nelson, L A Mayer, T C. Weber, K Moran, P B Flemings, and M K McNutt, "Scientific basis for safely shutting in the Macondo Well after the April 20, 2010 *Deepwater Horizon* blowout," Proceedings of the National Academy of Sciences **109**(50) 20268–20273 (2012).

R N Horne, *Modern well test analysis: A computer-aided approach*, Petroway, Palo Alto, California ISBN: 0962699217 (1997).

B-Z Hsieh, T-L Chen, C-C Tseng, G V Chilingar and Z-S Lin, "Case study of estimating gas loss from a producing well blowout," Journal of Petroleum Science and Engineering **70**(3-4) 327-333 (2010).

P A Hsieh, "Simulation of Reservoir Depletion and Oil Flow from the Macondo Well Following the Deepwater Horizon Blowout." Reston, VA: USGS Open-File Report 2010-1266 http://pubs.usgs.gov/of/2010/1266/ (2010).

P A Hsieh, "Application of MODFLOW for Oil Reservoir Simulation During the Deepwater Horizon Crisis," Ground Water **49**(3) May-June 319–323 (2011).

F P Incropera and D P DeWitt, "Introduction to Heat Transfer," John Wiley and Sons Inc., New York, NY (1985).

M M Kamal (Ed.), *Transient Well Testing,* Society of Petroleum Engineers, Richardson, Texas, USA, ISBN 978-1-55563-141-3 (2009).

J Lee, J B Rollins and J P Spivey, *Pressure Transient Testing,* Society of Petroleum Engineers Textbook Series, Volume 9, Richardson, Texas, USA, ISBN 978-1-55563-099-7 (2003).

B Liu, R Dessenberger, K McMillen, J Lach and M J Kelkar, "Water-Flooding Incremental Oil Recovery Study in Middle Miocene to Paleocene Reservoirs, Deep Gulf of Mexico," SPE 115669, proceedings of the Asia Pacific Oil & Gas Conference and Exhibition, Perth Australia, 20-22 October (2008).

Lubchenko, M K McNutt, G Dreyfus, S A Murawski, D M Kennedy, P T Anastus, S Chu and T Hunter, "Science in support of the *Deepwater Horizon* response," Proceedings of the National Academy of Sciences **109**(50) 20212-20221 (2012).

T McHargue, M J Pyrcz, M D Sullivan, J D Clark, A Fildani, B W Romans, J A Covault, M Levy, H W Posamentier and N J Drinkwater, "Architecture of turbidite channel systems on the continental slope: Patterns and predictions." Marine and Petroleum Geology **28** 728-743 (2011).

A J Love, C T Simmons and D A Nield, "Double-diffusive convection in groundwater wells," Water Resources Research **43** W08428, doi:10.1029/2007WR006001 (2007).

M McNutt, R Camilli, G Guthrie, P Hsieh, V Labson, B Lehr, D Maclay, A Ratzel and M Sogge, "Assessment of Flow Rate Estimates for the Deepwater Horizon / Macondo Well Oil Spill," National Incident Command, Interagency Solutions Group, Flow Rate Technical Group. http://www.doi.gov/deepwaterhorizon/loader.cfm?csModule=security/getfile&PageID=237763 (2011).

M K McNutt, S Chu, J Lubchenco, T Hunter, G Dreyfus, S A Murawski and D M Kennedy, "Applications of science and engineering to quantify and control the *Deepwater Horizon* oil spill," Proceedings of the National Academy of Sciences **109**(50) 20222–20228 (2012a).

M K McNutt, R Camilli, T C Cronec, G D Guthried, P A Hsieh, T B Ryerson, O Savas and F Shaffer, "Review of flow rate estimates of the *Deepwater Horizon* oil spill," Proceedings of the National Academy of Sciences **109**(50) 20260-20267 (2012b).

C S Matthews and D G Russell, *Pressure Buildup and Flow Tests in Wells,* Henry L. Dougherty Monograph Series, Volume 1, Society of Petroleum Engineers, Dallas, USA (1967).

M Muskat, *Physical Principles of Oil Production*, IHRDC Publishers, Boston, USA, ISBN: 0-934634-0706 (1981).

G H Newman, "Pore-Volume Compressibility of Consolidated, Friable, and Unconsolidated Reservoir Rocks Under Hydrostatic Loading," Journal of Petroleum Technology **25**(2) 129-134 (1973).

T A Newson and P Brunning, "Thermal Conductivity of Deepwater Offshore Sediments," International Journal of Offshore and Polar Engineering **14**(4) No TM-31 (2004).

H E Huppert and J S Turner, "Double-diffusive convection," J. Fluid Mechanics **106** 299-329 (1981).

C M Oldenburg, B M Freifeld, K Pruess, L Pan L, S Finsterle and GJ Moridis GJ, "Numerical simulations of the Macondo well blowout reveal strong control of oil flow by reservoir permeability and exsolution of gas," Proceedings of the National Academy of Sciences **109**(50) 20254–20259 (2012).

T L Osif, "The Effects of Salt, Gas, Temperature, and Pressure on the Compressibility of Water," SPE Reservoir Engineering **3** February 175-181 (1988).

R M Ostermeier, "Stressed Oil Permeability of Deepwater Gulf of Mexico Sands: Measurements and Theory," SPE Reservoir Formation Evaluation **11** 226-235 (1996).

R M Ostermeier, "Compaction Effects on Porosity and Permeability: Deepwater Gulf of Mexico Turbidites," Journal of Petroleum Technology February 68-74 (2001).

H W Posamentier, "Depositional elements associated with a basin floor channel-levee system: case study from the Gulf of Mexico," Marine and Petroleum Geology **20** 677–690 (2003).

H W Posamentier and V Kolla, "Seismic geomorphology and stratigraphy of depositional elements in deep-water settings," Journal of Sedimentary Research **73**(3) 367-388 (2003).

S E Pringle and R J Glass, "Double-diffusive finger convection in a solute system at fixed buoyancy ratio: Structural intricacy and length scale growth in Rayleigh space," Journal of Fluid Mechanics **462** 161-183 (2002).

R Raghavan, *Well test analysis*, Prentice Hall, Englewood Cliffs, New Jersey, USA, ISBN: 0139533656 (1993).

G N Ragagnin and M A S Moraes, "Seismic Geomorphology and Connectivity of Deepwater Reservoirs," SPE Reservoir Evaluation and Engineering **11**(4) 686-695 (2008).

H J Ramey, "Wellbore Heat Transmission," Journal of Petroleum Technology, April 427-435 (1962).

C M Reddy, J S Arey, J S Seewald, S P Sylva, K L Lemkau, R K Nelson, C A Carmichael, C P McIntyre, J Fenwick, G Todd Ventura, B A S Van Mooy and R Camilli, "Composition and fate of gas and oil released to the water column during the Deepwater Horizon oil spill," Proceedings of the National Academy of Sciences **109**(50) 20229–20234 (2012).

T B Ryerson, R Camilli, J D Kessler, E B Kujawinski, C M Reddy, D L Valentine, E Atlas, D R Blake, J de Gouw, S Meinardi, D D Parish, J Peischi, J S Seewald and C Warneke, "Chemical data quantify Deepwater Horizon hydrocarbon flow rate and environmental distribution," Proceedings of the National Academy of Sciences **109**(50) 20246–20253 (2012).

R M Saidikowski, "Numerical Simulations of the Combined Effects of Wellbore Damage and Partial Penetration," SPE 8204, proceedings of the SPE Annual Technical Conference and Exhibition, 23-26 September, Las Vegas, Nevada (1979).

M H Sharqawy, J H Lienhard V and S M Zubair. "The thermophysical properties of seawater: A review of existing correlations and data," Desalination and Water Treatment, **16** 354–380 (2010). http://dx.doi.org/10.5004/dwt.2010.1079

P Skalle, *Drilling Fluid Engineering*, bookboon.com, ISBN: 978-87-7681-929-3 (2011).

S V Stankus, I V Savchenko, A V Baginskii, O I Verba, A M Prokopev and R A Khairulin, "Thermal conductivity and thermal diffusivity coefficients of 12Kh18N10T stainless steel in a wide temperature range," High Temperature **46** 731-733 (2008).

T C Webera, A De Robertis, S F Greenaway, S Smith, L Mayera and G Rice, "Estimating oil concentration and flow rate with calibrated vessel-mounted acoustic echo sounders," Proceedings of the National Academy of Sciences 109(50) 20240–20245 (2012).

J Whelan, L Eglinton, L Cathles III, S Losh and H Roberts, "Surface and subsurface manifestations of gas movement through a N–S transect of the Gulf of Mexico," Marine and Petroleum Geology **22** 479–497 (2005).

C Wolfe, C Russell, N Luise and R Chhajlani, "Log-Based Pore Volume Compressibility Prediction – a Deepwater GoM Case Study," SPE 95545, proceedings of the SPE Annual Meeting, Dallas, Texas October (2005).

G R Wooley, "Computing Downhole Temperatures in Circulation, Injection and Production Wells," Journal of Petroleum Technology 1509-1522 (September) (1980).

R W Zimmerman, *Compressibility of Sandstones*, Elsevier Science Publishers, New York, NY, USA, ISBN: 0444-88325-8 (1991).

http://www.bp.com/liveassets/bp_internet/globalbp/globalbp_uk_english/incident_response/STAGING/local_assets/downloads_pdfs/BP_technical_audio_08032010.pdf

http://www.engineeringtoolbox.com/specific-heat-fluids-d_151.html

http://www.engineeringtoolbox.com/specific-heat-solids-d_154.html

http://www.engineeringtoolbox.com/overall-heat-transfer-coefficients-d_284.html

http://fluidflowvisualization.sandia.gov/double_diffusion.html

N.4   Additional Consideration Materials

Beg Bates	End Bates	Document Title / Description
ADR032-061971	ADR032-062078	Complete Report of the Modular Formation Dynamics Tester
ADX001-0014480	ADX001-0014482	Ex No._8625.pdf
BP-HZN-2179MDL00004086	BP-HZN-2179MDL00004086	M45AP 7 H513 32ppf 6 drift
BP-HZN-2179MDL00004086	BP-HZN-2179MDL00004086	M45AP 7 H513 32ppf 6 drift
BP-HZN-2179MDL00059145	BP-HZN-2179MDL00059167	Macondo Shallow Hazard
BP-HZN-2179MDL00059145	BP-HZN-2179MDL00059167	Macondo Shallow Hazard
BP-HZN-2179MDL00063016	BP-HZN-2179MDL00063016	Pencor, Sample Quality Assessment
BP-HZN-2179MDL00063084	BP-HZN-2179MDL00063084	Pencor, Volatile Oil Reservoir Study
BP-HZN-2179MDL00251209	BP-HZN-2179MDL00251212	2010-04-07 Daily Drilling Report No. 21
BP-HZN-2179MDL00251213	BP-HZN-2179MDL00251217	2010-04-08 Daily Drilling Report No. 22
BP-HZN-2179MDL00251218	BP-HZN-2179MDL00251221	2010-04-09 Daily Drilling Report No. 23
BP-HZN-2179MDL00251222	BP-HZN-2179MDL00251226	2010-04-10 Daily Drilling Report No. 24
BP-HZN-2179MDL00251227	BP-HZN-2179MDL00251230	2010-04-11 Daily Drilling Report No. 25
BP-HZN-2179MDL00251231	BP-HZN-2179MDL00251234	2010-04-12 Daily Drilling Report No. 26
BP-HZN-2179MDL00251235	BP-HZN-2179MDL00251238	2010-04-13 Daily Drilling Report No. 27
BP-HZN-2179MDL00251239	BP-HZN-2179MDL00251242	2010-04-14 Daily Drilling Report No. 28

Beg Bates	End Bates	Document Title / Description
BP-HZN-2179MDL00251243	BP-HZN-2179MDL00251246	2010-04-15 Daily Drilling Report No. 29
BP-HZN-2179MDL00251247	BP-HZN-2179MDL00251250	2010-04-16 Daily Drilling Report No. 30
BP-HZN-2179MDL00251251	BP-HZN-2179MDL00251255	2010-04-17 Daily Drilling Report No. 31
BP-HZN-2179MDL00251256	BP-HZN-2179MDL00251259	2010-04-18 Daily Drilling Report No. 32
BP-HZN-2179MDL00251260	BP-HZN-2179MDL00251265	2010-04-19 Daily Drilling Report No. 33
BP-HZN-2179MDL00251266	BP-HZN-2179MDL00251270	2010-04-20 Daily Drilling Report No. 34
BP-HZN-2179MDL00269659	BP-HZN-2179MDL00269659	BP - Zonal Isolation Requirements during Drilling Operations and Well Abandonment and Suspension
BP-HZN-2179MDL00269659	BP-HZN-2179MDL00269659	BP - Zonal Isolation Requirements during Drilling Operations and Well Abandonment and Suspension
BP-HZN-2179MDL00309089	BP-HZN-2179MDL00309089	1818_001
BP-HZN-2179MDL00309089	BP-HZN-2179MDL00309089	1818_001
BP-HZN-2179MDL00309089	BP-HZN-2179MDL00309089	Crossover 1818_001
BP-HZN-2179MDL00360844	BP-HZN-2179MDL00360844	BP - Gulf of Mexico SPU - Recommended Practice for Cement Design and Operations in DW GoM
BP-HZN-2179MDL00360844	BP-HZN-2179MDL00360844	BP - Gulf of Mexico SPU - Recommended Practice for Cement Design and Operations in DW GoM
BP-HZN-2179MDL00470598	BP-HZN-2179MDL00470598	Weatherford Laboratories, Core Weight Inventory
BP-HZN-2179MDL00470599	BP-HZN-2179MDL00470599	Weatherford Laboratories, Core Sample Inventory
BP-HZN-2179MDL00477088	BP-HZN-2179MDL00477088	BP-HZN-2179MDL00477088.pdf

Beg Bates	End Bates	Document Title / Description
BP-HZN-2179MDL00477088	BP-HZN-2179MDL00477088	BP-HZN-2179MDL00477088 .pdf
BP-HZN-2179MDL00640467	BP-HZN-2179MDL00640467	BP - E&P Segment Recommended Practice - Drilling and Completions Cementing Manual - HPHT Cementing Section
BP-HZN-2179MDL00640467	BP-HZN-2179MDL00640467	BP - E&P Segment Recommended Practice - Drilling and Completions Cementing Manual - HPHT Cementing Section
BP-HZN-2179MDL00894719	BP-HZN-2179MDL00894719	MDL 2179 Deposition Exhibit 8708
BP-HZN-2179MDL01299582	BP-HZN-2179MDL01299582	Email from Jesse Gagliano to Brian Morel re Lab test
BP-HZN-2179MDL01299741	BP-HZN-2179MDL01299741	Email from Jesse Gagliano to Anthony Cupit, et al., re Update Info for Prod Casing job
BP-HZN-2179MDL01608973	BP-HZN-2179MDL01609022	Schlumberger Report
BP-HZN-2179MDL01872218	BP-HZN-2179MDL01872218	Pencor Report
BP-HZN-2179MDL01872218	BP-HZN-2179MDL01872218	Pencor Report
BP-HZN-2179MDL02107723	BP-HZN-2179MDL02107723	Technical Assurance Memorandum - Sections2, 3 and 4
BP-HZN-2179MDL02107723	BP-HZN-2179MDL02107723	Technical Assurance Memorandum - Sections2, 3 and 4
BP-HZN-2179MDL02107724	BP-HZN-2179MDL02107724	TAM Chapter 5
BP-HZN-2179MDL02107724	BP-HZN-2179MDL02107724	TAM Chapter 5
BP-HZN-2179MDL02393883	BP-HZN-2179MDL02393883	Weatherford Rock Mechanics Testing & Analysis: Uniaxial Pore Volume Compressibility Tests
BP-HZN-2179MDL02394182	BP-HZN-2179MDL02394182	Weatherford Laboratories, Rotary Core Data
BP-HZN-2179MDL02394183	BP-HZN-2179MDL02394183	Weatherford Laboratories, Rock Mechanics Testing & Analysis, Rock Mechanics Final Report, Multi-Stage Triaxial Compressive Tests

Beg Bates	End Bates	Document Title / Description
BP-HZN-2179MDL02394184	BP-HZN-2179MDL02394184	BP Macondo Rock Mech Report HH-46949
BP-HZN-2179MDL02394184	BP-HZN-2179MDL02394184	BP Macondo Rock Mech Report HH-46949
BP-HZN-2179MDL02394185	BP-HZN-2179MDL02394185	Weatherford Laboratories, Pore Volume Compressibility Test - Pore Pressure Depeletion
BP-HZN-2179MDL02394186	BP-HZN-2179MDL02394186	Weatherford Laboratories, CoreLab_Stats Summary and Perm
BP-HZN-2179MDL02394187	BP-HZN-2179MDL02394187	Weatherford Laboratories, X-Ray Defraction
BP-HZN-2179MDL02900640	BP-HZN-2179MDL02900640	TAM Chapter 1
BP-HZN-2179MDL02900640	BP-HZN-2179MDL02900640	TAM Chapter 1
BP-HZN-2179MDL03139594	BP-HZN-2179MDL03139625	Geotap Pressure Transient Analysis
BP-HZN-2179MDL03198892	BP-HZN-2179MDL03198892	Capping Stack Schematic
BP-HZN-2179MDL03198892	BP-HZN-2179MDL03198892	Capping Stack Schematic
BP-HZN-2179MDL03290054	BP-HZN-2179MDL03290094	Post-Well Subsurface Technical Memorandum .doc
BP-HZN-2179MDL03290054	BP-HZN-2179MDL03290054	Post-Well Subsurface Technical Memorandum
BP-HZN-2179MDL03652749	BP-HZN-219MDL03652794	MDL 2179 Deposition Exhibit 8710
BP-HZN-2179MDL03742328	BP-HZN-2179MDL03742328	Comprehensive Analysis Report (Schlumberger MDT Field Report)
BP-HZN-2179MDL04440100	BP-HZN-2179MDL04440167	DataDump_MC252_K_303-8.csv
BP-HZN-2179MDL04440168	BP-HZN-2179MDL04440191	DataDump_MC252_K_303-6.csv

Beg Bates	End Bates	Document Title / Description
BP-HZN-2179MDL04440192	BP-HZN-2179MDL04440237	DataDump_MC252_K_303-1.csv
BP-HZN-2179MDL04440238	BP-HZN-2179MDL04440248	Macondo Depositional Models and Amplitude Maps
BP-HZN-2179MDL04440249	BP-HZN-2179MDL04440261	Macondo Technical Note (Preliminary Draft) – Well Integrity Test
BP-HZN-2179MDL04440249	BP-HZN-2179MDL04440261	MC252 WIT Pressure Measurement System Accuracy revA
BP-HZN-2179MDL04440262	BP-HZN-2179MDL04440262	Resistor Inaccuracy Tables – Error v. Pressure (VTD453_kv0.xls)
BP-HZN-2179MDL04440263	BP-HZN-2179MDL04440266	DataDump_MC252_PT_3K_2.csv
BP-HZN-2179MDL04440267	BP-HZN-2179MDL04440267	Macondo OOIP (ff9a70a171043e7d458cae0765f5aa5c)
BP-HZN-2179MDL04440268	BP-HZN-2179MDL04440367	DataDump_PT_3K_2.csv
BP-HZN-2179MDL04440368	BP-HZN-2179MDL04440381	Technical Note - Requirements for Sensor Data Collection and Transmission Rev 0
BP-HZN-2179MDL04440382	BP-HZN-2179MDL04440430	DataDump_MC252_K_303-2.csv
BP-HZN-2179MDL04440431	BP-HZN-2179MDL04440455	Well Inteegrity/Shut-In Discussion
BP-HZN-2179MDL04440456	BP-HZN-2179MDL04440465	Completions and Interventions-M252 Capping Stack ROV Procedures-Procedure Ops Note 2
BP-HZN-2179MDL04440466	BP-HZN-2179MDL04440532	DataDump_MC252_K_303-7.csv
BP-HZN-2179MDL04440557	BP-HZN-2179MDL04440583	Completions and Interventions - M252 Capping Stack ROV Procedures
BP-HZN-2179MDL04440584	BP-HZN-2179MDL04440612	DataDump_MC252_K_303-5.csv
BP-HZN-2179MDL04440613	BP-HZN-2179MDL04440613	MC252tagsforTrevor_10sInterval_Latest-1.xls

TREX-011553-R.0181

Beg Bates	End Bates	Document Title / Description
BP-HZN-2179MDL04440614	BP-HZN-2179MDL04440688	DataDump_MC252_K_303.csv
BP-HZN-2179MDL04440689	BP-HZN-2179MDL04440690	Intertek Constant Composition Expansion Tables 1 & 2 - e06636e3340751cc1966d2082b65fdfb
BP-HZN-2179MDL04440691	BP-HZN-2179MDL04440731	Powerpoint Presentation - Macondo-Petrophysics
BP-HZN-2179MDL04440732	BP-HZN-2179MDL04440732	Intertek CCE & Viscosity Tables - 2e9ee0e3675cc3b5acf22f1adea9089c
BP-HZN-2179MDL04440733	BP-HZN-2179MDL04440774	DataDump_MC252_K_303-3.csv
BP-HZN-2179MDL04440775	BP-HZN-2179MDL04440803	DataDump_MC252_K_303-4.csv
BP-HZN-2179MDL04440804	BP-HZN-2179MDL04440966	MC252DataDumpPT_3K_2.csv
BP-HZN-2179MDL04440967	BP-HZN-2179MDL04440967	Email Y. Wang to R. Merrill, et al. re OOIP and Data Ranges for MC252
BP-HZN-2179MDL04440968	BP-HZN-2179MDL04440968	Email from Y. Wang to M. Nass, et al. Attaching Preliminary EOS
BP-HZN-2179MDL04440969	BP-HZN-2179MDL04440976	Preliminary EOS
BP-HZN-2179MDL04440977	BP-HZN-2179MDL04440977	Intertek/Westport Multi-Stage Separator Test (MST Tables)
BP-HZN-2179MDL04440978	BP-HZN-2179MDL04440998	Intertek/Westport Multi-Stage Separator Test (Final Report)
BP-HZN-2179MDL04549798	BP-HZN-2179MDL04549798	ACTIVITY LOG Well integrity test Record rev6 7-15
BP-HZN-2179MDL04578104	BP-HZN-2179MDL04578104	Black Oil Tables from EoS for All Temps 11June2010
BP-HZN-2179MDL04808055	BP-HZN-2179MDL04808071	May 23 Sec. Salazar DH Review (Native)
BP-HZN-2179MDL04808055	BP-HZN-2179MDL04808071	May 23 Sec. Salazar DH Review (Native)

Beg Bates	End Bates	Document Title / Description
BP-HZN-2179MDL04826982	BP-HZN-2179MDL04826982	Riser General Data Sheet
BP-HZN-2179MDL04826982	BP-HZN-2179MDL04826982	Riser General Data Sheet
BP-HZN-2179MDL04843794	BP-HZN-2179MDL04843796	MDL 2179 Deposition Exhibit 10860.PDF
BP-HZN-2179MDL04899278	BP-HZN-2179MDL04899278	MDL 2179 Deposition Exhibit 9318.PDF
BP-HZN-2179MDL04923119	BP-HZN-2179MDL04923131	MDL 2179 Deposition Exhibit 10825.PDF
BP-HZN-2179MDL04927171	BP-HZN-2179MDL04927174	FW: FINAL Corrected Water Depth and Ambient Pressures at Key Stack Locations
BP-HZN-2179MDL04940401	BP-HZN-2179MDL04940401	MC252_DataDump_071810 (3)
BP-HZN-2179MDL04940401	BP-HZN-2179MDL04940401	MC252_DataDump_071810 (3)
BP-HZN-2179MDL05173765	BP-HZN-2179MDL05173768	M56 Net Rock Volume
BP-HZN-2179MDL05173765	BP-HZN-2179MDL05173768	M56 Net Rock Volume
BP-HZN-2179MDL05181294	BP-HZN-2179MDL05181319	June 22 2010 Macondo Review
BP-HZN-2179MDL05181294	BP-HZN-2179MDL05181319	June 22 2010 Macondo Review
BP-HZN-2179MDL05187231	BP-HZN2179MDL05187231	Email from Kate Baker to Marjorie and Steve Black re FW: Transmitter Calibrations, Section 4.2 Info
BP-HZN-2179MDL05187232	BP-HZN-2179MDL05187232	Tranmitter Calibration
BP-HZN-2179MDL05187232	BP-HZN-2179MDL05187232	Tranmitter Calibration
BP-HZN-2179MDL05223139	BP-HZN-2179MDL05223139	Weatherford - Summary of Effective Permeability to Oil Measurements
BP-HZN-2179MDL05223139	BP-HZN-2179MDL05223139	Weatherford - Summary of Effective Permeability to Oil Measurements

Beg Bates	End Bates	Document Title / Description
BP-HZN-2179MDL05441785	BP-HZN-2179MDL05441785	May 14-23 Pressure Measurements
BP-HZN-2179MDL05441785	BP-HZN-2179MDL05441785	May 14-23 Pressure Measurements (Native)
BP-HZN-2179MDL05604047	BP-HZN-2179MDL05604051	Depo Exh. 10452.pdf
BP-HZN-2179MDL05721745	BP-HZN-2179MDL05721755	May 16 Science Meeting Slides
BP-HZN-2179MDL05721745	BP-HZN-2179MDL05721755	May 16 Science Meeting Slides (Native)
BP-HZN-2179MDL05755276	BP-HZN-2179MDL05755277	MDL 2179 Deposition Exhibit 8776.PDF
BP-HZN-2179MDL05789875	BP-HZN-2179MDL05789876	MDL 2179 Deposition Exhibit 8775.PDF
BP-HZN-2179MDL05825079	BP-HZN-2179MDL05825083	MDL 2179 Deposition Exhibit 8581
BP-HZN-2179MDL05864773	BP-HZN-2179MDL05864774	MDL 2179 Deposition Exhibit 8777.PDF
BP-HZN-2179MDL05864804	BP-HZN-2179MDL05864805	MDL 2179 Deposition Exhibit 8774.PDF
BP-HZN-2179MDL06105310	BP-HZN-2179MDL06105313	MDL 2179 Deposition Exhibit 8770.PDF
BP-HZN-2179MDL06127378	BP-HZN-2179MDL06127378	MDL 2179 Deposition Exhibit 9324.PDF
BP-HZN-2179MDL06314451	BP-HZN-2179MDL06314453	BOP PT-B Data Summary 5.15.10
BP-HZN-2179MDL06314451	BP-HZN-2179MDL06314453	BOP PT-B Data Summary 5.15.10
BP-HZN-2179MDL06392037	BP-HZN-2179MDL06392041	MDL 2179 Deposition Exhibit 8767.PDF
BP-HZN-2179MDL06514658	BP-HZN-2179MDL06514659	MDL 2179 Deposition Exhibit 8700
BP-HZN-2179MDL06566208	BP-HZN-2179MDL06566233	Maconod RSDP - Predrill
BP-HZN-2179MDL06566208	BP-HZN-2179MDL06566233	Maconod RSDP - Predrill
BP-HZN-2179MDL06566258	BP-HZN-2179MDL06566259	MDL 2179 Deposition Exhibit 8773.PDF
BPHZN2179MDL06604337	BPHZN2179MDL06604337	Email from R. Benthien to P. Flemings re Deepwater unconfined slop channel complex

Beg Bates	End Bates	Document Title / Description
BPHZN2179MDL06604338	BPHZN2179MDL06604352	Unconfined Low Relief Slope Channel System
BPHZN2179MDL06604338	BPHZN2179MDL06604352	Unconfined Low Relief Slope Channel System
BP-HZN-2179MDL06605384	BP-HZN-2179MDL06605386	MDL 2179 Deposition Exhibit 8769.PDF
BP-HZN-2179MDL06629316	BP-HZN-2179MDL06629369	Depo Exh. 10459.pdf
BP-HZN-2179MDL06666023	BP-HZN-2179MDL06666034	MC252 WIT Pressure Measurement System Accuracy rev0
BP-HZN-2179MDL06666023	BP-HZN-2179MDL06666034	MC252 WIT Pressure Measurement System Accuracy rev0
BP-HZN-2179MDL06726208	BP-HZN-2179MDL06726208	MDL 2179 Deposition Exhibit 8772.PDF
BP-HZN-2179MDL06741948	BP-HZN-2179MDL06742177	Q4000 MC252 PT 3C
BP-HZN-2179MDL06741948	BP-HZN-2179MDL06742177	Q4000 MC252 PT 3C
BP-HZN-2179MDL06742178	BP-HZN-2179MDL06742178	Equations
BP-HZN-2179MDL06742178	BP-HZN-2179MDL06742178	Equations
BP-HZN-2179MDL06742179	BP-HZN-2179MDL06742231	MC252 HSR M PS
BP-HZN-2179MDL06742179	BP-HZN-2179MDL06742231	MC252 HSR M PS
BP-HZN-2179MDL06742232	BP-HZN-2179MDL06742232	Skandi MC252 PT 3K 1 2
BP-HZN-2179MDL06742232	BP-HZN-2179MDL06742232	Skandi MC252 PT 3K 1 2
BP-HZN-2179MDL06742233	BP-HZN-2179MDL06742233	MC252 PT 3K 1 1
BP-HZN-2179MDL06742233	BP-HZN-2179MDL06742233	MC252 PT 3K 1 1
BP-HZN-2179MDL06742234	BP-HZN-2179MDL06742234	Q4000 MC252 PT B 301 Offset

Beg Bates	End Bates	Document Title / Description
BP-HZN-2179MDL06742234	BP-HZN-2179MDL06742234	Q4000 MC252 PT B 301 Offset
BP-HZN-2179MDL06742238	BP-HZN-2179MDL06742238	Skandi MC252 PT 3K 1 1
BP-HZN-2179MDL06742238	BP-HZN-2179MDL06742238	Skandi MC252 PT 3K 1 1
BP-HZN-2179MDL06742239	BP-HZN-2179MDL06742607	Skandi MC252 PT C 302 2
BP-HZN-2179MDL06742608	BP-HZN-2179MDL06742608	Q4000 MC252 PT B 305
BP-HZN-2179MDL06742608	BP-HZN-2179MDL06742608	Q4000 MC252 PT B 305
BP-HZN-2179MDL06742609	BP-HZN-2179MDL06742609	Skandi MC252 PT K 303 1
BP-HZN-2179MDL06742609	BP-HZN-2179MDL06742609	Skandi MC252 PT K 303 1
BP-HZN-2179MDL06742613	BP-HZN-2179MDL06742613	Q4000 MC252 PT B 301
BP-HZN-2179MDL06742613	BP-HZN-2179MDL06742613	Q4000 MC252 PT B 301
BP-HZN-2179MDL06742614	BP-HZN-2179MDL06742718	Skandi MC252 HSR M PS
BP-HZN-2179MDL06742614	BP-HZN-2179MDL06742718	Skandi MC252 HSR M PS
BP-HZN-2179MDL06742720	BP-HZN-2179MDL06742720	Equations
BP-HZN-2179MDL06742720	BP-HZN-2179MDL06742720	Equations
BP-HZN-2179MDL06742721	BP-HZN-2179MDL06742826	Skandi MC252 PT B 301 Offset 2
BP-HZN-2179MDL06742721	BP-HZN-2179MDL06742826	Skandi MC252 PT B 301 Offset 2

Beg Bates	End Bates	Document Title / Description
BP-HZN-2179MDL06742965	BP-HZN-2179MDL06742965	Skandi MC252 PT B 301 1
BP-HZN-2179MDL06742965	BP-HZN-2179MDL06742965	Skandi MC252 PT B 301 1
BP-HZN-2179MDL06742966	BP-HZN-2179MDL06742966	Skandi MC252 PT 3K 2 1
BP-HZN-2179MDL06742966	BP-HZN-2179MDL06742966	Skandi MC252 PT 3K 2 1
BP-HZN-2179MDL06742968	BP-HZN-2179MDL06742968	Skandi MC252 PT C 302 1
BP-HZN-2179MDL06742968	BP-HZN-2179MDL06742968	Skandi MC252 PT C 302 1
BP-HZN-2179MDL06742969	BP-HZN-2179MDL06742969	Skandi MC252 PT 3C
BP-HZN-2179MDL06742969	BP-HZN-2179MDL06742969	Skandi MC252 PT 3C
BP-HZN-2179MDL06742970	BP-HZN-2179MDL06742970	MC252 PT C 302 2
BP-HZN-2179MDL06742970	BP-HZN-2179MDL06742970	MC252 PT C 302 2
BP-HZN-2179MDL06742973	BP-HZN-2179MDL06742973	Skandi MC252 PT B 305
BP-HZN-2179MDL06742973	BP-HZN-2179MDL06742973	Skandi MC252 PT B 305
BP-HZN-2179MDL06742974	BP-HZN-2179MDL06743163	Skandi MC252 PT K 303 2
BP-HZN-2179MDL06742974	BP-HZN-2179MDL06743163	Skandi MC252 PT K 303 2
BP-HZN-2179MDL06743166	BP-HZN-2179MDL06743166	Skandi MC252 PT B 301 Offset 1
BP-HZN-2179MDL06743166	BP-HZN-2179MDL06743166	Skandi MC252 PT B 301 Offset 1

Beg Bates	End Bates	Document Title / Description
BP-HZN-2179MDL06743280	BP-HZN-2179MDL06743280	Skandi MC252 PT 3K 2 3
BP-HZN-2179MDL06743280	BP-HZN-2179MDL06743280	Skandi MC252 PT 3K 2 3
BP-HZN-2179MDL06743284	BP-HZN-2179MDL06743284	MC252 PT 3K 2 1
BP-HZN-2179MDL06743284	BP-HZN-2179MDL06743284	MC252 PT 3K 2 1
BP-HZN-2179MDL06743478	BP-HZN-2179MDL06743478	MC252 PT B 301 1
BP-HZN-2179MDL06743478	BP-HZN-2179MDL06743478	MC252 PT B 301 1
BP-HZN-2179MDL06743479	BP-HZN-2179MDL06743479	Q4000 MC252 PT 3K 2
BP-HZN-2179MDL06743479	BP-HZN-2179MDL06743479	Q4000 MC252 PT 3K 2
BP-HZN-2179MDL06743482	BP-HZN-2179MDL06744008	MC252 PT K 303 2
BP-HZN-2179MDL06744009	BP-HZN-2179MDL06744009	MC252 PT 3K 2 2
BP-HZN-2179MDL06744009	BP-HZN-2179MDL06744009	MC252 PT 3K 2 2
BP-HZN-2179MDL06744010	BP-HZN-2179MDL06744010	MC252 PT K 303 1
BP-HZN-2179MDL06744010	BP-HZN-2179MDL06744010	MC252 PT K 303 1
BP-HZN-2179MDL06744011	BP-HZN-2179MDL06744011	MC252 PT B 305
BP-HZN-2179MDL06744011	BP-HZN-2179MDL06744011	MC252 PT B 305
BP-HZN-2179MDL06744066	BP-HZN-2179MDL06744066	Q4000 MC252 PT C 302

Beg Bates	End Bates	Document Title / Description
BP-HZN-2179MDL06744066	BP-HZN-2179MDL06744066	Q4000 MC252 PT C 302
BP-HZN-2179MDL06744067	BP-HZN-2179MDL06744202	Q4000 MC252 PT 3K 1 2
BP-HZN-2179MDL06744067	BP-HZN-2179MDL06744202	Q4000 MC252 PT 3K 1 2
BP-HZN-2179MDL06744204	BP-HZN-2179MDL06744204	Skandi MC252 HSR H2 BM
BP-HZN-2179MDL06744204	BP-HZN-2179MDL06744204	Skandi MC252 HSR H2 BM
BP-HZN-2179MDL06744773	BP-HZN-2179MDL06744878	Skandi MC252 PT B 301 2
BP-HZN-2179MDL06744773	BP-HZN-2179MDL06744878	Skandi MC252 PT B 301 2
BP-HZN-2179MDL06744880	BP-HZN-2179MDL06744880	Q4000 MC252 PT K 303
BP-HZN-2179MDL06744880	BP-HZN-2179MDL06744880	Q4000 MC252 PT K 303
BP-HZN-2179MDL06744882	BP-HZN-2179MDL06744882	MC252 PT B 301 Offset
BP-HZN-2179MDL06744882	BP-HZN-2179MDL06744882	MC252 PT B 301 Offset
BP-HZN-2179MDL06744883	BP-HZN-2179MDL06744883	MC252 HSR H2 BM
BP-HZN-2179MDL06744883	BP-HZN-2179MDL06744883	MC252 HSR H2 BM
BP-HZN-2179MDL06744884	BP-HZN-2179MDL06744884	Q4000 MC252 PT 3K 1 1
BP-HZN-2179MDL06744884	BP-HZN-2179MDL06744884	Q4000 MC252 PT 3K 1 1
BP-HZN-2179MDL06744885	BP-HZN-2179MDL06744885	MC252 PT B 301 2

Beg Bates	End Bates	Document Title / Description
BP-HZN-2179MDL06744885	BP-HZN-2179MDL06744885	MC252 PT B 301 2
BP-HZN-2179MDL06744992	BP-HZN-2179MDL06745325	MC252 PT 3C
BP-HZN-2179MDL06745326	BP-HZN-2179MDL06745326	Skandi MC252 PT 3K 1 3
BP-HZN-2179MDL06745326	BP-HZN-2179MDL06745326	Skandi MC252 PT 3K 1 3
BP-HZN-2179MDL06745327	BP-HZN-2179MDL06745327	Q4000 MC252 HSR H2 BM
BP-HZN-2179MDL06745327	BP-HZN-2179MDL06745327	Q4000 MC252 HSR H2 BM
BP-HZN-2179MDL06745329	BP-HZN-2179MDL06745329	Skandi MC252 PT 3K 2 2
BP-HZN-2179MDL06745329	BP-HZN-2179MDL06745329	Skandi MC252 PT 3K 2 2
BP-HZN-2179MDL06746267	BP-HZN-2179MDL06746267	MC252 PT C 302 1
BP-HZN-2179MDL06746267	BP-HZN-2179MDL06746267	MC252 PT C 302 1
BP-HZN-2179MDL06746268	BP-HZN-2179MDL06746268	MC252 PT 3K 1 2
BP-HZN-2179MDL06746268	BP-HZN-2179MDL06746268	MC252 PT 3K 1 2
BP-HZN-2179MDL06947350	BP-HZN-2179MDL06947351	Email from S. Gullion to M. Gochnour re RE Calibration Data
BP-HZN-2179MDL06947352	BP-HZN-2179MDL06947352	Data - Testing LDS at King South
BP-HZN-2179MDL06947352	BP-HZN-2179MDL06947352	Data - Testing LDS at King South
BP-HZN-2179MDL06947352	BP-HZN-2179MDL06947352	Testing LDS at King South on Horizon
BP-HZN-2179MDL06947352	BP-HZN-2179MDL06947352	Testing LDS at King South on Horizon

Beg Bates	End Bates	Document Title / Description
BP-HZN-2179MDL06990570	BP-HZN-2179MDL06990570	MDL 2179 Deposition Exhibit 8771.PDF
BP-HZN-2179MDL07033640	BP-HZN-2179MDL07033658	MDL 2179 Deposition Exhibit 10841.PDF
BP-HZN-2179MDL07066668	BP-HZN-2179MDL07066669	MDL 2179 Deposition Exhibit 10859.PDF
BP-HZN-2179MDL07087480	BP-HZN-2179MDL07087482	Macondo Technical Note - Depln for Well Control 21Jul vB.doc
BP-HZN-2179MDL07119924	BP-HZN-2179MDL07119925	Email from M. Gochnour to J. Tucker re RE: Sudsea pressures.
BP-HZN-2179MDL07119926	BP-HZN-2179MDL07119927	Email from M. Gochnour to M. Byrd re RE: Acoustic Data Acquisition - 12 Hour Look Ahead 2010-07-13 0620 hrs Rev 0
BP-HZN-2179MDL07206222	BP-HZN-2179MDL07206227	MDL 2179 Deposition Exhibit 8707
BP-HZN-2179MDL07279438	BP-HZN-2179MDL07279438	04-MC252_PT_3K_1-CORR2-Calculated-1
BP-HZN-2179MDL07279438	BP-HZN-2179MDL07279438	04-MC252_PT_3K_1-CORR2-Calculated-1
BP-HZN-2179MDL07279439	BP-HZN-2179MDL07279439	08-MC252_PT_3K_1-CORR2-Calculated-2
BP-HZN-2179MDL07279439	BP-HZN-2179MDL07279439	08-MC252_PT_3K_1-CORR2-Calculated-2
BP-HZN-2179MDL07279440	BP-HZN-2179MDL07279440	Equation_Corr
BP-HZN-2179MDL07279440	BP-HZN-2179MDL07279440	Equation_Corr
BP-HZN-2179MDL07279441	BP-HZN-2179MDL07279441	08-MC252_PT_3K_1-CORR2-Calculated-1
BP-HZN-2179MDL07279441	BP-HZN-2179MDL07279441	08-MC252_PT_3K_1-CORR2-Calculated-1
BP-HZN-2179MDL07279442	BP-HZN-2179MDL07279442	08-MC252_PT_3K_1-CORR2-Calculated-3
BP-HZN-2179MDL07279442	BP-HZN-2179MDL07279442	08-MC252_PT_3K_1-CORR2-Calculated-3
BP-HZN-2179MDL07279443	BP-HZN-2179MDL07279443	04-MC252_PT_3K_1-CORR2-Calculated-2
BP-HZN-2179MDL07279443	BP-HZN-2179MDL07279443	04-MC252_PT_3K_1-CORR2-Calculated-2
BP-HZN-2179MDL07279444	BP-HZN-2179MDL07279444	04-MC252_PT_3K_1-CORR2-Calculated-3
BP-HZN-2179MDL07279444	BP-HZN-2179MDL07279444	04-MC252_PT_3K_1-CORR2-Calculated-3
BP-HZN-2179MDL07279445	BP-HZN-2179MDL07279445	03-MC252_PT_3K_1-CORR2_R-Raw-2
BP-HZN-2179MDL07279445	BP-HZN-2179MDL07279445	03-MC252_PT_3K_1-CORR2_R-Raw-2

Beg Bates	End Bates	Document Title / Description
BP-HZN-2179MDL07279446	BP-HZN-2179MDL07279446	07-MC252_PT_3K_1-CORR2_R-Raw-1
BP-HZN-2179MDL07279446	BP-HZN-2179MDL07279446	07-MC252_PT_3K_1-CORR2_R-Raw-1
BP-HZN-2179MDL07279447	BP-HZN-2179MDL07279447	03-MC252_PT_3K_1-CORR2_R-Raw-1
BP-HZN-2179MDL07279447	BP-HZN-2179MDL07279447	03-MC252_PT_3K_1-CORR2_R-Raw-1
BP-HZN-2179MDL07279448	BP-HZN-2179MDL07279448	03-MC252_PT_3K_1-CORR2_R-Raw-3
BP-HZN-2179MDL07279448	BP-HZN-2179MDL07279448	03-MC252_PT_3K_1-CORR2_R-Raw-3
BP-HZN-2179MDL07279449	BP-HZN-2179MDL07279449	07-MC252_PT_3K_1-CORR2_R-Raw-3
BP-HZN-2179MDL07279449	BP-HZN-2179MDL07279449	07-MC252_PT_3K_1-CORR2_R-Raw-3
BP-HZN-2179MDL07279450	BP-HZN-2179MDL07279450	07-MC252_PT_3K_1-CORR2_R-Raw-2
BP-HZN-2179MDL07279450	BP-HZN-2179MDL07279450	07-MC252_PT_3K_1-CORR2_R-Raw-2
BP-HZN-2179MDL07383106	BP-HZN-2179MDL07383106	Pressure Measurement Network Architecture
BP-HZN-BLY00000001	BP-HZN-BLY00000193	Deepwater Horizon Accident Investigation Report (9/8/10)
BP-HZN-BLY00000194	BP-HZN-BLY00000194	Appendix A. Transocean Deepwater Horizon Rig Incident Investigation Into the Facts and Causation (April 23, 2010)
BP-HZN-BLY00000195	BP-HZN-BLY00000200	Appendix B. Acronyms, Abbreviations and Company Names
BP-HZN-BLY00000201	BP-HZN-BLY00000201	Appendix C Macondo Well Components of Interest
BP-HZN-BLY00000202	BP-HZN-BLY00000202	Appendix D Sperry-Sun Real-time Data Pits
BP-HZN-BLY00000203	BP-HZN-BLY00000203	Appendix E Sperry-Sun Real-time Data Surface Parameters
BP-HZN-BLY00000204	BP-HZN-BLY00000207	Appendix F Roles and Responsibilities for Macondo Well
BP-HZN-BLY00000208	BP-HZN-BLY00000219	Appendix G Analysis Determining the Likely Source of In Flow
BP-HZN-BLY00000220	BP-HZN-BLY00000231	Appendix H-Description of the BOP Stack and Control System
BP-HZN-BLY00000232	BP-HZN-BLY00000236	Appendix I. Deepwater Horizon Investigation Fault Trees
BP-HZN-BLY00000237	BP-HZN-BLY00000241	Appendix J. Halliburton Lab Results - #73909 2
BP-HZN-BLY00000242	BP-HZN-BLY00000275	Appendix K. Laboratory Analysis of Cementing Operations on the Deepwater Horizon (from

Beg Bates	End Bates	Document Title / Description
		CSI Technologies)
BP-HZN-BLY00000276	BP-HZN-BLY00000303	Appendix M. Summary Report Global Analysis Of Macondo 9 78-In X 7-In Production Casing 4992 ft Water Depth GoM (for Macondo Well Investigation) (from Stress Engineering)
BP-HZN-BLY00000304	BP-HZN-BLY00000370	Appendix N. Mississippi Canyon 252 No.1 (Macondo) Basis of Design Review
BP-HZN-BLY00000371	BP-HZN-BLY00000372	Appendix O. Industry Comparison Data on Long String Casing and Casing Liners in the Macondo Well Area
BP-HZN-BLY00000373	BP-HZN-BLY00000374	Appendix P. BP Deepwater Horizon Rheliant Displacement Procedure ÁʹMacondoÃ¶ OSC-G 32306 (M-I SWACO)
BP-HZN-BLY00000375	BP-HZN-BLY00000383	Appendix Q. Summary of The Effect of Spacer Fluid Composition and Placement on Negative-pressure Test
BP-HZN-BLY00000384	BP-HZN-BLY00000385	Appendix R. Fluid Compressibility Calculation
BP-HZN-BLY00000386	BP-HZN-BLY00000392	Appendix S. First Surface Indications of Well Flow and Pit Gain
BP-HZN-BLY00000393	BP-HZN-BLY00000401	Appendix T. Comparison of Events with Relevant Transocean Well Control Policies, Practices and Procedures
BP-HZN-BLY00000402	BP-HZN-BLY00000406	Appendix U. Riser Fluid Evacuation to Rig Floor
BP-HZN-BLY00000407	BP-HZN-BLY00000427	Appendix V. BP Deepwater Horizon GOM Incident Investigation Dispersion Analysis (from BakerRisk)
BP-HZN-BLY00000526	BP-HZN-BLY00000585	Appendix W. Report-Dynamic Simulations Deepwater Horizon Incident BP (from ae add energy)
BP-HZN-BLY00000586	BP-HZN-BLY00000592	Appendix X. Deepwater Horizon Blue Pod AMF System Batteries
BP-HZN-BLY00000593	BP-HZN-BLY00000596	Appendix Y. September 2009 Deepwater Horizon Follow-up Rig Audit
BP-HZN-BLY00000597	BP-HZN-BLY00000598	Appendix Z. Hydraulic analyses of BOP Control system(from Ultra Deep)
BP-HZN-BLY00000758	BP-HZN-BLY00000760	Appendix AA. Deepwater Horizon BOP Modifications Since Commissioning
BP-HZN-BLY-00111338	BP-HZN-BLY-00111338	BP - Cementing in hostile environments: Guidelines for obtaining isolation in demanding wells
BP-HZN-BLY-00111338	BP-HZN-BLY-00111338	BP - Cementing in hostile environments: Guidelines for obtaining isolation in demanding wells
BP-HZN-BLY00120160	BP-HZN-BLY00120160	mc0252_1_st01_bp_tops_sand
BP-HZN-BLY00120160	BP-HZN-BLY00120160	mc0252_1_st01_bp_tops_sand

Beg Bates	End Bates	Document Title / Description
BP-HZN-BLY00134336	BP-HZN-BLY00134345	DWP ELAS-TU-006 N-R Rev B 3-31-2010
BP-HZN-BLY00134336	BP-HZN-BLY00134345	DWP ELAS-TU-006 N-R Rev B 3-31-2010
BP-HZN-BLY00138899	BP-HZN-BLY00138907	Mid-bore Auto Fill Float Collar
BP-HZN-BLY00138899	BP-HZN-BLY00138907	Mid-bore Auto Fill Float Collar
BP-HZN-BLY00269184	BP-HZN-BLY00269185	RD070082C-S13-S1920Reamer20Shoe20720X208201-4-1
BP-HZN-BLY00269184	BP-HZN-BLY00269185	RD070082C-S13-S1920Reamer20Shoe20720X208201-4-1
BP-HZN-CEC011406	BP-HZN-CEC011406	Halliburton - 9.875" x 7" Foamed Production Casing Post Job Report
BP-HZN-CEC011406	BP-HZN-CEC011406	Halliburton - 9.875" x 7" Foamed Production Casing Post Job Report
BP-HZN-MBI00023865	BP-HZN-MBI00023865	Core Analysis Tracking Sheet
BP-HZN-MBI00023865	BP-HZN-MBI00023865	Core Analysis Tracking Sheet native
CAM_CIV_0148046	CAM_CIV_0148271	BOP Schematic (DWH BOP Stack O and M manual
DNV2011062210		DNV2011062210 - Laser Scanning Tracking Sheet
DW 0007239	DW 0007261	Depo Exh. 9734.pdf
DW 0007239	DW 0007261	Depo Exh. 9734.pdf
DW 0007272	DW 0007274	Depo Exh. 10423.pdf
DW 0007272	DW 0007274	Depo Exh. 10423.pdf
ERP001-003232	ERP001-003249	Ex No._8631.pdf
GMS001-000360	GMS001-000371	Gemini Summary of Work
IGS075-016276	IGS075-016385	Ex No._8635.pdf
IGS075-016276	IGS075-016385	Exhibit 8635.pdf
IGS075-018203	IGS075-018274	Ex No._8639.pdf
IGS075-018303	IGS075-018324	Ex No._8620.pdf
IGS076-001725	IGS076-001747	Ex No._8616.pdf
IGS078-001807	IGS078-001833	Ex No._8630.pdf
IGS092-010194	IGS092-010201	Ex No._8640.pdf
IGS092-010202	IGS092-010206	Ex No._8638.pdf
IGS092-010207	IGS092-010210	Ex No._8634.pdf
IGS606-016456	IGS606-016456	Ex No._8623.pdf
IGS606-016600	IGS606-016653	Ex No._8633.pdf
IGS606-038866	IGS606-038885	Ex No._8636.pdf
IGS622-000849	IGS622-000907	Gemini Preliminary Presentation
IGS628-009822	IGS628-009829	Ex No._8624.pdf
IGS628-009822	IGS628-009829	Email from S. Hickman to C. Enomoto et al. re Fwd: Geological evidence for aquifer
IGS629-000522	IGS629-000526	Ex No._8627.pdf
IGS629-001341	IGS629-001344	Ex No._8619.pdf

194

Beg Bates	End Bates	Document Title / Description
IGS629-003057	IGS629-003060	Ex No._8637.pdf
IGS642-000129	IGS642-000152	Ex No._8629.pdf
IMV267-051052	IMV267-051134	Gemini Final Presentation
IMV267-051416	IMV267-051419	Gemini Report
IMV365-018434	IMV365-018457	MDL 2179 Deposition Exhibit 9859.pdf
MDL 2179 Deposition Exhibit 8789_(23957589_1) (2).PDF	n/a	MDL 2179 Deposition Exhibit 8789_(23957589_1) (2).PDF
MDL 2179 Deposition Exhibit 9063_(23957804_1).PDF	n/a	MDL 2179 Deposition Exhibit 9063_(23957804_1).PDF
MDL 2179 Deposition Exhibit 9064_(23957808_1).PDF	n/a	MDL 2179 Deposition Exhibit 9064_(23957808_1).PDF
MDL 2179 Deposition Exhibit 9065_(23957823_1).PDF	n/a	MDL 2179 Deposition Exhibit 9065_(23957823_1).PDF
n/a	n/a	John Amos - SkyTruth - Gulf Oil Spill Rate Must be Much Higher than Stated
n/a	n/a	NYT Article Reporting 5000 bbl a day NOAA Estimate
n/a	n/a	Ian MacDonald -- SkyTruth - Gulf Oil Spill - New Spill Calculation
n/a	n/a	Crone, Chiang, Wereley -- NPR - Gulf Oil Spill May Far Exceed Government, BP Estimates _ NPR
n/a	n/a	Crone, Chiang, Wereley -- NPR - Transcript
n/a	n/a	Congressional Hearing - Sizing Up the BP Oil Spill - Transcript (Original)
n/a	n/a	Camilli - WHOI Prepared Congressional Statement
n/a	n/a	Camilli WHOI Presentation Plan
n/a	n/a	Werely - Congressional Presentation
n/a	n/a	FRTG Press Release
n/a	n/a	FRTG - Summary Preliminary Report
n/a	n/a	FRTG -Press Release McNutt Provide Updates on Progress of Scientific Teams
n/a	n/a	FRTG - Jun 8 - Pooling Report
n/a	n/a	FRTG - Plume Team Statement
n/a	n/a	WHOI Preliminary Report
n/a	n/a	FRTG - US Scientific Team Draws on New Data
n/a	n/a	FRTG Plume Team - PIV Report (Revised)
n/a	n/a	FRTG - Refined Estimate

195

Beg Bates	End Bates	Document Title / Description
n/a	n/a	Deepwater Horizon - BP Oil Budget - What happened to the oil
n/a	n/a	Deepwater Horizon MC252 Gulf Incident Oil Budget
n/a	n/a	Crone - Science Express - Magnitude of the 2010 Gulf of Mexico Oil Leak
n/a	n/a	PresComm - Flow Rate - Amount and Fate of Oil
n/a	n/a	PresComm - BP Comments to Oct 6 Working Paper No 3 - Amount and Fate of Oil
n/a	n/a	Oil Spill Calculator - Technical Documentation
n/a	n/a	PresComm - The Amount and Fate of the Oil (Revised)
n/a	n/a	Lehr IOSC - Computing Mass Balance for the Deepwater Horizon Spill (Presented May 26, 2011)
n/a	n/a	FRTG - Assessment of Flow Rate Estimates for the Deepwater Horizon-Macondo Oil Spill - (Combined)
n/a	n/a	(May-June) Hsieh, P - Application of Transient Analyiss to Macondo
n/a	n/a	Lehr IOSC Poster- Spill Response 10 Years Later
n/a	n/a	DOE-NL -- DJB marked with proprietary marked OUO - SAND_Report_on_Flow_Analysis_Studies
n/a	n/a	DOE-NL DWH Oil Re (Griffiths)_(18699619_1)
n/a	n/a	DNV Scan Protocol (Doc 2016-1 - Approved Protocol)
n/a	n/a	DNV BOP Report Volume I.PDF
n/a	n/a	DNV BOP Report Volume II Appendices.pdf
n/a	n/a	Addendum to DNV BOP Report.pdf
n/a	n/a	Hard Drive Data re Laser Scanning Subfolders (Outline).doc
n/a	n/a	DOE-NL -- DJB marked with proprietary marked OUO -SAND Report on Flow Analysis Studies 12-08-10.DOCX
n/a	n/a	PNAS Simulation Report
n/a	n/a	Complete report from Schlumberger's MDT test
n/a	n/a	Griffiths_Revised_6_2011
n/a	n/a	Revised_Ratzel_9_2011
n/a	n/a	SperrySun drilling data transmittal letter to Blunt
n/a	n/a	10-13-2010 Pre-decisional draft, Hsieh, Computer simulation of Reservoir Depletion and Oil Flow (IGS642-000215).pdf
n/a	n/a	Expert report of Morten Emilsen
n/a	n/a	Hsieh Modeling Presentation

Beg Bates	End Bates	Document Title / Description
n/a	n/a	Well Performance Second Edition
n/a	n/a	Applied Drilling Engineering Textbook
n/a	n/a	Oil Release from Well MC252 Following the Deepwater Horizon Accident.pdf
n/a	n/a	Supporting Information
n/a	n/a	Deposition of Jason LeBlanc
n/a	n/a	SIGNATURE LETTER AND ERRATA SHEET OF JASON LEBLANC
n/a	n/a	ATT00001.htm
n/a	n/a	ATT00002.htm
n/a	n/a	Depositon of Jason LeBlanc
n/a	n/a	2012-09-11 Hsieh, Paul - MINI - FINAL.pdf
n/a	n/a	2012-09-12 Hsieh, Paul - MINI - FINAL.pdf
n/a	n/a	Deposition of Paul Hsieh
n/a	n/a	Deposition of Paul Hsieh
n/a	n/a	Deposition of Paul Hsieh
n/a	n/a	Deposition of Paul Hsieh
n/a	n/a	Ex No._8615.pdf
n/a	n/a	Ex No._8617.pdf
n/a	n/a	Ex No._8618.pdf
n/a	n/a	Ex No._8621.pdf
n/a	n/a	2012-11-30 Shtepani, Edmond - FULL - FINAL.PDF
n/a	n/a	2012-11-30 McArthur, Steven - FULL - FINAL.PDF
n/a	n/a	2012-11-12 Gansert, Tanner - FULL - FINAL.PDF
n/a	n/a	2012-10-24 Wang, Yun - FULL - FINAL.PDF
n/a	n/a	2012-09-14 Pelphrey, Steve (Isotech) - FULL - FINAL.PDF
n/a	n/a	Merrill, Robert Vol 1 compressed.pdf
n/a	n/a	Merrill, Robert Vol 2 compressed.pdf
n/a	n/a	2013-01-30 Levitan, Michael - FULL - FINAL_(25040719_1).PDF
n/a	n/a	2013-01-31 Levitan, Michael - FULL - FINAL_(25043459_1).PDF
n/a	n/a	ADD Energy 30(b)(6) - Ole Rygg.pdf
n/a	n/a	Allen, Admiral Thad - FULL - FINAL 2012-09-24.PDF
n/a	n/a	Allen, Admiral Thad - FULL - FINAL 2012-09-25.PDF
n/a	n/a	Ballard, Adam - FULL - FINAL 2012-10-16.PDF
n/a	n/a	Ballard, Adam - FULL - FINAL 2012-10-17.PDF
n/a	n/a	Barnett, David - FULL - FINAL 2012-12-14.PDF
n/a	n/a	Bishop, Simon - FULL - FINAL 2012-09-27.PDF
n/a	n/a	Bishop, Simon - FULL - FINAL 2012-09-28.PDF
n/a	n/a	Bondurant, Charles - FULL - FINAL 2011-08-23.PDF

Beg Bates	End Bates	Document Title / Description
n/a	n/a	Bozeman, Walt - FULL - FINAL 2011-09-15.PDF
n/a	n/a	Chu, Steven - FULL - FINAL 2013-01-24.PDF
n/a	n/a	DeCoste, Albert Bud - FULL - FINAL 2012-12-05.PDF
n/a	n/a	Emilsen, Haug Morten - FULL - FINAL (REVISED) 2011-06-24.PDF
n/a	n/a	Emilsen, Haug Morten - FULL - FINAL 2011-06-23.PDF
n/a	n/a	Emilsen, Morten - FULL - FINAL 2011-12-08.PDF
n/a	n/a	Gochnour, Matthew - FULL - FINAL 2012-09-13.PDF
n/a	n/a	Gochnour, Matthew - FULL - FINAL 2012-09-14.PDF
n/a	n/a	Griffiths, Stewart - FULL - FINAL 2012-11-13.PDF
n/a	n/a	Griffiths, Stewart - FULL - FINAL 2012-11-14.PDF
n/a	n/a	Guthrie, George - FULL - FINAL 2012-11-15.PDF
n/a	n/a	Guthrie, George - FULL - FINAL 2012-11-16.PDF
n/a	n/a	Hill, Trevor - FULL - FINAL (CORRECTED) 2013-01-15.PDF
n/a	n/a	Hill, Trevor - FULL - FINAL 2013-01-14.PDF
n/a	n/a	Hunter, Thomas - FULL - FINAL 2012-10-30.PDF
n/a	n/a	Hunter, Thomas - FULL - FINAL 2012-10-31.PDF
n/a	n/a	Liao, Tony - FULL - FINAL 2013-01-10.PDF
n/a	n/a	Liao, Tony - FULL - FINAL 2013-01-11.PDF
n/a	n/a	Lockett, Timothy - FULL - FINAL (Corrected) 2012-12-18.PDF
n/a	n/a	Lockett, Timothy - FULL - FINAL 2012-12-19.PDF
n/a	n/a	Loos, Jaime - FULL - FINAL 2012-09-20.PDF
n/a	n/a	Maclay, Don - FULL - FINAL 2012-10-31.PDF
n/a	n/a	Maclay, Don - FULL - FINAL 2012-11-01.PDF
n/a	n/a	Mason, Michael - FULL - FINAL 2013-01-24.PDF
n/a	n/a	Mason, Michael - FULL - FINAL 2013-01-25.PDF
n/a	n/a	McNutt, Marcia - Full - FINAL 2012-10-24.PDF
n/a	n/a	McNutt, Marcia - FULL - FINAL 2012-10-25.PDF
n/a	n/a	O'Neill, Brian - FULL - FINAL 2012-09-12.PDF
n/a	n/a	Ratzel, Arthur - FULL - FINAL 2012-10-17.PDF
n/a	n/a	Ratzel, Arthur - FULL - FINAL 2012-10-18.PDF

Beg Bates	End Bates	Document Title / Description
n/a	n/a	Ritchie, Ph.D., Bryan - FULL - FINAL 2012-10-04.PDF
n/a	n/a	Ritchie, Ph.D., Bryan - FULL - FINAL 2012-10-05.PDF
n/a	n/a	Saidi, Farah - FULL - FINAL 2013-01-10.PDF
n/a	n/a	Saidi, Farah - FULL - FINAL 2013-01-11.PDF
n/a	n/a	Sogge, Mark Kenneth - FULL - FINAL 2012-09-18.PDF
n/a	n/a	Sogge, Mark Kenneth - FULL - FINAL 2012-09-19.PDF
n/a	n/a	Tooms, Paul - FULL- FINAL 2011-06-16.PDF
n/a	n/a	Tooms, Paul - FULL- FINAL 2011-06-17.PDF
n/a	n/a	SPE-113888 Evaluation of Confidence Intervals Europec 2008
n/a	n/a	Horne - Uncertainty in Well Test Interpretation.pdf
n/a	n/a	Onur - Nonlinear Regression - The information content of pressure.pdf
n/a	n/a	Expert Report of Mohan Kelkar and Rajagopal Raghavan
n/a	n/a	Consideration Materials List of Mohan Kelkar and Rajagopa Raghavan
n/a	n/a	Expert Report of Mehran Pooladi-Darvish
n/a	n/a	Consideration Materials List of Mehran Pooladi-Darvish
n/a	n/a	Expert Report of Aaron Zick
n/a	n/a	Consideration Materials List of Aaron Zick
n/a	n/a	Pooladi-Darvish, Mehran Expert Modeling Runs
n/a	n/a	Modeling files from Pooladi-Darvish
n/a	n/a	Consideration Materials List of Mohan Kelkar and Rajagopa Raghavan (Revised)
n/a	n/a	Consideration Materials List of Mohan Kelkar and Rajagopa Raghavan (Revised)
n/a	n/a	Kelkar_relied upon modeling runs
n/a	n/a	3MC252 WTA 02-Apr-2013_DRAFT1.pptx
n/a	n/a	Incropera, Frank P. and David P. DeWitt, Introduction to Heat Transfer
n/a	n/a	Expert Report of Stewart Griffiths
n/a	n/a	Whitson ALL-T=35-SSF.ecl.xls
n/a	n/a	Whitson ALL-T=160F-SSF.ecl.xls
n/a	n/a	Whitson ALL-T=180F-SSF.ecl.xls
n/a	n/a	Whitson ALL-T=200F-SSF.ecl.xls
n/a	n/a	Whitson ALL-T=210-SSF.ecl.xls
n/a	n/a	Whitson ALL-T=220F-SSF.ecl.xls
n/a	n/a	Whitson T=243F-SSF-ALL.xls
n/a	n/a	Torres-Verdin Maps
n/a	n/a	Trusler PT-3k-2 data

Beg Bates	End Bates	Document Title / Description
n/a	n/a	Whitson Single-phase-density-20130306
n/a	n/a	Trusler PT-3k-1 data
PC-00057	PC-00083	MDL 2179 Deposition Exhibit 8711
PC-00057	PC-00083	Depo Exh. 8711.pdf
PC-00084	PC-00085	MDL 2179 Deposition Exhibit 8591
PC-00093	PC-00093	MDL 2179 Deposition Exhibit 8703
PC-00119	PC-00121	MDL 2179 Deposition Exhibit 8712
PC-00142	PC-00147	MDL 2179 Deposition Exhibit 8580
PC-00153	PC-00157	MDL 2179 Deposition Exhibit 8594
PC-00173	PC-00175	MDL 2179 Deposition Exhibit 8706
PC00176	PC00177	MDL 2179 Deposition Exhibit 8592
PC-00188	PC-00189	MDL 2179 Deposition Exhibit 8588
PC-00215	PC-00220	MDL 2179 Deposition Exhibit 8701
PC-00263	PC-00264	MDL 2179 Deposition Exhibit 8596
PC-0027	PC-00230	MDL 2179 Deposition Exhibit 8705
PC-00278	PC-00278	MDL 2179 Deposition Exhibit 8595
PC-00284	PC-00284	MDL 2179 Deposition Exhibit 8702
PC-00287	PC-00289	MDL 2179 Deposition Exhibit 8597
PC-00294	PC-00294	MDL 2179 Deposition Exhibit 8590
PC-00296	PC-00297	MDL 2179 Deposition Exhibit 8713
PC-00306	PC-00308	MDL 2179 Deposition Exhibit 8593
PC-00342	PC-00343	MDL 2179 Deposition Exhibit 8704
PC-00344	PC-00344	MDL 2179 Deposition Exhibit 8589
PC-00351	PC-00353	MDL 2179 Deposition Exhibit 8582
PC-00566	PC-00567	MDL 2179 Deposition Exhibit 8598
PC-00568	PC-00568	MDL 2179 Deposition Exhibit 8599
PC-00569	PC-00570	MDL 2179 Deposition Exhibit 8583
PC-00569	PC-00570	Depo Exh. 8583.pdf
PC-00596	PC-00597	MDL 2179 Deposition Exhibit 8584
PC-00596	PC-00597	Depo Exh. 8584.pdf
PC-00598	PC-00599	MDL 2179 Deposition Exhibit 8585
PC-00598	PC-00599	Depo Exh. 8585.pdf
PC-01874	PC-01882	MDL 2179 Deposition Exhibit 8587
PC-03132	PC-03140	MDL 2179 Deposition Exhibit 8586
PC-03132	PC-03140	Depo Exh. 8586.pdf
PNL003-003308	PNL003-003365	Ex No._8628.pdf
PNL032-036391	PNL032-036415	MDL 2179 Deposition Exhibit 8709
PNL032-036391	PNL032-036415	Depo Exh. 8709.pdf
SAT007-008716	SAT007-008725	Ex No._8622.pdf
SNL043-007022	SNL043-007022	Email from S. Griffiths to C. Ammerman, et al re well flow rates and total discharge
SNL043-007023	SNL043-007029	MC252 Well Flow Analysis Using Measured BOP Pressures
SNL043-007034	SNL043-007035	Griffiths – Reply to Ron's questions regard model
SNL043-007524	SNL043-007526	Email from S. Griffiths to R. Dykhuizen re Re: well flow rates and total discharge
SNL110-002599	SNL110-002599	Ex No._8626.pdf

Beg Bates	End Bates	Document Title / Description
SNL111-002483	SNL111-002484	Email from S. Griffiths to R. Dykhuizen re Re: griffith assumptions
SNL111-002485	SNL111-002487	Email from S. Griffiths to A. Ratzel and M. Tatro re FW: summary of your model
SNL116-002820	SNL116-002823	Ex No._8632.pdf
STC-MDL-0003092	STC-MDL-0003147	Depo Exh. 10455.pdf
STC-MDL-0004070	STC-MDL-0004094	Depo Exh. 10454.pdf
WFT-MDL-00039232	WFT-MDL-00039232	plug-17805_00-0.jpg
WFT-MDL-00039234	WFT-MDL-00039234	plug-18069_80-0.jpg
WFT-MDL-00039235	WFT-MDL-00039235	plug-18077_00-0.jpg
WFT-MDL-00039236	WFT-MDL-00039236	plug-18081_80-0.jpg
WFT-MDL-00039237	WFT-MDL-00039237	plug-18083_00A-0.jpg
WFT-MDL-00039238	WFT-MDL-00039238	plug-18087_00-0.jpg
WFT-MDL-00039239	WFT-MDL-00039239	plug-18121_00-0.jpg
WFT-MDL-00039240	WFT-MDL-00039240	plug-18124_90-0.jpg
WFT-MDL-00039241	WFT-MDL-00039241	plug-18127_00-0.jpg
WFT-MDL-00039242	WFT-MDL-00039242	plug-18131_90-0.jpg
WFT-MDL-00039243	WFT-MDL-00039243	plug-18134_10-0.jpg
WFT-MDL-00039244	WFT-MDL-00039244	plug-18143_90-0.jpg
WFT-MDL-00039245	WFT-MDL-00039245	plug-18147_90-0.jpg
WFT-MDL-00039246	WFT-MDL-00039246	plug-18157_90-0.jpg
WFT-MDL-00039247	WFT-MDL-00039247	plug-18166_00-0.jpg
WFT-MDL-00039248	WFT-MDL-00039248	plug-18188_00-0.jpg
WFT-MDL-00039271	WFT-MDL-00039271	17706.90_3-1R_uv_l.jpg
WFT-MDL-00039272	WFT-MDL-00039272	17706.90_3-1R_wl_l.jpg
WFT-MDL-00039273	WFT-MDL-00039273	17805.00_3-2R_uv_l.jpg
WFT-MDL-00039274	WFT-MDL-00039274	17805.00_3-2R_wl_l.jpg

Beg Bates	End Bates	Document Title / Description
WFT-MDL-00039275	WFT-MDL-00039275	18030.60_2-1R_uv_l.jpg
WFT-MDL-00039276	WFT-MDL-00039276	18030.60_2-1R_wl_l.jpg
WFT-MDL-00039277	WFT-MDL-00039277	18067.90_2-2R_uv_l.jpg
WFT-MDL-00039278	WFT-MDL-00039278	18067.90_2-2R_wl_l.jpg
WFT-MDL-00039279	WFT-MDL-00039279	18069.80_3-4R_uv_l.jpg
WFT-MDL-00039280	WFT-MDL-00039280	18069.80_3-4R_wl_l.jpg
WFT-MDL-00039281	WFT-MDL-00039281	18072.00_3-5R_uv_l.jpg
WFT-MDL-00039282	WFT-MDL-00039282	18072.00_3-5R_wl_l.jpg
WFT-MDL-00039283	WFT-MDL-00039283	18074.90_3-6R_uv_l.jpg
WFT-MDL-00039284	WFT-MDL-00039284	18074.90_3-6R_wl_l.jpg
WFT-MDL-00039285	WFT-MDL-00039285	18080.00_3-7R_uv_l.jpg
WFT-MDL-00039286	WFT-MDL-00039286	18080.00_3-7R_wl_l.jpg
WFT-MDL-00039287	WFT-MDL-00039287	18081.80_3-8R_uv_l.jpg
WFT-MDL-00039288	WFT-MDL-00039288	18081.80_3-8R_wl_l.jpg
WFT-MDL-00039289	WFT-MDL-00039289	18083.00_3-9R_uv_l.jpg
WFT-MDL-00039290	WFT-MDL-00039290	18083.00_3-9R_wl_l.jpg
WFT-MDL-00039291	WFT-MDL-00039291	18084.90_3-10R_uv_l.jpg
WFT-MDL-00039292	WFT-MDL-00039292	18084.90_3-10R_wl_l.jpg
WFT-MDL-00039293	WFT-MDL-00039293	18087.00_2-4R_uv_l.jpg
WFT-MDL-00039294	WFT-MDL-00039294	18087.00_2-4R_wl_l.jpg
WFT-MDL-00039295	WFT-MDL-00039295	18114.90_3-11R_uv_l.jpg
WFT-MDL-00039296	WFT-MDL-00039296	18114.90_3-11R_wl_l.jpg
WFT-MDL-00039297	WFT-MDL-00039297	18121.00_3-12R_uv_l.jpg
WFT-MDL-00039298	WFT-MDL-00039298	18121.00_3-12R_wl_l.jpg

Beg Bates	End Bates	Document Title / Description
WFT-MDL-00039299	WFT-MDL-00039299	18124.90_3-14R_uv_l.jpg
WFT-MDL-00039300	WFT-MDL-00039300	18124.90_3-14R_wl_l.jpg
WFT-MDL-00039301	WFT-MDL-00039301	18127.00_3-15R_uv_l.jpg
WFT-MDL-00039302	WFT-MDL-00039302	18127.00_3-15R_wl_l.jpg
WFT-MDL-00039303	WFT-MDL-00039303	18129.10_3-16R_uv_l.jpg
WFT-MDL-00039304	WFT-MDL-00039304	18129.10_3-16R_wl_l.jpg
WFT-MDL-00039305	WFT-MDL-00039305	18131.90_3-17R_uv_l.jpg
WFT-MDL-00039306	WFT-MDL-00039306	18131.90_3-17R_wl_l.jpg
WFT-MDL-00039307	WFT-MDL-00039307	18134.10_3-18R_uv_l.jpg
WFT-MDL-00039308	WFT-MDL-00039308	18134.10_3-18R_wl_l.jpg
WFT-MDL-00039309	WFT-MDL-00039309	18141.90_3-19R_uv_l.jpg
WFT-MDL-00039310	WFT-MDL-00039310	18141.90_3-19R_wl_l.jpg
WFT-MDL-00039311	WFT-MDL-00039311	18143.90_3-20R_uv_l.jpg
WFT-MDL-00039312	WFT-MDL-00039312	18143.90_3-20R_wl_l.jpg
WFT-MDL-00039313	WFT-MDL-00039313	18147.90_3-21R_uv_l.jpg
WFT-MDL-00039314	WFT-MDL-00039314	18147.90_3-21R_wl_l.jpg
WFT-MDL-00039315	WFT-MDL-00039315	18150.00_3-22R_uv_l.jpg
WFT-MDL-00039316	WFT-MDL-00039316	18150.00_3-22R_wl_l.jpg
WFT-MDL-00039317	WFT-MDL-00039317	18154.00_3-23R_uv_l.jpg
WFT-MDL-00039318	WFT-MDL-00039318	18154.00_3-23R_wl_l.jpg
WFT-MDL-00039319	WFT-MDL-00039319	18157.90_3-24R_uv_l.jpg
WFT-MDL-00039320	WFT-MDL-00039320	18157.90_3-24R_wl_l.jpg
WFT-MDL-00039321	WFT-MDL-00039321	18161.00_3-25R_uv_l.jpg
WFT-MDL-00039322	WFT-MDL-00039322	18161.00_3-25R_wl_l.jpg

Beg Bates	End Bates	Document Title / Description
WFT-MDL-00039323	WFT-MDL-00039323	18163.10_1-2R_uv_l.jpg
WFT-MDL-00039324	WFT-MDL-00039324	18163.10_1-2R_wl_l.jpg
WFT-MDL-00039325	WFT-MDL-00039325	18166.00_3-26R_uv_l.jpg
WFT-MDL-00039326	WFT-MDL-00039326	18166.00_3-26R_wl_l.jpg
WFT-MDL-00039327	WFT-MDL-00039327	18167.50_3-27R_uv_l.jpg
WFT-MDL-00039328	WFT-MDL-00039328	18167.50_3-27R_wl_l.jpg
WFT-MDL-00039329	WFT-MDL-00039329	18174.00_1-3R_uv_l.jpg
WFT-MDL-00039330	WFT-MDL-00039330	18174.00_1-3R_wl_l.jpg
WFT-MDL-00039331	WFT-MDL-00039331	18178.00_3-29R_uv_l.jpg
WFT-MDL-00039332	WFT-MDL-00039332	18178.00_3-29R_wl_l.jpg
WFT-MDL-00039333	WFT-MDL-00039333	18180.10_3-30R_uv_l.jpg
WFT-MDL-00039334	WFT-MDL-00039334	18180.10_3-30R_wl_l.jpg
WFT-MDL-00039335	WFT-MDL-00039335	18183.10_3-31R_uv_l.jpg
WFT-MDL-00039336	WFT-MDL-00039336	18183.10_3-31R_wl_l.jpg
WFT-MDL-00039337	WFT-MDL-00039337	18188.00_1-4R_uv_l.jpg
WFT-MDL-00039338	WFT-MDL-00039338	18188.00_1-4R_wl_l.jpg
WFT-MDL-00039339	WFT-MDL-00039339	18214.40_3-33R_uv_l.jpg
WFT-MDL-00039340	WFT-MDL-00039340	18214.40_3-33R_wl_l.jpg
WFT-MDL-00039341	WFT-MDL-00039341	18232.90_3-35R_uv_l.jpg
WFT-MDL-00039342	WFT-MDL-00039342	18232.90_3-35R_wl_l.jpg
WFT-MDL-00039343	WFT-MDL-00039343	plug-17706_90-0.jpg
WFT-MDL-00039344	WFT-MDL-00039344	plug-18067_90-0.jpg
WFT-MDL-00039345	WFT-MDL-00039345	plug-18072_00-0.jpg
WFT-MDL-00039346	WFT-MDL-00039346	plug-18074_90-0.jpg

Beg Bates	End Bates	Document Title / Description
WFT-MDL-00039347	WFT-MDL-00039347	plug-18080_00-0.jpg
WFT-MDL-00039348	WFT-MDL-00039348	plug-18083_00-0.jpg
WFT-MDL-00039349	WFT-MDL-00039349	plug-18084_90-0.jpg
WFT-MDL-00039350	WFT-MDL-00039350	plug-18114_90-0.jpg
WFT-MDL-00039351	WFT-MDL-00039351	plug-18123_00-0.jpg
WFT-MDL-00039352	WFT-MDL-00039352	plug-18129_10-0.jpg
WFT-MDL-00039353	WFT-MDL-00039353	plug-18141_90-0.jpg
WFT-MDL-00039354	WFT-MDL-00039354	plug-18150_00-0.jpg
WFT-MDL-00039355	WFT-MDL-00039355	plug-18154_00-0.jpg
WFT-MDL-00039356	WFT-MDL-00039356	plug-18161_00-0.jpg
WFT-MDL-00039357	WFT-MDL-00039357	plug-18163_10-0.jpg
WFT-MDL-00039358	WFT-MDL-00039358	plug-18167_50-0.jpg
WFT-MDL-00039359	WFT-MDL-00039359	plug-18170_90-0.jpg
WFT-MDL-00039360	WFT-MDL-00039360	plug-18174_00-0.jpg
WFT-MDL-00039361	WFT-MDL-00039361	plug-18178_00-0.jpg
WFT-MDL-00039362	WFT-MDL-00039362	plug-18180_10-0.jpg
WFT-MDL-00039363	WFT-MDL-00039363	plug-18183_10-0.jpg
WFT-MDL-00039364	WFT-MDL-00039364	plug-18184_90-0.jpg
WFT-MDL-00039365	WFT-MDL-00039365	plug-18214_40-0.jpg
WFT-MDL-00039366	WFT-MDL-00039366	plug-18231_00-0.jpg
WFT-MDL-00039367	WFT-MDL-00039367	plug-18232_90-0.jpg
WFT-MDL-00039368	WFT-MDL-00039368	plug-18235_80-0.jpg
WFT-MDL-00039385	WFT-MDL-00039385	plug-18030_60-0.jpg
WFT-MDL-00039587	WFT-MDL-00039588	MDL 2179 Deposition Exhibit 9053_(23957629_1).PDF

Beg Bates	End Bates	Document Title / Description
WFT-MDL-00039615	WFT-MDL-00039615	1-1.jpg
WFT-MDL-00039616	WFT-MDL-00039616	1-2.jpg
WFT-MDL-00039617	WFT-MDL-00039617	2-1.jpg
WFT-MDL-00039618	WFT-MDL-00039618	3-1.jpg
WFT-MDL-00039619	WFT-MDL-00039619	3-2.jpg
WFT-MDL-00039620	WFT-MDL-00039620	3-3.jpg
WFT-MDL-00039621	WFT-MDL-00039621	3-4.jpg
WFT-MDL-00039622	WFT-MDL-00039622	3-5.jpg
WFT-MDL-00039623	WFT-MDL-00039623	3-6.jpg
WFT-MDL-00039624	WFT-MDL-00039624	3-7.jpg
WFT-MDL-00039625	WFT-MDL-00039625	3-8.jpg
WFT-MDL-00039695	WFT-MDL-00039695	18030.60_2-1R_uv.jpg
WFT-MDL-00039696	WFT-MDL-00039696	18030.60_2-1R_wl.jpg
WFT-MDL-00039697	WFT-MDL-00039697	18069.80_3-4R_uv.jpg
WFT-MDL-00039698	WFT-MDL-00039698	18069.80_3-4R_wl.jpg
WFT-MDL-00039699	WFT-MDL-00039699	18072.00_3-5R_uv.jpg
WFT-MDL-00039700	WFT-MDL-00039700	18072.00_3-5R_wl.jpg
WFT-MDL-00039701	WFT-MDL-00039701	18074.90_3-6R_uv.jpg
WFT-MDL-00039702	WFT-MDL-00039702	18074.90_3-6R_wl.jpg
WFT-MDL-00039703	WFT-MDL-00039703	18080.00_3-7R_uv.jpg
WFT-MDL-00039704	WFT-MDL-00039704	18080.00_3-7R_wl.jpg
WFT-MDL-00039705	WFT-MDL-00039705	18081.80_3-8R_uv.jpg
WFT-MDL-00039706	WFT-MDL-00039706	18081.80_3-8R_wl.jpg
WFT-MDL-00039707	WFT-MDL-00039707	18083.00_3-9R_uv.jpg

Beg Bates	End Bates	Document Title / Description
WFT-MDL-00039708	WFT-MDL-00039708	18083.00_3-9R_wl.jpg
WFT-MDL-00039709	WFT-MDL-00039709	18084.90_3-10R_uv.jpg
WFT-MDL-00039710	WFT-MDL-00039710	18084.90_3-10R_wl.jpg
WFT-MDL-00039711	WFT-MDL-00039711	18087.00_2-4R_uv.jpg
WFT-MDL-00039712	WFT-MDL-00039712	18087.00_2-4R_wl.jpg
WFT-MDL-00039713	WFT-MDL-00039713	18121.00_3-12R_uv.jpg
WFT-MDL-00039714	WFT-MDL-00039714	18121.00_3-12R_wl.jpg
WFT-MDL-00039715	WFT-MDL-00039715	18124.90_3-14R_uv.jpg
WFT-MDL-00039716	WFT-MDL-00039716	18124.90_3-14R_wl.jpg
WFT-MDL-00039717	WFT-MDL-00039717	18129.10_3-16R_uv.jpg
WFT-MDL-00039718	WFT-MDL-00039718	18129.10_3-16R_wl.jpg
WFT-MDL-00039719	WFT-MDL-00039719	18131.90_3-17R_uv.jpg
WFT-MDL-00039720	WFT-MDL-00039720	18131.90_3-17R_wl.jpg
WFT-MDL-00039721	WFT-MDL-00039721	18141.90_3-19R_uv.jpg
WFT-MDL-00039722	WFT-MDL-00039722	18141.90_3-19R_wl.jpg
WFT-MDL-00039723	WFT-MDL-00039723	18143.90_3-20R_uv.jpg
WFT-MDL-00039724	WFT-MDL-00039724	18143.90_3-20R_wl.jpg
WFT-MDL-00039725	WFT-MDL-00039725	18147.90_3-21R_uv.jpg
WFT-MDL-00039726	WFT-MDL-00039726	18147.90_3-21R_wl.jpg
WFT-MDL-00039727	WFT-MDL-00039727	18150.00_3-22R_uv.jpg
WFT-MDL-00039728	WFT-MDL-00039728	18150.00_3-22R_wl.jpg
WFT-MDL-00039729	WFT-MDL-00039729	18154.00_3-23R_uv.jpg
WFT-MDL-00039730	WFT-MDL-00039730	18154.00_3-23R_wl.jpg
WFT-MDL-00039731	WFT-MDL-00039731	18157.90_3-24R_uv.jpg

Beg Bates	End Bates	Document Title / Description
WFT-MDL-00039732	WFT-MDL-00039732	18157.90_3-24R_wl.jpg
WFT-MDL-00039733	WFT-MDL-00039733	18161.00_3-25R_uv.jpg
WFT-MDL-00039734	WFT-MDL-00039734	18161.00_3-25R_wl.jpg
WFT-MDL-00039735	WFT-MDL-00039735	18163.10_1-2R_uv.jpg
WFT-MDL-00039736	WFT-MDL-00039736	18163.10_1-2R_wl.jpg
WFT-MDL-00039737	WFT-MDL-00039737	18166.00_3-26R_uv.jpg
WFT-MDL-00039738	WFT-MDL-00039738	18166.00_3-26R_wl.jpg
WFT-MDL-00039739	WFT-MDL-00039739	18174.00_1-3R_uv.jpg
WFT-MDL-00039740	WFT-MDL-00039740	18174.00_1-3R_wl.jpg
WFT-MDL-00039741	WFT-MDL-00039741	18178.00_3-29R_uv.jpg
WFT-MDL-00039742	WFT-MDL-00039742	18178.00_3-29R_wl.jpg
WFT-MDL-00039743	WFT-MDL-00039743	18180.10_3-30R_uv.jpg
WFT-MDL-00039744	WFT-MDL-00039744	18180.10_3-30R_wl.jpg
WFT-MDL-00039745	WFT-MDL-00039745	18183.10_3-31R_uv.jpg
WFT-MDL-00039746	WFT-MDL-00039746	18183.10_3-31R_wl.jpg
WFT-MDL-00039747	WFT-MDL-00039747	18232.90_3-35R_uv.jpg
WFT-MDL-00039748	WFT-MDL-00039748	18232.90_3-35R_wl.jpg
WFT-MDL-00039838	WFT-MDL-00039838	18069.80-18083.00.jpg
WFT-MDL-00039839	WFT-MDL-00039839	18084.90-18141.90.jpg
WFT-MDL-00039840	WFT-MDL-00039840	18147.90-18163.10.jpg
WFT-MDL-00039841	WFT-MDL-00039841	18166.00-18183.10.jpg
WFT-MDL-00054278	WFT-MDL-00054278	plug-18074_9-0.jpg
WFT-MDL-00054279	WFT-MDL-00054279	plug-18087_0-0.jpg
WFT-MDL-00054280	WFT-MDL-00054280	plug-18131_9-0.jpg

Beg Bates	End Bates	Document Title / Description
WFT-MDL-00054281	WFT-MDL-00054281	plug-18141_9-0.jpg
WFT-MDL-00054282	WFT-MDL-00054282	plug-18150_0-0.jpg
WFT-MDL-00054283	WFT-MDL-00054283	plug-18129_1-0.jpg
WFT-MDL-00082902	WFT-MDL-00082902	MDL 2179 Deposition Exhibit 9069_(23957831_1).PDF
WFT-MDL-00082904	WFT-MDL-00082904	MDL 2179 Deposition Exhibit 9067 - Clean_(24675966_1).PDF
WFT-MDL-00129170	WFT-MDL-00129172	MDL 2179 Deposition Exhibit 9070_(23957834_1).PDF
WFT-MDL-00129617	WFT-MDL-000129618	MDL 2179 Deposition Exhibit 9066 - Clean_(24675970_1).PDF
WFT-MDL-00131648	WFT-MDL-00131649	MDL 2179 Deposition Exhibit 9068 - Clean_(24675968_1).PDF